THE
PHYSICAL REVIEW
A Journal of Experimental and Theoretical Physics Established by E. L. Nichols in 1893
VOL. 58, NO. 12 DECEMBER 15, 1940 SECOND SERIES

Counter Studies on Cosmic Rays at Sea Level

GEORGE O. ALTMANN, *Fordham University, New York, New York*
H. N. WALKER, *College of Engineering, New York University, New York, New York*
AND
VICTOR F. HESS, *Fordham University, New York, New York*
(Received August 29, 1940)

Part I: Rossi transition curves for lead up to 400 g/cm² were studied with a triple coincidence counter arrangement in various geometrical configurations with shower angles from 4° to 60°; variations of cosmic-ray intensities were recorded simultaneously with a twofold vertical coincidence set and every point of the transition curves corrected accordingly. Even with small angle showers in an arrangement practically identical with Bothe and Schmeiser's no second maximum of the Rossi curve could be found. Absorption of shower particles and back scattering were studied.

Part II: Time variations were recorded with a vertical coincidence set giving daily mean values for one year in New York City. The temperature coefficient for the winter months (−0.155 percent per degree C) is about 5 times greater than the one for the summer months (−0.033). The total seasonal variation (maximum in winter, minimum in summer and fall) amounts to about 5.6 percent and is reduced to about 2.8 percent when the values are corrected for the same temperature. Thus a true seasonal variation with an amplitude of ±1.4 percent was found, in agreement with measurements elsewhere with ionization chambers. Various nonperiodic changes in cosmic-ray intensity were studied: the effect of the passage of cold and warm fronts, of the passage of barometric depressions and the effect of magnetic storms. The magnitude of these effects, as recorded in a vertical coincidence set agrees very well with the effects found with ionization chambers.

INTRODUCTION

IN the spring of 1939 cosmic-ray studies were begun in the Physics Department of Fordham University under the direction of the senior author (V.F.H.).

The following is a report on some preliminary work done on production of showers, absorption of shower particles, back scattering and on time variations observed with coincidence counter arrangements.

PART I: STUDY OF PRODUCTION AND ABSORPTION OF SHOWERS

During the Cosmic-Ray Symposium in Chicago (June, 1939) the existence or nonexistence of the second maximum, found first in 1934 by Ackermann and Hummel and by Drigo,[1] at a thickness of about 17 cm in lead (30 cm in iron) was a matter of controversy among several participants of this convention. Shortly before, Nielsen, J. E. Morgan and K. Z. Morgan[2] had published experiments on the shower production in iron up to thicknesses of 320 g/cm² at various shower angles and had not found a second maximum around 200 g/cm² as expected with either large or small angle showers. This is contradictory to the findings of Bothe and

[1] A. Ackermann and I. N. Hummel, Naturwiss. 22, 169 and 170 (1934); A. Drigo, Ricerca Scient. 5, 88, 89 (1934).
[2] W. M. Nielsen, J. E. Morgan and K. Z. Morgan, Phys. Rev. 55, 995 (1939).

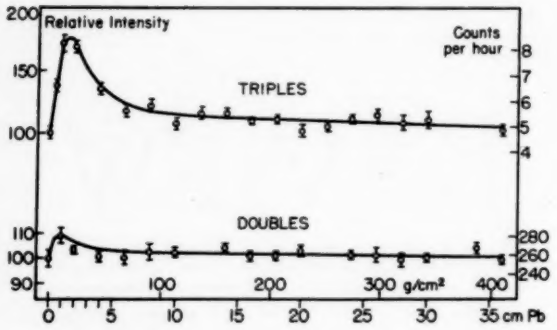

FIG. 1. Rossi transition curves for lead. The shower angle was 9.6°.

Schmeiser.[3] Bothe pointed out that the higher penetrating power of small angle showers may be mainly responsible for the second maximum of the Rossi curve and he published a curve where, with a shower angle of 4°, the second maximum was very well pronounced and nearly as high as the first maximum at 1–2 cm of lead while with an angle of 15° in the neighborhood of the critical thickness no hump at all was visible. Clay and Jonker[4] on the other hand found with a shower angle of 39° only a very slight indication of a second hump.

It seemed interesting to study the Rossi transition curve for lead up to thicknesses of more than 30 cm of the scattering block with double and triple coincidence counter sets and in various geometrical arrangements in order to clarify, if possible, the contradictory statements of the authors cited above.

Each point of the curve necessitated a recording of coincidences for several days, and since time variations of the general intensity of cosmic rays (barometer effect, air mass effect, magnetic storms, etc.) may amount to several percent it seemed advantageous to correct for time variations as much as possible by having a second set of apparatus giving the vertical coincidence counting rate for every day of operation at the same time.

1. Experimental arrangement

Two sets of three Geiger-Müller counting tubes arranged in a Rossi circuit with the usual extension amplifiers and recording units operating watch recorders were used for most experiments. A third set consisted of a twofold coincidence arrangement with the two counters set up permanently in a vertical plane and was operated continuously for almost one year to obtain the average cosmic-ray intensity for each day.

In the first-mentioned triple coincidence apparatus large Geiger-Müller counting tubes were used (diameter of the copper cathode cylinders 3 cm, length 30 cm).

The three high voltage sources used throughout these experiments were constructed by one of us (H.N.W.) and were similar to the stabilized high voltage circuit devised by N. S. Gingrich.[5] It was found desirable to make certain changes in the circuit. A description of this will be published elsewhere.

Most of the experiments were performed in the basement laboratory of Fordham University where the temperature changes encountered during the year are relatively small, namely between 20 and 27°C.

For reasons given above we thought it necessary to reduce all counts to normal barometric pressure. The barometer effect was determined with our twofold coincidence set.

2. Experiments with various angle showers

Since the second maximum was found first with arrangements where rather wide showers were causing the coincidences[6] we carried out one series of experiments where the three counters were placed parallel to each other in a horizontal plane with their centers 5 cm apart and the lead scatterer set up directly above this row of counters ("Hummel arrangement").

We obtained the typical Rossi transition curve with a first maximum at 1.3 cm lead. No second maximum between 10 and 20 cm was discernible.

The next series was taken with the usual "triangle arrangement." Here again no clear indication of a second maximum for lead thicknesses between 15 and 25 cm was found. Another series with the counter cross section forming an isosceles triangle of 30° (extended for a period of 2 months) showed slight indications of a hump

[3] K. Schmeiser and W. Bothe, Naturwiss. **25**, 669 (1937); Ann. d. Physik **32**, 161 (1938); W. Bothe, Rev. Mod. Phys. **11**, 282 (1939).
[4] J. Clay, Rev. Mod. Phys. **11**, 287 (1939).
[5] N. S. Gingrich, Rev. Sci. Inst. **7**, 207 (1936).
[6] D. K. Froman and J. C. Stearns, Rev. Mod. Phys. **10**, 133 (1938).

and at least greater irregularities between 14 and 24 cm of lead.

Therefore we tried next an experiment where single rays and very narrow showers could cause coincidences. Three counters were placed above each other in a vertical plane, with the scattering lead plates above them. Double coincidences of the first two upper tubes and triple coincidences of all three tubes were registered separately for various thicknesses of the scattering lead up to 21 cm. For the double coincidences the shower angle as measured from the lower surface of the scattering plate to the contour of the middle tube was 12°, for the triples (as taken from the scattering block to the contour of the bottom tube) only 7°. This experiment, therefore, gives an approximate comparison of the Rossi curves at these two angles. The first maximum of these transition curves, well pronounced in both cases, was reached at about 2 cm.

Again no second maximum, at thicknesses beyond 15 cm lead was found.

It may be noted also that in this particular arrangement a great percentage of coincidences is due to single rays and therefore these curves still cannot be considered as unambiguous evidence against the possible existence of this second maximum.

3. Narrow angle showers

Next we carried out a long series of coincidence counting with a triangular arrangement, where the top tube (1) was placed directly under the scattering lead block (its thickness was varied in small steps from 0 to 36 cm of lead) while the lower two tubes (2) and (3) were arranged 25 cm from the upper tube. The minimum shower angle of two-particle showers effecting all three tubes or the two lower tubes (doubles) was thus about 9.6°. The total number of double coincidences used for each point of the following curves was from 1000 to 5000 (average counting rate 260 c/hr.), for triples 250 to 1700 (average counting rate 5 to 8 c/hr.). The actual counting rates for each thickness of the scattering block (22 cm×33 cm) were corrected for accidentals and then reduced to normal pressure.

The statistical errors computed for each individual point are indicated in Fig. 1.

At first glance we see that indications for a second hump are very slight. The curve for triples shows upward deviations at 13 and 25 cm slightly greater than the statistical error but none at 20 cm. The double coincidence curve is smooth showing no hump except at the rather well-known first maximum between 1 and 2 cm of lead.

This curve indicates that double coincidences in our arrangement were to a great extent caused by side showers and two-particle showers traveling downwards in oblique directions from the scattering surface to the two bottom counters. Dubious points were repeatedly checked.

The next step was to choose an arrangement which was identical to the one used by Bothe and Schmeiser.[3] In order to get a higher absolute counting rate these authors placed four counters at such a distance from the lower surface of the lead scatterer that the angle subtended from any point near the center of the lead surface to the centers of the lower two counters was only 4°. Counters 1 and 2 were connected in parallel and triple coincidences between these upper tubes (1 and 2) with the lower counters 3 and 4 were registered. This arrangement is shown in Fig. 2. Between the two rows of counters a lead plate of 0.7 cm thickness was placed and a lead bar of 1 cm thickness was used between counters 3 and 4. The 0.7-cm lead plate between the two rows of counters was used to exclude any soft shower

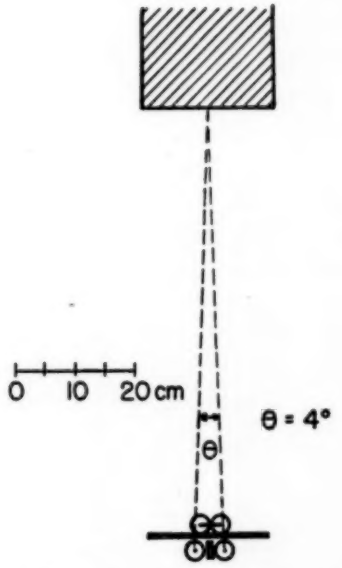

FIG. 2. Arrangement of counters for experiments similar to those of Bothe and Schmeiser.

particles which would tend to blur the effect of the hard narrow showers sought. The 1-cm lead bar used as a partition wall between the two lower counters served the same purpose and was also used by Zeiller[7] and by Schmeiser and Bothe.

These authors also reported that the second maximum was relatively more pronounced when the experiments were performed in the basement instead of on the top floor. This again would indicate that the hard component (mesotrons) is mainly responsible for the second maximum. We, therefore, made all experiments in the basement of the Physics Building of Fordham University with four stories above the experimental arrangement.

The curve shows no indication of any second hump, in complete contradiction to the findings of Bothe and Schmeiser who claim that the second maximum shows up clearly in narrow angle showers. We are at a loss to explain this disagreement. A final experiment was a repetition of the last described, but with no lead plates between the two rows of counters and with increased surface of the scatterer (30 cm×33 cm). The result was again negative.

4. Absorption of shower particles and back scattering

The absorption of shower particles was studied by using a triple coincidence set with two counters in a vertical plane, the third in a parallel position, but out of line, while the scatterer (lead) was placed above the third counter. The great inhomogeneity of the shower particles was demonstrated by the fact that for the thicknesses of the absorbing plates (between the second and third counter) up to 6 cm lead the absorption coefficient shows a steady decrease.

Back scattering was studied with three parallel counters in a horizontal plane. The secondary radiation created in a block of lead (2 cm thick) was gradually absorbed in interposed sheets of aluminum (which itself gives a very small back scattering effect). The absorption coefficient in aluminum of secondary radiation from lead scattered backwards was found as 5.02 cm^{-1}.

TABLE I. *Monthly means of cosmic-ray intensity.*

Month	Uncorrected Intensity c/hr.	Barometric Pressure Inch Hg	Barometer Corrected Intensity c/hr.	Temperature °F	Temperature-Corrected Intensities Uniformly c/hr.	Temperature-Corrected Intensities Seasonally c/hr.
Jan.	112.9	29.79	111.6	25.2	109.2	109.2
Feb.	—	—	—	—	—	—
Mar.	109.7	29.77	108.3	35.0	107.1	106.9
Apr.	108.1	29.78	106.8	46.0	106.3	106.4
May	108.9	29.76	107.5	59.6	108.3	107.7
June	108.0	29.76	106.6	68.4	108.2	106.9
July	107.5	29.88	106.8	74.6	108.9	107.3
Aug.	107.2	29.81	106.1	76.8	108.3	106.6
Sep.	106.4	29.89	105.8	67.4	107.2	106.1
Oct.	106.4	29.87	105.7	56.4	106.3	105.8
Nov.	109.3	29.99	108.9	43.2	108.3	108.3
Dec.	111.4	29.69	109.9	36.2	108.7	108.6
Average	108.7	29.82	107.6	53.5	107.9	107.3

[7] O. Zeiller, Zeits. f. Physik **96**, 121 (1935).

Part II: Time Variations

1. Barometer effect

Cosmic-ray daily means were obtained from readings taken at about 8 A.M. each day, throughout the year. Two argon-oxygen filled G-M tubes (effective area 1 cm×15 cm) were used in form of a telescope—the distance of the axes of the tubes in the vertical was 4 cm. The readings were taken from July 28, 1939, to July 31, 1940, with the exception of almost all of February.

Barometer data were taken from the publications and records of the New York Meteorological Observatory in Central Park (courtesy Mr. Morris). In order to obtain the mean barometric pressure corresponding to our 24-hour periods, the 2 P.M. and 9 P.M. data were averaged with the 7 A.M. datum of the successive day and related to the reading taken around 8 A.M.

The simple class correlation method was used for computation of the barometer coefficient and correlation coefficient (r). The barometer coefficient found was $k=-2.18$ percent of intensity per cm Hg ($r_{i,b}=-0.349$). All data were reduced to 30.00 inches Hg.

Table I may give an idea of the actual amount of this correction. This table gives the monthly means of cosmic-ray intensity uncorrected, the barometric pressure, the temperature, the cosmic-ray intensities reduced to 30.00 inches barometric pressure, and also the intensities corrected for temperature effect, as discussed in the following paragraph, reduced to 10°C (50°F).

2. Temperature effect

a. Correction with uniform coefficients.—Hourly temperature data were obtained from the Monthly Meteorological Summary of the Weather Bureau, Battery Place, New York City, through the courtesy of Dr. James H. Kimball. The daily mean temperature was computed corresponding to the 24-hour periods for which cosmic-ray intensity averages were obtained. The correlation of these averages with the mean temperatures of the same periods was thus found to be $r(i, T_d) = -0.482$ (T_d standing for daily temperature means). The temperature coefficient α_d was found to be $\alpha_d = -0.154$ percent of intensity per degree centigrade. The means for every day were then reduced to 50° Fahrenheit, resulting in the monthly means given in the table (under "Uniformly temperature-corrected intensities").

To exclude statistical fluctuations further, monthly barometer corrected means were directly correlated with the monthly temperature means. Here a much better correlation was obtained, namely $r(i, T_m) = -0.832$, but the coefficient was found to be essentially the same: $\alpha_m = -0.150$ percent of intensity per degree centigrade.

b. Correction with variable coefficients.—From the work done by Hess and collaborators in Tyrol a seasonal variation of the temperature coefficient was to be expected.[8] The fact that the temperature coefficient in turn depends upon temperature (being much smaller in summer) indicates that the air mass distribution is differently correlated with the same change of ground temperature in summer and in winter.

In order to investigate this dependency of the temperature coefficient two separate correlations were made for winter and summer. The result is given in the following table, the symbols employed being the same as before.

Summer	T°F = 73.3	$r = -0.054$	$\alpha = -0.033$ percent/°C
Winter	31.2	-0.272	-0.155 percent/°C

c. Discussion.—The absolute values of the temperature coefficient for the whole year found by us with our coincidence counter arrangement (-0.15) agrees very well with Blackett's theoretical value and with experimental values obtained with ionization chambers. The latter according to Compton and Gill[9] are small in the equatorial zone and reach a maximum of -0.25 percent per degree centigrade at latitudes beyond the "knee." In the geomagnetic latitude of New York (51°N) therefore our value seems somewhat low, but it must be remembered that at about the same geomagnetic latitude, Clay and Bruins[10] in Amsterdam found a value of -0.21 percent per degree, while on the Hafelekar (Austria) the average α for several years was about -0.1.

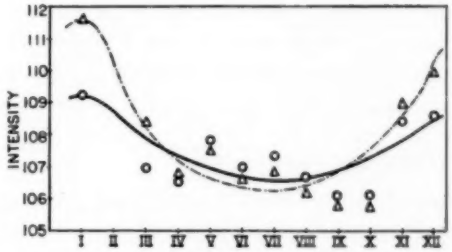

FIG. 3. Seasonal variation of cosmic-ray intensity.

The large variation of α from winter to summer found first at this station in Central Europe[8] is now fully confirmed by our measurements in New York. There is no doubt that the coefficients in the hot season are much smaller indicating that correlation between ground temperature and cosmic-ray intensity becomes almost zero.

d. Seasonal variation.—Figure 3 shows the seasonal variation of cosmic-ray intensity according to our measurements in 1939/40. The broken line corresponds to the barometer corrected values (without temperature correction) which are indicated by small triangles. The full line curve (points indicated by small circles) corresponds to the values corrected to a mean temperature (10°C), with two different coefficients of α (as mentioned in Section *b*), for the winter and summer months.

From the two curves it is quite obvious that the seasonal variation cannot be explained solely as a thermal effect although the temperature correction reduces the amplitude of the

[8] V. F. Hess, Rev. Mod. Phys. **11**, 153 (1939); Phys. Rev. **57**, 781 (1940).

[9] A. H. Compton and P. S. Gill, Rev. Mod. Phys. **11** 136 (1939); P. S. Gill, Phys. Rev. **55**, 1154 (1939).

[10] J. Clay and E. M. Bruins, Physica **6**, 628 (1939).

seasonal change from about ±2.8 to about ±1.4 percent. This is in good agreement with results of a recent analysis of the Hafelekar data by the senior author.[11]

3. The front passage effect

Loughridge and Gast[12] presented evidence of an effect of the passage of air mass fronts on cosmic-ray intensities at the point of passage.

To study the effect of front passage on our counter telescope, front data were obtained from the weather stations at LaGuardia and Newark Airports.

During the whole year, 53 cold fronts and 14 warm fronts were usable for our purposes. Of the 53 cold fronts, 29 were accompanied by an increase of cosmic-ray intensity upon passage, two showed no change and 22 showed a decrease. The changes varied between +8.5 and −7.5 counts per hour, but give on the average an increase of +0.8 percent intensity per cold front passage.

Of the 14 warm fronts 7 were accompanied by an increase and an equal number by a decrease, the latter, however, being preponderant in value. The average was −0.7 percent intensity per warm front passage. Both of the values check well with the ones obtained by Loughridge and Gast.

4. The effect of the position of barometric lows

Y. Nishina, Y. Sekido, H. Simamura and H. Arakawa[13] published a survey of cosmic-ray intensities of Tokyo according to direction and distance of that city with respect to the relative position of depressions (lows): the center of the depression is taken as the center of 5 concentric circles with radii 222, 444, 667, 889 and 1111 km, (2 degrees latitude), respectively. Diameters were drawn at intervals of 30° dividing the 4 rings in 12 sections each, but leaving the innermost circle as single whole section, thus totaling 49 sections. This scheme was applied so that one diameter coincided with the north-south direction. The same scheme was used for our New York data. The 109 positions of the depressions and their respective times were taken from the 6-hourly weather maps which were also used to obtain front passage data.

It was found that about half the lows centered about a northwesterly position, making the number of cases for the other sections rather small and subject to great statistical uncertainties. The scheme showed clearly a maximum of cosmic-ray intensity in the southwest to south-southwest and a minimum in the northeast of the center of the depression. This is in good qualitative agreement with the Japanese findings. An indication of a smaller minimum in the West seems to exist also and the negative area is slightly more extended than for Tokyo, covering even the center.

5. The magnetic storm effect

Magnetic storm data were obtained from the Magnetic Observatory of Cheltenham, Maryland which are published[14] and from a private communication of the Department of Terrestrial Magnetism, Carnegie Institution of Washington, D. C. giving the report which appears in September in the same journal. The reports give the exact time of a magnetic disturbance, i.e., its beginning, its end and its time of maximal activity, as well as the ranges of the deviation of the declination, the vertical and the horizontal intensities. However, they do not give the sign of the deviations from normal values nor the average deviation on a disturbed day which should be expected to have a closer relation to cosmic-ray intensity changes. Our numerical results, in this connection, must be taken with precaution.

The cosmic-ray intensities of the day of maximal disturbance were taken and compared with the preceding undisturbed or little disturbed day. It was found that out of 20 magnetic storms (in the course of 11 months) 16 lowered the cosmic-ray intensity and 4 increased it. In the latter 4 cases the ranges of variations of the horizontal intensity H were, however, relatively small, namely not higher than 225 gammas, whereas the ranges for the negative (lowering) cases extended up to 850 gammas. Furthermore it could be clearly seen that there was a rough proportionality between

[11] V. F. Hess, Phys. Rev. **57**, 781 (1940).
[12] D. Loughridge and P. Gast, Phys. Rev. **56**, 1169 (1939); **58**, 194A (1940).
[13] Y. Nishina, Y. Sekido, H. Simamura and H. Arakawa, Nature **145**, 703 (1940).
[14] Cheltenham Magnetic Observatory, Terr. Mag. Atmos. Elec. **44**, 400 (1939); **45**, 48 (1940); **45**, 227 (1940).

the ranges and the (negative) differences of the intensity rates of corresponding counting periods yielding a correlation coefficient of $r_{i,H}=-0.56$ and a "magnetic storm coefficient," $m=-1.97$ percent of cosmic-ray intensity per percentage range of H. The cosmic-ray intensities used for this correlation had been corrected for pressure and temperature.

Considering the fact that in our analysis not individual magnetic storm effects but rather a general mean of this effect is obtained, it is of the expected order of magnitude (-2 percent). In individual magnetic storms this effect may be -15 percent, in others almost zero.[15]

[15] S. E. Forbush, Terr. Mag. Atmos. Elec. **43**, 203 (1938). Following a suggestion of Dr. J. A. Fleming our results on day to day variations of cosmic-ray intensities were compared by Dr. S. E. Forbush with results from the Compton model C meter placed at the Observatory at Cheltenham, Maryland. It was found that variations observed at both stations over the whole 11-month period were in good agreement.

Summing up our results on time variations it has been shown that it is possible to get cosmic-ray data with sufficient accuracy over a period of one year with a very simple double coincidence counter telescope. They allow conclusions on the variation of the temperature effect during the year, on the seasonal effect, on air mass effects connected with the passage of lows or of cold and warm fronts and on the magnetic storm effects.

The authors wish to thank Dr. W. F. G. Swann for placing the facilities of the Bartol Research Foundation at their disposal. They also express their indebtedness to Dr. J. A. Fleming, Director of the Department of Terrestrial Magnetism, to Dr. James H. Kimball (New York Meteorological Observatory) and to the Meteorological Staff of the Airports in Newark and La Guardia Field, Queens, N. Y., for supplying the necessary magnetic and meteorological data.

DECEMBER 15, 1940 PHYSICAL REVIEW VOLUME 58

The Genetic Relation Between the Electronic and Mesotronic Components of Cosmic Rays Near and Above Sea Level

G. Bernardini, B. N. Cacciapuoti, B. Ferretti, O. Piccioni and G. C. Wick
Universities of Rome, Bologna and Padua, Italy

(Received May 21, 1940)

The hypothesis that the cosmic-ray electrons observed at sea level are mostly due to the disintegration of the mesotrons has been tested (a) by comparing the ratio *soft component/hard component*, found at sea level in free air, with the same ratio found at 2050 m under a dense absorbing layer; (b) by comparing the Rossi curves for small showers under the same conditions; (c) by an especially detailed study of the increase of the soft component with increasing altitude. The results indicate that the proper lifetime of the mesotron is at least four microseconds and that the soft radiation observed at sea level is not entirely due to secondary processes of the mesotron.

§1. Introduction

It is now generally believed that the mesotrons, which form the penetrating component of cosmic rays, are unstable and have a mean life of a few microseconds. The evidence bearing on this very important hypothesis is twofold. First, the instability of the mesotron easily explains the long known and puzzling fact of the anomalous absorption of the hard component in air.[1] Second, there is the evidence concerned with the secondaries ("disintegration electrons") emitted when the mesotron disintegrates.[2]

The work described in this paper is chiefly concerned with this second aspect of the problem, which seems to us to be in a far more unsettled state than is generally thought. The

[1] H. Euler and W. Heisenberg, Ergeb. d. exakt. Naturwiss. **17**, 1 (1938); see also B. Rossi, Rev. Mod. Phys. **11**, 296 (1939).

[2] The mesotron is usually identified with Yukawa's hypothetical particle which disintegrates spontaneously into an electron and a neutrino. H. Yukawa, Proc. Phys. Math. Soc. Japan **17**, 48 (1935); further literature in the papers of reference 1.

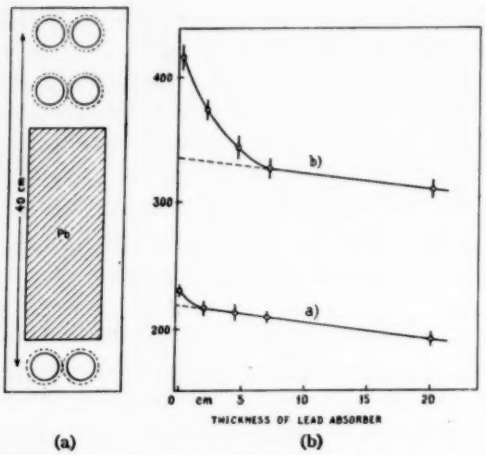

FIG. 1. (a) First arrangement of counter telescope. (b) Curve *a*, absorption curve of the vertical rays under a thick vault, equivalent to 4 or 5 m water; Curve *b*, absorption curve in open air; both curves at Rome.

striking confirmations which the instability hypothesis has received from experiments of the first kind have generated a strong confidence that the "disintegration electrons" can be found in some way. But—apart from *one* beautiful Wilson-chamber photograph obtained by Williams and Roberts[3] after the experiments here described were completed—a direct experimental confirmation of their existence is still wanting.

The evidence brought forward so far is indirect in that it is based on detailed calculations of certain delicate effects with the cascade theory of showers. Let us call E and M, respectively, the electronic and mesotronic components of cosmic rays; further, call R that part of the electronic component which is just degraded shower radiation due to electronic primaries of very high energy, I the electronic secondaries produced by the interaction of the mesotrons with the matter they traverse, and D the disintegration electrons. Thus the "R" component is independent of the mesotrons, and $E=R+I+D$. The "interaction component" I is known to be small. It may account for 20 or 25 percent of E, as given by our apparatus (see §3). The evidence mentioned above tends to prove that R is negligible at sea level, so that the main part of the soft component must be due to the disintegration electrons D. The evidence rests on three arguments: (1) Heitler's calculations[4] show that the latitude effect of the R component at sea level cannot exceed 1 percent. Therefore, *if the latitude effect of the soft component is about as large as that of the hard one* (10 percent), only a small fraction of the soft rays can be due to R; (2) the "difference curves" of Bowen, Millikan and Neher[5] follow closely the theoretical multiplication curves at great altitudes; near sea level they indicate the presence of an excess radiation which must be due to D; (3) the R component at sea level must be due to high energy primaries which are also responsible for the extended air showers and, according to Euler, for the large Hoffman bursts; from the known frequency of the large bursts Euler evaluates R at sea level and finds that it is negligible.[6]

On arguments (1) and (2) one may remark that the difference curve used in (2) must refer, of course, to the soft component alone. Thus both (1) and (2) rest essentially *on the latitude effect of the soft component at sea level*, the experimental value of which *is still uncertain, and may be quite small.* Thus it is difficult to prove a contradiction even with the extreme—and probably untrue—assumption that $D=0$, since in this case the latitude effect to be expected (taking into account the I electrons) would be 3 or 4 percent, which is not quite incompatible with the experiments.[7]

As regards argument (3), we shall come back to it in the last section. In the experiments described in this paper we have tried to follow

[3] E. J. Williams and G. E. Roberts, Nature **145**, 102 (1940).

[4] W. Heitler, Proc. Roy. Soc. **161**, 261 (1937); also L. W. Nordheim, Phys. Rev. **53**, 694 (1938).

[5] J. S. Bowen, R. A. Millikan and H. V. Neher, Phys. Rev. **52**, 80 (1937); H. J. Bhabha and W. Heitler, Proc. Roy. Soc. **159**, 432 (1937); J. F. Carlson and J. R. Oppenheimer, Phys. Rev. **51**, 220 (1937); H. Snyder, Phys. Rev. **53**, 960 (1938); R. Serber, Phys. Rev. **54**, 317 (1938).

[6] H. Euler, Zeits. f. Physik **116**, 73 (1940); we are deeply indebted to Professor Heisenberg for telling us about these results before the publication.

[7] For a discussion of the results on the latitude effect until 1938 see: T. H. Johnson, Rev. Mod. Phys. **10**, 193 (1938). More recently P. Auger, R. Grégoire, R. Maze and B. Goldschmidt, Comptes rendus **209**, 794 (1939) have found that the small showers are, if at all, much less latitude sensitive than the vertical coincidences. This may indicate that the latitude effect of the soft component is smaller than 5 percent. The same authors have also measured the latitude effect of the vertical coincidences with and without a lead shield between the counters; they do not state, however, whether a value for the latitude effect of the soft component can be safely inferred from their results. See also G. Occhialini, Comptes rendus **208**, 101 (1939).

a more direct line of attack, based on the simple theoretical prediction that the number of disintegration electrons in equilibrium with the hard rays in a dense medium should be negligible (perhaps 2 percent of the hard rays). Hence if the intensities of the soft and hard components are measured first at sea level in free air and then at a certain height above sea level under a layer of dense material having, as closely as possible, the same atomic number as air and equivalent in stopping power to the air layer between the two altitudes, one should find: (a) many more electrons in the first experiment, if the electrons present at sea level are mostly disintegration electrons, (b) the same number of electrons in both experiments, if the electrons are *not* disintegration electrons.

Measurements under conditions approaching those of the first or the second case can be found in the literature, but it is hard to judge whether a comparison is allowed. This is, perhaps, the reason why certain results of Auger[8]—who found $E/M=0.30$ under a layer of ice 4 m thick at Jungfraujoch, and again, the same value at sea level in free air—have not been regarded as a serious objection to the disintegration hypothesis. In our experiment, described in §4, the two measurements were made, of course, with the same apparatus and the conditions were as similar as was feasible.

The experiment, however, has failed to give any certain sign of the existence of the disintegration electrons; this can be understood if the R component is not entirely negligible at sea level, so that the fraction due to the D electrons becomes smaller. From the quantitative discussion we draw the conclusion (§7) that the proper lifetime of the mesotron must be at least four microseconds.

This lower limit is in contradiction with some recent careful determinations by the "anomalous absorption" method;[9] it is compatible, however, with other equally recent results by the same method.[10]

The evidence from the experiment in §4 has been extended and substantiated by a study of the Rossi curves for small showers (§5) under the same conditions as in the previous section, and by an investigation of the increase of the soft component with altitude in the immediate vicinity of sea level (§6). Previous results of Cacciapuoti[11] had already shown that the increase of the soft component is somewhat more rapid than one would expect on the hypothesis that the electrons observed near sea level are the result of the disintegration of the mesotron.

§2. Apparatus

All the measurements have been made with Geiger-Müller counters having a cylindrical brass cathode enclosed in glass and filled with an argon-alcohol mixture following the prescriptions of Trost[12] (10 percent alcohol, pressure 11 cm). The thickness of the counter walls (including the cathode) was equivalent to about 4–5 mm Al. The useful length of the counters was about 28 cm. All the counters had an

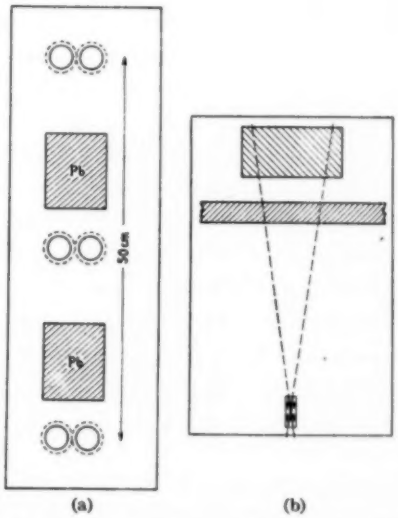

Fig. 2. (a) Second arrangement of counter telescope. (b) Position of the telescope relative to the roof and absorbing layer of earth (Cervinia 2050 m).

[8] P. Auger and L. Leprince Ringuet, *Les Rayons Cosmiques* (Actualités Scient. Hermann 340, Paris, 1936); P. Auger, L. Leprince Ringuet and P. Ehrenfest, J. de phys. et rad. **2**, 58 (1936).

[9] B. Rossi, H. van Norman Hilberry and J. Barton Hoag, Phys. Rev. **57**, 461 (1940); W. M. Nielsen, C. M. Ryerson, L. W. Nordheim and K. Z. Morgan, Phys. Rev. **57**, 158 (1940).

[10] M. Ageno, G. Bernardini, B. N. Cacciapuoti, B. Ferretti and G. C. Wick, Ricerca Scient. **10**, 1073 (1939); Phys. Rev. **57**, 945 (1940); M. A. Pomerantz, Phys. Rev. **57**, 3 (1940).

[11] B. N. Cacciapuoti, Ricerca Scient. **10**, 680 (1939).

[12] A. Trost, Zeits. f. Physik **105**, 399 (1937).

efficiency of 97 or 98 percent under working conditions.

The measurements of §3—which were already completed when the main work was planned—were made with the counter telescope shown in Fig. 1(a). Lead absorbers were inserted as shown in the figure. The pairs of neighboring counters were connected in parallel and were used as single counters.

For the later work (§§4 and 6) the geometry of the telescope was slightly improved, as shown in Fig. 2(a), but apart from this no essential change was introduced in the apparatus. In all these measurements with counter telescopes the triple coincidences between the three pairs were measured at the same time as the double coincidences between the two extreme pairs. The excess of the double over the triple coincidences was, of course, mostly due to chance coincidences, and gave a useful check on the regularity of operation of the apparatus. As a further check the number of single pulses from each counter was determined at intervals of an hour.

§3. The "Interaction" Electrons (Component *I*)

The intensity of the *I* component of the soft radiation can be determined by a measurement of the number of electrons in equilibrium with the mesotrons under a layer of dense material fulfilling the following conditions: The depth below sea level must be sufficient to make it quite certain that the degraded shower radiation is negligible; on the other hand, if the result has to be used as an indication of the *I* component in air, the depth should not be so large as to cause a great change in the spectrum of the hard component;[13] finally, the distance of the counter set from the dense layer should be large enough to prevent any effect due to the coherence of secondaries.[14]

Although such measurements have already been made several times, we thought it advisable to make a new determination. A counter telescope (Fig. 1(a)) was set vertically under the center of one of the great vaults of the Basilica di Massenzio (Rome). The minimum thickness of these vaults has been evaluated at about 4 or 5 m (water equivalent). The counters were about 30 m under the top of the vault; under these conditions we measured the absorption curve of the radiation in lead. Since the counters were mounted in a thin Al box on a rolling table, they could be removed every second hour from under the vault into free air, where the absorption curve was also taken for comparison. The results, which were reported in a preceding paper,[15] are summarized in Table I and in Fig. 1(b).

We evaluate the intensity of M by linear extrapolation from the 7 cm and 20 cm lead points to 0 cm; E is then obtained by difference from the zero lead point. In this way we get: $E/M=0.05$ under the vault; $E/M=0.25$ in free air, in accord with the results of Auger,[8] and—as regards the value in air—of many others.[16]

Under the vault, E should consist only of I electrons; the atomic number Z of the elements contained in the vault is somewhat larger than that of air. Since it is unlikely that I/M is a decreasing function of Z, we conclude that,

Table I. *Threefold coincidences per hour.*

Pb cm	0	2	4.5	7	20
Under the vault	230.8 ±4.3	218.8 ±5.8	214.0 ±6.2	211.6 ±4.3	191.6 ±5.3
In free air	413.1 ±9.6	375.7 ±9.7	343.7 ±9.9	327.3 ±8.5	316.2 ±8.4

Table II. *Threefold coincidences per hour.*

Pb cm	Cervinia (2050 m) Under 170 g/cm²	Under 7 g/cm²	Under 170 g/cm²	Under 7 g/cm²	Rome (50 m) In Free Air
0	283±6.8	405±7.9	295±7.5	383±13.8	225±4.2
5	240±4.8	286±7.5		279± 7.9	184±3.7
10	210±4.8	252±5.2	227±5.3	247± 8.9	174±3.3
20	206±5.6	240±5.8	210±5.4	244± 8.4	168±3.5

[13] W. M. Nielsen and K. Z. Morgan, Phys. Rev. **54**, 246 (1938); see also J. R. Oppenheimer, H. Snyder and R. Serber, Phys. Rev. **57**, 75 (1940).

[14] L. Jánossy, Proc. Roy. Soc. **167**, 499 (1938).

[15] G. Bernardini, B. N. Cacciapuoti and B. Ferretti, Ricerca Scient. **10**, 731 (1939). Since this experiment plays an essential role in the final discussion (§7) we have asked Drs. Santangelo and Scrocco to repeat the experiment with a slightly different apparatus in a wide gallery, 6 m high, 5 m wide, under a limestone layer equivalent to about 10 m of water. They have found $E/M \approx 0.05$. (To appear shortly in the Ricerca Scient.)

[16] B. Rossi, Zeits. f. Physik **82**, 151 (1933); P. Auger, *Kernphysik* (Springer, Berlin, 1936); R. H. Woodward and J. C. Street, Phys. Rev. **49**, 198 (1936).

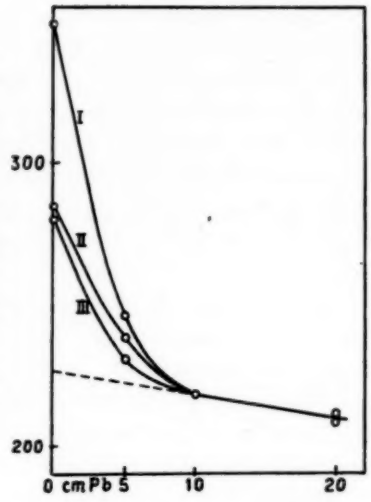

FIG. 3. Comparison between the absorption curves for vertical rays. Curve I, at Cervinia (2050 m) under a thin roof; Curve II, at Cervinia under an absorbing layer 170 g/cm² thick; Curve III, at Rome (50 m) in open air (under 0.5 mm Al). Curves I and II have been multiplied by suitable factors so as to make the points at 10 cm of lead coincide.

also in air, I/M cannot be larger than about 5 percent of M, or about 20 percent of the total electronic radiation measured by our apparatus in free air.

§4. The Disintegration Electrons (Component D)

We now come to the experiment whose principle was laid down in the introduction.[17] A counter telescope (Fig. 2(a)) was brought to Cervinia (2050 m) and placed vertically in a large room 4.2 m high. The concrete roof of the room was covered with a layer of earth 6×2 m broad, 1 m high weighing 1.3 tons/m². The underlying part of the roof had a weight of about 0.4 ton/m² so that the total mass above the counters was 170 g/cm². The general arrangement is shown in Fig. 2(b). The absorbing layer could be considered as roughly equivalent in absorbing power to the air layer between 0 and 2050 m altitude. It was, in fact, somewhat less than equivalent in g/cm², but account must be taken also of the slightly greater atomic number of the material ($Z=10$ or 12). The electronic component under that layer can, therefore, be compared with that present at sea level, in the sense that has been previously explained.

Under these conditions we measured the absorption curve of the vertical rays in lead, together with the absorption curve in lead under a thin wooden roof of about 7 g/cm² thickness, the two measurements being made in four alternative runs, the results of which are given in the columns 2 to 5 in Table II.

The data for the absorption curve in free air near sea level (Rome), with the same apparatus, are given in the sixth column; during this measurement the apparatus was enclosed in a thin aluminum box (0.5 mm thick).

These results are also represented in Fig. 3. The intensity of the hard component has been extrapolated linearly, as before, from the 10- and 20-cm lead points, and the soft component has been obtained by difference from the zero lead point as before. One finds:

(a) at Cervinia under a 170 g/cm² layer $E/M=0.27\pm0.03$
(b) at Cervinia under a 7 g/cm² layer $E/M=0.56\pm0.03$
(c) at Rome under practically 0 layer $E/M=0.27\pm0.03$

As stated previously, the intensity of the D electrons should be negligible under the thick layer; I is not greater than 0.05 M. Hence, we should expect the value (*a*) to be considerably smaller than (*c*). So the rather large number of electrons found in case (*a*) is puzzling; it must be largely due to electrons which are *not* secondaries of the mesotron, and which are able to make themselves felt through the thick layer. Hence, also, at sea level a considerable fraction of the soft component must be due to the degraded shower radiation R (discussion in §7).

§5. The Rossi Curve

The results just described are in harmony with those of Auger and his collaborators,[8] but they are a little difficult to reconcile with the instability hypothesis. We have, therefore, sought an independent check in the study of the transition curve for small showers at Cervinia under a layer of concrete and bricks of about 175 g/cm²[18] and for comparison at Rome in free air in a thin aluminum box (0.5 mm thick) and within the Physical Institute of the University under 35 g/cm² of concrete. At great depths, where the soft rays are certainly in equilibrium with the hard component, the Rossi curve exhibits only a rapid increase unto saturation without any marked maximum; it was, therefore, of interest to see whether the Rossi curve under the thick

[17] Preliminary reports have been published—Ricerca Scient. **10**, 809 (1939) and **10**, 1010 (1939).

[18] For certain reasons these measurements could not be made exactly at the same place as those of §4; the absorbing layer, however, was roughly equivalent.

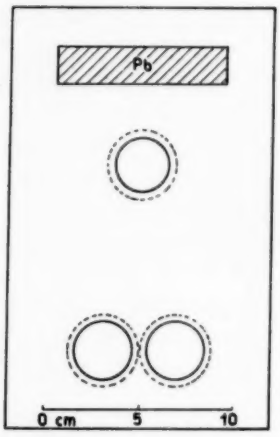

FIG. 4. Arrangement of coincidence set of three counters.

layer of Cervinia would exhibit the ordinary maximum or not.

The measurements were made with a coincidence set of three counters (Fig. 4) having a useful length of 27 cm and very similar to the counters used in the previous work. Lead plates were placed on the apparatus as shown in the figure. The arrangement is far from ideal: It has a strong bias for very small showers, and so the maximum of the Rossi curve is not so high as with other arrangements; the maximum occurs at a lead thickness somewhat smaller than the ordinary one, which is also understandable. The arrangement was chosen merely because of the high rate of counting, which was a great advantage, owing to the short time available at Cervinia. The results are given in Table III and Fig. 5(a).[19]

Thus even under the dense layer there is a pronounced maximum followed by a marked decrement which strongly indicates the existence of an electronic component which is not yet in equilibrium with the mesotrons, thus confirming our previous conclusions.

There is, nevertheless, a certain difference between the three curves of Fig. 5(a), which requires some comment. The maximum for the free air curve is considerably higher than in the two other curves. The interpretation of this fact is not unique; it may be due to the fact that the electrons observed under a layer of concrete are more degraded than the electrons in air (the mean atomic number of the medium is higher than that of air, and so the critical energy of shower theory is lower; the height of the maximum is quite sensitive to a change in the ratio *electron energy/critical energy* as is shown by the fact that the maximum is 10 times as large under lead as under aluminum). It might also be interpreted as an indication of the presence of disintegration electrons in air. In view of the results of §4, the first interpretation seems more likely.

At any rate it must be strongly emphasized, that the marked decrease after the maximum, observed at Cervinia under the thick layer, cannot be simply due to a transition effect from concrete to lead. In order to secure this point, the measurements have been extended recently to greater depths below sea level.[20] The measurements were made in the Physical Institute in Rome, under concrete layers of 35, 100 and 160 g/cm², respectively. The apparatus was always kept at a distance from the ceiling comparable to that in Cervinia. The result is given by the three curves of Fig. 5(b). Curve 3° shows clearly that, with our apparatus at least, no transition effect can explain the shape of the curve found in Cervinia. The comparison of the two curves, measured under comparable thicknesses of dense matter, namely curve 3° of Fig. 5(a) and curve 3° of Fig. 5(b) is very striking and lends strong support to our previous conclusions.

§6. INCREASE OF THE SOFT COMPONENT WITH HEIGHT

The curve of the logarithmic intensity of the vertical rays (electrons+mesotrons) as a function of depth below the top of the atmosphere shows a definite change of slope just above sea

TABLE III. *Frequency of showers (per hour).*

Pb cm	Cervinia (2050 m) Under 175 g/cm²	Rome (50 m) Under 35 g/cm²	Rome (50 m) In Free Air
0	23.0±1.4	20.6±1.1	17.6±0.8
4		38.0±2.3	51.6±1.6
8	42.7±2.7	45.6±1.7	66.6±1.6
12	41.8±2	46.5±1.6	72.8±1.6
16	41.4±2.2	48.2±2.6	71.3±2.2
28	36.1±2		51.8±1.8
50	29.9±1.8	29.3±1.6	37.9±1.9
100	25.8±1.5	24.8±1.5	24.7±1.6

[19] See also G. Bernardini, B. N. Cacciapuoti, Ricerca Scient. **10**, 933 (1939).

[20] We wish to thank Dr. G. Palmieri for her valuable collaboration in these measurements.

level (Pfotzer[21]). The same holds, of course, for the experiments with ionization chambers, but we prefer here to think of the vertical rays only. The change of slope indicates the increasing importance of the hard component.

For our problem it would be of interest to see whether *the curve for the soft component alone* exhibits a similar bend. It is certain that at 3500 m there is still some degraded shower radiation. If the electrons at sea level were entirely due to secondary processes of the mesotron, then the bend should occur between 3500 m and sea level and should be detectable by a sufficiently detailed study in this region.

Some preliminary results of Cacciapuoti have been extended[11] and the results are presented here. Previous measurements by others were chiefly concerned with higher altitudes; in experiments near sea level only two rather distant points (as, for instance, 0 and 3500 m) had been compared, as far as we know. We have aimed at a greater detail and accuracy, using also the intensity of the hard component as a check on the consistency of the results as will be presently shown. By means of the counter telescope (Fig. 2(a)) several absorption curves of the vertical rays in lead have been determined at Rome (50 m), Antey (1050 m), Cervinia (2050 m) and Pian Rosà (3460 m). The different thicknesses of lead were interchanged at intervals of an hour. At Rome the measurements were made in an aluminum box, with 1 mm thick walls; at Antey and Cervinia under a thin roof (about 3 g/cm² thick), at Pian Rosà within a wooden hut. The triple coincidences measured, together with the statistical standard errors are given in Table IV.

We shall assume that these coincidences represent single particles going through the counter telescope; actually two corrections should be made, one for air showers and one for a slight change of efficiency of the apparatus at the greater altitudes, due to the greater number of single pulses in each counter; it was found[22] that the two corrections were both small and nearly canceled each other.

By means of Table IV we can compare the

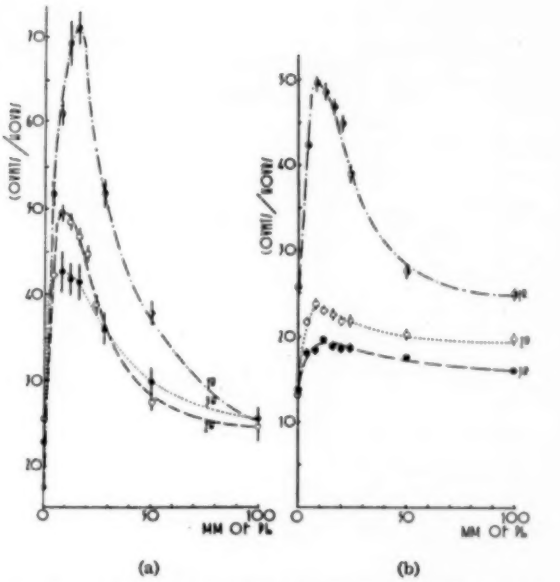

FIG. 5. (a) Rossi curves for small showers at Cervinia (2050 m) and Rome (50 m). 1°—Rossi curve at Rome, open air (under 0.5 mm Al); 2°—Rossi curve at Rome under a layer of concrete 35 g/cm² thick; 3°—Rossi curve at Cervinia under a layer 175 g/cm² thick. (b) Rossi curves at Rome (50 m) under various absorbing layers. 1°—Concrete layer 35 g/cm² thick (same curve as 2° of (*a*)); 2°—Concrete layer 100 g/cm² thick; 3°—Concrete layer 160 g/cm² thick.

intensity *versus* altitude curves of the soft and hard components. In order to get an idea of the effect on the final result of the somewhat arbitrary assumptions which must be made in the separation of the total intensity into the contributions due to the two components, we have examined several assumptions (Fig. 6).

As regards the hard component M, we have drawn two intensity *vs.* altitude curves (the two upper curves in the figure), assuming that M is proportional to the radiation, M', filtered by 10 cm of lead, or alternatively to the radiation M'' filtered by 20 cm of lead. The two curves are sufficiently smooth—an indication of the constancy of the apparatus during the measurements—and consistent with each other.[23] They are also in accord with the well-known absorption anomaly in air; this is shown by the full dots, which are the points of the curve for M'', shifted to lower altitudes corresponding to a change in pressure by 70 g/cm², the mass of air

[21] G. Pfotzer, Zeits. f. Physik **102**, 41 (1936).

[22] For the method used in evaluating the corrections see our paper of reference 10.

[23] The two points at 3460 m are not very satisfactory, however; the quite large absorption between 10 and 20 cm of lead is puzzling; we hope to investigate this point in greater detail.

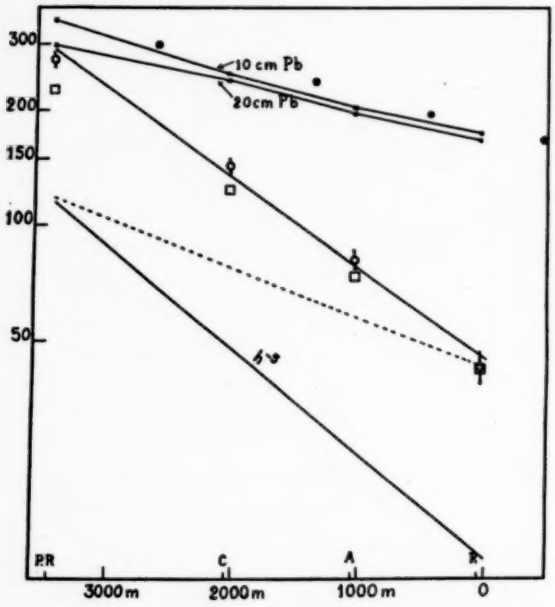

FIG. 6. Law of increase with height of the various components of cosmic rays (vertical intensity). The abscissae give the height above sea level. The points marked *P.R.*, *C*, *A* and *R* correspond to Pian Rosà, Cervinia, Antey and Rome, respectively. The intensities (log scale) are coincidences per hour. The two upper curves give the intensity of the hard component, filtered by 10 and 20 cm of lead, respectively. The anomalous absorption of the hard component in air is exhibited by the black dots as explained in the text. The open circles and the square dots give the intensity of the soft component evaluated in two different ways. The dotted line gives the number of electronic secondaries due to the disintegration of the mesotron, to be expected if the proper lifetime of the mesotron is 2 microseconds. The straight line marked h^{-2} represents for comparison the law of increase of small showers found by Regener and Ehmert[27] between 350 and 760 mm Hg.

which should be equivalent in stopping power to $20-10=10$ cm of lead, if there were no anomaly.[10] The full dots lie consistently higher than the curve for M', as one should expect if the absorption in air is anomalously large.

As regards the soft component E, we have first assumed E to be proportional to the difference between the total intensity and the intensity of the radiation filtered by 5 cm of lead, as given by the second and third columns, respectively, (Table IV). The result is represented by the square dots in Fig. 6. Strictly speaking, the quantity which must be subtracted from the total intensity is the intensity M_0 of the hard component extrapolated to zero lead thickness. Assuming a constant absorption coefficient $\mu=0.005$ cm^{-1} for the hard component in lead, we may evaluate M_0 from the data of the fourth or alternatively the fifth column of Table IV ($M_0=1.05\ M'$ or alternatively $=1.10\ M''$). Taking the arithmetical mean of the two values thus obtained and subtracting from the total intensity we get the E values corresponding to the open circles in Fig. 6. (The errors indicated are purely *statistical* and do not include, therefore, the (probably larger) uncertainties involved in the procedure of extrapolation.)

Now, looking at Fig. 6, we do not see any evidence of a bend in the curve for the soft radiation. Unfortunately the accuracy of the E values is rather poor and a small bend could well escape our notice. Nevertheless it is nearly certain—especially in view of the similar result previously obtained by Cacciapuoti[11]—that the slope of the E curve *at sea level* is definitely larger than the slope of the M curve, and also larger than the slope to be expected for the D electrons. These are given in the figure by the dotted line.

Thus the results of this section also lend some support to the conclusion that *the soft radiation observed at sea level is not entirely due to secondary processes of the mesotron.*

§7. DISCUSSION

Euler and Heisenberg[1] have given a widely used formula for the number D of disintegration electrons in equilibrium with the mesotronic component M

$$D/M=-\frac{9}{8}\frac{X_0 mc}{E_0\tau_0}, \qquad (1)$$

neglecting a small term, unimportant in air. Here m is the mass of the mesotron, E_0 and X_0 are, respectively, the critical energy and the unit length of shower theory (in the Bhabha-Heitler form). In this theory the energy loss per cm path due to ionization is: $a=\ln 2\cdot E_0/X_0$

TABLE IV. *Threefold coincidences per hour, for various absorber thicknesses.*

ALTITUDE	0 CM PB	5 CM PB	10 CM PB	20 CM PB
3460 m	620 ±13	391.5±7.7	348±6	300 ±6
2050 m	407 ± 6.7	283 ±5.4	251±4.4	241.5±4.8
1050 m	297 ± 6	224 ±5	205±4.5	196 ±4.2
50 m	224.5± 4.2	184 ±3.7	174±3.2	168 ±3.5

so that the above formula becomes

$$D/M=0.78\frac{mc}{a\tau_0}. \qquad (1a)$$

Using a simple idea of Williams,[24] we may show that these formulae probably give a somewhat exaggerated value for the ratio D/M. As is well known, the probability of disintegration dw of a mesotron of momentum p in the path dx is $dw=(m/p\tau_0)dx$. The disintegration electron gets, on the average, half the mesotron energy, that is $\frac{1}{2}cp$ (assuming $p\gg mc$). As Williams points out, the total electron path in the shower initiated by the disintegration electron can be evaluated without a detailed knowledge of the multiplication mechanism, since the whole energy must be finally dissipated by ionization, assuming a constant energy loss per cm path: a, the total electron path in the shower must be given by $cp/2a$. From this it easily follows that the ratio D/M is:

$$D/M=\tfrac{1}{2}mc/a\tau_0, \qquad (2)$$

which is about 0.64 times the value given by (1) and (1(a)).

Williams' assumption of a constant ionization loss is admittedly rough, but in the detailed shower theory even cruder assumptions have to be made. Actually formula (2) should, rather, give an upper limit, since it includes the total electronic path, while a counter telescope only counts electrons from a certain energy upwards. This correction is probably quite large; on the other hand, in deriving (2), we have neglected the fact that the D electrons belong to showers started at a greater altitude, let us say 3 or 4 units X_0 (that is roughly the distance after which a shower reaches its maximum size) above the place where D and M are measured. This means that the evaluation has to be raised by 10 or 20 percent. Taking the two corrections together, we still think that (2) should represent an upper limit.

Because of the fact that the energy loss a is proportional to pressure, the ratio (2) must slowly increase with increasing altitude, as already remarked by Euler and Heisenberg. Thus the dotted line of Fig. 6 has a slightly greater slope than the curve for the hard component.

Let us now consider the results of §§3 and 4 more closely. The experiment of §3 is important in that it shows that the large number of electrons found at Cervinia under the dense layer cannot be simply due to a large increase of the I component in clay as compared to air (due to the difference in atomic number). We shall assume that I is always of the order of 5 percent of M. As already stated, we take the data at Cervinia under the dense layer (§4) as a measure of the number $I+R$ of "interaction"+"degraded shower radiation" electrons which one should find at sea level in open air. Then we find (referring all intensities to $M=100$):

$$I+R \quad =27\pm3$$
$$I+R+D=27\pm3,$$

so that:

$$D=0\pm4.2 \quad \text{or:} \quad D<10 \qquad (3)$$

as a statistically safe upper limit.

If we accept the upper limit (3), then a lower limit to the proper lifetime of the mesotron ensues (Eq. (2)):

$$mc/a\tau_0<1/5.$$

If we take $a=3000$ ev/cm, $mc^2=80$ Mev we finally get:

$$\tau_0>4.4\times10^{-6}\text{ sec.} \qquad (4)$$

In Eqs. (3) and (4) we have so far considered the statistical errors only. The most dangerous source of errors, however, may lie in coherence and other geometrical effects. Auger and Grivet have found,[25] for instance, that the apparent intensity of the soft component (that is the absorption by the first 5 or 10 cm of lead) is much increased if one of the counters is protected by lateral screens.

It is not entirely clear whether one is justified in taking the values obtained in this way as a true measure of the soft component; at any rate, the experiment shows how strongly results can be affected by such factors. We incline to the view, however, that the use of lateral screens in

[24] E. J. Williams, Proc. Roy. Soc. **172**, 194 (1939); an evaluation on very similar lines of the *ionization* due to the disintegration secondaries has been recently published by B. Rossi, Phys. Rev. **57**, 469 (1940).

[25] P. Auger and T. Grivet, Rev. Mod. Phys. **11**, 232 (1939).

such experiments can introduce disturbing secondary effects (like the creation of showers in the shield by rays which pass through the two upper counters and miss the lower one).

Until such problems are clarified by further experiments, we shall accept the lower limit (4) with great caution, especially in view of the low values for τ_0 obtained by some authors.[9] On the other hand, the recent discovery by Fermi[26] of an effect of density on ionization losses should mean that the older evaluation of τ_0 by Euler and Heisenberg[1] must be increased well above three microseconds.

Let us now examine to what extent conclusion (3) is compatible with Euler's argument (see §1). Euler shows that the spectrum of the primary rays probably follows a power law with an exponent $y=1.8\pm0.17$; then, assuming $y=1.8$, he shows that the intensity of R at sea level is only $\frac{1}{5}$ of the electronic radiation observed. Now from (3) we see that only 37 percent of the electrons, at most, can be due to D, and only about 60 percent can be secondaries of the mesotron at all $(I+D)$. So R is at least 40 percent of the observed radiation. The discrepancy from Euler is only a factor 2, which is compatible with the uncertainty of the exponent y as given by Euler.

As Professor Heisenberg has kindly pointed out to us, however, the value of y not only determines the value of R at sea level, but also —and perhaps more accurately—the slope of the intensity *vs.* altitude curve. From Serber's table[5] we find

	$y=1.6$	1.7	1.8
$-\frac{1}{R}\frac{dR}{dh}=$	0.397	0.435	0.470,

where h, the depth below the top of the atmosphere, is measured in units of shower theory ($h=25$ corresponds to sea level). According to our measurements (Fig. 6) the soft component in the vicinity of sea level may well increase according to the law $E\sim h^{-5}$ found by Regener and Ehmert[27] for the small showers. Component I must increase like the hard component M and component D like M/h, according to (2). Thus we find, at sea level,

$$-\frac{h}{I}\frac{dI}{dh}=1.3, \quad -\frac{h}{D}\frac{dD}{dh}=2.3, \quad -\frac{h}{E}\frac{dE}{dh}=5.$$

Assuming the percentage of I as known (20 percent) the percentages of D and R are then determined. One finds that R/E takes the values 0.38, 0.34, 0.31 according as $y=1.6$, 1.7 or 1.8. This evaluation is admittedly rough because of the low accuracy of the slope for the E curve, but it shows at least that there is *no very serious discrepancy* between our conclusions and Euler's work. The slope for the E curve might be smaller than $5/h$ and then R would become negligible. On the other hand it is hardly likely that the slope is *larger* than $5/h$. Hence the above evaluation might be used to show that the percentage of the electronic radiation due to the R electrons cannot exceed 40 percent.

We wish, finally, to mention an evaluation of τ_0 by Pomerantz,[10] on lines somewhat similar to ours. He evaluates $I/M=0.05$ in air, in accord with our value. He then finds that the ratio E/M is 0.19 and concludes, neglecting the degraded shower radiation altogether, that D/M is 0.14. From this ratio, and by means of Eq. (1), he then deduces the value $\tau_0=6$ microseconds. Although this value of τ_0 is in agreement with our conclusions, some differences must be pointed out. If, instead of (1), we use formula (2) we get, from $D/M=0.14$, a value $\tau_0=3.2$ microseconds (which, by the way, is in better accord with the other values found by Pomerantz by a different method). Moreover, the rather low number of soft rays found by Pomerantz illustrates once more how sensitive such measurements are on the apparatus. If we had treated our value $E/M=0.27$ in the same manner as Pomerantz, that is, neglecting the shower radiation altogether, we would have found 2 microseconds.

The investigations described in this paper have been made possible by a generous grant from the "Consiglio Nazionale delle Ricerche—Comitato per la Geofisica."

Thanks are due also to the Società Anonima Cervinia for several facilities.

[26] E. Fermi, Phys. Rev. **57**, 485 (1940).
[27] E. Regener and A. Ehmert, Zeits. f. Physik **111**, 501 (1939).

A Study of the Production and Absorption of Mesotrons in the Substratosphere

MARCEL SCHEIN, E. O. WOLLAN AND GERHART GROETZINGER
Ryerson Physical Laboratory, University of Chicago, Chicago, Illinois
(Received October 28, 1940)

In a coincidence-counter experiment carried out in an airplane at altitudes up to 9.3 km (22.9 cm Hg) an attempt was made to observe the production of mesotrons in an 8-cm lead block by some non-ionizing radiation other than photons. From our results it would seem that the number of mesotrons so created is not greater than about five percent of the total number of mesotrons at this altitude. The experiment was also designed to give the absorption of mesotrons in lead of 19-cm and 27-cm thickness as a function of the altitude. From these data and from those obtained previously for 10 cm of lead we have constructed an energy spectrum of the mesotrons at an altitude of 6.7 km. At this altitude about 33 percent of all the mesotrons have energies below 5.2×10^8 ev while at sea level a very small fraction of the mesotrons have energies in this range. This is in accord with the finding of many slow mesotrons in the cloud-chamber experiments of Herzog and Bostick at these altitudes.

PREVIOUS experiments[1] indicate that mesotrons can be produced in high altitudes by a non-ionizing radiation. To identify, if possible, this non-ionizing radiation we have carried out some experiments in an airplane in which, for the producing layer, a larger thickness of lead was used than previously. Furthermore, a lead block of 6-cm thickness was placed above the whole counter apparatus to eliminate photons as possible agents producing mesotrons.

The arrangement of the apparatus is shown in Fig. 1. The Geiger-Mueller counters 1 and 5 were 5.1 cm in diameter and had an effective length of 40 cm. The counters 2, 3 and 4 were 2.5 cm in diameter and had an effective length of 20 cm. The counter tubes were filled with a mixture of argon and petroleum ether, and were of the self-quenching type. The efficiency of each individual tube was very close to 1.

Counters 1, 2, 3 and 4 constituted one fourfold coincidence set and counters 2, 3, 4 and 5 constituted another. The solid angle of the top fourfold counter set was just covered by the bottom counter and likewise the solid angle of the bottom fourfold set was just covered by the top counter. The whole solid angle was filled with lead.

Each of the two coincidence circuits had a resolving power of 3×10^{-5} second which was directly determined with a cathode-ray oscilloscope.

In the first flight a circuit was used similar to that described by Schein, Jesse and Wollan[1] except that the resistances in the grid and the plate circuit of the first stage of amplification were reduced to 10^5 ohms. In the second flight a modified multivibrator circuit was used.[2] The coincidence counts of the two fourfold sets were separately recorded on a rotating film in the same way as by Schein, Jesse and Wollan.[1]

On account of the high resolving power of the coincidence circuits (3×10^{-5} second) the number of fourfold accidentals was negligible even at 9.3 km (highest altitude reached). Because of the rapid increase of the soft component of cosmic rays with altitude, the single counting rate of the individual Geiger-Mueller tube becomes very great. This will result in a decreased efficiency in recording coincidences unless the time constant of the tubes is sufficiently short. The time constant of each counter tube was determined with the cathode-ray oscilloscope and found to be 2×10^{-5} sec. which is sufficiently short that no change in efficiency greater than one percent could be expected.

The apparatus was arranged to record: (a) the number of penetrating ionizing particles which pass through all five counters; (b) those which pass through the top fourfold set and do not pass through counter 5 because they are either stopped or are scattered out in the bottom 8 cm of lead; (c) those cases in which an ionizing particle passes through the lower four counters 2, 3, 4

[1] M. Schein and V. C. Wilson, Rev. Mod. Phys. **11**, 292 (1939); M. Schein, W. P. Jesse and E. O. Wollan, Phys. Rev. **57**, 874 (1940).

[2] A description of this circuit will be published in a paper of G. Groetzinger in the Rev. Sci. Inst.

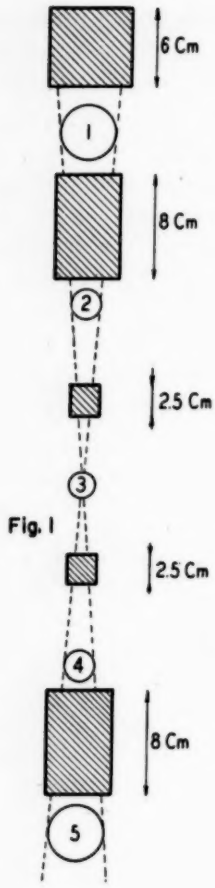

Fig. 1

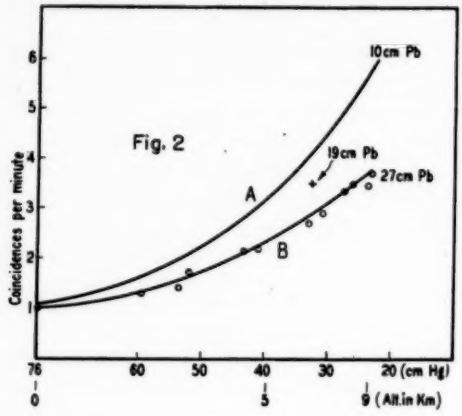

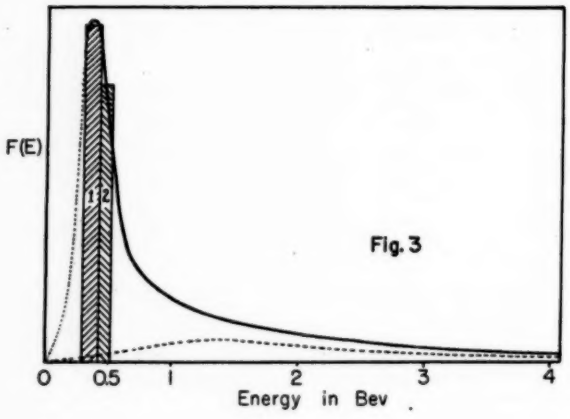

FIG. 1. Arrangement of counters.
FIG. 2. Mesotron intensity as a function of altitude for two different lead thicknesses.
FIG. 3. Energy spectrum of mesotrons. Solid curve at about 6.7 km altitude, dashed curve at sea level.

and 5 without being accompanied by an ionizing particle through the upper counter.

Except for the effect of scattering of mesotrons by the upper 8-cm lead block into the bottom set without hitting the top counter, (c) gives a measure of the production of mesotrons in the upper 8-cm lead block by a non-ionizing radiation.

The 6-cm lead block was placed above the upper counter tube to eliminate photons as possible agents in producing excess mesotrons in the upper 8-cm lead block. The probability is small that a photon after passing through 6 cm of lead would emerge without being accompanied by an electron which would set off the top counter and hence have the same effect as an ionizing particle. Therefore any non-ionizing radiation which does not cause a discharge of counter 1 (not accompanied by electrons) and produces mesotrons in the upper 8-cm lead block must be of a more penetrating type such as neutrons, neutrettos, or neutrinos.

Two flights were made. The first on December 17, 1939, the second on April 30, 1940. In the first flight the minimum pressure reached was 25.7 cm of mercury (8.2 km); in the second, 22.9 cm of mercury (9.3 km). The pressure was recorded with the same type of barometer as used by Jesse[3] in the balloon experiments.

THE PRODUCTION OF MESOTRONS

To determine whether or not there was a measurable production of mesotrons in the upper 8-cm lead block we compared the number of fourfold coincidences in the top and bottom counter set. Using the data from the second flight on December 17, in the altitude range between 5.2 km and 7.4 km[4] we obtained the following

[3] W. P. Jesse, Phys. Rev. **58**, 281 (1940).
[4] Because of the failure of the top counter tube we have data for both fourfold sets only up to 7.4 km and above the altitude we have complete data only for the lower fourfold set.

results. The number of fourfold coincidences in the *upper* counter set not accompanied by a simultaneous coincidence in the lower set was found to be 22 ± 3 percent of the cases in which a simultaneous coincidence occurred in both sets (fivefold coincidence). The number of fourfold coincidences in the *lower* set not accompanied by a fivefold was found to be *9.7±3 percent*. This excess of *12 percent* in the upper set must then have been due to the stopping of mesotrons which had insufficient energy to traverse the lower 8-cm lead block.

At sea level we found that *8.1±2 percent* of the number of fourfold coincidences in the bottom set were unaccompanied by fivefold coincidences and within experimental error the same value was found for the top fourfold coincidence set. This shows that the excess in the bottom set is within statistical accuracy the same at sea level as at altitudes between 5.2 and 7.4 km.

The 8-cm lead block between counter 1 and 2, which constituted our producing layer, is four times as large as that used in the experiments of Schein, Jesse and Wollan,[1] in which mesotrons produced by a non-ionizing radiation (of any type) constituted about 15 percent of the vertical mesotron intensity at 7.5 km altitude. Since in the present experiment no effect of this type larger than about five percent was observed, the evidence is in favor of photons as the main agent responsible for the observed production of mesotrons.

Even if neutrons are capable of producing mesotrons, their energy would have to be greater than 2.9×10^8 ev (the minimum energy which would enable a mesotron to penetrate the 13 cm of lead in our lower fourfold counter set). According to Bethe, Korff and Placzek,[5] the large number of neutrons observed at high altitudes by Korff[6] can be accounted for if they are produced with an initial energy of about 30×10^6 ev, which would rule them out as a mesotron-producing agent.

An independent test for the presence of neutrons of high energy was made in the flight on April 30, by placing a block of paraffin of 35-cm thickness above the apparatus. If neutrons of high energy were present in any abundance one would expect that protons would be ejected with sufficient energy to penetrate our counter train and thus give rise to an increase in the counting rate of the coincidence sets. If the cross section for the scattering of neutrons by protons (3×10^{-23} cm^2)[7] which is known up to about 5×10^6 ev energy is taken to be approximately valid for high energy neutrons it can be shown that in this thickness of paraffin the probability of ejecting a proton by a neutron is practically unity. Since we observed with the paraffin no change in the coincidence counting rate within the experimental error of *4 percent* we can conclude that high energy neutrons are not present in altitudes up to 9.3 km to the extent of more than about *4 percent* of our observed mesotron intensity.

Intensity of mesotrons

In Fig. 2 are shown curves for the variation of the intensity of mesotrons as a function of the pressure down to 23.0 cm Hg. Curve *B* represents the data from the two airplane flights for the lower fourfold coincidence set. One can see from Fig. 1 that there were 13 cm of lead between the counters and 14 cm above the counters which gives a total lead thickness of 27 cm. For comparison of the intensity for different thicknesses of lead we have made use of the recent unpublished balloon measurements of Schein, Jesse and Wollan for 10 cm of lead between the counter tubes. These data are plotted as curve *A*.

Because curves *A* and *B* are obtained with two different sets of apparatus it was necessary to make a comparison of the counting rate of both sets at sea level. Nielsen and Morgan and others[8] have made absorption measurements of mesotrons in different thicknesses of lead at sea level. Since in these experiments the lead was placed between the counters, it may be objected that a small part of the effect is due to scattering of mesotrons. However, this would constitute a second-order effect so far as we are here concerned. Making a small correction for scattering we have taken 5 percent as a difference of the

[5] H. A. Bethe, S. A. Korff and G. Placzek, Phys. Rev. **57**, 573 (1940).
[6] S. A. Korff, Rev. Mod. Phys. **11**, 211 (1939).
[7] H. A. Bethe, Rev. Mod. Phys. **9**, 69 (1937).
[8] W. M. Nielsen and K. Z. Morgan, Phys. Rev. **54**, 245 (1938); P. Auger, L. Leprince-Ringuet and P. Ehrenfest, Jr., J. de phys. et rad. **7**, 58 (1936); B. Rossi, *La Radiation Cosmique* (Hermann, Paris, 1930).

number of mesotrons passing through 10 cm and those passing through 27 cm of lead at sea level.

The large difference in the ordinates of curves A and B in higher altitudes as shown in Fig. 2 can be affected only slightly by scattering of the mesotrons since 14 cm out of the 17 cm of lead (which represents the difference in the thicknesses for the two cases) was placed above the counters. Hence this difference must be ascribed to mesotrons which are stopped in the additional 17 cm of lead.

If we take this loss as entirely due to ionization, which must be very nearly the case for mesotrons, we can get some idea of the energy distribution of the mesotrons at these altitudes. Taking the ionization loss as 1.4×10^7 ev per cm of lead[9] and adding twice the rest mass of the mesotron (7.5×10^7) in units of ev we obtain 2.9×10^8 ev as the energy which a mesotron must have to traverse 10 cm of lead and 5.2×10^8 ev to traverse 27 cm of lead. The difference between the ordinates of the two curves represent those mesotrons which have energies between these two values. We see that for the maximum altitude reached (9.3 km) about $\frac{1}{3}$ of the measured number of mesotrons have energies in this interval.

When the data for the counting rate in the upper fourfold coincidence set are considered in comparison with that for the lower fourfold set we obtain a measure of the number of those mesotrons which can traverse the upper 19 cm of lead but are not able to traverse the total of 27 cm and thus be recorded in the lower set. This represents the number of those mesotrons which have energies lying between 4.2×10^8 ev and 5.2×10^8 ev. We have not represented these data in the form of a curve since the total number of counts which we obtained with the upper set was considerably less than that with the lower set. Taking all the data between 5.2 and 7.4 km we obtain a point for the number of mesotrons stopped in the lower 8 cm of lead at an average altitude of about 6.7 km which is represented by a cross in Fig. 2.

The high energy part of the mesotron spectrum, i.e., mesotrons of energies greater than about 5×10^9 ev will be practically the same at 6.7 km altitude as at sea level, since the change in energy by ionization and decay for these energies is very small between these altitudes. At sea level the number of mesotrons above 5×10^9 ev represents about 10 percent of the total mesotron intensity.[10] Since at 6.7 km the total mesotron intensity is increased by a factor of 4 over the sea level value, the mesotrons with energies above 5×10^9 ev at this altitude now represent only 2.5 percent of those present.

In Fig. 3 we have represented by the two blocks the number of mesotrons $F(E)dE$ in the above-mentioned energy intervals. The area under block 1 represents 18 percent and that under block 2 represents 12 percent of the total number of mesotrons with energies greater than 2.9×10^8 ev (energy required to traverse 10 cm of lead). Making use of the fact that 2.5 percent of the mesotrons have energies above 5×10^9 ev we have represented the energy spectrum as a solid line, the area under which is 97.5 percent in the energy interval of 2.9×10^8 ev to 5×10^9 ev. The low energy part of the spectrum, i.e., below 2.9×10^8 ev has been indicated by the dotted line as containing an area of about 10 percent of the total. This estimate has been taken from the cloud-chamber data of Herzog.[11]

For comparison with the mesotron spectrum at sea level we have included as the dashed curve the data of previous investigations.[12] This dashed curve has been drawn to have an area of 25 percent of that of the solid curve corresponding to the ratio of 4 : 1 in the mesotron intensities at 6.7 km altitude (curve A, Fig. 2) and sea level. Without any claim for accuracy concerning the shape of the energy spectrum of the mesotrons at 6.7 km altitude it is nevertheless obvious that the maximum of the spectrum is shifted to a much lower energy than that at sea level and also that many of these slow mesotrons are absorbed before reaching sea level. From Fig. 6 of the paper of Schein, Jesse and Wollan[1] we see that the absorption coefficient of mesotrons remains almost constant above an altitude of 6 km. Hence, it is to be expected that the mesotron spectrum in the low energy range between

[9] J. G. Wilson, Proc. Roy. Soc. **A172**, 517 (1939).

[10] D. J. Hughes, Phys. Rev. **57**, 592 (1940).

[11] G. Herzog, Phys. Rev. **57**, 337 (1940).

[12] P. M. S. Blackett, Proc. Roy. Soc. **A159**, 1 (1936); H. Jones, Rev. Mod. Phys. **11**, 235 (1939).

2.9×10^8 ev and 2×10^9 ev is not much different from that shown in Fig. 3 even at much higher altitudes.

To investigate the influence of lateral showers on the results obtained in the present experiments, in the flight on December 17, 1939 the middle counter tube No. 3 was moved out of the line of the remaining counters. Registering for half an hour the lateral showers, the counting rate at an altitude above 5.2 km was found to be 3 percent of that with all the counters in line. This indicates that in our arrangement the lateral showers do not give any appreciable contribution to the observed fourfold coincidences and, therefore, our results are not influenced by them.

The authors wish to express their appreciation to Professor A. H. Compton for his interest in and his support of this investigation.

DECEMBER 15, 1940 PHYSICAL REVIEW VOLUME 58

Neutron Studies of Order in Fe-Ni Alloys*

F. C. Nix,
Bell Telephone Laboratories, New York, New York

AND

H. G. Beyer and J. R. Dunning
Columbia University, New York, New York

(Received October 24, 1940)

Neutron transmission measurements are used to study order in Fe–Ni alloys. The difference in neutron transmission between fully annealed and quenched alloys when plotted against the nickel content displays a broad peak around Ni_3Fe and falls to vanishingly small values near 35 atomic percent Ni and pure Ni. The higher the degree of order the greater the neutron transmission. The substitution of 2.3 atomic percent Mo or 4.1 atomic percent Cr for Fe in the annealed 78 atomic percent Fe–Ni alloy caused a decrease in the neutron transmission, relative to the annealed 78 atomic percent Fe–Ni alloy, of 15.6 and 21.2 percent, respectively. The cold working of an annealed binary 75 atomic percent Ni alloy, a treatment known to produce disorder, gave rise to a decrease of 20.6 percent in neutron transmission. These results demonstrate that neutron techniques serve as a useful tool to study order in Fe–Ni alloys, and suggest that they can be extended to study other solid state phenomena.

THE previous work of Whitaker and Beyer[1,2] has shown that slow neutron interaction may be modified by the physical state of the material which the neutrons traverse. The dependence of neutron interaction on physical parameters of the system affords a possibility of investigating solid state phenomena. If only one parameter in a system be varied, changes in the neutron interaction may be correlated with the parameter in question. In the research reported here this approach was employed to investigate order in Fe–Ni alloys.

The measurements were made with neutrons diffusing from paraffin at room temperature. These neutrons have an energy distribution which corresponds to a de Broglie wave-length spectrum with the most probable wave-length in the region of 1.7 angstroms. The spacings of atoms in a crystal are of about this magnitude, so that interference phenomena should occur when these neutrons interact with matter in the solid state.

Although x-rays are very suitable for studying many aspects of the solid state there exist many problems where x-ray studies yield inconclusive results. This is the situation in the case of superstructures in alloys with the relative intensity of the super-structure lines depending on the difference in scattering powers of the constituent atoms.

In general, x-ray scattering is proportional to the number of electrons in the atoms (unless near

* Publication assisted by the Ernest Kempton Adams Fund for Physical Research of Columbia University.

[1] M. D. Whitaker and H. G. Beyer, Phys. Rev. **55**, 1101 (1939).

[2] H. G. Beyer and M. D. Whitaker, Phys. Rev. **57**, 976 (1940).

an absorption edge) and the addition of one unit of charge to the nucleus and one electron to an outer shell produces only a slight change in the scattering power. On the other hand the addition of an extra particle to the nucleus may completely change the response of the system to a slow neutron and neighboring elements in the periodic table may not only differ greatly in their scattering power for neutrons but important phase shift changes in the scattered wave may occur.

The presence of an ordered phase in alloys[3,4] can be established (or at least inferred) from a study of several physical properties such as electrical conductivity, the effect of plastic deformation on electrical conductivity, specific heats, thermal expansitivity, magnetic properties, etc. At the beginning of this work there was no direct unequivocal evidence, such as x-ray super-structure lines, for the presence of an ordered structure in Fe–Ni alloys. It was also of much interest to determine whether or not the presence of "short range order," i.e., ordered regions approaching the size of two atoms along an edge could be detected from neutron scattering. The most reliable evidence[5] indicates that x-ray super-structure lines are not detectable in Cu_3Au when the ordered domains are of a size less than

TABLE I. *Effect on relative transmissions of the addition of a third component to the* Fe–Ni *alloys.*

ALLOY	RELATIVE TRANSMISSION
78 Fe–Ni annealed	0.500
4.1 Chromium annealed*	0.422
2.3 Molybdenum annealed*	0.394
78 Fe–Ni cold worked	0.397
4.1 Chromium cold worked	0.402
2.3 Molybdenum cold worked	0.369

* The annealing conditions were chosen to develop high initial permeability as discussed above.

16–18 atoms along an edge. There is the further possibility that the presence of out-of-step domains may complicate the situation and prevent the appearance of super-structure lines even though the individual domains were sufficiently large.

[3] F. C. Nix and W. Shockley, Rev. Mod. Phys. **10**, 1 (1938).
[4] F. C. Nix, J. App. Phys. **8**, 783 (1937).
[5] C. Sykes and F. W. Jones, Proc. Roy. Soc. London **157**, 213 (1936).

PREPARATION OF ALLOYS

A series of iron-nickel alloys including pure iron and nickel were prepared from carbonyl iron and high purity electrolytic nickel in a vacuum induction furnace. The alloys were then subjected to a homogenizing anneal at 1000 degrees C. Pairs of samples were prepared from the cast and homogenized ingots which were 4 by 4 by 0.31 cm in size. All samples were then annealed in a vacuum induction furnace at about 900 degrees C in order to establish comparable grain size in both specimens. One sample of each composition was then annealed in a vacuum induction furnace containing low vapor pressure oil in the bottom of the vacuum chamber. The specimens were suspended on a fine tungsten wire which was fused at the end of the annealing period permitting the samples to drop into the oil bath. This drastic quench should suppress all ordering processes possessing a relaxation time greater than a fraction of a second. The remaining specimens of each of the pairs were then placed in evacuated glass tubes and subjected to prolonged annealings in order to permit the establishment of a large degree of order. They were held at a temperature of 490 degrees C for a period of 700 hours and then slowly cooled to 360 degrees C over a period of 340 hours. This treatment should be suitable for establishing a very high degree of order in the 75 atomic percent Ni alloy and should also produce a high degree of order in samples of other compositions from 85 to 45 atomic percent Ni. Unfortunately very little information is available concerning the optimum ordering temperatures in alloys other than Ni_3Fe, consequently it is extremely difficult to obtain comparable degrees of order as a function of composition. From studies of electrical conductivity of Fe–Ni alloys to be reported later we know that both quenched and annealed alloys are ordered, the difference being in the degree of order.

The Fe–Ni–Cr and Fe–Ni–Mo samples were prepared in a high frequency induction furnace and cold rolled from a plate $\frac{3}{4}$ in. in thickness down to a $\frac{1}{4}$ in. plate. Magnetic measurements show this treatment to give initial permeabilities of 492 and 178, respectively. A suitable heat treatment followed by slow cooling provoked an

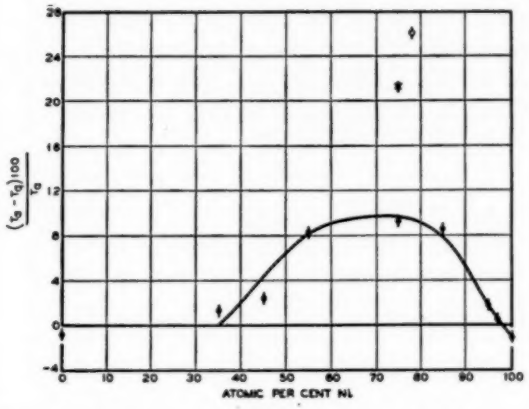

FIG. 1. Difference in neutron transmission *versus* composition (·). T_a, transmission of annealed plate; T_q, transmission of quenched plate. Cold worked plate relative to an annealed plate (*x*). 2.3 atomic percent Mo, Fe–Ni–Mo cold worked plate, relative to annealed 78 atomic percent Ni, Fe–Ni alloy (*o*).

increase in the initial permeabilities to 5400 and 15,100, respectively.

EXPERIMENTAL TECHNIQUE

The general arrangement for the neutron measurements is the same as used previously in the Columbia laboratories.[2]

Neutrons from a 500 to 750-mC Rn–Be source were slowed in a paraffin "howitzer" at room temperature. The emerging neutron beam was highly collimated by a cadmium lined tubular shield filled with boron carbide.

The detector consisted of a BF_3 ionization chamber connected to a linear amplifier and scaling system recorder. Samples to be tested were placed at the midpoint of the neutron beam. Under these geometrical conditions neutrons scattered by the sample through angles greater than 4 degrees did not reach the detector.

Method of observations

In these experiments it was more important to measure accurately the relative difference in neutron transmission between two samples, rather than the absolute value of the neutron transmission, since the samples had the same chemical composition and geometrical shape and differed only in that one of each pair had been quenched and the other annealed as described above. Hence in general, only cyclic measurements of the relative neutron transmission were made, although in some cases absolute transmissions were determined, as shown in Table II. The thicknesses of the samples were the same and in general gave an average neutron transmission of approximately 50 percent.

Precision.—30,000 to 150,000 neutrons were generally counted for each sample so that precision of the determinations of the difference in transmission was less than 1 percent.

Results

The transmission differences between annealed and quenched alloys were studied as a function of the nickel content. Pure iron and nickel were included as a check on the experimental technique of the preparation of the samples. Representing by T_q and T_a the transmission of the quenched and annealed plates, respectively, the values of $(T_a - T_q)100/T_a$ for various concentrations of Ni are:

At. % Ni	100	97	95	85	75	55	45	35	0
$100(T_a - T_q)/T_a$	−0.9	0.4	1.8	8.5	9.3	8.2	2.5	1.3	−0.6

The effects of cold working by compression and of quenching on the neutron transmissions were also ascertained for comparison. The relative transmissions of the annealed, quenched, and cold worked 75-atomic percent Ni samples are:

TREATMENT	ANNEALED	QUENCHED	COLD WORKED
Transmission	0.500	0.454	0.397

The effect of adding a third component to the Fe–Ni alloys was studied with plates containing 4.1 atomic percent Cr and 2.3 atomic percent Mo substituted for some of the Fe, in the 78 atomic percent Ni alloy. Mo and Cr have smaller slow neutron cross sections than Fe, the values being 7×10^{-24} cm² and 6×10^{-24} cm² as contrasted

TABLE II. *Observed neutron cross sections for a series of* Fe–Ni *alloys.*

ATOMIC PERCENT Ni OF Fe-Ni ALLOYS	CROSS SECTION $\times10^{24}$ cm^{-2} ADDITIVE (EXPECTED)*	OBSERVED	PERCENT CHANGE
78 (annealed)	18.2	12.5	31.3
78 (quenched)	18.2	15.5	14.8
78 (cold worked) (containing 2.3 at. % Mo)	18.1	18.0	0
45	15.6	15.5	0

* Additive values computed from neutron cross sections of polycrystalline Fe, Ni and Mo.

with 12×10^{-24} cm^2 for Fe. The relative transmissions are given in Table I.

The results are graphically presented in Fig. 1.

Table II shows the observed neutron cross sections for a series of Fe–Ni alloys together with the cross sections assuming additivity.

Discussion of Results

The differences in neutron transmission between the quenched and annealed alloys can be measured at compositions where super-structure x-ray lines cannot be detected even by refined x-ray technique. Super-structure lines have been detected only in 70[6] and 75[6] atomic percent Ni alloys,[7,8] whereas reliable differences in neutron transmission can be measured in the entire composition region from 45 to 90 atomic percent Ni. It is possible that neutrons reveal the presence of considerably smaller ordered domains than are disclosed by x-rays; this could account for the different results obtained by the two methods.

It has also been shown[6] that cold working of both annealed and quenched Fe–Ni alloys around the Ni_3Fe region provokes an increase in the electrical resistivity. Cold working of an ordered Cu_3Au alloy gives rise to a similar increase in electrical resistivity, and here the accompanying disappearance of the x-ray super-structure lines with cold working in the latter alloy shows that the increase in the electrical resistivity is correlated with the destruction of order. The results of neutron transmission studies indicate that a similar correlation occurs in Fe–Ni alloys. Thus the neutron results lead to the conclusion that both quenched and annealed Fe–Ni alloys in the region around Ni_3Fe are ordered, the difference being simply in the degree of order.

In the case of the ternary alloys containing 4.1 atomic percent Cr and 2.3 atomic percent Mo the neutron transmissions of both cold worked and annealed alloys are appreciably smaller than that of the binary Fe–Ni alloy of the same Ni content, indicating a lesser degree of order in the ternary alloys. It is also of interest to note that a heat treatment suitable to increase the initial permeability from 178 to 15,100 in the Mo–Fe–Ni alloy changes the neutron transmission difference, relative to the binary Fe–Ni alloy, only from 26.2 percent to 21.2 percent. This heat treatment was such as to cause some increase in the degree of order; however, the small change observed in neutron transmission could not be accounted for by the large change in initial permeability.

It should be pointed out that magnetic polarization effects do not play any appreciable part in the neutron transmission changes observed in these researches. The Fe–Ni–Mo alloy, which has the highest initial permeability, should be most transparent from magnetic polarization considerations, whereas actually this alloy scatters more neutrons than the other alloys. Furthermore; the transmission changes reported in this paper are very much larger than observed with magnetic polarization effects and, in addition, neutron transmission changes due to magnetic polarization have only been observed with very high magnetizing fields.[9]

The results are very consistent, with the assumption that changes in degree of order affect the neutron transmission, in that where large deviations from additivity occur, the thermal treatments and cold working, which are known to produce changes in order, are effective in changing the neutron transmission.

Conclusions

These results clearly show that neutron transmission measurements provide a very sensitive technique for studying changes of order in Fe–Ni alloys. Such measurements are able to give quantitative comparisons of the effect of various physical processes, such as cold working and thermal treatments, in changing the state of order.

In the particular case of Fe–Ni alloys studied in these experiments, the sensitivity of the neutron transmission technique may be due in part to large phase-shift differences in the waves scattered by the Fe and Ni nuclei. If this is true, then the method will not be equally sensitive for all alloys, but it should be applicable to many.

[6] O. Dahl, Zeits. f. Metallkunde **28**, 133 (1936).
[7] F. E. Haworth, Phys. Rev. **56**, 289 (1939).
[8] P. Leech and C. Sykes, Phil. Mag. **27**, 742 (1939).
[9] J. R. Dunning, P. N. Powers and H. G. Beyer, Phys. Rev. **51**, 51, 371 (1937).

Thresholds for the Proton-Neutron Reactions of Lithium, Beryllium, Boron, and Carbon

R. O. Haxby,† W. E. Shoupp,* W. E. Stephens‡ and W. H. Wells
Westinghouse Research Laboratories, East Pittsburgh, Pennsylvania

(Received August 30, 1940)

The energy threshold for the production of neutrons by bombardment of targets of Li, Be, B, and C with high energy protons has been measured with a boron trifluoride ionization chamber, surrounded with paraffin, as a neutron detector. The energy of the protons was calibrated against the 0.862-Mev $F(p, \gamma)$ resonance. With H_2^+ and H_3^+, this calibration was extended to 1.724 Mev and 2.586 Mev. The thresholds are: Li^7, 1.86 Mev; Be^9, 2.03 Mev; B^{11}, 2.97 Mev and C^{13}, 3.20 Mev. From these values can be calculated the mass differences $Be^7-Li^7=0.87$ Mev, $B^9-Be^9=1.08$ Mev, $C^{11}-B^{11}=1.97$ Mev and $N^{13}-C^{13}=2.22$ Mev. B^9 is shown to be certainly unstable with respect to disintegration into Be^8+H^1. The $N^{13}-C^{13}$ difference agrees closely with the maximum positron energy from N^{13}, and thereby confirms the voltage scale.

Introduction

THE first observation of a (p, n) reaction was made by DuBridge, Barnes, and Buck.[1] The excitation curve was shown to have a definite threshold first by measuring the radioactivity[2] produced as a function of proton energy, and later by measuring the neutron[3] yield as a function of proton energy. The $Li^7(p, n)Be^7$ [3] and Be^9 [4] thresholds have been measured by means of the neutron induced activity in silver foils. The thresholds of these two reactions are of interest because they furnish the best way of measuring the masses of the nuclei Be^7 and B^9. We have redetermined these thresholds as accurately as possible. The $B^{11}(p, n)C^{11}$ threshold has not heretofore been measured; in fact the reaction itself has only recently been detected.[5] The $C^{13}(p, n)N^{13}$ threshold closes a reaction and mass-doublet cycle whose components have been very accurately measured. If the neutrino mass is zero, this cycle gives a good check on the voltage calibration. The precise measurement of these thresholds, or rather the precise intercomparison of these thresholds with γ-ray resonances, was a good way of testing the performance of the Westinghouse pressure electrostatic generator, and of exhibiting its principal feature, namely, accurate and easy control of voltage. Preliminary results have already been reported.[6]

Experiment

The Westinghouse pressure electrostatic generator[6] was the source of the high energy protons. The magnetically deflected spot of mass one was used so that there was no possibility of contamination of the beam by deuterons. The target arrangement is shown in Fig. 1, in which the aperture in the Faraday cage was small enough to insure that all protons entering the cage hit the target. The alignment was checked visually by means of quartz plate which could be let down over the target. The proton beam current was integrated by a device similar to the one described by Herb.[7] Neutrons coming from the target were slowed down in the block of paraffin and detected by means of the BF_3 ionization chamber inserted in the paraffin near the target. The BF_3 ionization chamber was patterned after the one described by Powers[8] and is shown in Fig. 2. The quartz insulation and Picein sealing wax first tried were replaced by hard rubber insulation and soft rubber gaskets to make a stronger and more convenient structure. This insulation lasts at least four months, and can be easily changed. Commercial BF_3 was used to fill

* Westinghouse Research Fellow.
† Now with Sperry Gyroscope Company.
‡ Now at Stanford University.
[1] DuBridge, Barnes, and Buck, Phys. Rev. **51**, 995 (1937).
[2] DuBridge, Barnes, and Buck, Phys. Rev. **53**, 447 (1938).
[3] J. E. Hill and G. E. Valley, Phys. Rev. **55**, 678A (1939).
[4] J. E. Hill, Phys. Rev. **57**, 567A (1940).
[5] W. H. Barkas, Phys. Rev. **56**, 287 (1939).
[6] Haxby, Shoupp, Stephens, and Wells, Phys. Rev. **57**, 348 and 567 (1940); Wells, Haxby, Shoupp, and Stephens, Phys. Rev. **58**, 162 (1940).
[7] Herb, Kerst, and McKibben, Phys. Rev. **51**, 691 (1937).
[8] P. N. Powers, Phys. Rev. **54**, 827 (1938).

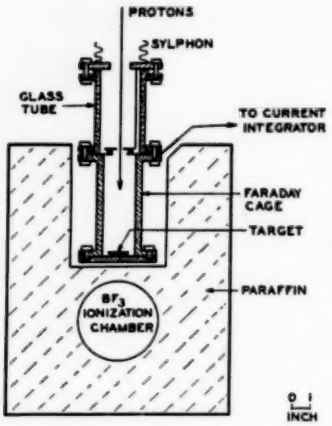

FIG. 1. Arrangement of target, paraffin, and BF_3 ionization chamber.

the ionization chamber to two atmospheres pressure. A 954 acorn tube was found convenient to use for a first stage of the linear amplifier, and was mounted on the ionization-chamber box. The linear amplifier has four resistance-capacity coupled stages[9] that feed a thyratron which drives a scaling circuit[10] and in turn actuates a Cenco counter. The thyratron was biased to count pulses approximately $\frac{1}{3}$ of the maximum α-particle pulses, this being about twice the background level. A potential of 2000 volts was used on the ionization chamber.

The voltage with which the protons are accelerated was measured by a generating voltmeter in which the principle of the compensating voltage plate described by Harnwell and Van Voorhis[11] was used. In this voltmeter, the generating voltmeter itself is used only to detect the absence of inhomogeneities in the field behind the voltage plate. Voltage is applied to this voltage plate until it coincides with an equipotential surface of the field from the high potential electrode. This condition is detected by the absence of pick-up in the generating voltmeter part. The high potential is then proportional to the voltage on the voltage plate and is measured by means of precision resistors and a good milliammeter.

The first voltmeter tried is shown diagrammatically in Fig. 3. The shutter and voltage plates consist of opposite quadrants. The pick-up plate was stationary and not sectored. The shutter was grounded through a slip ring and brush. This voltmeter worked well except that the presence of the front grounded plate and lack of proper alignment of the plates made it impossible to get a perfect balance point. The output from the pick-up plate as viewed in an oscillograph gave a complex pattern which was adjusted to an arbitrary but easily reproduced "balance pattern." This voltmeter was calibrated and checked for linearity against the 0.862-Mev fluorine gamma-ray resonance using H^+, HH^+, and HHH^+. The calibration curve was linear to an accuracy of 0.2 percent, but did not go through the origin. The limitation in accuracy was due to difficulty in setting the "balance pattern" on the oscillograph. Introduction of a pre-amplifier further distorted the pattern. To eliminate the imperfect balance effect (and hence eliminate the possibility that change in amplifier characteristics would shift the balance) a new and simpler voltmeter was made and is shown in Fig. 4. Here, instead of a rotating shutter and stationary pick-up plate, a rotating sectored pick-up plate was used. Since the pick-up plate is used only as a null detector, the a.c. amplifier gain need not be accurately constant. Variation in the brush resistance is unimportant, as long as it remains much less than the input resistance in the amplifier. To insure adequate brush contact, two brushes in parallel are provided for the pick-up plates. The most serious disadvantage is that the distance between the voltage plate and the pick-

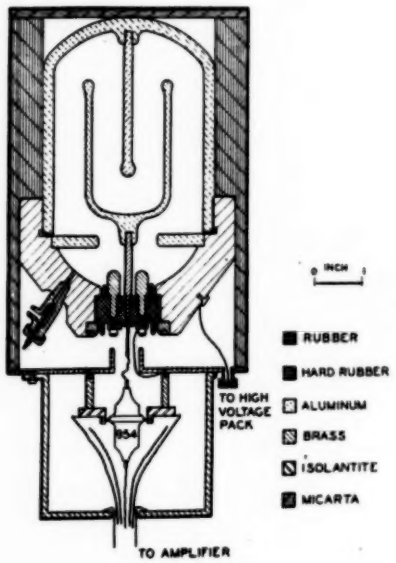

FIG. 2. Diagram of BF_3 ionization chamber.

[9] J. R. Dunning, Rev. Sci. Inst. **5**, 387 (1934).
[10] W. G. Shepherd and R. O. Haxby, Rev. Sci. Inst. **7**, 425 (1936).
[11] G. P. Harnwell and S. N. Van Voorhis, Rev. Sci. Inst. **4**, 540 (1933).

up plate must remain accurate to the precision desired in the voltage measurement. End play in the motor ball bearings is the probable limitation in accuracy of this spacing at present. With this voltmeter (using precision resistors and a potentiometer to measure the voltage on the voltage plate) readings can be reproduced to 0.2 percent and the voltage scale is linear to about 0.2 percent. This linearity was checked by measuring the 0.862-Mev fluorine gamma-ray resonance with H^+, HH^+, and HHH^+ at 0.862, 1.724, and 2.586 Mev. The yield of gamma-rays as a function of generating voltmeter reading is shown in Fig. 5. The gamma-rays are measured by a Geiger counter using otherwise the same procedure described by the Wisconsin group.[12] Hence their value of 0.862 Mev for the main resonance was used in our work. This value is ½ percent less than the value 0.867 Mev given by Heydenburg from a thick target measurement.[13] Both values are based on the value 0.440 Mev for the $Li^7(p, \gamma)$ resonance. This value was measured at Washington, D. C. by a calibrated resistance voltmeter to 2 percent[14] and checked at Wisconsin.[15] However, the voltage scale used at Washington was calibrated to 1 percent by absolute measurement of the proton scattering in argon.[13] Hence, our voltage scale is accurate in absolute value to about 1½ percent by this method of calibration. As will be discussed later, the $C(p, n)$ threshold measurement is a good check on our voltage calibration.

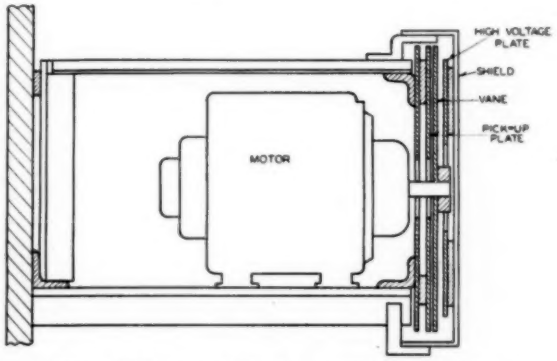

FIG. 3. Diagram of first generating voltmeter.

[12] Bernet, Herb, and Parkinson, Phys. Rev. **54**, 398 (1938).
[13] Heydenburg, Hafstad, and Tuve, Phys. Rev. **56**, 1078 (1939).
[14] Hafstad, Heydenburg, and Tuve, Phys. Rev. **50**, 504 (1936).
[15] Parkinson, Herb, Bernet, and McKibben, Phys. Rev. **53**, 642 (1938).

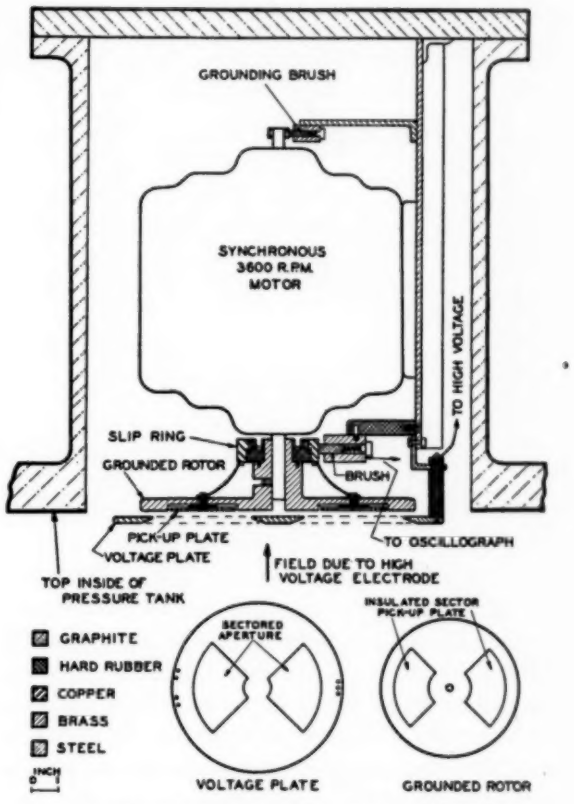

FIG. 4. Diagram of second generating voltmeter.

RESULTS

The number of neutrons counted by the detector per proton current integrator count was plotted as a function of proton energy read on the generating voltmeter to give the curves shown in Figs. 6 to 11. In our first exploratory experiments we used a BF_3 Geiger counter[16] surrounded by several pieces of paraffin. A $Be(p, n)$ yield curve taken with the counter is shown in Fig. 6. The BF_3 ionization chamber had a sensitivity about 40 times greater than the counter, and we were then able to investigate more carefully the dotted rectangle of Fig. 6. The resulting curve is shown in Fig. 7. With the second generating voltmeter we were able to increase the voltage resolution and secure the curve which is shown in Fig. 8. In all these curves the vertical lines through the points represent the statistical uncertainty of the number of counts. The horizontal lines represent the variation of voltage during a reading, as read on the generating

[16] S. A. Korff and W. E. Danforth, Phys. Rev. **55**, 980 (1939).

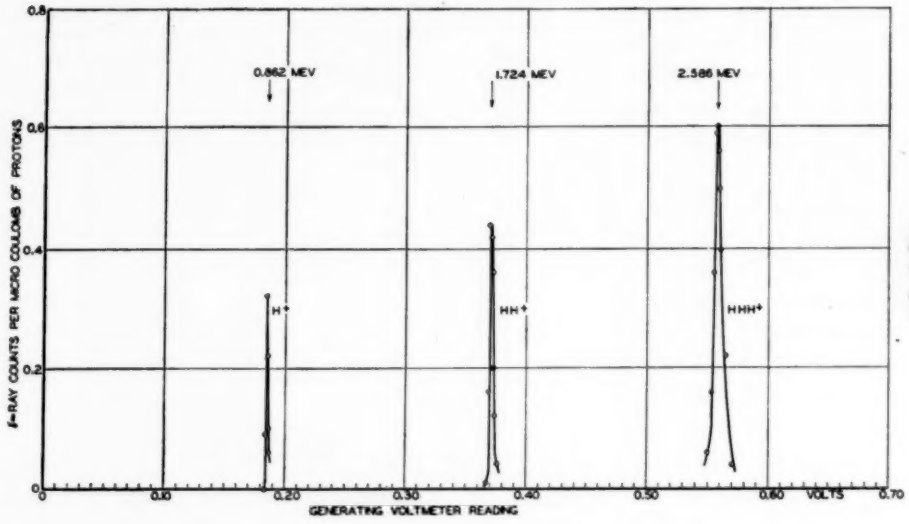

FIG. 5. Thin target γ-ray yield curve for the $F(p, \gamma)$ 0.862-Mev resonance taken with H^+, HH^+, and HHH^+ at $E_p = 0.862$ Mev, 1.724 Mev, and 2.856 Mev.

voltmeter. The ripple or any fast variation in voltage could not be read on the generating voltmeter, and can only be estimated from the width of a thin target γ-ray resonance curve assuming all the width to be experimental. The width at half-maximum varied from 3 kv to 10 kv for a 1-kv thick target, and seems to depend on the length of time of the readings and also on some uncontrollable features of the generator. There seems to be a tendency for the voltage to drop below, rather than fluctuate around, the value read on the generating voltmeter; this may explain the occasional points below the general run of points on the excitation curves. The reproducibility of the thresholds is about 0.2 percent, and is of the same order as the accuracy of calibration against the $F(p, \gamma)$ resonance. The curve of Fig. 8 is the best evidence we have for the sharpness of these (p, n) thresholds. Here the resolving power seems to be as good as 0.05 percent and the curve intercepts the background without any evidence of tailing. This resolution is better than we have obtained from γ-ray curves, and is probably due to the short time required to take the readings. It will be noticed that there is an appreciable neutron background in the $Be(p, n)$ curve. This effect is ascribed to the secondary reaction system $Be^9(p, d)$, $Be^9(d, n)$ and could probably be reduced by using a thin Be target.

The yield curve for $Li^7(p, n)$ is shown in Fig. 9. It is to be noted that the background is quite small. In fact, it is the same as the natural background and is probably due to natural α-particles from the walls of the ionization chamber and to cosmic-ray neutrons.[17] Because of the small background and large yield from this reaction, its threshold can be observed visually by watching the linear amplifier monitor oscilloscope. The voltage at which neutron pulses appear visually on the screen is taken as the threshold. These values, shown by the arrows on the curve, agree quite well with the

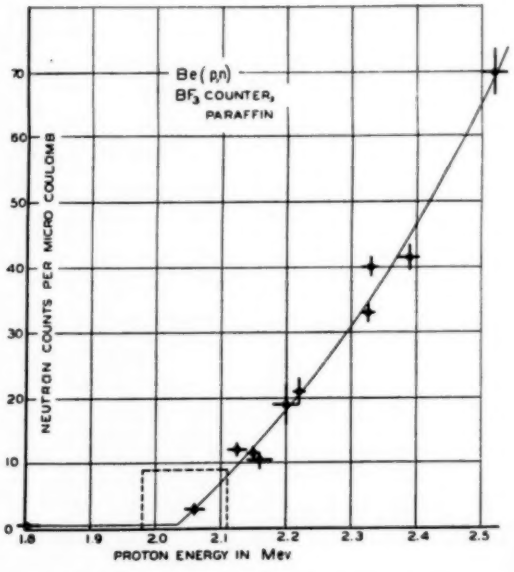

FIG. 6. Thick target neutron yield curve for $Be(p, n)$ taken with BF_3 Geiger counter, a few pieces of paraffin, and the first generating voltmeter.

[17] C. G. Montgomery and D. D. Montgomery, Phys. Rev. **56**, 10 (1939).

extrapolated value. The $B^{11}(p, n)$ yield curve is given in Fig. 10, and $C^{13}(p, n)$ in Fig. 11. The yield from $C^{13}(p, n)$ is distinctly smaller than the others, and is consistent with the fact that C^{13} is only 1 percent of carbon. Both the B and C curves have appreciable backgrounds of undetermined origin.

A summary of the observed threshold energies E_p of the (p, n) reactions investigated is given in Table I. The probable errors given are only those involved in the comparison of these values with the 0.862-Mev $F(p, \gamma)$ resonance. As has been pointed out, this value of 0.862 Mev is known to an absolute accuracy of only $1\frac{1}{2}$ or 2 percent.

Discussion

The general (p, n) reaction may be written as

$$_zX^A + {}_1H^1 \rightarrow {}_{z+1}Y^A + {}_0n^1 + Q_1,$$

where Q_1 is actually negative, since the reaction is endoergic and the value of Q_1 is given in terms of the measured threshold of proton bombarding energy E_p, as

$$Q_1 = -\left(\frac{A}{A+1}\right)E_p.$$

The product nucleus Y may return to X either by emitting positrons,

$$_{z+1}Y^A \rightarrow {}_zX^A + {}_{-}e + {}_{+}e + \mu + E_+$$

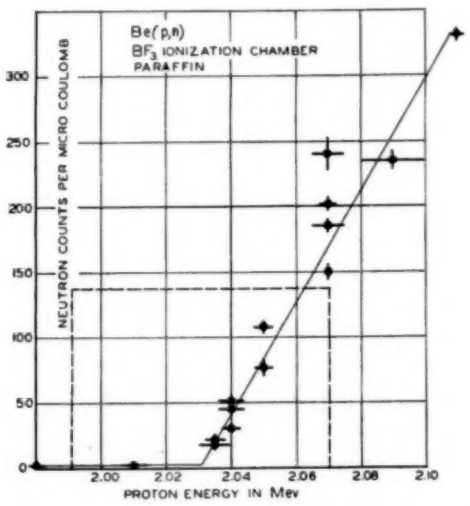

FIG. 7. Thick target neutron yield curve for $Be(p, n)$, taken with BF_3 ionization chamber in paraffin and with the first generating voltmeter.

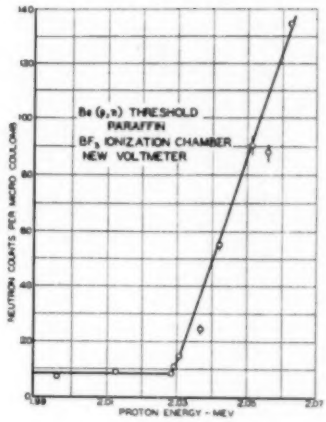

FIG. 8. Thick target neutron yield curve for $Be(p, n)$ taken with BF_3 ionization chamber in paraffin and with the second generating voltmeter.

or by K-electron capture

$$_{z+1}Y^A \rightarrow {}_zX^A + \mu + Q_2.$$

In these equations, X, Y, refer to atomic masses $_{-}e$ and $_{+}e$ to the rest mass of the electron and positron, μ to the rest mass of the neutrino, and Q_2 to the total kinetic energy of the products. In the case of the positron emitters E_+ is the maximum energy of the positron spectrum.

First we can give the masses of the Y nuclei by putting our results together with other measured values for the X masses and adopting the value

$$({}_0n^1 - {}_1H^1) = 0.750 \pm 0.056 \text{ Mev}.$$

This value is derived from Mattauch's[18] mass-spectroscopic value,

$$(HH - D) = 1.433 \pm 0.002 \text{ Mev}.$$

or alternatively on the value of Bainbridge and Jordan[19]

$$(HH - D) = 1.424 \pm 0.04 \text{ Mev}.$$

Also involved in $({}_0n^1 - {}_1H^1)$ is the value for the dissociation energy of the deuteron $({}_0n^1 + {}_1H^1 - {}_1D^2)$. There are four experimental values for this, as follows:

(a)	2.17 ±0.04 Mev	(c)	2.18 ±0.07
(b)	2.189±0.0022	(d)	2.174±0.05

The sources of these are (a) Bethe's correction[20] of the Cambridge cloud-chamber range, (b) Stetter and Jentschke's[21] ionization-chamber

[18] J. Mattauch, Zeits. f. tech. Physik **12**, 578 (1939).
[19] K. T. Bainbridge and E. B. Jordan, Phys. Rev. **49**, 883 (1936).
[20] H. A. Bethe, Phys. Rev. **53**, 313 (1938).
[21] G. Stetter and W. Jentschke, Zeits. f. Physik **110**, 214 (1938).

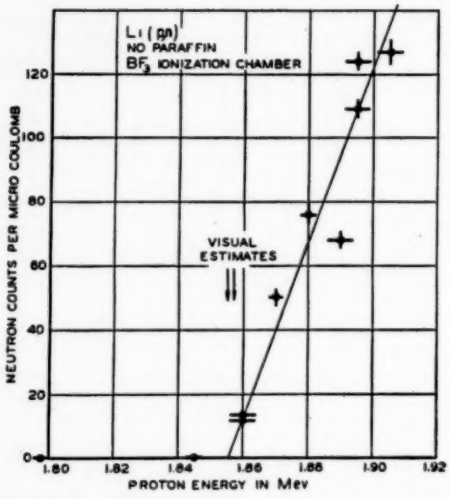

FIG. 9. Thick target neutron yield curve for LiOH(p, n) taken with BF_3 ionization chamber and with the first generating voltmeter.

work, (c) Richardson and Emo[22] cloud-chamber range, and (d) Rogers and Rogers[23] cloud-chamber curvature. A weighted average of these gives

$$({}_0n^1+{}_1H^1-{}_1D^2)=2.183\pm0.017 \text{ Mev}$$

from which the stated value of $({}_0n^1-{}_1H^1)$ is derived. If, more conservatively, one uses the Bainbridge and Jordan value for (HH−D) and the Bethe value for $({}_0n^1+{}_1H^1-{}_1D^2)$, the result is

$$({}_0n^1-{}_1H^1)=0.750\pm0.02 \text{ Mev}.$$

This value for $({}_0n^1-{}_1H^1)$, together with our observed values of Q_1 from Table I and the following assumed masses for the X nuclei give these values for the Y nuclei,

X, Li^7	7.01814±0.00011	Ref. (24)	Y, Be^7	7.01908±0.00011
Be^9	9.01484±0.00013	(25)	B^9	9.01600±0.00013
B^{11}	11.01286±0.00020	(26)	C^{11}	11.01499±0.00020
C^{13}	13.00766±0.00015	(26)	N^{13}	13.01004±0.00015

The value $E_p=1.85$ Mev for the $Li^7(p, n)$ threshold is somewhat lower than that observed by Hill and Valley,[3] but is within their experimental uncertainty. Recently, Hudson, Herb, and Plain[27] found a sharp rise in γ-ray intensity at $E_p=1.83$ Mev which, as they mention, may be due to neutrons from $Li^7(p, n)$.

Knowledge of the Be^7-Li^7 mass difference makes possible a discussion of the branching ratio of the K-capture activity of Be^7. When Be^7 captures a K electron, it may go to Li^7 in the normal state, in which case the energy taken away by the emitted neutrino is 0.87 Mev; likewise it may go to excited $(Li^7)^*$, which subsequently emits a 0.45 Mev γ-ray,[28] in which case the emitted neutrino carries off only 0.87−0.45=0.42 Mev. On the β-decay theory, using the Fermi interaction assumption for allowed transitions, the relative likelihoods of the two modes of disintegration should be as the square of the released neutrino energy, or 0.232 for the ratio of $(Li^7)^*$ to Li^7 yield. Similarly with the Konopinski-Uhlenbeck form the variation is as the fourth power of the released neutrino energy or 0.054. The Gamow-Teller[29] spin dependent form assuming the two states of Li^7 to be $^2P_{3/2}$ (ground) and $^2P_{\frac{1}{2}}$ (excited) gives a value of 0.149 for the ratio. The experimental estimate[28] of the ratio is quite crude, and puts it only in the range 0.03 to 0.3, and so does not afford a decisive comparison with the theories. A more accurate experimental value would be interesting.

In regard to the Be(p, n) reaction, one might

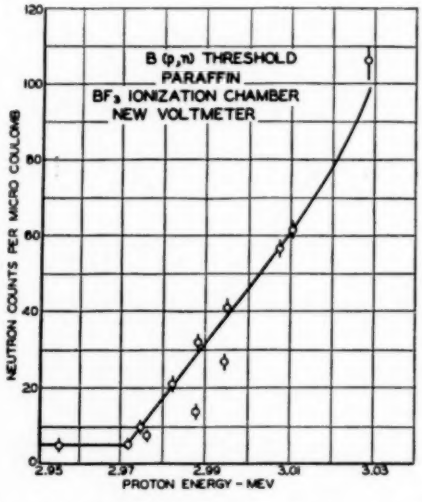

FIG. 10. Thick target neutron yield curve for $B_4C(p, n)$ taken with BF_3 ionization chamber in paraffin and with second generating voltmeter.

[22] J. R. Richardson and L. Emo, Phys. Rev. **53**, 234 (1938).
[23] F. T. Rogers, Jr., and M. M. Rogers, Phys. Rev. **55**, 269 (1939).
[24] N. M. Smith, Jr., Phys. Rev. **56**, 548 (1940); Allison, Miller, Perlow, Skaggs, and Smith, Phys. Rev. **58**, 178 (1940).
[25] Allison, Skaggs, and Smith, Phys. Rev. **57**, 550 (1940).
[26] W. H. Barkas, Phys. Rev. **55**, 691 (1940).
[27] Hudson, Herb, and Plain, Phys. Rev. **57**, 587 (1940).
[28] Rumbaugh, Roberts, and Hafstad, Phys. Rev. **54**, 657 (1938).
[29] G. Gamow and E. Teller, Phys. Rev. **49**, 895 (1936); B. O. Grönblum, Phys. Rev. **56**, 508 (1939).

expect an alternative reaction producing neutrons to be the noncapture disintegration,

$$_4Be^9+_1H^1\rightarrow_4Be^8+_0n^1+_1H^1+Q_1.$$

Since the threshold for γ-ray disintegration of Be^9 has been found[30] to be 1.63 ± 0.05 Mev, the expected threshold of this reaction would be $1.81[=(10/9)\times1.63]$ Mev, definitely below the observed threshold of 2.03 Mev. Because of background, we can only detect a reaction cross section greater than 10^{-27} cm^2 within 0.2 Mev of the threshold. This is in accord with a theoretical estimate of Guth (private communication) that the cross section is about 10^{-28} cm^2 at 0.3 Mev above the threshold.

The observed energy difference (B^9-Be^9) would permit a positron radioactivity with maximum positron energy of 0.06 Mev or a K-electron capture. Such positron activity was not observed by Hill.[4] We looked for K-capture activity, by inserting a bombarded Be target into a Geiger counter, but found none. One may account for the absence of such activity in B^9 by the fact that B^9 is unstable with regard to dissociation into Be^8+H^1. This explanation follows at once from the fact that the $Be^9(p, n)B^9$ threshold is 0.20 Mev higher than the $Be^9(p, pn)Be^8$ threshold, as already discussed. Hence we conclude that the $Be^9(p, n)B^9$ reaction is immediately followed by the $B^9\rightarrow Be^8+H^1$ disintegration or perhaps a $B^9\rightarrow He^4+He^4+H^1$ disintegration. This was originally suggested as a possibility by Hill. The unstability of B^9 was predicted by Bethe from binding energy considerations.[31]

TABLE I. *Summary of results.*

Target $_zX^A$	Threshold Energy E_p* (Mev)	Reaction Energy Q_1 (Mev)	$Y-X$ or Q_1 (Mev)	Max. Positron Energy E_+ (Mev)
Li^7	1.85 ± 0.02	1.62 ± 0.02	0.87 ± 0.03	—
Be^9	2.03 ± 0.01	1.83 ± 0.01	1.08 ± 0.02	—
B^{11}	2.97 ± 0.01	2.72 ± 0.01	1.97 ± 0.02	0.95 ± 0.02
C^{13}	3.20 ± 0.03	2.97 ± 0.03	2.22 ± 0.04	1.20 ± 0.04

Mass Differences

Be^7-Li^7	$(9.4\pm0.3)\times10^{-4}$ m.u.
B^9-Be^9	$(11.6\pm0.2\times10^{-4})$ m.u.
$C^{11}-B^{11}$	$(21.3\pm0.2\times10^{-4})$ m.u.
$N^{13}-C^{13}$	$(23.8\pm0.4\times10^{-4})$ m.u.

* Values based on 0.862 Mev for the $F(p, \gamma)$ resonance. The stated uncertainties cover those in our comparison with this value. There is an additional uncertainty in these values of slightly less than 1 percent due to the uncertainty of this absolute value. Previously the uncertainty of the fluorine value was about 2 percent, but this seems to be considerably reduced in view of the results for the carbon cycle discussed below.

[30] Collins, Waldman, and Guth, Phys. Rev. **56**, 876 (1939).

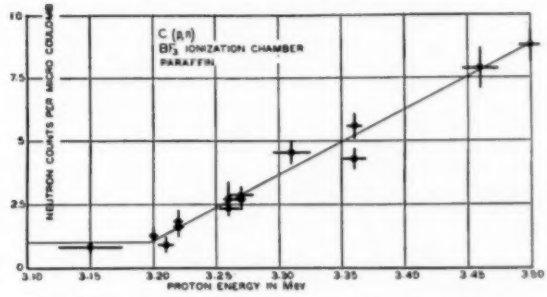

FIG. 11. Thick target neutron yield curve for $C(p, n)$ taken with BF_3 ionization chamber in paraffin and with first generating voltmeter.

The observed boron threshold is interesting in that it leads to a prediction of 0.95 ± 0.02 Mev for the maximum positron energy from C^{11}, which is definitely lower than the values 1.15 and 1.03 ± 0.03 Mev previously reported.[32] However, the most recent measurement, 0.95 ± 0.05 Mev, is in perfect agreement with our result.[33]

The boron threshold also permits a calculation of the $B^{10}(d, n)$ reaction in combination with other known data:

$$B^{11}(p, n)C^{11}=-2.72\pm0.03 \text{ Mev}$$
$$B^{10}(d, n)C^{11}=Q$$
$$B^{10}H-B^{11}=10.80\pm0.1$$
$$HH-D=1.433\pm0.002.$$

The $B^{10}H-B^{11}$ difference is from Bainbridge and Jordan.[34] These combine to give $Q=6.65\pm0.11$, which, at a bombarding energy of $E_D=1.0$ Mev, would give 6.85 ± 0.1 Mev for the energy of the neutrons emitted at 90° to the deuteron beam. The neutrons ascribed to this reaction by Bonner and Brubaker[35] have an energy of 6.15 ± 0.2 Mev, as measured by Staub and Stephens,[36] so it would seem that the neutrons are probably really due to $B^{11}(d, n)$ and that the neutrons from $B^{10}(d, n)$ have not as yet been measured.

In the case of the carbon threshold, Q_1 enables

[31] H. A. Bethe, Phys. Rev. **54**, 436 (1938).
[32] Fowler, Delsasso, and Lauritsen, Phys. Rev. **49**, 561 (1936); B. L. Moore, Phys. Rev. **57**, 355A (1940).
[33] Barkas, Creutz, Delsasso, Fox, and White, Phys. Rev. **57**, 562A (1940).
[34] K. T. Bainbridge and E. B. Jordan, Phys. Rev. **51**, 385 (1937).
[35] T. W. Bonner and W. M. Brubaker, Phys. Rev. **50**, 308 (1936).
[36] H. Staub and W. E. Stephens, Phys. Rev. **53**, 212A (1938).

TABLE II. *Coulomb differences in Mev.*

PAIR	Q_1	TRITON MODEL	HOMOGENEOUS DISTRIBUTION MODEL	CENTRAL NUCLEUS MODEL
Be^7-Li^7	1.62 ± 0.03	1.72	1.86	1.85
B^9-Be^9	1.83 ± 0.02		2.28	1.83
$C^{11}-B^{11}$	2.72 ± 0.02	2.72*	2.68	2.84
$N^{13}-C^{13}$	2.97 ± 0.04		3.03	2.98*

* Calculated values fitted to these values.

us to close an energy cycle in which the only unknown quantity is the rest mass of the neutrino. If we regard this as zero from evidence from β-decay theory, then this cycle gives an independent check on the accuracy of our voltage scale. Or if we accept the voltage scale as calibrated from the $F(p, \gamma)$ resonance, the result gives an upper limit for the rest mass of the neutrino. The reactions involved are

$$ {}_6C^{13}+{}_1H^1\rightarrow{}_7N^{13}+{}_0n'+Q_1 $$

$$ {}_7N^{13}\rightarrow{}_6C^{13}+{}_+e+{}_-e+\mu+E_+. $$

Using the previously cited value for

$$ ({}_0n^1-{}_1H^1)=0.750\pm0.02 \text{ Mev}, $$

our value for $Q_1=-2.970\pm0.05$ Mev and the value obtained by Lyman[37] for the maximum energy of the positron spectrum $E_+=1.198\pm0.006$ Mev, we get for the rest mass of the neutrino

$$ \mu=-({}_0n^1-{}_1H^1)-({}_+e+{}_-e)-E_+-Q_1, $$

$$ \mu=-0.750\pm0.02-1.021-1.198\pm0.006+2.970\pm0.05, $$

$$ \mu=0.001\pm0.056 \text{ Mev}. $$

Hence if one accepts the voltage calibration, the results indicate the neutrino rest mass is probably less than one-tenth the electron rest mass. Or if one believes that the neutrino rest mass is zero, the close balance gives a very good check (to better than 1 percent) of the absolute voltage scale used in this work.

[37] E. M. Lyman, Phys. Rev. **55**, 234A (1939).

The reaction energy Q_1, as given in Table I, is also the "Coulomb difference" or the difference in binding energy between pairs of isobaric nuclei for which $Z=\frac{1}{2}A\pm\frac{1}{2}$. Since these pairs differ only in the interchange of a neutron and proton, this binding energy difference indicates the amount of Coulomb repulsion of the interchanged proton (assuming n–n and p–p forces are equal). It is interesting to compare the observed values with various calculated values, as shown in Table II.[38] The Be^7-Li^7 value is closest to that calculated on the alpha-triton model.[39] This might be expected, since this model also gives the spin and magnetic moment of Li^7 and for this pair the binding of alpha to triton is less than the intra group binding. The B^9-Be^9 value is remarkably well fitted by the central nucleus model.[40] This seems to indicate that the extra proton is in a p state outside a closed alpha-particle shell. The other two pairs and also pairs of higher atomic number[38] agree quite well with calculations on the homogeneous distribution model,[40] indicating that from here on the nuclei behave, in this respect at least, as if the nuclear particles were homogeneously distributed in a sphere of radius $=1.46A^{\frac{1}{3}}\times10^{-13}$ cm.

In conclusion, the experiments presented here have demonstrated the value of the large pressure electrostatic generator for precision measurements in nuclear physics. The sharpness of the thresholds of the (p, n) reactions indicates that they will be useful as calibration points in high voltage work.

We wish to express our appreciation of the generous support of this work by the Westinghouse Electric and Manufacturing Company, and of the friendly help and discussions with Dr. L. W. Chubb, Director, and Dr. E. U. Condon, Associate Director of the Westinghouse Research Laboratories.

[38] W. E. Stephens, Phys. Rev. **57**, 938L (1940).
[39] H. Brown and D. R. Inglis, Phys. Rev. **55**, 1182 (1939).
[40] H. A. Bethe, Phys. Rev. **54**, 436 (1938).

Protons from Carbon and Aluminum Bombarded by Deuterons

H. L. SCHULTZ,* W. L. DAVIDSON,† JR. AND L. H. OTT
Sloane Physics Laboratory, Yale University, New Haven, Connecticut
(Received October 5, 1940)

The design of a cloud chamber and the technique of its use are described. With it a study of the protons from deuteron bombardment of carbon and aluminum has been made. The group corresponding to the ground state of C^{13} appears to be single. The protons from Al^{27} show a general distribution in agreement with the work of McMillan and Lawrence; but analysis into groups is difficult as there appear to be many such, with small spacing. Curves are shown from which any group structure can be inferred. The homogeneity of the deuteron beam was tested by scattering the deuterons from a thin gold foil: It is homogeneous to within 0.15 Mev.

INTRODUCTION

PROPORTIONAL counters and ionization chambers have been used almost exclusively in studies of the group structure of charged particles emitted in nuclear transmutations. These methods have disadvantages, in particular when a cyclotron is employed. Weak groups are hard to detect in the presence of a high neutron background. The necessity of a high counting level for discriminating against β- and γ-radiations makes the determination of absolute yields a difficult problem. This feature may lead to incorrect values of the relative intensities of groups of different width and symmetry.

Theoretical considerations indicate that the density of nuclear energy levels varies rapidly with excitation energy and number of particles of which the nucleus is composed. Resolution is important in investigations of groups from heavier nuclei where counting methods may show definite groups with larger spacings than predicted by theory.

An attempt has been made to overcome the above difficulties in studies of dp reactions by allowing the emitted protons to register in an expansion chamber. Bower and Burcham[1] have applied this method in experiments on proton groups from fluorine bombarded by deuterons, and have pointed out that it affords a means of achieving high resolving power without serious limitation of solid angle. A desirable feature of the method is that the determination of relative amplitudes of groups does not involve an integration of the incident beam intensity.

This paper gives the results of a cloud-chamber investigation of the protons from carbon and aluminum bombarded by 3.2-Mev deuterons produced in the Yale cyclotron. General details of construction and performance of this cyclotron have already been mentioned.[2]

APPARATUS AND EXPERIMENTAL PROCEDURE

The cloud chamber, 17 cm in diameter, is of the moving diaphragm type. Best results were obtained with a semirigid diaphragm made by cementing a circular aluminum plate $\frac{3}{32}''$ thick to the rubber diaphragm itself. Argon and ethyl alcohol vapor were used with a relative stopping power of 1.18 as determined both by calculation and calibration with Th C′ alpha-particles. This mixture has the advantage that much fewer recoils and disintegrations produced by neutrons are noted than would be the case with air.

Single photographs were taken with an automatic camera. Since the tracks were highly collimated in a horizontal plane, stereoscopic photographs were unnecessary. Two high speed argon-filled discharge tubes of the design by Edgerton[3] served to give ample illumination. With Agfa Ultraspeed Panchromatic film enough light was present to permit an aperture of $f:9$, thus providing good depth of focus. This lighting scheme proved to be quite successful and convenient. A photograph of tracks is shown in Fig. 1.

* Now at University of Buffalo, Buffalo, New York.
† Now at B. F. Goodrich Co., Akron, Ohio.
[1] J. C. Bower and W. E. Burcham, Proc. Roy. Soc. **173**, 379 (1939).
[2] E. Pollard, W. L. Davidson, Jr. and H. L. Schultz, Phys. Rev. **57**, 1117 (1940).
[3] H. E. Edgerton, K. J. Germeshausen and H. E. Grier, Phot. J. **76**, 198 (1936).

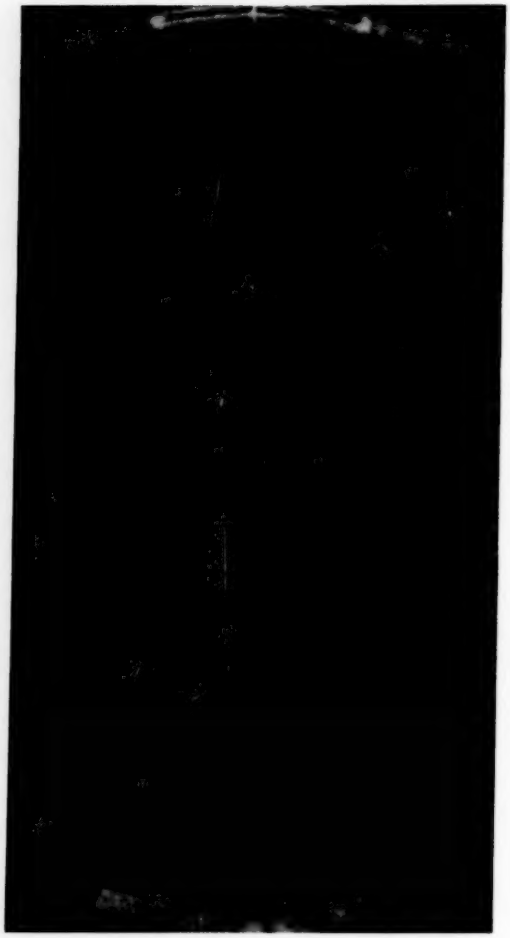

FIG. 1. Protons from aluminum bombarded by deuterons.

Solid targets were mounted directly in the target chamber of the cyclotron. For targets in gaseous form a special cell was built into the target box and isolated from the acceleration chamber by a 2.7-cm air equivalent foil. Protons from the target passed down an evacuated tube and entered the cloud chamber 45 cm from the target proper. All observations were made at a mean angle of 87° with respect to the incident beam, with an angular spread of less than 4° in the horizontal plane and a spread not exceeding $\frac{1}{2}$° in the vertical. Particles suffering small angle scattering with the walls of the evacuated tube were prevented from entering the slot in the cloud chamber by a series of diaphragms. Fog produced by background radiations from the cyclotron was not at all troublesome. In order to make each track clearly distinguishable, an effort was made to keep the number per expansion less than fifteen.

Groups were caused to end successively in the expansion chamber by interposing aluminum foils between the chamber and target. Each foil represented one-half of the total absorption experienced by a particle traversing the diameter of the chamber. This gave rise to overlapping of data with consecutive foils, and thus data taken with different foils could be properly joined up so as to permit the determination of relative intensities of groups.

HOMOGENEITY OF THE CYCLOTRON BEAM

A knowledge of the homogeneity in energy of the incident beam used for bombardment is essential in experiments of the kind being described. Several methods first used in the estimation of spread in energy of the deuteron beam were: (1) visual observation of the beam in air; (2) measurement of the beam current to a collector as a function of absorption introduced in the path of the beam. These preliminary measurements indicated a spread of 0.5 Mev. However, these methods are open to considerable error, and our final estimation is based on the following experiment.

The number-range distribution of deuterons scattered from the beam by a thin gold foil (1 mm air equivalent) was obtained by allowing the scattered particles to enter the cloud chamber. In this case a relative stopping power of 0.71 was used. The angular divergence of the scattered beam was made less than 2°. Figure 2 shows the results. The observed distribution has a width at half-maximum of 0.19 Mev. It is difficult to estimate how much of this width is caused by range straggling introduced by the foils and gas in the chamber. From the distribution curve the difference between extrapolated and mean range is 8 percent of the mean range. Theoretically, if the incident beam were homogeneous, this quantity would be expected to be about 2 percent. If one allows for non-uniformity in the thickness of the foils, 5 percent may be taken as a reasonable figure for the beam itself.

The lower energy peak of small intensity may perhaps be attributed to inelastic scattering. However, if that is the case it is difficult to understand why this peak should be well defined

in view of the close spacing of nuclear levels in gold. Most likely, it is to be associated with two more or less effectively defined ion centers from which ions are withdrawn for acceleration. This condition will of course depend strongly upon the magnetic field corrections used to get a beam, available dee voltage, and clearance between deflector plate and dee. It should be noted that our cyclotron employs the simple filament ion source, and hence ions can be withdrawn from more than one point.

These results indicate a better degree of homogeneity in energy than found with other cyclotrons.[4] This is no doubt because in our case small radiofrequency power input (2 kw) has been used. This, together with a small clearance between deflector plate and dee, imposes the requirement that the beam energy be accurately defined in order that it may be withdrawn into the target chamber.

Protons from C^{12}

The assumption of Russell-Saunders coupling between spins and orbital momenta in the nucleus C^{13} suggests a doublet of which the lower level is the ground state.[5] The separation between the components of the doublet might be expected to be of the order of a few tenths of a Mev with an intensity ratio of 2 : 1, i.e., ratio of statistical weights of the two levels. Whether the spin of the ground state is $\frac{1}{2}$ or $\frac{3}{2}$ depends upon the particular nuclear model chosen. The assumption of a doublet character is in accord with observations of Richardson[6] that a 280-kev γ-ray appears to be emitted in the transition $N^{13} \rightarrow C^{13} + e^+$; also, additional support of this assumption is found in the work of Cockcroft and Lewis[7] who found that the group of protons from carbon bombarded by deuterons is wider than the deuteron-deuteron group. The opposite should be expected if the carbon group is associated with a single level in C^{13}.

An attempt to observe a definite asymmetry in the group of protons arising in the reaction $C^{12}(dp)C^{13}$ has been made with the cloud-chamber method of detection. The higher available energy of 3.2 Mev for bombardment, and hence longer proton range is an advantage since the range-energy relation operates in separating groups more than at low energies.

Several kinds of carbon targets were used. The first consisted of a thin (less than 1 mm air equivalent) layer of Aquadag on a gold foil.

A number-range curve plotted from these data involving several thousand tracks exhibited a definite asymmetry on the low energy side. However, other elements involving shorter and longer range contamination groups were also present as impurities. For that reason, these data were discarded. Final observations were made on purified CH_4 in the gas target cell. The sample kindly supplied by Professor Watson was estimated to contain less than 0.1 percent by volume of the usual impurities, O and N. With a pressure of 14 cm in the cell, the effective thickness of the target was 2 mm air equivalent. A series of diaphragms defining the beam and emerging protons made it impossible for any particle emitted from the walls to reach the cloud chamber directly. It should be noted that only about one-half of the width of the incident beam was used. Hence, the homogeneity in this case probably was somewhat better than shown in Fig. 2.

The results are depicted in Fig. 3. Tracks were grouped so that they ended in intervals of 3 mm. The group appears to be quite symmetrical with a width at half-maximum of 0.6 Mev in good

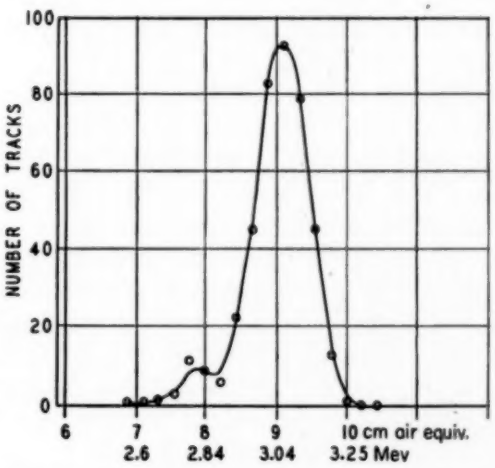

Fig. 2. Number-range distribution of deuterons scattered by a 1-mm air equivalent Au foil. Energy of beam = 3.2 Mev; beam current = 10^{-8} amp.

[4] M. C. Henderson and M. G. White, Rev. Sci. Inst. 9, 19 (1938).
[5] M. E. Rose and H. A. Bethe, Phys. Rev. 51, 205 (1937).
[6] J. R. Richardson, Phys. Rev. 53, 610 (1938); 55, 609 (1939).
[7] J. D. Cockcroft and W. B. Lewis, Proc. Roy. Soc. 154, 261 (1936).

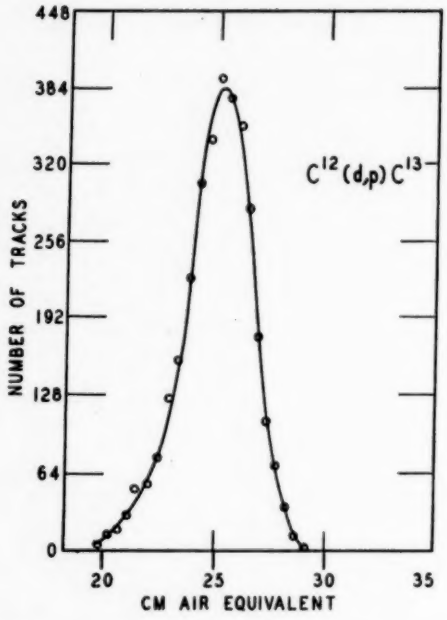

FIG. 3. Protons from carbon bombarded by deuterons. Target in the form of CH_4.

agreement with the work of Cockcroft and Lewis. If the group is a doublet and, a 2 : 1 ratio of intensities of the two components is assumed the separation must be much less than 285 kev. Richardson[8] has also looked for this fine structure and reported a negative result, although details of his work are not given. Watase and Itoh[9] have confirmed the existence of the 285-kev gamma-ray in the spectrum of N^{13}. However, in a private communication Dr. Itoh has kindly pointed out that he finds no indication of the 285-kev excited level in C^{13} from an analysis of the β-ray spectrum of N^{13}.

The curve shown in Fig. 3 does exhibit some asymmetry near the axis on the low energy side, with possibly a slight irregularity at 21.4 cm range. The latter may be accounted for by statistical fluctuations. The asymmetry noted may be connected with the weak low energy component in the deuteron beam. Some additional straggling introduced by the foil isolating the target cell from the cyclotron vacuum chamber, and small but finite target thickness are contributing factors.

[8] T. R. Richardson, Phys. Rev. **55**, 1129A (1939).
[9] Y. Watase and J. Itoh, Proc. Phys. Math. Soc. Japan **21**, 389 (1939).

PROTONS FROM ALUMINUM

The reaction $Al^{27}(dp)Al^{28}$ was first studied by McMillan and Lawrence[10] using an ionization chamber. Their results indicate the presence of five groups with possible intermediate groups that are unresolved. The cloud-chamber method just described has been applied to this problem in the hopes of obtaining higher resolution in the presence of a rather high neutron background from this element. A target of 1.4 mm air equivalent was employed. Tracks ending in 7-mm intervals were grouped together and the number plotted against range as shown in Fig. 4. Correction has been made for the variation of relative stopping power with energy in the aluminum foils[11] used to cause different groups to end successively in the chamber. Some adjustment was necessary to make the data taken with each additional foil join up with those preceding. However, the adjustment was small in each case, and thus the ordinates represent quite accurately the number of tracks actually observed.

The broad fluctuations in the curve may be taken to represent groups in rough agreement with the work of McMillan and Lawrence. However, there are indications that each may be complex, particularly in view of the large width. The end group appears to be complex and consist of at least three components. The fact that the curve does not drop to low or zero value, except possibly in the interval 66–70 cm also suggests a greater number than 5 groups. The authors feel that possibly these broad maxima do not involve individual levels in the Al^{28} residual nucleus, but on the other hand, represent regular fluctuations

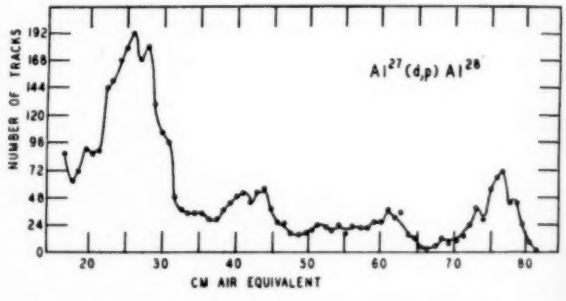

FIG. 4. Protons from a 1.6-mm air equivalent target of Al.

[10] E. McMillan and E. O. Lawrence, Phys. Rev. **47**, 343 (1935).
[11] 1.52 mg/cm^2 = 1 cm air.

in the density (per unit energy) of Al^{28} levels, thus giving the appearance of single groups. Similar tendencies have been noticed in unpublished experiments done at this laboratory on other elements in this mass range. However, in some cases (e.g. Ne and A) pronounced groups are observed where the minima between groups is low compared to the maxima in these groups. This may be taken as evidence for the assumption that the density of nuclear levels is not only a function of the total number of particles from a statistical viewpoint but also depends critically upon the characteristics of a given nucleus, i.e., to what degree the nucleus approximates a closed-shell configuration in neutrons and protons. It is of interest to recall the work of Plain, Herb, Hudson and Warren[12] who found a large number of levels from observations on the excitation function for γ-rays produced in the reaction $Al^{27}(p, \gamma)Si^{28}$.

In comparing the present results on aluminum with those of McMillan and Lawrence it appears that the relative intensity of the groups is different from that published by the above writers. Perhaps this discrepancy results from the fact that the present experiment was conducted at higher bombarding energies, the higher excitation being responsible for this difference in relative intensities. Similar effects have been noted by Pollard, Davidson and Schultz[2] in the case of boron bombarded by deuterons. More likely it is caused by the difference in technique of detection.

In conclusion, it is a pleasure to thank Professor Ernest Pollard for much valuable help and advice. The writers are also indebted to Dr. M. E. Rose for discussion. A grant from the George Sheffield Fund is gratefully appreciated.

[12] G. P. Plain, R. G. Herb, C. M. Hudson and R. E. Warren, Phys. Rev. **57**, 187 (1940).

DECEMBER 15, 1940 PHYSICAL REVIEW VOLUME 58

Protons from the Separated Isotopes of Carbon and Neon under Deuteron Bombardment

HOWARD L. SCHULTZ* AND WILLIAM W. WATSON
Sloane Physics Laboratory, Yale University, New Haven, Connecticut

(Received October 5, 1940)

The protons arising from the bombardment by 2.54-Mev deuterons of CH_4 gas enriched in C^{13} isotope and neon enriched in Ne^{22} have been studied with a cloud chamber. It is shown that the yield of long range protons from the $C^{13}(dp)C^{14}$ reaction is less than four percent of the yield of shorter range protons from the $C^{12}(dp)C^{13}$ reaction at this deuteron energy. This low yield means that the half-life of C^{14} discovered by Ruben and Kamen is considerably less than their estimate and is probably about 100 years. In neon the longest range group of protons discovered by Pollard and Watson is shown to be complex, with an indicated doublet width of the ground state of Ne^{21} of 0.44 Mev. The only proton group definitely indicated for the Ne^{22} bombardment occurs at about 30 cm range.

INTRODUCTION

RECENT improvements in the production of separated isotopes have immediate application to problems in nuclear physics. In studies of proton groups emitted in transmutations, samples enriched in one or more of the isotopes are necessary where: (1) Proton emission caused by the rare isotope is normally so small as to make detection difficult even in the absence of interfering groups from the more abundant isotopes; (2) the group caused by the rare isotope may be fairly strong but be overlapped by equally prominent groups from the abundant species. The transmutation of C^{13} by deuterons is an example of (1), while the situation in the case of neon may follow (2).

This paper presents the results of experiments on the protons from carbon enriched in C^{13} and on neon with and without enrichment in Ne^{22}. The cloud-chamber method of detection of

* Now at the University of Buffalo.

groups described in another paper[1] has been employed. The protons from both elements have previously been studied with the aid of counting technique. For work of this kind with separated isotopes it is more advantageous to use cloud-chamber detection as it enables the counting of every particle and hence the accurate measurements of relative yields.

Production of the Separated Isotopes

The separated isotopes for these bombardment experiments were produced by the thermal diffusion method, as already described by one of us.[2] In particular the "heavy" neon was one of the samples used by Pollard and Watson,[3] with an Ne^{20}/Ne^{22} abundance ratio of about 84/16 as against the normal ratio of 90/10. The heavy methane has been produced in a six-unit, all-copper thermal diffusion apparatus, with a total column length of 12 meters. This apparatus is an extension of the two-unit model which increased the C^{13} content of the CH_4 to 2.77 times the normal amount.[2] Preceding these two 2-meter columns there were placed two additional columns identical in all respects except that the gap space between the hot and cold surfaces was increased $\frac{1}{16}$ inch, while following the two original columns two with this gap space decreased by $\frac{1}{16}$ inch were installed. These changes in dimensions were limited by available sizes of copper pipe, but the "staggering" effect thus produced is not far from that indicated by the Furry, Jones and Onsager theory[4] in order to give a maximum separation factor. All units are based on G. E. $\frac{1}{2}$-inch Calrod heaters with the hot coupling pipes all grouped together around a center post and wound with a common heater, the whole constituting a compact assembly of volume about eight liters.

Without the "staggering" of columns this six-unit model would be expected to give a factor of $(2.77)^3$ or 21. Actually one sample of heavy methane withdrawn after 36 days of operation showed a C^{13} content 22.4 times that in ordinary methane, with indications that equilibrium had not yet been reached and that considerable nitrogen was being accumulated, probably from a small leak in the apparatus. The CH_4 sample withdrawn for the transmutation experiments consisted of 15.6 percent C^{13}, the enrichment being limited by a rather fast withdrawal rate of about 55 cm^3 per day and possibly by increasing accumulation of nitrogen found in the withdrawn gas.

Protons from Carbon

Protons from C^{12} bombarded by deuterons are well known. The yield is quite prolific at bombarding energies of 3 Mev. On the other hand, the transmutation of C^{13} according to $C^{13}(dp)C^{14}$ is not as easily observed. Studies of this reaction have been carried out by two means: (1) observations on the production of radioactive C^{14};[5] (2) direct study of the emitted protons. The latter has been aided by the determination of the mass of C^{14} by Bonner and Brubaker[6] through the reaction $N^{14}(np)C^{14}$. Pollard[7] has detected a weak group at 81 cm range (3.2-Mev incident beam) from a thick target of carbon, while Bower and Burcham[8] using the cloud-chamber method in experiments on proton groups from fluorine found a contamination group which they attribute to C^{13}. On the other hand, Holloway and Moore[9] failed to find this group even though they employed concentrated C^{13}.

Recently, however, Bennett, Bonner, Hudspeth and Watt,[10] using targets prepared from methane with both increased and decreased C^{13} content, have reported measurements on these long range protons from the deuteron bombardment of C^{13}. With an ionization chamber they find that for 1.22-Mev deuterons the ratio of the proton yield from this reaction to that from $C^{12}(dp)C^{13}$ is 6.5 percent for like numbers of

[1] H. L. Schultz, W. L. Davidson, Jr. and L. H. Ott, this issue.
[2] W. W. Watson, Phys. Rev. **57**, 899 (1940).
[3] E. Pollard and W. W. Watson, Phys. Rev. **58**, 12 (1940).
[4] W. Furry, R. Jones and L. Onsager, Phys. Rev. **55**, 1083 (1939).
[5] E. McMillan, Phys. Rev. **49**, 875 (1936); S. Ruben and M. D. Kamen, *ibid.* **57**, 549 (1940); M. D. Kamen and S. Ruben, *ibid.* **58**, 194 (1940).
[6] T. W. Bonner and W. M. Brubaker, Phys. Rev. **49**, 778 (1936).
[7] E. Pollard, Phys. Rev. **56**, 1168 (1939).
[8] J. C. Bower and W. E. Burcham, Proc. Roy. Soc. **173**, 379 (1939).
[9] M. G. Holloway and B. L. Moore, Phys. Rev. **57**, 1086A (1940).
[10] W. E. Bennett, T. W. Bonner, E. Hudspeth and B. E. Watt, Phys. Rev. **58**, 478 (1940).

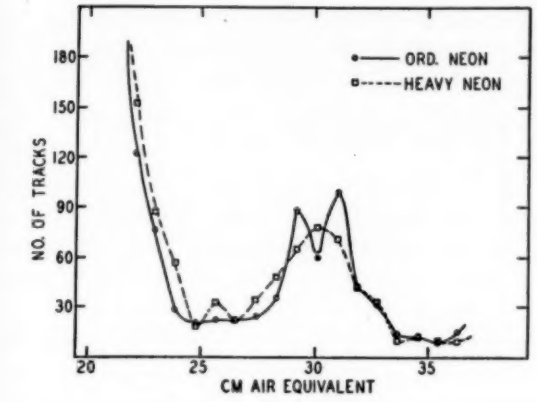

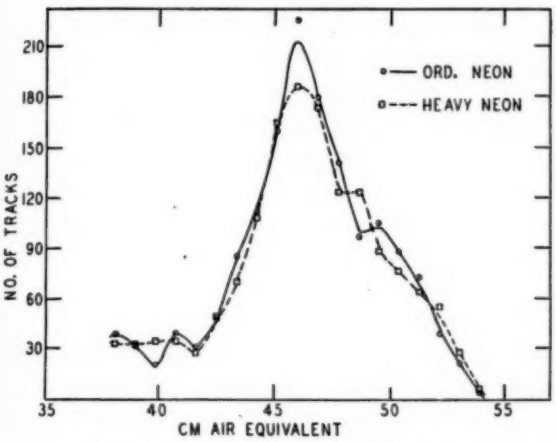

FIGS. 1A (top) and 1B (bottom). Number-range distribution of protons from normal and "heavy" samples of neon bombarded by deuterons.

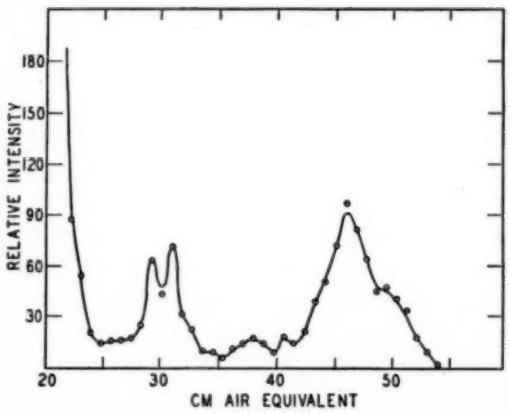

FIG. 1C. Composite curve plotted in terms of arbitrary scale along the ordinate to indicate relative intensities of groups for ordinary neon. Data of Figs. 1A and 1B have been used and adjusted as explained in the text.

atoms. Our cloud-chamber observations are in fair agreement with this value.

Importance attaches to an accurate knowledge of this yield since on it is based the estimate of the half-life of C^{14} recently discovered by Ruben and Kamen.[5] The half-life is too long for direct measurement and must be deduced from a knowledge of the number of atoms of C^{14} formed in a bombardment. From the figures given by Pollard, Ruben and Kamen estimate a half-life of 1000 years for C^{14}. The lower figures of Bennett, Bonner, Hudspeth and Watt would imply a half-life considerably less, about 200 years.

The CH_4 enriched in C^{13} was used at 18 cm pressure in the gas target cell with an effective thickness of 3 mm air equivalent. This sample was purified by condensation with liquid air. Preliminary observations showed a weak but definite group ending at 70 cm range (effective beam energy, 2.54 Mev) in good agreement with mass values assuming that C^{13} was responsible for this group. At the same time, however, protons of much longer range were present, suggesting nitrogen contamination. The sample was then purified much more thoroughly by repeated condensation, pumping off the undesirable residue each time. After this procedure a total of only four tracks of range greater than 35 cm (i.e., passing through chamber), two of which were of doubtful origin, were observed as compared to 720 ending in the chamber due to C^{12}. Since the number of long range tracks was so small, no attempt was made to locate their range by introducing additional foils between the cloud chamber and target. The sample of CH_4 may still have contained about one percent of uncondensed gas, which probably was mostly nitrogen. Hence one or more of these few long range tracks could possibly be from nitrogen.

With a C^{13}/C^{12} abundance ratio of 0.156 in the enriched sample, it must be concluded that the yield from C^{13} is less than four percent of that for C^{12} at the present deuteron energy. This ratio is considerably smaller than that estimated by Pollard (30 percent) and by Bower and Burcham (10 percent) but in fair agreement with that given by Bennett, *et al.* However, Pollard worked at somewhat higher energy, where no doubt the excitation curve for the less probable reaction is steeper than for the C^{12} to C^{13} transition. But it is doubtful whether this difference can be so pronounced as to account for the high yield given, and it is likely that in

his experiments the yield from $C^{12} \rightarrow C^{13}$ was underestimated.

In order to investigate the origin of the weak 70-cm group found with the first sample of enriched CH_4, tank nitrogen was put into the gas target cell at 8 cm pressure. Protons of 70 cm were again observed in somewhat greater numbers. Although nitrogen has not been investigated in detail, there is indication of a new group at a Q value of 5.9 Mev from that element. This weak group does not seem to be the one found by Holloway and Moore.[11]

Protons from Neon

Ordinary neon and neon enriched in the heavier isotope (Ne^{20}/Ne^{22} abundance ratio of 84/16) were bombarded in the gas target cell. Figure 1A shows the results with no absorption between the cloud chamber and target proper other than the basic, while Fig. 1B depicts the data taken with an additional 18-cm absorption in the form of aluminum foils. The first set of data just overlaps the second. In each figure the needed adjustment of one curve with respect to the other has been made so that the same total number of tracks is represented.

Figure 1C represents a combination of the data for the normal sample plotted on a scale of relative intensity of groups. In order to do this these two sets of data from Figs. 1A and 1B were joined so that the total number of tracks passing completely through the chamber with no additional absorption equaled the number ending in the chamber with the additional foils.

There are indications that the broad group of protons distributed about the maximum at 46 cm range is complex, and that it arises very largely from the Ne^{20} in both gas samples. The total number of tracks represented by the plots in Fig. 1B is large enough to guarantee that the irregularity and asymmetry on the high energy side of this group are real. This less intense group of protons on the high energy side has an extrapolated range of 54.2 cm while that of the more intense component comes at about 48.5 cm. This interval of roughly 0.44 Mev may well represent the doublet splitting of the ground state of the Ne^{21} nucleus formed in the reaction.

The Ne^{21} nucleus is also formed in the reaction $Na^{23}+H^2 \rightarrow Ne^{21}+He^4$ studied by Murrell and Smith.[12] It would be interesting to see whether the doublet structure of the ground state also appears here. However, their maximum energy group is somewhat overlapped by an oxygen group, and in addition the difference of 0.4 Mev would represent only a small difference in α-particle range. Hence it is difficult to say whether or not this doubling is present in their case.

Between 35 cm and 42 cm range there seem to be a number of weak proton groups, with one at 40 cm due to Ne^{22}. Also at about 30 cm range we observe a definite difference between the protons from ordinary neon and those from the neon enriched in the heavy isotope. Whereas there is an apparent doubling of the proton group at 30 cm with ordinary neon, the group appears single when the gas with the larger Ne^{22} content is bombarded. At about this range then there seems to be definitely a proton group resulting from the deuteron bombardment of Ne^{22}.

Associated with the doublet at 30.2 cm and 33.5 cm the Q values are 2.78 and 2.94 Mev, respectively. This is apparently the first excited state of Ne^{21}. As for the Ne^{23} resulting from the Ne^{22} bombardment, the proton group at 40 cm has a corrected extrapolated range of 41.5 cm which is a Q value of 3.5 Mev. The first excited state of Ne^{23} comes then at about 2.85 Mev, the mean of the values of the first excited state of the Ne^{21} nucleus.

These results with neon are in substantial agreement with those of Pollard and Watson[3] obtained by amplifier detecting methods. As already noted in this earlier work, the bombardment of Ne^{22} does not give rise to any strong proton groups, in agreement with the fact that the induced radioactivity of the resulting Ne^{23} is weak. It is evident that a considerably greater concentration of Ne^{22} is necessary in order to establish definitely the location of all the proton groups from this isotope.

We wish to thank Professor Ernest Pollard for much helpful advice and encouragement, and Dr. D. Rittenberg of Columbia University for the mass-spectrometer analysis giving the C^{13} enrichment.

[11] M. G. Holloway and B. L. Moore, Phys. Rev. **56**, 705 (1939).

[12] E. B. M. Murrell and C. L. Smith, Proc. Roy. Soc. **173**, 410 (1939).

Broadening, Asymmetry and Shift of Rubidium Resonance Lines under Different Pressures of Helium and Argon up to 100 Atmospheres

CH'EN SHANG-YI*
Norman Bridge Laboratory, California Institute of Technology, Pasadena, California
(Received September 23, 1940)

A new absorption tube was constructed which made feasible the study of the pressure effects of foreign gases on the absorption lines of alkali vapors of homogeneous density and temperature. In addition to helium and argon at pressures up to 100 atmospheres, hydrogen was used up to 20 atmospheres. Up to relative density 46 the broadening is proportional to the concentration of helium or argon gas. The slopes of the half-width *vs.* relative density curves are 0.735 cm^{-1} and 0.594 cm^{-1} per unit relative density of helium for $^2P_{3/2}$ and $^2P_{\frac{1}{2}}$ components, respectively, and the corresponding values for argon are 0.855 cm^{-1} and 0.627 cm^{-1} per unit relative density. Helium produces a violet, argon a red asymmetry. The degree of asymmetry increases as the concentration of foreign gas increases, and is comparatively much greater for argon. For argon the asymmetry of the $^2P_{3/2}$ component is greater than that of the $^2P_{\frac{1}{2}}$ component, while for helium the reverse is true. Argon produces a greater shift than helium. The former produces a strong red shift, the latter a violet shift. For both gases the shift of the $^2P_{\frac{1}{2}}$ component is greater than that of the $^2P_{3/2}$ component. For helium the shift appears to be proportional to the relative density, and the shift of the longer wave-length component is about twice as great as that of the shorter wave-length component, while for argon the shifts for the doublet components are quite close, and the relation between shifts and relative densities obeys in general the 3/2 power relationship. Optical collision diameters as calculated from the half-width data are 13.37A and 7.753A for Rb–A and Rb–He, respectively. From the measurements of the amount of total absorption from the line contours, f values and the transition probabilities were evaluated.

INTRODUCTION

TO realize the advantages of the corrosion resistant MgO windows,[1] in absorption measurements on metallic vapors it is necessary to design a mounting for them which will remain pressure-tight during repeated heating and cooling of the tube. Margenau and Watson[2] made an absorption tube whose windows could be heated, but they confessed to only partial success at overcoming leakage. Prior to that time high pressure tubes were of the old form with water cooling at both ends.[3] Under such conditions it is impossible to determine many physical constants from the measurement of the absolute absorption coefficients because the optical path in the absorbing vapor is unknown and neither the absorbing nor the perturbing atom have a homogeneous concentration in the tube. In addition experimental troubles arise of the kind pointed out by Ny and the author[3] and later confirmed by Füchtbauer and Heesen.[3]

In the present research, an absorption tube was made which is perfectly pressure-tight both at low and at high pressures. The pressure effects of helium and argon on the resonance lines of rubidium were studied under pressures up to 100 atmospheres (also with hydrogen up to 20 atmospheres). Furthermore, MgO windows were used so that the length of the optical path in the rubidium vapor was known. The optical collision diameters, and the area under the absorption line contours, were determined, leading to the evaluation of the oscillator strength of the atom and of the transition probabilities.

APPARATUS AND EXPERIMENTAL PROCEDURE

The construction of the absorption tube is shown in Fig. 1. A is a steel pressure tube $1\frac{1}{2}$ inches in diameter with $\frac{3}{16}$ inch wall thickness. At the middle of the tube was connected very strongly by iron soldering a side tube S about 7 inches long whose end was ready to connect by a union with a cross tube. Inside the pressure tube was placed an inner absorption tube about 26 cm long with an MgO window $\frac{3}{4}$ inch in diameter and $\frac{1}{8}$ inch thick at each end. The ends were closed tightly by pressing the MgO windows on the sharp edges of the tube ends. At the central part of the tube there was a side-tube

* Research Fellow of the China Foundation for the Promotion of Education and Culture. Now at Yenching University, Peiping, China.

[1] J. Strong and R. T. Brice, J. Opt. Soc. Am. **25**, 207 (1935).

[2] H. Margenau and W. W. Watson, Phys. Rev. **44**, 92 (1933).

[3] For example: Ny Tsi-Zé and Ch'en Shang-Yi, Phys. Rev. **51**, 567 (1937); **54**, 1045 (1938); C. Füchtbauer and W. v. Heesen, Zeits. f. Physik **113**, 323 (1939).

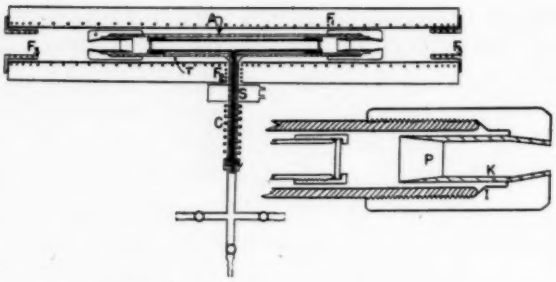

FIG. 1. The absorption tube.

thinner than S. This thinner side-tube was screwed to the inner absorption tube and could be taken off very easily.

The essential difficulty in constructing the pressure tube was to make the pressure-tight windows whose construction is shown in the insert of Fig. 1. The whole window frame was made of the same material as that of the main pressure tube except the Pyrex glass window P and the Kovar cone K which held the window. When the window frame is screwed on to the ends of the pressure tube, the inclined part, I, of the frame is pressed very tightly on the round and smooth end of the pressure tube. This serves as an excellent and permanent pressure seal because the tube end and the window frame contract or expand equally at various temperatures.

The thin Kovar cone was united with the steel frame by silver soldering. Before the glass window was put in position the Kovar cone was ground so that it fitted very nicely with the polished conical glass. Very thin aluminum rings were employed in the gasket.[4] The Pyrex glass was pressed into the Kovar cone while the whole was heated to about 250°C at which temperature the aluminum ring became soft. As Kovar metal has nearly the same coefficient of expansion as that of Pyrex glass, the window was tightly fitted in the cone at all temperatures. The slight difference between the expansion of the two materials was taken up by the elasticity of the thin cone.

The Pyrex glass window was 2 cm thick and $\frac{3}{4}$ inch in diameter and the angle of the cone was about 5°. If the angle was greater than 7° the window leaked even with the above method. Obviously, there will be no difficulty if the Pyrex glass is replaced by fused quartz when observations are to be made in the ultraviolet region.

The absorption tube was uniformly heated by the furnace F_1 which was made by winding Chromel wire on steel cyclinders covered by asbestos paper. The whole furnace, F_1, consisted of two sections which were connected at the position of the side tube. The windings were so made that when the side tube was heated by a small furnace, F_2, the main absorption tube could be heated uniformly to about 240°C as shown by the thermocouple probe. When the furnace had to be heated to still higher temperatures, additional furnaces, F_3, were added on both ends. They were used to compensate the heat loss of the ends to the surroundings.

The furnace F_2 was made by simply winding the resistance wire around the side tube protected by asbestos paper and mica. The furnaces F_3 were made by first winding the heating wire on a cylinder covered with asbestos then putting it inside another bigger cylinder forming a very compact and removable heating unit. The temperature of the absorption tube was measured by an Alumel-Chromel thermocouple, whose hot junction was fastened tightly by a steel ribbon on the pressure tube at the position T in the figure. The whole furnace was placed in a box full of asbestos powder. As the side tube had to be put below the absorption tube the box was placed on a table with a large hole in the center. In this way the cold gas in the side tube would not flow into the absorption tube on account of its density being higher than that of the hot gas in the main tube.

Water cooling was applied immediately outside of the heating box to cool the side tube. The upper jacket was composed of two semicylindrical vessels which could be applied and taken off much more conveniently than the copper coils below. The function of the water cooling was not only to keep the cross tube and the needle valves cooled but also to condense the rubidium vapor if it escaped from the absorption tube A. Thus this arrangement served to give a connection between the outer and the inner tubes for the foreign gas, but not for the alkali vapor.

[4] Copper rings were tried. They did not work because of the hardness of copper. Gold rings would be even better than aluminum because gold is softer and has a still higher melting point.

Three needle valves were used; one led to the pressure tank containing foreign gas, one to the pressure gauge, and one to the high vacuum pump. Between the valve and the gas tank was a thick-walled copper tubing and a condensing spiral to feed the foreign gas back into the tank after the experiment was completed. Three pressure gauges were used. They served to measure the pressure in three ranges, 1–300 lb., 1–600 lb., and 1–3000 lb. They were calibrated by means of a standard pressure gauge. The first two gauges were calibrated to read pressures accurately to 1 lb., while the third one could be read to 10 lb.

The helium gas[5] was obtained originally from evaporation of liquid helium, and was once more purified by an absorption method to eliminate contaminations by the sealing liquid during storage. The total impurity at the source is estimated to be smaller than 0.01 percent. The small trace of impurity would be hydrogen. The argon tank was supplied by the Ohio Chemical and Manufacturing Company, Cleveland. The purity was 99.6 percent. The impurity would be nitrogen. The hydrogen tank was supplied by the Cryogenic Laboratory of this Institute. The gas was claimed to be about 99.5 percent pure.

During experiment the absorption tube was first cleaned and the absorbed gas in the tube wall was removed by long pumping and heating. Then metallic rubidium, which was prepared by reducing RbCl with Ca, was introduced into the absorption tube in a current of nitrogen. With the 21-foot grating and a high intensity tungsten filament lamp the absorption spectrum of rubidium was taken when the pure foreign gas was admitted into the tube and the tube was heated to a certain temperature. The temperature was adjusted at each pressure of the foreign gas so that the absorption was less than total in the center of the resonance lines in order that true line contours could be registered.[6] To measure the density gradations in the absorption lines, the plate (Eastman Type $I-R$) was calibrated by a step weakener placed in the plateholder just on one side of each absorption line. An iron arc spectrum was superposed on both sides of the main exposure as a comparison.

Results and Discussion

(a) Broadening

The half-widths of the Rb resonance lines broadened by different concentrations of helium, argon, and hydrogen are tabulated in Table I. As shown in Fig. 2 the half-widths turn out to be proportional to the relative densities of these gases, indicating the predominance of velocity broadening even in this high pressure range. The slopes of these curves are 0.735 cm^{-1} and 0.594 cm^{-1} per unit relative density of helium for $^2P_{3/2}$ and $^2P_{1/2}$ components, respectively, and the corresponding values for argon are 0.855 cm^{-1} and 0.627 cm^{-1} per unit relative density.

It is to be noted that the broadening by argon is greater than that by helium and the broadening of the shorter wave-length component is slightly greater than that of the longer wave-length one for both gases. Watson and Margenau[7] and Hull[8] have shown in their results for sodium (with H_2, N_2 and A) and potassium (with N_2 and A) that there is no significant difference between the half-widths of the doublet components for resonance lines and also for the second doublet of the K principal series. But Petermann[9] found that the blue Cs doublet and the corresponding K doublet show about 20 percent greater broadening for the shorter wave-length component when broadened by hydrogen. Ny and the author[10] found that for helium and neon the half-width of the $^2P_{1/2}$ component of the second doublet of Rb principal series is greater than that of the $^2P_{3/2}$ component, while for argon the half-width of the $^2P_{1/2}$ component is slightly greater. In the present research the results for argon are in harmony with

[5] Thanks are due to Professor A. Goetz, the Director of the cryogenic laboratory of California Institute, for his generous permission and help in using his pure helium.

[6] In order to approach as much as possible the theoretical assumptions it is certainly desirable to use low temperatures so that the influence of atomic motion of Rb be eliminated. But, since the area under the absorption line contour depends on the concentration of absorbing atoms, the line will be diffused out when it is broadened; therefore the temperature of the absorption tube had to be raised to a high value, so that the absorption of the line could be easily measureable.

[7] H. Margenau and W. W. Watson, Phys. Rev. **44**, 92 (1939).

[8] G. F. Hull, Phys. Rev. **50**, 1148 (1936).

[9] Petermann, Zeits. f. Physik **87**, 96 (1933).

[10] Ny Tsi-Zé and Ch'en Shang-Yi, Phys. Rev. **52**, 1158 (1937).

TABLE I. *Broadening, asymmetry and shift of the resonance lines of* Rb *produced by* He, A, *and* H_2.

P ATM.	T °K	RELATIVE DENSITY	HALF-WIDTH IN CM^{-1} 7947	7800	ASYMMETRY (7947) (1)	(2)	(7800) (1)	(2)	SHIFT 7947	7800
				(*a*) *Rubidium/helium*						
									(violet)	(violet)
3.95	447	2.41	1.61	1.79	0.95	0.911	1.00	0.988	0.39	0.19
8.98	455	5.39	3.07	3.69	0.98	0.967	1.01	0.990	1.85	0.95
20.48	461	12.13	7.86	9.18	0.97	0.843	0.98	0.961	2.89	1.52
41.10	463.5	24.21	16.95	17.08	0.78	0.772	0.88	0.874	5.76	2.26
77.29	569	37.08	21.74	27.80	0.83	0.782	0.90	0.832	7.54	2.62
96.62	579.5	45.52	27.80	33.21	0.86	0.777	0.99	0.748	10.88	4.40
98.79	581.5	46.36	—	34.46						
				(*b*) *Rubidium/argon*						
									(red)	(red)
2.72	440	1.69	1.30	1.21	1.07	1.128	1.41	1.538	0.82	0.36
6.12	515	3.24	2.76	3.16	1.39	1.588	1.50	1.654	1.03	0.48
10.21	517.5	5.39	3.37	3.42	1.56	1.661	1.50	1.702	1.69	1.33
19.94	527	10.33	7.22	7.29	1.79	1.975	1.71	1.912	4.63	3.99
41.16	552	20.36	15.10	19.46	1.42	1.387	1.60	1.641	11.01	9.64
71.44	569	34.28	22.65	32.39	1.38	1.374	1.80	1.825	20.23	19.63
85.73	576.0	40.63	24.99	34.48	1.33	1.395	1.58	1.658	24.17	26.04
97.98	576	46.44	28.00	39.02	1.36	1.352	1.63	1.568	29.90	29.85
				(*c*) *Rubidium/hydrogen*						
									(violet)	(red)
3.47	457	2.07	—	—	—	—	—	—	1.32	1.33
20.00	462	11.82	7.73	10.26	1.18	—	1.00	—	1.63	1.61

those of the author's former experiment for the second member of Rb principal series. The difference between the half-widths of the doublet components detected both by the former[11] and by the present researches suggests again that the perturbing effect of neighboring atoms (similar or dissimilar) may be different for different j values.

(b) Asymmetry

In the 6th–9th columns of Table I the asymmetry of the broadened Rb resonance lines produced by He, A and H_2 are given both in the ratios of the red half to the blue half of the half-widths as listed in the sixth and the eighth columns represented by (1) and in the ratios of the areas under the red half to those under the violet half of the line contour as represented by (2).

Helium produces a violet asymmetry, while argon produces a red asymmetry. The degree of asymmetry increases as the concentration of helium or argon increases. For helium the degree of asymmetry is a little greater for the longer wave-length component, while for argon the degree of asymmetry for the shorter wave-length component is greater. For argon the degree of asymmetry first increases very rapidly with the increase of concentration, then attains a weak maximum around relative density 10; finally the asymmetry drops slightly to a nearly constant value. The degree of asymmetry produced by helium is comparatively much lower than that produced by argon. The asymmetry was small when the relative density was below 10, but increased gradually with the increase of concentration. The asymmetry produced by the hydrogen is quite small.

The values listed under the columns numbered (1) and (2) permit interesting comparison of the two ways of describing the nature of the asymmetry of the line contours. The first way (the ratios of the halves of the half-widths as represented by (1)) gives in general the asymmetry at nearly the central portion of the line. The asymmetry at the far wings is not given. While the second way (the ratios of the areas under the line contour as represented by (2)) is a more sensitive way of measuring the asymmetry for the asymmetry of the line affects the area more conspicuously than it does the half-width. The asymmetries were most pronounced near the

[11] Ch'en Shang-Yi, Phys. Rev. **58**, 884 (1940).

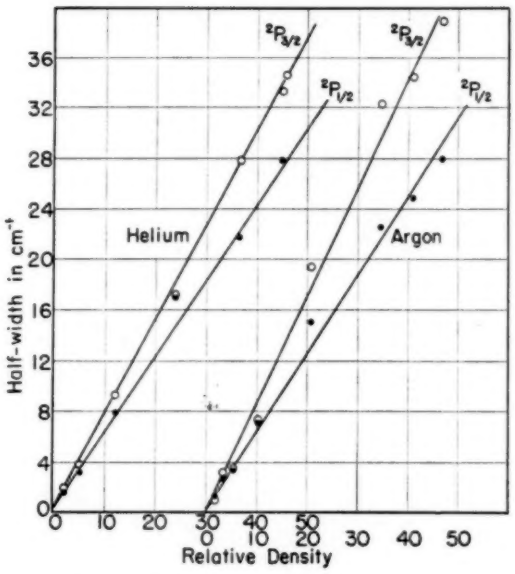

FIG. 2. Half-width *vs.* relative density.

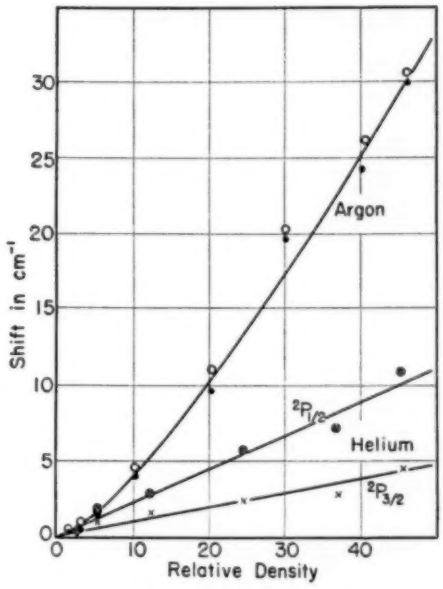

FIG. 3. Shift *vs.* relative density.

base of the line. The values of the eighth and the ninth columns for helium in the table give a good illustration.

Although three figures are recorded in expressing the degree of asymmetry, the last figure has very little significance as regards the accuracy of measurement. The chief source of error is in the planimetric measurement near the end of the wings. The wing stretched very far on both sides of the wings especially the side which showed asymmetry, a little error in tracing the line contour would affect the area by a considerable amount.

(c) Shift

The displacement of the central maxima of the Rb resonance lines produced by helium and argon are also given in Table I, and are plotted in Fig. 3. Argon produced a greater shift than helium. The former produces a strong red shift while the latter a violet shift. For both gases the shift of the $^2P_{1/2}$ (λ7947) component is greater than that of the $^2P_{3/2}$ (λ7800) component. This phenomenon is shown very obviously in Fig. 4.

In Fig. 4 is given a direct comparison of the positions of the Rb resonance lines, with and without the effects of foreign gases. Figure 4(a) is the spectra taken with the absorption tube containing pure rubidium vapor at very low pressure (10^{-2} mm Hg), Fig. 4(b) is that taken when the pure Rb vapor pressure was increased to about 4 mm Hg, and Figs. 4(c) and (d) are the spectra taken when foreign gases were introduced. As pointed out in the previous article,[11] and also shown here, the very small shift of Rb resonance lines caused by the pressure of its own vapor, and the large shift of the lines produced by foreign gases are strikingly illustrated.

It is well known that the shift of the resonance lines produced by foreign gases is the smallest among the series lines.[12] Thus it is easy to imagine that under so large a foreign gas pressure (100 atmospheres) the shift for higher series members would be as large as one hundred angstrom units.

It is to be noted from Fig. 3 that for helium the shift appears to be proportional to the relative density, while for argon there is a noticeable departure from the linear relationship. For argon the shifts for the two doublet components are very nearly the same, while for helium the shift of the longer wave-length component is about twice as great as for the shorter wave-length component. Hydrogen produces a violet shift on the longer wave-length component and a red shift on the shorter wave-length component.

The difference between shifts of the two components has already been pointed out by Mar-

[12] For instance, see Füchtbauer, Schulz and Brandt, Zeits. f. Physik **90**, 403 (1934); Ny Tsi-Zé and Ch'en Shang-Yi, Phys. Rev. **51**, 567 (1937); **54**, 1045 (1938).

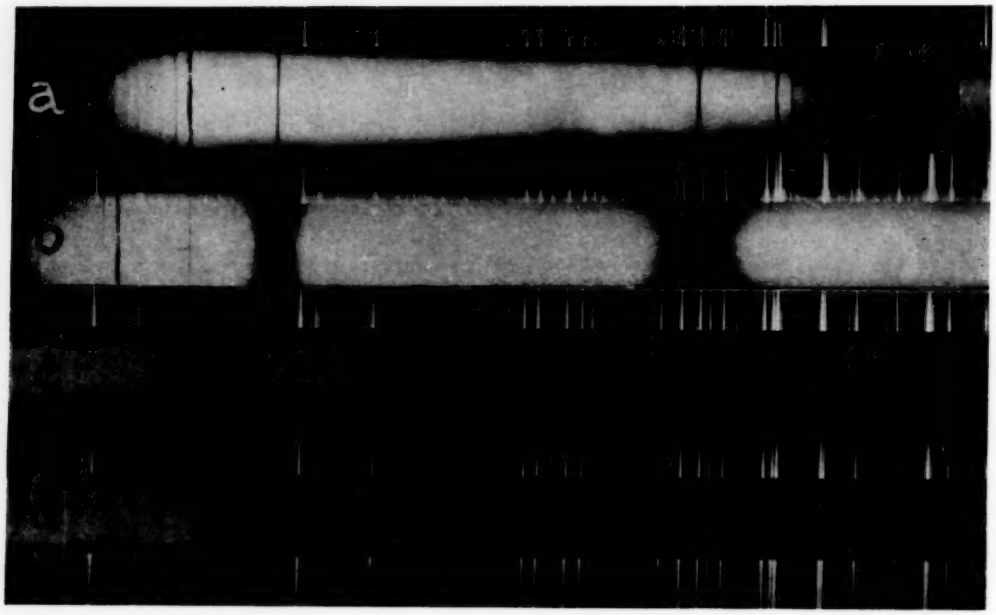

FIG. 4. Positions of rubidium resonance lines. (a) Under 10^{-2} mm pressure pure vapor ($T=190°C$). (b) Under 4 mm Hg pressure pure vapor ($T=347°C$). (c) Under 97.98 atmospheres argon ($T=303°C$). (d) Under 96.62 atmospheres helium ($T=306.5°C$).

genau and Watson[7] and Hull[8] in their experiments on effects of nitrogen and argon on potassium resonance lines and also by Ny and the author[10] in their experiment on the effects of rare gases on the second member of Rb absorption series.

The relation between the shift and the relative density is still an unsolved problem. Both the linear and the quadratic relations were predicted and observed. Ny and the author[10] found that for argon the shift of the second member of Rb principal series appears to be proportional to the square of the relative density in conformation with Kuhn's theory.[13] In the present case, however, the shift of the lines produced by helium is linearly proportional to the relative density, but for argon the relation between shift and relative densities obeys in general the 3/2 power relationship. The accuracy of locating the positions of the maxima of these lines was estimated; the greatest possible error should not be more than 2 percent. It is evident that, for low members, the relationship between shift and relative density depends on the nature of foreign gas added as well as the member of the series and

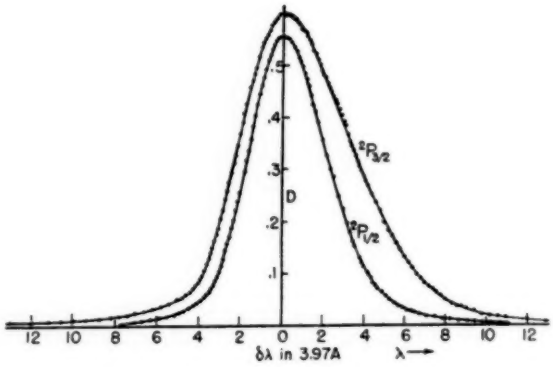

FIG. 5A. $\text{Log}_{10}\, I_0/I$ *vs.* δλ. Argon pressure 97.98 atmospheres; ($T=576°K$).

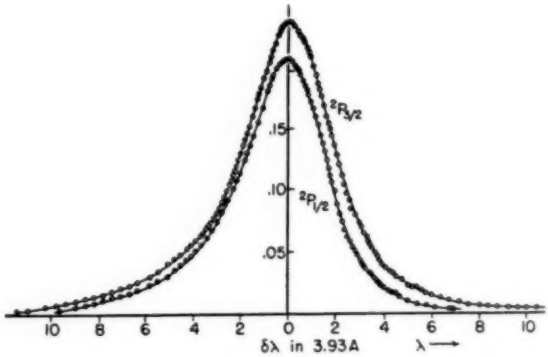

FIG. 5B. $\text{Log}_{10}\, I_0/I$ *vs.* δλ. Helium pressure 96.92 atmospheres; ($T=579.5°K$).

[13] H. Kuhn, Phil. Mag. **18**, 987 (1934); Phys. Rev. **52**, 133 (1937).

the nature of the absorbing atom. Further theoretical investigation seems very desirable.

(d) The evaluation of f values and transition probabilities

Oscillator strengths and transition probabilities were computed from the amount of the total absorption[14] $\int_0^\infty (n\kappa)d\nu$ which was obtained by graphical integration of the line contours as illustrated in Figs. 5*A* and 5*B*. Thus

$$\int_0^\infty (n\kappa)d\nu = (2.303\times 3\times 10^{10}/4\pi l\lambda)\int_0^\infty D\delta\lambda,$$

where $D=\log_{10} I_0/I$, and $n\kappa$ is the electron theory absorption coefficient. According to radiation theory the oscillator strength of the atoms, i.e., the f value, is

$$f=(4\nu m/ne^2)\int_0^\infty (n\kappa)d\nu$$

and the transition probability, A, is

$$A=(4\pi/cnh)\int_0^\infty (n\kappa)d\nu$$

$$=(\pi e^2/ch\nu m)f.$$

Substituting the numerical constants

$$f=(6.086\times 10^6/n)\int_0^\infty (n\kappa)d\nu \quad \text{for } \lambda 7800$$

$$=(5.974\times 10^6/n)\int_0^\infty (n\kappa)d\nu \quad \text{for } \lambda 7947$$

TABLE II. *The f values of* Rb *resonance lines under different pressures of foreign gases.*

T°K	p MM Hg	n	R.D.	f_2	f_1
		(a) *Rubidium/helium*			
447	1.25×10^{-2}	2.71×10^{14}	2.41	0.780	0.467
455	1.79×10^{-2}	3.81×10^{14}	5.39	0.614	0.323
461	2.32×10^{-2}	4.88×10^{14}	12.13	0.463	0.253
463.5	2.582×10^{-2}	5.404×10^{14}	24.21	0.307	0.186
569	1.00	1.70×10^{16}	37.08	0.202	0.152
579.5	1.337	2.238×10^{16}	45.52	0.0884	0.0742
		(b) *Rubidium/argon*			
440	9.00×10^{-3}	1.98×10^{14}	1.69	0.595	0.281
515	1.58×10^{-1}	1.98×10^{15}	3.24	0.582	0.301
517.5	2.023×10^{-1}	3.792×10^{15}	5.39	0.503	0.264
527	2.78×10^{-1}	5.12×10^{15}	10.33	0.511	0.253
552	6.08×10^{-1}	1.07×10^{16}	20.36	0.378	0.220
569	1.00	1.70×10^{16}	34.28	0.253	0.172
576.0	1.214	2.044×10^{16}	40.63	0.304	0.194
576	1.214	2.04×10^{16}	46.44	0.305	0.197

[14] Cf. H. Margenau and W. W. Watson, Rev. Mod. Phys. **8**, 29 (1936).

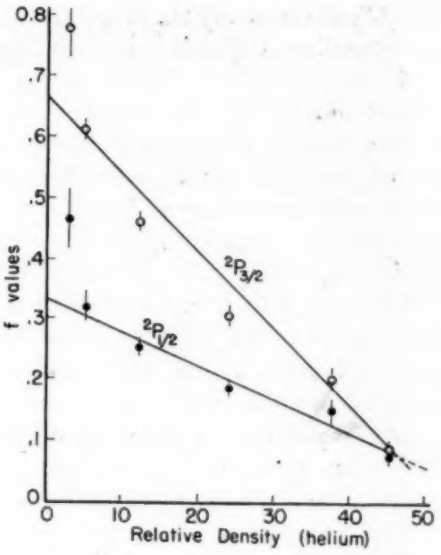

FIG. 6A. f values *vs.* relative density of helium.

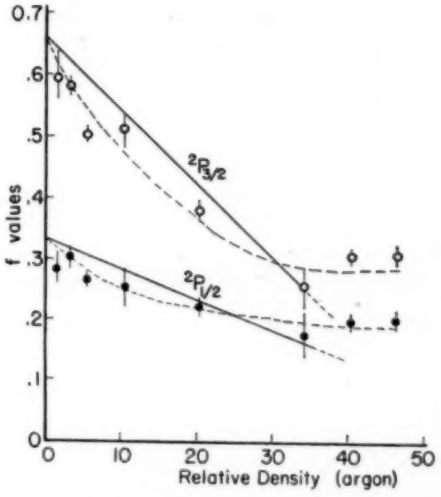

FIG. 6B. f values *vs.* relative density of argon.

and

$$A=1.050\times10^{10}f \quad \text{for } \lambda 7800$$

$$=1.070\times10^{10}f \quad \text{for } \lambda 7947.$$

In Table II are listed the f values when the lines were broadened by foreign gases. There p and n stand for the vapor pressure and the concentration of the alkali vapor and R. D. the relative density of foreign gas. The f values of the resonance lines without the presence of foreign gases were found by extrapolating to zero density of foreign gas as shown in Figs. 6*A* and 6*B*. The results are 0.33 and 0.66 for the $^2P_{1/2}$

and the $^2P_{3/2}$ components, respectively, and the corresponding transition probabilities are 6.93×10^9 and 3.53×10^9. These results agree with the results of Na, K and Cs resonance lines as measured by Minkowski, etc.[15] As shown in Figs. 6A and 6B readings for low foreign gas concentrations were not as accurate owing to the inaccuracy in obtaining $\int_0^\infty(n\kappa)d\nu$. Also the readings for argon in Fig. 6B are not as good as those for helium. This might be due to the fact that the argon was not as pure as the helium; impurities such as O_2, N_2 and H_2[16] would remove some Rb atoms causing a decrease in absorption. Great care was taken to heat the absorption tube for a long time after the foreign gas was inserted, in order to be sure that the saturation of the alkali vapor in the absorption tube was recovered after the vapor had been condensed by the cold foreign gas or caught by impurity atoms.

(e) The optical collision diameters

These can be computed from the observed half-widths, using the relation

$$\rho^2=[\pi\Delta\nu_{\frac{1}{2}}/2n(2\pi kT)^{\frac{1}{2}}][mM/(m+M)]^{\frac{1}{2}}$$

where m and M are the masses of the absorbing and of the perturbing atoms, respectively; taking

$$\Delta\nu_{\frac{1}{2}}/n=0.665\ \text{cm}^{-1}\ \text{for helium}$$
$$=0.741\ \text{cm}^{-1}\ \text{for argon},$$

which are the mean values for the doublet components. Then for argon and Rb $\rho=13.37$A, while for helium and Rb $\rho=7.75$A.

Finally, the author takes pleasure in expressing his gratitude to Professor I. S. Bowen for his supervision throughout the research. He is also indebted to Messrs. J. Pearson and S. C. Lin for their help in various ways.

[15] Cf. A. C. G. Mitchell and M. W. Zemansky, *Resonance Radiation and Excited Atoms* (Macmillan, 1934), p. 146.

[16] N_2 and H_2 will react with rubidium when the pressure is increased higher than about thirty atmospheres.

DECEMBER 15, 1940 PHYSICAL REVIEW VOLUME 58

Pressure Effects of Hydrogen and Nitrogen on the Second Doublet of Rb Principal Series

CH'EN SHANG-YI AND PAO CHIA-SHAN
Physics Department, Yenching University, Peiping, China

(Received October 11, 1940)

Pressure effects of nitrogen and hydrogen on the second doublet of the rubidium principal series, were studied at pressures up to 13 atmospheres. Both for hydrogen and nitrogen the $^2P_{3/2}$ component broadens more conspicuously than the $^2P_{\frac{1}{2}}$ one, and the relationship between the half-width and the relative density is linear. Nitrogen produces a red shift for both components, while hydrogen has a weaker red shift for $^2P_{3/2}$ and a stronger violet shift for $^2P_{\frac{1}{2}}$. The departure from a linear relationship between shift and the density of the perturbing gases is quite manifest. Study of the line contours reveals marked asymmetry, toward the red in the case of nitrogen and slightly toward the blue for hydrogen. The relationship between the half-width and the shift is discussed.

INTRODUCTION

IN sequel to the previous observations on the pressure effects of rare gases on the second doublet of rubidium principal series,[1] the same problem was studied with hydrogen and nitrogen at pressures up to 13 atmospheres. The experimental procedure was essentially the same as that of the previous research. Commercially pure hydrogen and nitrogen (the purity was about 99.5 percent) were used. The results obtained in the present research were compared with those for other alkalis.

[1] Ny Tsi-Zé and Ch'en Shang-Yi, Phys. Rev. **52**, 1158 (1937).

Results and Discussion

(a) Broadening

The results of broadening of the second doublet of the rubidium principal series perturbed by hydrogen and nitrogen are given in the fourth and fifth columns of Table I. These values are expressed in terms of half-width in cm^{-1} of the two doublet components, and are plotted in Fig. 1. It is to be noted that hydrogen produces a much greater broadening than nitrogen, and that a marked difference between the half-widths of the doublet components appears. The difference of the doublet components has also been observed by Ny and Ch'en in their experiment on rubidium perturbed by rare gases.[1] In hydrogen and in nitrogen the half-width of the $^2P_{3/2}$ component is greater than that of the $^2P_{\frac{1}{2}}$ component. The relationship between the half-width and the relative density is linear for nitrogen but for hydrogen the relationship is found to be linear for foreign gas concentrations up to relative density 6. Beyond this point, the half-width increases more rapidly than linearly.

(b) Shift

The results of measurements of the shift of the doublet components produced by the two gases are given in the sixth and the seventh columns of Table I, and are plotted in Fig. 2. All these curves show noticeable departure from linear relationship. Thus the values of the slopes shown in Table II are rather approximate.

In hydrogen the $^2P_{\frac{1}{2}}$ component has a violet shift, whereas the $^2P_{3/2}$ component shifts slightly towards the red. The shift of the former is nearly three times as much as that of the latter. Nitrogen, however, produces a red shift for both components of the doublet, in agreement with the other alkali metals.

(c) Asymmetry

The degree of asymmetry is described by the ratio of the red half to the blue half of the half-width, as shown in the last two columns of Table I. The relation between the asymmetry and the relative density is shown in Fig. 3. Nitrogen produces a strong red and hydrogen a weak violet asymmetry.

In general, a red shift is followed by a red asymmetry and vice versa. But here, for hydrogen, the $^2P_{3/2}$ component has a slight red shift and

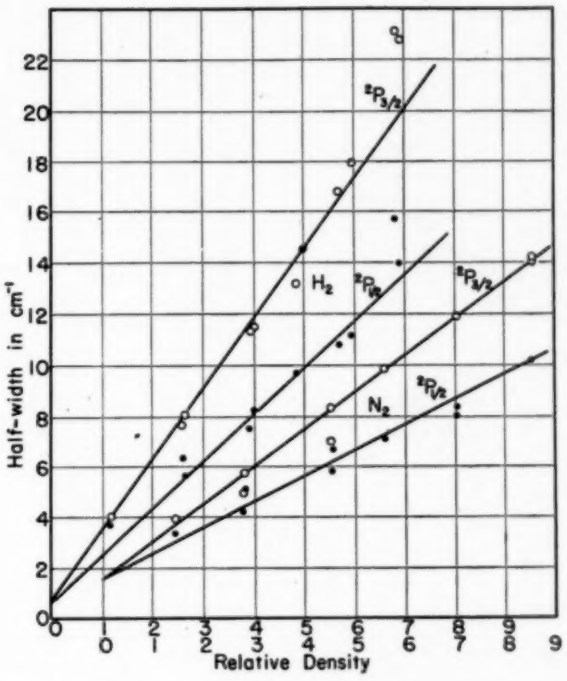

FIG. 1. Half-width in cm^{-1} *vs.* relative density.

TABLE I. *Broadening, asymmetry and shift of the second doublet of rubidium principal series perturbed by hydrogen and nitrogen.*

p atmos.	t °K	Relative Density	Half-Width (cm^{-1}) (λ4202)	Half-Width (cm^{-1}) (λ4216)	Shift (cm^{-1}) (λ4202)	Shift (cm^{-1}) (λ4216)	Asymmetry (λ4202)	Asymmetry (λ4216)
			(a) Rubidium in hydrogen		(red)	(violet)		
1.78	422	1.17	4.06	3.52	0.18	0.62	0.98	1.00
4.07	421	2.57	7.60	6.31	0.30	1.01	0.86	1.07
4.09	432	2.62	7.99	5.62	0.30	0.92	0.96	0.98
6.59	458	4.01	11.45	8.08	0.42	1.56	0.97	0.90
6.71	476	3.93	11.29	7.42	0.48	1.62	1.01	0.97
8.65	495	4.82	13.11	10.54	0.54	1.86	0.97	0.79
10.78	504	5.95	17.92	11.19	0.77	2.63	0.78	0.84
10.79	521	5.70	16.74	10.72	0.65	2.34	0.86	0.76
13.24	524	6.90	22.75	13.94	1.04	3.45	0.82	0.85
13.25	530	6.83	23.10	15.76	0.92	3.81	0.82	0.88
			(b) Rubidium in nitrogen		(red)	(red)		
2.15	414	1.42	3.85	3.32	—	0.09	1.20	1.10
4.13	401	2.81	5.75	5.01	1.63	0.53	1.14	1.22
4.14	406	2.78	4.91	4.13	1.25	0.36	1.03	1.13
6.81	410	4.53	6.90	5.71	1.84	0.92	1.44	1.44
6.86	414	4.52	8.22	6.69	2.05	1.27	1.52	1.28
8.65	424	5.58	10.58	7.03	3.07	1.92	1.41	1.03
10.67	415	7.02	11.82	7.96	4.04	2.46	1.71	1.15
10.64	414	7.02	11.87	8.23	4.31	2.57	1.57	1.01
12.79	409	8.53	13.97	10.07	5.62	4.08	1.55	1.03
12.88	415	8.52	14.18	10.07	5.74	4.17	1.47	1.02

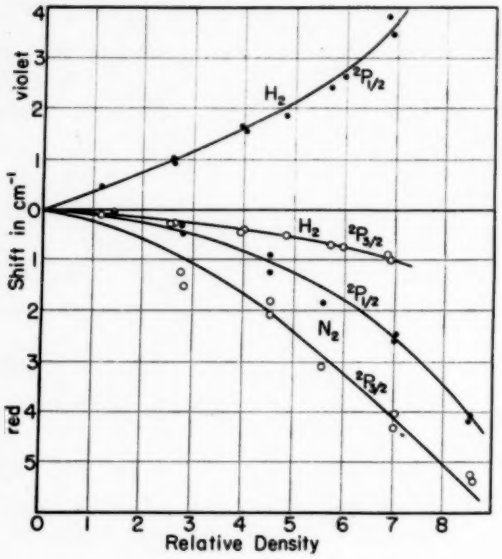

FIG. 2. Shift in cm^{-1} *vs.* relative density.

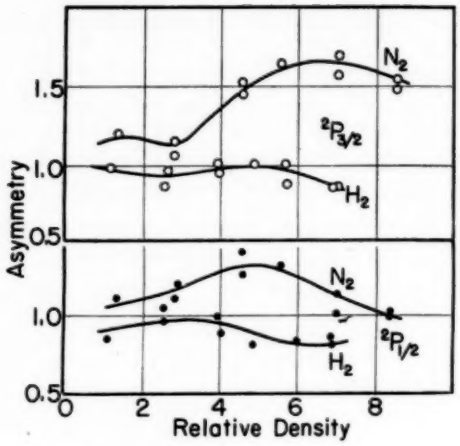

FIG. 3. Asymmetry *vs.* relative density.

a violet asymmetry, an exception like that for Cs 3876 observed by Füchtbauer and Gössler.[2]

(d) Precision of results

The precision of the results is already illustrated in Table I in which duplicate readings for different relative densities of foreign gases are given. When the temperature of the absorption tube was adjusted so that the absorption for λ4202 component had a suitable value for photometric determinations, the λ4216 component always showed an absorption that was too low. Consequently the absorption peaks for the latter were not high so that the irregularities of the microphotometer deflections could easily blur them. This will give too big a value for the half-width and also inaccuracy in the asymmetry (in general nearer to unity) and in the shift. On the other hand, when the temperature of the absorption tube was too high so that the absorption peaks had too high an absorption, the half-width data would be too low and asymmetry would again be nearer to unity. When the pressure was high so that the lines were highly broadened the position of maximum absorption could not be determined very accurately. Inaccuracy in determining shift would also mean an inaccuracy in determining asymmetry because the latter is expressed in terms of ratios of the red to the violet half of the half-width.

(e) Comparison with other results

The relation between half-width and shift is shown in Table II. All those values marked with a "?" are rather approximate because of the nonlinear relationship between the shift and the relative density. The values for the resonance lines of rubidium are taken from the author's previous research,[3] and those for the potassium resonance lines are taken from Hull's work.[4]

TABLE II. *Relationship between half-width and shift.*

SPECTRAL LINES AND PERTURBING GASES	$\Delta\nu_{\frac{1}{2}}/d$ (cm^{-1})	$\Delta\nu/d$ (cm^{-1})	$\Delta\nu_{\frac{1}{2}}/\Delta\nu$
Rb 7947–He	0.594	0.228	2.6
Rb 7800–He	0.735	0.092	8.0
Rb 7947–A	0.627	0.51 (?)	1.2
Rb 7800–A	0.855	0.51 (?)	1.7
Rb 7947–H_2	0.65 (?)	0.4 (?)	1.6
Rb 7800–H_2	0.87 (?)	0.4 (?)	2.2
Rb 4216–H_2	2.86	0.14 (?)	20.4
Rb 4202–H_2	1.87	0.45 (?)	4.2
Rb 4216–N_2	1.51	0.52 (?)	2.9
Rb 4202–N_2	1.01	0.38 (?)	2.7
K 7665–A	1.01	0.360	2.8
K 7699–A	1.01	0.420	2.4
K 7665–N_2	0.82	0.300	2.7
K 7699–N_2	0.82	0.360	2.3

[2] C. Füchtbauer and F. Gössler, Zeits. f. Physik **93**, 648 (1935).

[3] Ch'en Shang-Yi, Phys. Rev. **58**, 1051 (1940).

[4] G. F. Hull, Jr., Phys. Rev. **50**, 1148 (1936).

This table, together with Table II in Margenau and Watson's paper,[5] and Table II in Ny and Ch'en's[6] paper gives a complete tabulation of all available results for testing Margenau's theory. The varying of the ratio $\Delta\nu_{\frac{1}{2}/\Delta\nu}$ between 1.2 and 8 is certainly not strong support for it.[7]

Finally the authors wish to thank Dr. Ny Tsi-Zé, Director of Institute of Physics, National Academy of Peiping, for his interest and encouragement.

[5] H. Margenau and W. W. Watson, Rev. Mod. Phys. **8**, 44 (1936).
[6] Ny Tsi-Zé and Ch'en Shang-Yi, Phys. Rev. **52**, 1160 (1937).
[7] Thanks to Dr. H. Kuhn of the Clarendon Laboratory, Oxford, for his private communication to one of the authors regarding the point.

DECEMBER 15, 1940 PHYSICAL REVIEW VOLUME 58

On the Theory of the Magnetic Resonance Method of Determining Nuclear Moments

A. F. STEVENSON
Department of Applied Mathematics, University of Toronto, Toronto, Canada
(Received June 27, 1940)

Two refinements of the theory of the resonance method of determining magnetic moments as given by Rabi are considered quantitatively: (1) A correction is included because of the fact that an oscillating, rather than a rotating, field is used, (2) the "end effect" pointed out by Millman is taken into account. The results caused by (1) agree with those found by Bloch and Siegert, but the method of calculation is simpler. In the case of (2), it is shown that, under assumptions which mean that the effect is small, and which are usually well satisfied in practice, the effect can be worked out without making more than very general assumptions as to the nature of the field in the end regions. Results are given for the displacement of the maximum, and the asymmetry in the curve, which depend on the sign of the magnetic moment. The sign of the displacement is in agreement with experiment, but that of the asymmetry is not; the discrepancy can, however, be explained when account is taken of the inhomogeneity of the velocities in the beam. The effects increase as the square of the amplitude of the oscillating field.

1.

THIS paper is concerned with two refinements of the theory of the molecular beam resonance method of determining nuclear magnetic moments as developed by Rabi and his collaborators.[1] In the first place, there is included a correction resulting from the fact that in the experiments an *oscillating* magnetic field is used, whereas Rabi's original theory[2] assumed a *rotating* field. Secondly, the "end effect" due to the passage of the beam into the region of the oscillating field is considered quantitatively. This effect was pointed out by Millman,[3] who showed that it was of importance as enabling the *sign* of the magnetic moment to be determined experimentally.

It is evident that both effects can be made small by choosing the proper experimental conditions, but it seems desirable, nevertheless, to have some quantitative estimate of them. The first ("nonrotating") effect has already been considered by Bloch and Siegert[4] in a paper which appeared after the present calculations were begun; but inasmuch as the method of calculation used here is simpler than that of these authors, it is perhaps still of interest to include a brief account of it. Our results agree with theirs as far as this part of the calculation is concerned.

2.

We consider only the case where we deal, effectively, with a single atom for which $I=\frac{1}{2}$, $J=0$. The case where I is arbitrary and $J=0$ can be deduced from this simple one by means

[1] I. I. Rabi, S. Millman, P. Kusch and J. R. Zacharias, Phys. Rev. **55**, 526 (1939), and subsequent papers.
[2] I. I. Rabi, Phys. Rev. **51**, 652 (1937), and reference 1.
[3] S. Millman, Phys. Rev. **55**, 628 (1939).
[4] F. Block and A. Seigert, Phys. Rev. **57**, 522 (1940).

of an elegant result due to Majorana.[5] Let, then ξ, η denote the probability amplitudes for the states in which the z component of angular momentum is $+\frac{1}{2}\hbar$, $-\frac{1}{2}\hbar$, respectively, and let (H_x, H_y, H_z) be the components of magnetic field acting on the atom. The equations for ξ, η are then

$$\begin{aligned} i\hbar\dot{\xi} &= -\mu[H_z\xi+(H_x-iH_y)\eta], \\ i\hbar\dot{\eta} &= -\mu[-H_z\eta+(H_x+iH_y)\xi], \end{aligned} \tag{1}$$

where μ is the nuclear magnetic moment, reckoned positive if it is directed in the same sense as the nuclear spin.

In order to explain the "end effect," we reproduce in Fig. 1 a schematic diagram of the circuit producing the oscillating magnetic field, as given by Millman.[3] An oscillating source of current is applied at A, H, and the circuit consists of the bent copper tubing $A\,B\cdots H$, $O\,O'$ being the direction of the beam. The portions AB, GH, CD, EF of the circuit are parallel and at right angles to BC, FG. We take a system of right-handed axes as shown, with the y axis in the direction of the beam. In addition to the oscillating field, a strong uniform field is applied in the direction Oz (or zO). Over most of the path of the beam where the oscillating field is effective (within OO'), this field is of constant amplitude in the x direction. But in the neighborhood of O or O', there is an end effect which causes its amplitude and direction to change. It is evident that if the nonrotating and end effects are both small, we can (to the first order) consider them separately, and simply superpose the results.

We seek first a solution of Eqs. (1) for the region within OO' where the field is what we shall term "purely oscillatory" (i.e., of constant amplitude in the x direction). We put then in (1)

$$H_x=H_1\cos(\omega t+\delta), \quad H_y=0, \quad H_z=\pm H,$$

where H_1 is the amplitude of the oscillating field of frequency $\omega/2\pi$, H the magnitude of the uniform field, and the + or − sign is to be taken according as the direction of H is Oz or zO. We assume $H_1 \ll H$, since this is so in all the experiments. Equations (1) then become

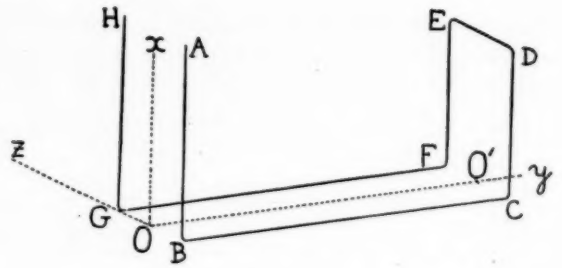

FIG. 1. Schematic diagram of the circuit producing the oscillating magnetic field.

$$\begin{aligned} ia\dot{\xi} &= \xi+\alpha[e^{-i(\omega t+\delta)}+e^{i(\omega t+\delta)}]\eta, \\ ia\dot{\eta} &= -\eta+\alpha[e^{i(\omega t+\delta)}+e^{-i(\omega t+\delta)}]\xi, \end{aligned} \tag{2}$$

where[6]

$$a=\pm\hbar/|\mu|H, \quad \alpha=H_1/2H(\alpha\ll 1). \tag{3}$$

The sign of a will be of importance when we come to discuss the end effect: $a>0$ if $\mu>0$ and H is in the direction zO. The direction of H can be conveniently related to the sense of rotation of the oscillating field caused by the end effect (cf. reference 3). It is easily seen from Fig. 1 that the end effects at O and O' are such as to rotate the oscillating field about the direction zO in the positive (right-hand screw) sense. We therefore have the rule: *$a>0$ if $\mu>0$ and the end effect is such as to rotate the oscillating field about the direction of the uniform field in the positive sense; if either the sign of μ or the sense of rotation is reversed, the sign of a is reversed.*

If (2) be solved by assuming ξ, η to be power series in α, the first approximation shows that, if $\eta=0$ initially, then η remains permanently small, of order α, unless $|a\omega\pm 2|$ is itself small of the order α. In this case, secular terms, or terms of large amplitude, arise, which shows that this method of solution then breaks down when large time intervals are considered.[7] For sufficiently short time intervals, however, the method of solution as power series in α is still applicable, and we shall use it in discussing the end effect.

[5] E. Majorana, Nuovo Cimento 9, 43 (1932).

[6] We should also write $\alpha=\pm H_1/2H$. We can, however, still retain the definition (3) by suitably altering the phase δ; the final results are independent of δ.

[7] The higher approximations will in any case introduce secular terms, because of the method of solution. The first approximation is, however, a sufficient indication.

The critical case $a\omega=\pm 2$, for which the transition probability need not be small even though α is small, arises when

$$H=H_0=\hbar\omega/2|\mu|. \tag{4}$$

H_0 is the field for which the Larmor precession frequency is $\omega/2\pi$. When $H\sim H_0$, the important terms in α in (2), which give rise to the secular terms, are the first ones within the square bracket in each equation if $a>0$, and the second ones if $a<0$. Neglecting the unimportant terms is equivalent to replacing the oscillating field by a rotating field of half the amplitude (the sense of rotation depending on the sign of a); the *presence* of these terms gives rise to the nonrotating effect.

Let us consider the case $a>0$. It is then convenient to put

$$\eta=e^{i(\omega t+\delta)}\eta'. \tag{5}$$

Equations (2) then become

$$\begin{aligned} ia\dot{\xi}&=\xi+\alpha[1+e^{2i(\omega t+\delta)}]\eta',\\ ia\dot{\eta}'&=(\alpha\omega-1)\eta'+\alpha[1+e^{-2i(\omega t+\delta)}]\xi. \end{aligned} \tag{6}$$

The important terms in α are now the constant ones. We first recall the solution when only these terms are retained. It can be written

$$\begin{aligned} \xi&=Ae^{i\lambda_1 t}+Be^{i\lambda_2 t},\\ \eta'&=-kAe^{i\lambda_1 t}+(1/k)Be^{i\lambda_2 t}, \end{aligned} \tag{7}$$

where A, B are arbitrary constants, and

$$\left.\begin{aligned} &a\lambda_1=-1+\alpha k, \quad a\lambda_2=-1-\alpha/k,\\ &k=\beta+(1+\beta^2)^{\frac{1}{2}},\\ &\beta=(1/\alpha)(1-|a|\omega/2)=2(H-H_0)/H_1. \end{aligned}\right\} \tag{8}$$

With the initial conditions $\xi=1$, $\eta=\eta'=0$ when $t=0$, we find for the probability of the transition $+\frac{1}{2}\hbar\rightarrow-\frac{1}{2}\hbar$, P, say ($P=|\eta|^2$),

$$P=(1+\beta^2)^{-1}\sin^2[\psi(1+\beta^2)^{\frac{1}{2}}], \tag{9}$$

where

$$\psi=\alpha t/|a|=|\mu|H_1 l/2\hbar v, \tag{10}$$

l being the length of the purely oscillating field, and v the velocity of the atom. The result (9) for the transition probability, which is independent of the sign of a, is that obtained by Rabi.[2]

If $\psi<\pi$, P has a maximum for $\beta=0$, or $H=H_0$; the optimum value of ψ is $\pi/2$, i.e., the optimum value of H_1 is $\pi\hbar v/|\mu|l$. For larger values of ψ, P may have a *minimum* for $\beta=0$, or maxima other than $\beta=0$ may be of importance. The half-width of the P curve (width at half-maximum), regarding P as a function of β, or H,[8] depends on ψ. For $\psi=\pi/2$, the half-maximum values are at about $\beta=\pm 0.8$, so that the half-width ΔH is about $0.8H_1$.

It should be noted, however, that (9) and (10) apply for an atom of definite velocity v. Actually, the beam will contain atoms (or molecules) of different velocities, and an average over these velocities must be taken. This will have the effect of "smoothing out" the ($\sin^2$)-term in (9), making this factor more nearly a constant, so that P will probably *always* have a maximum for $\beta=0$. The value of P at this maximum, and the half-width, will also be affected by this averaging process. That this effect is operative can be seen from the experimental curves, which show no trace of the subsidiary maxima demanded by (9).

3.

We consider now the nonrotating effect, and sketch a method of approximating to the solution of the complete Eqs. (6) for small α. We first note, from (9) and (8), that within the important part of the P curve in the neighborhood of the maximum, which is all that we need be concerned with, $|\beta|$ varies between 0 and a quantity of the order of unity, and hence $||a|\omega-2|\sim\alpha$, $k\sim 1$, $1/k\sim 1$.

Equations (6), being linear with periodic coefficients, possess an integral which is accurately of the form

$$\xi=e^{i\lambda' t}f(t), \quad \eta'=e^{i\lambda' t}g(t), \tag{11}$$

where f, g are periodic functions with the same period $(2\pi/\omega)$. In general, there will be two independent integrals of this form. From (7), we have, for the zero-order solution corresponding

[8] We shall always regard P in this manner, as in most of the experiments H is varied and the other parameters kept constant. In some of the latest experiments, however (P. Kusch, S. Millman and I. I. Rabi, Phys. Rev. 57, 765 (1940)), H is kept constant, and the frequency ω varied. The shape of the curve is exactly similar in this case, since β is a linear function of both H and ω.

to (11), $\lambda'=\lambda_1$, $g/f=-k$, or $\lambda'=\lambda_2$, $g/f=1/k$. Considering the integral for which $\lambda'\sim\lambda_1$, we therefore assume expansions of the form

$$f=1+\alpha f_1+\alpha^2 f_2+\cdots,\quad g=-k+\alpha g_1+\alpha^2 g_2+\cdots,$$
$$\lambda'=\lambda_1+c_1\alpha+c_2\alpha^2+\cdots.$$

We then obtain a series of equations for the f's and g's which can be solved in succession. The condition that only periodic terms shall occur determines the constants c, and also effectively determines the arbitrary constants arising in the course of the work; any indeterminacy which remains is equivalent to multiplying the integral (11) by a constant factor. The method is sufficiently well known, and the calculations need not be reproduced in detail.[9] In a similar manner, we can find an integral of the form (11) for which $\lambda'\sim\lambda_2$. With a convenient choice of the arbitrary constants, we thus obtain as the general solution of (2), for $a>0$, and correct to the first order in α,[10]

$$\xi=Ae^{i\lambda_1' t}\left[1+\frac{\alpha k}{4}\left(-\frac{2}{k^2+1}+e^{2i\phi}\right)\right]+Be^{i\lambda_2' t}\left[1+\frac{\alpha k}{4}\left(-\frac{2}{k^2+1}-\frac{1}{k^2}e^{2i\phi}\right)\right],$$
$$e^{-i\phi}\eta=-kAe^{i\lambda_1' t}\left[1-\frac{\alpha k}{4}e^{-2i\phi}\right]+\frac{1}{k}Be^{i\lambda_2' t}\left[1+\frac{\alpha k}{4}e^{-2i\phi}\right],$$

where

$$a\lambda_1'=a\lambda_1+\frac{\alpha^2}{4}\cdot\frac{k^2-1}{k^2+1},\quad a\lambda_2'=a\lambda_2-\frac{\alpha^2}{4}\cdot\frac{k^2-1}{k^2+1},$$
$$\phi=\omega t+\delta,$$

and A, B are arbitrary constants. If $a<0$, we need only change the sign of ϕ throughout, if we retain the definitions (8) of k, λ_1, λ_2.

With the initial conditions $\xi=1$, $\eta=0$ when $t=0$, we obtain for the transition probability, for either sign of a, correct to the first order in α,

$$P=(1+\beta^2)^{-1}[1-(\alpha/2)\beta(1+\beta^2)^{-1}]\sin^2[\psi(1+\beta^2)^{\frac{1}{2}}(1-(\alpha/4)\beta(1+\beta^2)^{-1})].$$

We have omitted terms proportional to $\cos 2\delta$, $\sin 2\delta$, since we are dealing with a *beam* of particles, and must therefore average over the initial phases δ.[4] To the same order, we may write

$$P=(1+\beta'^2)^{-1}\sin^2[\psi(1+\beta'^2)^{\frac{1}{2}}],$$

where $\beta'=\beta+\alpha_0/4$, $\alpha_0=H_1/2H_0$.

Comparing with (9), we see that the shape of the curve is unaltered, but that the maximum is shifted to $\beta=-\alpha_0/4$, or

$$H=H_0-H_1^2/16H_0$$

in agreement with the result of Bloch and Siegert.[4] It will be seen that our method is more straightforward than theirs, which requires somewhat elaborate transformations.[11]

4.

We consider now the end effect. While the atom is under the influence of the end effects at O or O' (Fig. 1), there will be both x and y components to the oscillating field,[12] these components depending on the y coordinate of the atom as well as the current in the circuit. We therefore put in (1)

$$H_x=X(y)H_1\cos(\omega t+\delta),\quad H_y=Y(y)H_1\cos(\omega t+\delta),\quad H_z=\pm H,$$

where $X(y)$ denotes, at any moment, the ratio of the amplitude of H_x at the point whose coordinate is y to the amplitude at a point where the field is purely oscillatory, and $Y(y)$ denotes a similar ratio for H_y. Equations (1) then become, in the same notation,

$$ia\dot{\xi}=\xi+\alpha(X-iY)[e^{-i(\omega t+\delta)}+e^{i(\omega t+\delta)}]\eta,$$
$$ia\dot{\eta}=-\eta+\alpha(X+iY)[e^{i(\omega t+\delta)}+e^{-i(\omega t+\delta)}]\xi. \qquad (12)$$

Evidently X and Y are functions with an upper bound of the order unity. Consideration of

[9] See, for instance, the very full account in Moulton *et al.*, *Periodic Orbits* (Carnegie Institution, Washington, 1920), Chap. 1, Section 3. We can also proceed direct from Eqs. (2).

[10] It can be shown that in order to calculate P to the first order, it is necessary to calculate λ' to the *second* order.

[11] The slightly more general case considered by them can be treated with equal facility by the present method, as can also the case (not considered by them) where the oscillating field has a component parallel to the uniform field. In this latter case, the effect is of the same order of magnitude as the "nonrotating" effect.

[12] A possible z component would only give rise to a second-order effect. Cf. reference 11.

the field arising from the circuit of Fig. 1 shows that X and Y are positive in the neighborhood of O, while $X>0$, $Y<0$ in the neighborhood of O'. The end effects will be negligible except in regions in the neighborhood of O and O' whose length is of the order b, where b denotes the distance GB between the wires. The actual circuit may not conform very well to the idealized one of Fig. 1; but if the latter represents at all well the general features of the circuit, it is evident that the above statements are true.

We further define a parameter ϵ by

$$\epsilon=\alpha b/|a|v=|\mu|H_1 b/2\hbar v=\psi b/l, \qquad (13)$$

and assume

$$\epsilon\ll 1, \quad v/b\omega\ll 1. \qquad (14)$$

It will be shown that we can then integrate (12) approximately without making any further assumptions as to the functions X and Y beyond the very general ones already mentioned.

From (13), we see that the first of (14) is satisfied if $b/l\ll 1$, provided ψ has a value which does not differ much from the optimum one, namely $\pi/2$. The condition $b/l\ll 1$ is well satisfied in the actual apparatus. According to measurements given by Millman,[3] the distance between the axes of the wires is about $\frac{1}{4}$ cm, and the length of the circuit about 6 cm, so that $b/l\sim 1/25$. In a later form of the apparatus described,[13] $b/l\sim 1/50$. The second of (14) is also usually well satisfied; thus for $v=10^5$ cm/sec., $\omega/2\pi=3$ megacycles, $b=\frac{1}{4}$ cm, we have $v/b\omega\sim 1/45$.

The assumptions (14) ensure, as we shall see, that the end effect is *small*. The second assumption is not essential to the method of solution, but simplifies the analysis. It will be shown that the end effects are proportional to ϵH_1, and therefore increase as H_1^2. Hence H_1 must be increased beyond the optimum value in order to bring out the end effects prominently.

We suppose now that the end effect at O lasts from $t=-t_1$ to $t=0$, the purely oscillating field from $t=0$ to $t=T$, and the end effect at O' (which need not be identical with that of O) from $t=T$ to $t=T+t_2$. We suppose $a>0$ for definiteness. For $O<t<T$, the solution (neglecting the nonrotating effect) is given by (7). During the end effects, we solve (12) for ξ, η as power series in α.

For $-t_1<t<0$, we assume, with the initial conditions $\xi=1$, $\eta=0$ when $t=-t_1$,

$$\begin{aligned}\xi&=e^{-(i/a)(t+t_1)}+\alpha\xi_1+\alpha^2\xi_2+\cdots,\\ \eta&=\alpha\eta_1+\alpha^2\eta_2+\cdots,\end{aligned} \qquad (15)$$

where the initial conditions require the vanishing of $\xi_1, \eta_1, \cdots$ for $t=-t_1$. The first approximation gives

$$ia\dot{\xi}_1-\xi_1=0,$$

$$ia\dot{\eta}_1+\eta_1=(X+iY)[e^{i(\omega t+\delta)}+e^{-i(\omega t+\delta)}].$$

Hence, taking account of the initial conditions,

$$\xi_1=0,$$

$$\eta_1=-(i/a)e^{(i/a)(t+t_1)}\left[e^{i(\delta-\omega t_1)}\int_{-t_1}^{t}(X+iY)e^{i(\omega-2/a)(t+t_1)}dt+e^{-i(\delta-\omega t_1)}\int_{-t_1}^{t}(X+iY)e^{i(\omega+2/a)(t+t_1)}dt\right].$$

Changing the variable of integration from t to $y(dy/dt=v)$ in both integrals, and using (13), we therefore have

$$\alpha\eta_1(0)=-i\epsilon e^{it_1/a}\left[e^{i(\delta-\omega t_1)}\int_{y_1}^{y_2}(X+iY)e^{i(\omega-2/a)(y-y_1)/v}(dy/b)\right.$$
$$\left.+e^{-i(\delta-\omega t_1)}\int_{y_1}^{y_2}(X+iY)e^{i(\omega+2/a)(y-y_1)/v}(dy/b)\right], \qquad (16)$$

where y_1, y_2 are the values of y at the beginning and end of the end effect at O.

Now, as remarked in Section 3, $|a\omega-2|$ is (for $a>0$) of the order α within the important part of the P curve, so that, since $(y_2-y_1)\sim b$ according to our assumptions, the argument of the exponential

[13] J. M. B. Kellogg, I. I. Rabi, N. F. Ramsey and J. R. Zacharias, Phys. Rev. **56**, 728 (1939).

in the first integral in (16) is of order $\alpha b/av=\epsilon$. Hence the first integral in (16) is, in absolute value, of the order unity, and we can put the exponential in this integral equal to 1 if we are only working to the first order in ϵ. In the second integral in (16), on the other hand, the argument of the exponential $\sim\omega(y-y_1)/v$. From the second of (14), we therefore see that the real and imaginary parts of this integral are rapidly oscillating functions with an upper bound of the order unity within the domain of integration, and the absolute value of the second integral will not exceed $v/b\omega$ in order of magnitude. Hence, to the first order in ϵ and $v/b\omega$ we can neglect the second integral in (16), and can write

$$\alpha\eta_1(0)=-i\epsilon e^{i(t_1/a+\delta-\omega t_1)}(I_1+iI_2),$$

where

$$I_1=\int_{y_1}^{y_2}Xdy/b, \quad I_2=\int_{y_1}^{y_2}Ydy/b. \tag{17}$$

I_1, I_2 are positive dimensionless quantities of the order unity.

Thus $|\alpha\eta_1(0)|\sim\epsilon$, and it is clear that the development (15) is justifiable, and that a good approximation is obtained by stopping at the first term. To the first order in ϵ, $v/b\omega$ we therefore have, from (15),

$$\xi(0)=e^{-it_1/a}, \quad \eta(0)=-i\epsilon e^{i(t_1/a+\delta-\omega t_1)}(I_1+iI_2). \tag{18}$$

Similarly the end effect at O' is dealt with. We assume, analogously to (15),

$$\xi=\xi(T)e^{-(i/a)(t-T)}+\alpha\xi_1+\cdots, \quad \eta=\eta(T)e^{(i/a)(t-T)}+\alpha\eta_1+\cdots,$$

and find, to the same order,

$$\eta(T+t_2)=e^{it_2/a}[\eta(T)-i\epsilon e^{i(\delta+\omega T)}(I_1'+iI_2')\xi(T)], \tag{19}$$

where

$$I_1'=\int_{y_1'}^{y'_2}Xdy/b, \quad I_2'=\int_{y_1'}^{y_2'}Ydy/b, \tag{20}$$

and y_1', y_2' are the values of y at the beginning and end of the end effect at O'. The constants I_1', I_2' are also of the order unity, and $I_1'>0$, $I_2'<0$. It is not necessary to give the value of $\xi(T+t_2)$.

We now use (18) to determine the arbitrary constants A, B in (7), calculate $\xi(T)$, $\eta(T)$ from (7), and then use (19) to determine $\eta(T+t_2)$. To the first order we find

$$\exp i[(1/a)(t_1-t_2)-(\omega T+\delta)]\cdot(k+1/k)\eta(T+t_2)=-e^{i\lambda_1 T}+e^{i\lambda_2 T}$$
$$-i\epsilon[(I_1+iI_2)(ke^{i\lambda_1 T}+(1/k)e^{i\lambda_2 T})+(I_1'+iI_2')((1/k)e^{i\lambda_1 T}+ke^{i\lambda_2 T})]. \tag{21}$$

Equation (21) applies for $a>0$. In a similar manner the calculation for $a<0$ is carried through, and we find that we need merely change the signs of ω, δ, ϵ where they occur explicitly in (21), if we retain the definition (13) of ϵ. With the help of (8), and using $T=l/v$, we find from (21) that the transition probability, $P=|\eta(T+t_2)|^2$, can be expressed, correct to the first order, in the form

$$P=(1+\beta^2)^{-1}(1-2\epsilon C\beta)\sin^2[\psi'(1+\beta^2)^{\frac{1}{2}}], \tag{22}$$

where

$$\psi'=\psi+\epsilon C', \quad C=I_2-I_2', \quad C'=I_1+I_1'.$$

Equation (22) holds, of course, only within the important part of the P curve ($|\beta|\lesssim 1$), and is for the case $a>0$. If $a<0$, we must change the sign of ϵ in the second factor of (22) (but *not* in the definition of ψ'!). The constants C, C' are positive, and of order unity.[14]

The presence of the constant C' merely has the

[14] A rough estimate of them may be made by supposing that the circuit of Fig. 1 consists of ideal linear circuits AB, BC, $\cdots$, with right angles at B, $\cdots$, and which can be treated as being of infinite length in comparison with b. For the field in the neighborhood of 0 we then find

$$2X=1+2y(b^2+4y^2)^{-\frac{1}{2}}, \qquad 2Y=b^2/(b^2+4y^2)$$

and can suppose that the end effect at 0 is confined (say) to the region $-3b/2\leqslant y\leqslant 3b/2$. We then find

$$I_1=I_1'=1.5, \qquad I_2=-I_2'=0.625,$$

whence $C=1.25$, $C'=3.0$.

effect of increasing the effective length l of the circuit, and is unimportant; but the presence of the second factor in (22) shifts the maximum of the P curve and introduces an asymmetry. Always working to the first order in ϵ, and taking the case $a>0$ again, we find that the maximum occurs at

$$\beta=-C\epsilon/(1-\psi'\cot\psi'),$$

or

$$H=H_0-C\epsilon H_1/(1-\psi'\cot\psi'). \tag{23}$$

For $\psi'=\pi/2$, this becomes

$$H=H_0-C\epsilon H_1/2. \tag{24}$$

The shift of the maximum given by (23) is toward the low field side if $\psi'<\pi$, and it is probable that when an average over molecular velocities is taken, the shift is always in this direction (cf. the discussion in Section 2). Thus, *the maximum is shifted to the low field or high field side according as a is positive or negative.* As already discussed, the sign of a depends on the sign of μ and the direction of the uniform field relative to the circuit. This result is in accordance with the results of Millman.[3]

As regards the asymmetry, (22) makes the curve steeper on the low field or high field side of the maximum according as a is positive or negative, which is precisely the *opposite* of the result found experimentally. The discrepancy can, however, be explained when the already mentioned averaging over molecular velocities is taken into account. For this would make the ($\sin^2$)-terms in (22) more nearly a constant, and would probably have the effect of reversing the asymmetry. This is certainly the case if we assume as a rough approximation that the ($\sin^2$)-terms in (22) can be put equal to a constant. The values of β for which P has half the maximum value are then given by

$$\beta'=1-\epsilon C, \quad -1-\epsilon C,$$

where $\beta'=\beta+\epsilon C$, so that the origin for β is transferred to the maximum. Hence the *difference* in the half-widths on either side of the maximum is $2\epsilon C$, or, in terms of H,

$$\Delta H_1-\Delta H_2=C\epsilon H_1, \tag{25}$$

the curve being wider on the low field or high field side according as a is positive or negative. The displacement of the maximum is again given by (24).

A quantitative comparison of our results with experiment is scarcely possible at present, since the value of H_1 is not usually made clear in the experiments, and most of the curves are given for one direction only of the uniform field, so that only the asymmetry can be judged, for which, as pointed out, the averaging over molecular velocities is of importance. A possible source of comparison is furnished by Fig. 3 of Millman's paper,[3] where curves for LiCl molecules are shown with both directions of the uniform field. If we assume that (24) and (25) hold for this case, we see that the difference in the half-widths for either curve should be equal to the distance between the intensity minima (P maxima) of the two curves. Actually, the difference in the half-widths is only about one-half of this. The discrepancy can be accounted for by the fact that (25) is obtained by quite a crude assumption as to velocity averaging.

The calculations of this section all relate to the case where the end effect is *small* ($\epsilon\ll 1$). If the amplitude of the oscillating field H_1 is so large that our analysis becomes inapplicable, it is not surprising that the P curve becomes more complicated and may show additional maxima.[3] But for most purposes it is, of course, *desirable* to make the end effect small.[15]

I wish to acknowledge some helpful suggestions made by the referee.

[15] *Note added in proof.*—The end effect could be reduced by rotating the loop $CDEF$ of the circuit (Fig. 1) through 180° about CF, should such a change be feasible, for this would change the sign of I_2', and hence reduce C.

Scattering Matrix of Radioactive States[1]

G. BREIT
University of Wisconsin, Madison, Wisconsin
(Received October 28, 1940)

The method of complex eigenvalues is generalized to many dimensional problems by means of the scattering matrix. It is essential to allow for the existence of a background matrix on which the resonance is superposed. The "radioactive state" (i.e., the state with complex energy for which waves in all disintegration channels are outgoing) determines the damping constants of the resonance formulas. Phase constants [Eq. (6.2)] responsible for displacements of observable resonance peaks with respect to the real part of the complex eigenvalue of the energy are also determined by the radioactive state. The background matrix is restricted by the above-mentioned damping constants and phase constants to a considerable extent, leaving free in its specification an n-1-dimensional symmetric unitary matrix for the case of n channels. The equations presented do not include the case of continuously variable energy distribution among disintegration products.

THE notion of the scattering matrix has been introduced by Wheeler[2] for the discussion of scattering in the approximation of the resonating group structure. Radioactive quantum-mechanical states with complex energy have been introduced by Gamow[3] and the resonance scattering of one body by a central field can be described conveniently by means of the radioactive state. Resonance scattering for a system having several modes of decay can also be understood by means of the radioactive state by an extension of the argument used for the one-body problem.[4] This extension is being carried out below and makes use of a general scattering matrix. It is found that the energy dependence of the scattering and disintegration cross sections is given approximately by the formula for resonance competition derived by Wigner and the writer. The scattering matrix is found to consist of resonance-like terms superposed on a background. Restricting conditions on the background are found to follow as a general consequence of the wave equation. For two competitive modes of disintegration the background part of the scattering matrix is fixed to within one real parameter. For three competitive modes there enter three real parameters. For n modes the parameters involved are those contained in the matrix elements of an n-1-dimensional symmetric unitary matrix. A partial object of the present note is to eliminate, in the discussion of the resonance formula, special considerations regarding the interaction between particles.

THE SCATTERING MATRIX

The system of particles will be assumed to have no spin and the particles will be assumed to be nonidentical. The wave equation is

$$\left[-\sum_1^m \frac{\hbar^2}{2M_i}\left(\frac{\partial^2}{\partial x_i^2}+\frac{\partial^2}{\partial y^2{}_i}+\frac{\partial^2}{\partial z_i^2}\right)+V-E\right]\psi=0. \quad (1)$$

The potential energy depends only on the relative distance between particles so that conservation of momentum, angular momentum and parity hold. It is supposed that it is energetically possible for the system to break up into pairs of fragments in several ways. The possibility of breakup into triplets or quadruplets of fragments

[1] Professor E. P. Wigner mentioned to the writer that one can use the scattering matrix for an improved understanding of resonance phenomena more than a year ago. At the end of 1939 he had considerable success in this direction which was mentioned briefly in conversation. These considerations will be described by him jointly with L. Eisenbud in a forthcoming paper in the *Reviews of Modern Physics*. The present note is thus not an independent investigation because of its origin in the knowledge that useful relations can be obtained by means of the scattering matrix. The reason for publishing is that the scattering matrix is here related to the method of complex eigenvalues and the approach differs in this way from that of Wigner and Eisenbud who have arrived at the results before the present author.

[2] J. A. Wheeler, Phys. Rev. **52**, 1107 (1937).

[3] G. Gamow, Zeits. f. Physik **51**, 204 (1928).

[4] G. Breit and F. L. Yost, Phys. Rev. **48**, 203 (1935); G. Breit, *ibid.* **40**, 127 (1932); A. J. F. Siegert, *ibid.* **56**, 750 (1934); G. Breit, *ibid.* **58**, 506 (1940). See pages 509–517 in latter paper.

is neglected. The discussion does not apply, therefore, to $(n, 2n)$ reactions except insofar as the emission of neutrons may be treated as a succession of two processes.

The region of configuration space in which the system has separated into two definitely formed and noninteracting fragments will be called a *channel*. Within each channel the wave function is a sum of products of functions describing the motion of the center of mass of the whole system, the internal coordinates of each fragment and finally the relative motion of the particles with respect to each other. The latter factor may in its turn be represented as a sum of products of angular functions corresponding to different angular momenta and radial factors depending only on the distance between the fragments. The product of the angular factor, the factors representing the internal motion within the fragments and the factor containing the coordinates of the center of mass of the system will be referred to as u.

The transformation

$$X=(M_1x_1+M_2x_2)/(M_1+M_2), \quad x=x_2-x_1$$

represents the introduction of the center of mass and relative coordinates for a pair of particles. Its determinant is 1. The internal coordinates for each fragment can be introduced by a succession of such transformations. The centers of mass of each fragment are then used in such a transformation to introduce the relative coordinates of the fragments with respect to each other and the center of mass of the whole system. The Jacobian of the transformation from the original coordinates is unity and the normalization integral of the whole wave function retains its form.

Within the channels the wave function can be represented as

$$\psi=\sum_l[a_l\exp(ik_lr_l)+b_l\exp(-ik_lr_l)]u_l/r_l, \qquad k_l=\mu_lv_l/\hbar. \tag{1.1}$$

The index l specifies here the channel, the state of the fragments and the relative angular momentum of the fragments; a_l, b_l are constants; μ_l, v_l, r_l are respectively the reduced mass, relative velocity and distance between the fragments. Each term in the above sum corresponds to a mode of disintegration. All modes of disintegration in the same channel correspond to the same μ_l, r_l. The function u_l is normalized so that $|u_l|^2$ gives unity when integrated over the coordinates of the center of mass of the system, the internal coordinates of each fragment and the angular coordinates of the relative position of the fragments.

Special solutions are now considered for a system having n independent modes of disintegration. Within the channels these are given by

$$\psi^j=\sum_l\varphi_l{}^ju_l; \qquad \varphi_l{}^j=[\delta_{jl}\exp(-ik_lr_l)+a_{lj}\exp(ik_lr_l)]/r_l. \tag{1.2}$$

Each ψ^j is obtained by solving (1) subject to the boundary condition of there being only one incident wave $u_j\exp(-ik_jr_j)/r_j$. The matrix (a_{lj}) is called the scattering matrix. Although a solution of Eq. (1) is practically impossible some information can be obtained by studying the a_{lj}.

A surface is passed so as to cut across the channels. Within each channel the surface satisfies the equation $r_l=$const. The radius of a sphere inscribed into the surface is made $\gg m\times$range of force. The wave function on the surface is thus negligible except at the channels. From Eq. (1) one obtains

$$\psi^j\sum\frac{1}{M_i}\Delta_i\psi^m-\psi^m\sum\frac{1}{M_i}\Delta_i\psi^j=0.$$

This formula is integrated through the $3m$-dimensional volume contained within the surface and the integral is transformed into a surface integral by Green's theorem. The transformation from the original coordinates to the channel variables takes the form of orthogonal transformations if one uses $(M_i)^{\frac{1}{2}}x_i$ instead of x_i and $\mu^{\frac{1}{2}}$ times relative coordinate at each stage. To each r_l there correspond the coordinates X_l, Y_l, Z_l which correspond to $\mu_l{}^{\frac{1}{2}}X_l$, $\mu_l{}^{\frac{1}{2}}Y_l$, $\mu_l{}^{\frac{1}{2}}Z_l$ in the Euclidean space. In the integrand there corresponds to them

$$\sum_{x,y,z}\frac{1}{\mu_l}\frac{\partial}{\partial X_l}\left(\psi^j\frac{\partial\psi^m}{\partial X_l}-\psi^m\frac{\partial\psi^j}{\partial X_l}\right).$$

The factor μ_lv_l brought down by differentiation on account of Eq. (1.1) combines with $1/\mu_l$ leaving v_l. Only terms with the same l contribute

to the result because the u_l are orthogonal to each other and because the channels do not overlap on the surface. One obtains on substituting Eq. (1.2)

$$v_l a_{lj} = v_j a_{jl}. \tag{2}$$

This relation holds for real or complex E. For real E one obtains additional simple relations by considering ψ^{i*} and ψ^m in Green's formula *viz.*

$$\sum_k v_k a^*_{kj} a_{kl} = \delta_{jl} v_l. \tag{2.1}$$

It is convenient to introduce

$$b_{kl} = (v_k/v_l)^{\frac{1}{2}} a_{kl} \tag{2.2}$$

for which

$$b_{kl} = b_{lk}, \quad \sum b^*_{kl} b_{kj} = \delta_{lj}. \tag{2.3}$$

The latter of these equations shows that $\|b_{kl}\|$ is a unitary matrix. According to Eq. (2.2) there are $|b_{kl}|^2$ systems leaving by way of the disintegration mode k per unit incident system in state l. Relations (2.3) have as a consequence the conservation of the number of systems as has been pointed out by Wheeler. The symmetry of $\|b_{lk}\|$ means detailed balance at high temperatures.

Complex Energies

For complex energies it is also possible to use a scattering matrix. Equation (2.1) does not hold in this case and the matrix $\|b_{lk}\|$ is not unitary. It is symmetric, however. The values of E will have in most of the calculation negative imaginary parts. In such cases v will be taken to have positive real and negative imaginary parts. The factors $\exp[i\mu vr/\hbar]$, $\exp[-i\mu vr/\hbar]$ will have exponentially increasing and decreasing amplitudes for large r. The energy states of the fragments still correspond to real internal energies. For values of E with a small imaginary part one has solutions of the wave equation which are similar to solutions for real E as long as one does not go too far out in the channels. If the imaginary part of E is not sufficiently small, however, there will be no predominance of the rapidity of decrease of states with negative kinetic energy in the channels over the decrease of $\exp[-i\mu vr/\hbar]$ and the distinction between the interior and exterior of the channel disappears. The imaginary part of E will be supposed to be sufficiently small so that this does not happen.

For a suitably chosen complex $E = E_e$ it may be possible to have

$$\varphi_l = \alpha_l \exp(ik_l r_l)/r_l, \tag{3}$$

so that only outgoing waves are present in the channels. Such solutions are, of course, impossible for real energies, since their existence would contradict the conservation of the number of systems. The state (3) will be referred to as the radioactive state. Its normalization is immaterial at this stage. By superposing solutions of the form (1.2) it should be possible to obtain (3). This can only happen if some of the a_{lj} become infinite at $E = E_e$. The simplest possibility for this will be considered

$$a_{lj} \cong \frac{c_{lj}}{E - E_e} + d_{lj}. \tag{3.1}$$

Here the c_{lj}, d_{lj} are constants and the equation is meant to be only an approximation in the neighborhood of the complex eigenvalue. On the other hand the number of independent solutions of the wave equation must be still n. There must exist, therefore, $n-1$ linearly independent combinations of the ψ^j for which the solution is not (3). The equation

$$\sum_{j=1}^{n} c_{lj} \lambda_j = 0 \tag{3.2}$$

must have, therefore, $n-1$ linearly independent solutions and all the minors of $\det \|c_{lj}\|$ are zero. According to Eq. (2) one has

$$v_l c_{lj} = v_j c_{jl} \tag{3.3}$$

and one obtains, therefore, as the general form of c_{lj}

$$c_{lj} = (v_j/v_l)^{\frac{1}{2}} C_l C_j. \tag{3.4}$$

The wave equation (1) is real. If $E = E_e^*$ there must exist, therefore, an *antiradioactive state* consisting entirely of incoming waves and it should be possible to superpose the solutions ψ^i linearly so as to obtain this state. The required linear combination is $\sum a_i^* \psi^i(E_e^*)$ because only with this combination are the ratios of the coefficients of $\exp(-ik_l r_l)$ correct. From Eq. (3.4) it follows that one may take

$$h^{\frac{1}{2}} \alpha_j = v_j^{-\frac{1}{2}} C_j; \quad c_{lj} = v_j \alpha_l \alpha_j \hbar \tag{3.5}$$

and hence

$$\sum_j v_j^{-1} C_j^* \left[\frac{c_{lj}}{E_c^* - E_c} + d_{lj} \right] = 0, \qquad (3.6)$$

because the terms $\exp(ik_l r_l)$ must disappear in the antiradioactive state. One has in Eq. (3.6) n conditions on the d_{lj}. Formally, according to this presentation, one must use complex v_j, v_l in Eqs. (3.4) and (3.6). The approximation (3.1), however, is not exactly consistent with Eq. (2) for constant c_{lj} as E is varied. Since it is important to represent scattering for real E, the real values of v_j, v_l corresponding to $E=(E_c+E_c^*)/2$ will be used.

It will be shown next that the restrictions on $\|d_{lj}\|$ imposed by Eq. (3.6) are such that $\|b_{lj}\|$ is unitary for real E. On account of Eq. (2) it is convenient to introduce

$$q_{lj} = (v_l/v_j)^{\frac{1}{2}} d_{lj} = q_{jl}, \qquad (4)$$

so that

$$b_{lj} = C_l C_j/(E-E_c) + q_{lj} \qquad (4.1)$$

and

$$\sum_i b_{ij} b_{il}^* = \frac{C_j C_l^*}{|E-E_c|^2} \sum_i |C_i|^2 + \frac{C_j}{E-E_c} \sum_i C_i q_{il}^* + \frac{C_l^*}{E-E_c^*} \sum_i C_i^* q_{ij} + \sum_i q_{ij} q_{il}^*. \qquad (4.2)$$

The first three terms in this formula depend on E and it appears strange that this could be reconciled with the unitary nature of $\|b_{lj}\|$ expressed by Eq. (2.3). The relations (3.6), however, connect the q_{lj} with the C_l in such a way that only the last term in Eq. (4.2) survives. Substituting (3.4) into (3.6) one has

$$\sum_i q_{ij} C_j^* = \frac{C_i}{E_c - E_c^*} \sum_j |C_j|^2. \qquad (4.3)$$

This formula and its complex conjugate are used in (4.2) and the first three terms are then seen to cancel. One has, therefore,

$$\sum_i q_{ij} q_{il}^* = \delta_{lj}. \qquad (4.4)$$

These, however, are the necessary and sufficient conditions for $\|q_{ij}\|$ to be a unitary matrix. It is necessary for $\|q_{ij}\|$ to be unitary in order that $\|b_{ij}\|$ be unitary. The unitary symmetric nature of $\|q_{ij}\|$ together with (4.3) is also sufficient for the unitary, symmetric nature of $\|b_{ij}\|$.

In the above presentation Eq. (4.3) has been obtained from a consideration of the antiradioactive state. It may possibly be preferred to use the notion of the radioactive state only to the extent of suggesting the form (4.1) as an approximation for the scattering matrix close to resonance. This may be done either through Eq. (3.2) as has been explained or else this form can be made reasonable by observing that for $E \cong E_c$ the ratios of the b_{lj} for fixed j are equal to the ratios of the corresponding C_l. This means that any single incident wave of type $(u_l/r_l)\exp[-ik_l r_l]$ gives rise for $E \cong E_c$ to a multiple of the radioactive state. Having decided on (4.1) as the desired approximation one can derive the relations (4.3) as well as the unitary symmetric nature of $\|q_{ij}\|$ from the consideration of the scattering matrix for real E alone as follows. Since $b_{lj}=b_{jl}$ it follows from (4.1) that $q_{lj}=q_{jl}$. Substituting (4.1) into the left side of (4.2), one obtains (4.2). On the other hand the left side of (4.2) $=\delta_{jl}$ which is independent of E. Rearranging the right side of (4.2) one has

$$\frac{C_j}{E-E_c}\left[\frac{C_l^*}{E_c-E_c^*}\sum_i |C_i|^2 + \sum_i C_i q_{il}^*\right] + \frac{C_l^*}{E-E_c^*}\left[\frac{C_j}{E_c^*-E_c}\sum_i |C_i|^2 + \sum_i C_i^* q_{ij}\right] + \sum_i q_{ij} q_{il}^* - \delta_{jl} = 0. \qquad (4.5)$$

This relation is of the form $A_1/(E-E_c)+A_2/(E-E_c^*)+B=0$ where A_1, A_2, B are independent of E and it must be satisfied for all real E. It follows that $B=0$ and that either $E_c=E_c^*$ (which is not the case) or else $A_1=A_2=0$. From $B=0$ one obtains (4.4) so that $\|q_{ij}\|$ is unitary. $A_2=0$ says that either $C_l^*=0$ or else the square bracket multiplying C_l^* in (4.5) vanishes. Varying l in (4.5) from 1 to n and keeping j fixed, one will find at least one $C_l^* \neq 0$. Otherwise there is no resonance scattering. The square bracket in (4.5) is, therefore $=0$ for any j so that Eq. (4.3) holds for all i.

The matrix $\|q_{ij}\|$ gives the *background* to the resonance scattering. It is reasonable that it turns out to be unitary and symmetric because

for large $|E-E_c|b_{ij} \geqq q_{ij}$. The conditions (4.3) will now be studied.

The Background Matrix and Mean Life

Making use of the fact that $\|q_{ij}\|$ is unitary and symmetric one solves (4.3) for C_i^* and obtains

$$\sum q_{ij}^* C_j = \frac{E_c - E_c^*}{\sum_j |C_j|^2} C_i^* \tag{5}$$

and comparing this with the complex conjugate of (4.3) one has

$$|E_c - E_c^*| = \sum_j |C_j|^2 = \sum_j v_j |\alpha_j|^2 h. \tag{5.1}$$

The quantity $\frac{1}{2}|E_c - E_c^*|$ is the absolute value of the imaginary part of E_c and $|E_c - E_c^*|$ is, therefore, the resonance half-width. According to Eq. (5.1) this half-width is equal to the sum of partial half-widths $|C_j|^2 = \hbar v_j |\alpha_j|^2$ each of which is associated with one of the modes of disintegration. One has here a connection between the numerators of the dispersion terms of the scattering matrix and the resonance width. Equation (5.1) has a simple meaning in terms of mean life. For $E = E_c$ the time-dependent wave equation has a solution of the form (3) with a time factor $\exp[-iE_c t/\hbar]$. The reciprocal of the mean life of this state is $|E_c - E_c^*|/\hbar$ and according to (5.1) this transition probability can be considered as the sum of elementary transition probabilities $\hbar^{-1}|C_j|^2 = v_j |\alpha_j|^2$.

On the other hand, another formula for the mean life is obtained from Eq. (1) and its complex conjugate for the radioactive state. Eliminating V by multiplication with ψ_c^* and ψ_c and subtraction and then applying Green's theorem one obtains on account of Eq. (3)

$$\frac{E_c^* - E_c}{hi} \int |\psi_c|^2 d\tau \leqq \sum v_l |\alpha_l|^2, \tag{5.2}$$

so that comparing with (5.1)

$$\int |\psi_c|^2 d\tau \leqq 1. \tag{5.3}$$

This means that the normalization of the radioactive state made by setting $\alpha_j = \hbar^{-\frac{1}{2}} v_j^{-\frac{1}{2}} C_j$ is such as to give (5.3), i.e., one system in the region of configuration space out of which the wave function leaks into the channels; $|C_j|^2/\hbar$ is thus the rate of disintegration caused by the mode j.

According to (5.2) the imaginary part of E_c is negative. On account of (5.1) one has, therefore,

$$\sum_j |C_j|^2 = i(E_c - E_c^*) \tag{6}$$

and hence from Eq. (4.3) one has

$$\sum_j q_{lj} C_j^* = i C_l \tag{6.1}$$

as the conditions on $\|q_{lj}\|$ that must be required in addition to having it unitary and symmetric. These conditions can be simplified by letting

$$C_j = \rho_j \exp(-i\theta_j) \tag{6.2}$$

with ρ_j real and positive and θ_j real. Substituting this into (6.1) one has

$$\sum_j p_{lj} \rho_j = \rho_l, \tag{6.3}$$

$$p_{lj} = i^{-1} q_{lj} \exp[i(\theta_j + \theta_l)]. \tag{6.4}$$

The matrix $\|p_{lj}\|$ is symmetric and unitary as a consequence of the same properties of $\|q_{lj}\|$. Besides it is restricted by (6.3). For many modes of disintegration the restrictions (6.3) allow considerable freedom on p_{lj} because these restrictions mean that $\|p_{lj}\|$ has an eigenvalue 1 and that the vector corresponding to this eigenvalue is parallel to $(\rho_1, \rho_2, \cdots, \rho_n)$. The most general form of p_{lj} is obtained as follows.

One considers the general transformation of n variables $x_1, \cdots, x_n$, $x_i' = \sum p_{ij} x_j$ simultaneously with $x_i = \sum S_{ij} y_j$, $x_i' = \sum S_{ij} y_j'$. The matrix S_{ij} is taken to be real orthogonal. One has then

$$y_i' = \sum (S^{-1} p S)_{ij} y_j. \tag{6.5}$$

One makes besides

$$S_{1i}^{-1} = \rho_i / (\sum \rho_j^2)^{\frac{1}{2}} = S_{i1}. \tag{6.6}$$

One has

$$(S^{-1} p S)_{ij} = \sum S_{ik}^{-1} p_{kl} S_{lj} = \sum S_{ki} p_{lk} S_{jl}^{-1} = (S^{-1} p S)_{ji}.$$

Hence $S^{-1}pS$ is symmetric and unitary. Conversely if it is symmetric and unitary then p is also. On account of (6.6) one has

$$y_1' = \sum \rho_i x_i' / (\sum \rho_j^2)^{\frac{1}{2}} = \sum_{ij} \rho_i p_{ij} x_j / (\sum \rho_j^2)^{\frac{1}{2}}$$
$$= \sum_j \rho_j x_j / (\sum \rho_j^2)^{\frac{1}{2}} = y_1, \tag{6.7}$$

where $\sum \rho_i p_{ij} = \rho_j$ has been used in accordance with (6.3). Comparing (6.7) with (6.5) one sees that $(S^{-1}pS)_{1j} = \delta_{1j}$. Since $S^{-1}pS$ is symmetric $(S^{-1}pS)_{j1} = \delta_{j1}$. The only nonvanishing element in the first row and column of $S^{-1}pS$ is the diagonal element which is unity. The elements $(S^{-1}pS)_{ij}$ with i, j running from 2 to n must be, therefore, those of an n-1-dimensional symmetric unitary matrix U. Aside from these requirements the conditions used do not restrict U. Conversely for any symmetric unitary U one can form

$$\|p_{ij}\| = S\begin{pmatrix} 1 & 0 \\ 0 & U \end{pmatrix} S^{-1} \tag{6.8}$$

and (6.3) as well as the other conditions for $\|p_{ij}\|$ are then satisfied.

Examples

One mode

The scattering matrix consists of one element. The notation is simplified by dropping the suffixes. One has $p=1$, $q=ie^{-2i\theta}$, $C=\rho e^{-i\theta}$, $E_c - E_c^* = -i\rho^2$ and

$$a = b = \frac{C^2}{E - E_c} + ie^{-2i\theta} = ie^{2i(K-\theta)}, \tag{7}$$

where

$$e^{2iK} = (E - E_c^*)/(E - E_c), \tag{7.1}$$

so that K is real and varies from 0 to π as E passes through $(E_c + E_c^*)/2$ from smaller to larger values. The asymptotic form of $r\varphi$ is

$$r\varphi \sim e^{-ikr} + e^{i(kr + 2K - 2\theta)}$$

and

$$-\frac{1}{2i} e^{iL\pi/2} r\varphi \sim \sin(kr - L\pi/2) - \frac{1}{2i} e^{i(kr - L\pi/2)}\left[1 + ie^{i(2K - 2\theta + L\pi)}\right]. \tag{7.2}$$

If the channel represents disintegration with relative angular momentum L, the second term represents the addition to the function usually called F_L. The square of the absolute value of this term is

$$\sin^2\left[K - \theta + (2L-1)\pi/4\right]$$

and the scattering cross section is

$$\sigma_s = (2L+1)(\lambda^2/\pi)\sin^2\left[K - \theta + (2L-1)\pi/4\right]. \tag{7.3}$$

According to (7.1) the rate of variation of K with E is a maximum for $E = (E_c + E_c^*)/2$ and there is a correspondingly rapid variation of the argument of $\sin^2$ in (7.3) at this energy.

Two modes

The matrix U in Eq. (6.8) has one element and its most general form is $e^{2i\xi}$ with a real ξ. The general form of $\|p_{ij}\|$ is thus easily obtained. Substituting it into (4.1) one has

$$\|b_{ij}\| = ie^{2iK}\begin{pmatrix} c^2 e^{-2i\theta_1}, & cse^{-i(\theta_1+\theta_2)} \\ cse^{-i(\theta_1+\theta_2)}, & s^2 e^{-2i\theta_2} \end{pmatrix} + ie^{2i\xi}\begin{pmatrix} s^2 e^{-2i\theta_1}, & -cse^{-i(\theta_1+\theta_2)} \\ -cse^{-i(\theta_1+\theta_2)}, & c^2 e^{-2i\theta_2} \end{pmatrix} \tag{8}$$

with

$$c = \rho_1/(\rho_1^2 + \rho_2^2)^{\frac{1}{2}}, \quad s = \rho_2/(\rho_1 + \rho_2)^{\frac{1}{2}} \tag{8.1}$$

and K as in Eq. (7.1). To the modes of disintegration 1 and 2 there correspond angular momenta of relative motion L_1, L_2. By means of the above matrix one forms the asymptotic solutions

$$-\frac{1}{2i} e^{iL_1\pi/2} r_1\varphi_1' \sim \sin(k_1 r_1 - L_1\pi/2) - \frac{1}{2i}\left\{e^{i(k_1 r_1 - L_1\pi/2)} + i\left[c^2 e^{2iK} + s^2 e^{2i\xi}\right] e^{i(k_1 r_1 + L_1\pi/2 - 2\theta_1)}\right\};$$

$$-\frac{1}{2i} e^{iL_1\pi/2} r_2\varphi_2' \sim -\tfrac{1}{2}(v_1/v_2)^{\frac{1}{2}} cs\left[e^{2iK} - e^{2i\xi}\right] e^{i(k_2 r_2 - \theta_1 - \theta_2 + L_1\pi/2)}.$$

These formulas give the collision cross sections $\sigma_{1\to 1}$, $\sigma_{1\to 2}$ corresponding to incidence in channel 1

giving rise to scattering and disintegration via channel 2, respectively. One obtains in this way

$$\frac{\sigma_{1\to 2}}{(2L_1+1)\Lambda_1^2}=\frac{\sigma_{2\to 1}}{(2L_2+1)\Lambda_2^2}=\frac{\rho_1^2\rho_2^2}{\pi(\rho_1^2+\rho_2^2)^2}\sin^2(K-\xi) \tag{8.3}$$

and

$$\begin{aligned}\sigma_{1\to 1}+\sigma_{1\to 2}&=\frac{2L_1+1}{\pi}\Lambda_1^2[\rho_1^2\cos^2(K-\Theta_1)+\rho_2^2\cos^2(\xi-\Theta_1)]/(\rho_1^2+\rho_2^2),\\ \sigma_{2\to 2}+\sigma_{2\to 1}&=\frac{2L_2+1}{\pi}\Lambda_2^2[\rho_2^2\cos^2(K-\Theta_2)+\rho_1^2\cos^2(\xi-\Theta_2)]/(\rho_1^2+\rho_2^2).\end{aligned} \tag{8.4}$$

Here

$$2\Theta_i=2\theta_i-(2L_i+1)\pi/2. \tag{8.5}$$

Equation (8.3) shows the well-known reciprocity of cross sections which may be derived by considerations of detailed balance. *Resonance* is again defined most simply as that energy at which dK/dE is a maximum. According to (8.3) this energy can be determined, in principle, from a graph of $\sigma_{1\to 2}$ against E which may then be used also for a determination of ξ as well as ρ_1/ρ_2. The latter quantity cannot be determined uniquely from $\sigma_{1\to 2}$ and $\sigma_{2\to 1}$ since ρ_1/ρ_2 and ρ_2/ρ_1 can be interchanged. The width of resonance determines $\rho_1^2+\rho_2^2$ and hence in principle one has from the experimental $\sigma_{1\to 2}$ two possibilities for ρ_1^2, ρ_2^2 as well as values of ξ and $(E_c+E_c^*)/2$. It is obviously possible to use these values in data on $\sigma_{1\to 1}+\sigma_{1\to 2}$ and to test by means of the first equation (8.4) the validity of this formula.

Equation (8) gives a unitary symmetric matrix independently of whether Eq. (7.1) is obeyed or not. The only essential point is that K, θ_1, θ_2, c, s be real and that $c^2+s^2=1$. Discarding Eq. (7.1) and adopting (8) *ad hoc* one still obtains (8.3) and (8.4) but without an explicit connection between $\rho_1^2+\rho_2^2$ and the width of resonance. Such a connection is not necessary, however, in such a formulation because (8.3), (8.4) are homogeneous of degree zero in ρ_1, ρ_2. Only c, s enter into the observable cross sections. Such a formulation can also be tested experimentally by using (8.3) to determine $K-\xi$ as a function of the energy. On the assumption that the maximum of (8.3) corresponds to $\sin^2(K-\xi)=1$ one obtains cs and hence the first Eq. (8.4) contains only one adjustable constant $\xi-\Theta_1$.

The contribution due to $K-\Theta_1$ in (8.4) varies with E while the term in $\cos^2(\xi-\Theta_1)$ is independent of the energy and behaves as a background. If $\rho_2^2\gg\rho_1^2$ the background may be large in comparison with the maximum fluctuation in $\sigma_{1\to 1}+\sigma_{1\to 2}$ near resonance which is $(2L_1+1)\Lambda_1^2\rho_1^2/\pi(\rho_1^2+\rho_2^2)$. Thus, for example, Eq. (8.4) does not exclude the possibility of a scattering + disintegration cross section of slow neutrons of the order Λ_n^2, the resonance contribution on the other hand is limited to $\sim\Lambda_n^2\rho_n^2/(\rho_n^2+\rho_\gamma^2)$ which is of the same order as the capture cross section. The maximum value of $\sigma_{1\to 1}+\sigma_{1\to 2}$ for best values of $K-\Theta_1$, $\xi-\Theta_1$ is $(2L_1+1)\Lambda_1^2/\pi$.

Intensity Changes in Cameron Bands of CO Excited by Electron Impact

GEORGE E. HANSCHE*
Mendenhall Laboratory of Physics, Ohio State University, Columbus, Ohio
(Received September 21, 1940)

Relative intensities of the $^3\Pi-{}^1\Sigma$ Cameron bands and the $^1\Pi-{}^1\Sigma$ fourth positive bands of CO excited by impact of electrons of various energies at various pressures indicate that (1) intense Cameron bands can be obtained at pressures up to 0.025 mm, in contrast with an upper limit of 0.005 mm found in our electrodeless discharge experiments and (2) the excitation function of the Cameron bands has two maxima, like that of a $^3P-{}^1S$ atomic transition.

INTRODUCTION

DATA on electron-impact excitation functions for band systems are very meager. Bernard[1] has shown that the maximum of the experimentally determined excitation function of the auroral bands of N^+_2 shifts rapidly to higher voltages at increasing pressures when multiple electron impacts start but that of the $^3\Pi-{}^3\Pi$ second positive bands of N_2 with a sharp maximum at 16 volts is independent of pressure. Bernard's experimental results are in good agreement with those of both Bundy[2] and Herrmann.[3] Bundy also obtained an excitation function for the comet-tail bands of CO^+ which was similar to his N^+_2 curve.

Previous experiments[4] on intensity variations of the $^3\Pi-{}^1\Sigma$ Cameron bands of CO in an electrodeless discharge have shown that the intensity of these bands as compared with neighboring fourth positive bands increases very abruptly with a decrease in pressure. Consequently, a study of the excitation function of the Cameron bands compared with that of the fourth positive bands was undertaken in the hope of explaining this intensity relationship. The present paper represents the results of this investigation.

EXPERIMENTAL

A metal tube shown in Fig. 1 was used throughout these experiments. It was constructed in two sections joined in a threaded joint, *A*. The upper half of the tube was threaded on the inside so that supports for the filament, *F*, and grid, *G*, could be fixed at any desired height. Electrical connections made through the top of the tube were insulated from the metal by means of Pyrex capillary tubing, *I*, which was in turn sealed with wax. The top of the tube was water cooled to keep the wax from softening. The lower half of the tube contained the Faraday cage, *C*, in which the electrons were collected, and two quartz windows, *Q*, through which the discharge in the field-free space, *B*, could be observed and photographed.

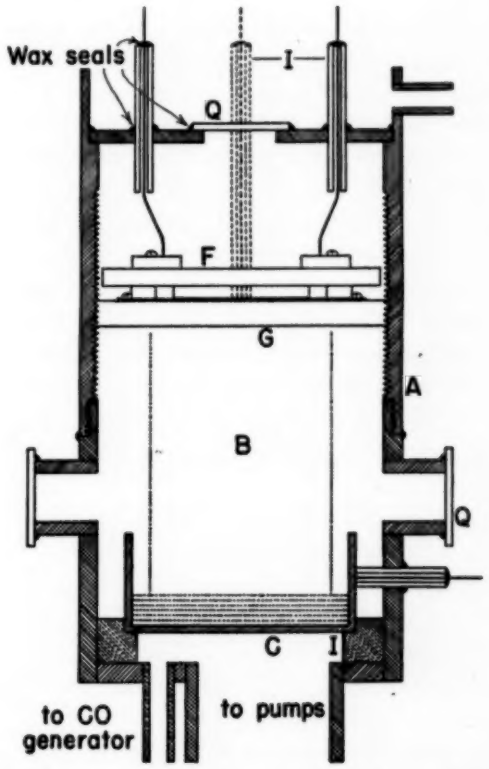

FIG. 1. Discharge tube for controlled electron impacts. *A*, threaded joint at which tube may be taken apart; *B*, field-free space; *C*, Faraday cage; *F*, filament support; *G*, position of grid; *I*, glass insulators; *Q*, quartz windows.

* Now at Rose Polytechnic Institute, Terre Haute, Indiana.

[1] R. Bernard, Ann. de physique **13**, 5 (1940).
[2] F. P. Bundy, Phys. Rev. **52**, 698 (1937).
[3] O. Herrmann, Ann. d. Physik **25**, 166 (1935).
[4] G. E. Hansche, Phys. Rev. **57**, 289 (1940).

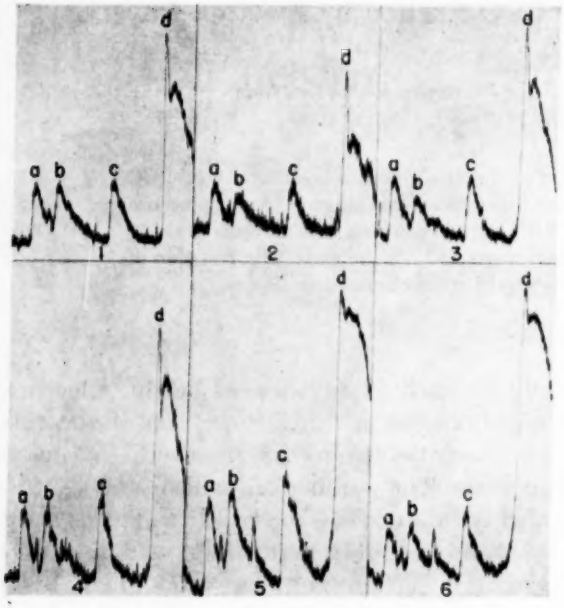

FIG. 2. Microphotometer traces of CO bands (see Table I for exposure data): *a*, (4, 12) fourth positive. *b*, (0, 1) Cameron. *c*, (5, 13) fourth positive. *d*, (0, 0) first negative (CO^+).

The filaments were made from strips of platinum foil 0.0015 inch thick, 0.5 inch long and about 0.2 inch wide. One side of each strip was frayed with scissor cuts, each cut being exactly halfway across the strip to keep the resistance uniform along the entire length of the strip. After being cut, the jagged edges were bent over and flattened against the smooth part of the foil thus furnishing a rough surface to which the activating material could cling. The filaments were spot-welded in place with the jagged sides next to the grid and then coated with oxides of barium and strontium. Nine filaments were connected in series to furnish the emitting surface.

The discharge tube was connected directly to a two-inch brass single-stage oil diffusion pump backed by a Hyvac mechanical pump. A CO generator, needle valve and liquid-air trap served to maintain a continuous flow of gas. The pressure was measured by means of a Pirani gauge.

The electrical circuit was similar to that used by Bernard[1] except that only one grid was used. The filament-to-grid voltage was supplied by two *B*-eliminators in series.

A Steinheil quartz prism spectrograph of 40 cm focal length served to obtain the spectrograms. Both Eastman 40 plates, sensitized with Eastman ultraviolet sensitizing solution, and Ilford type *Q* plates were used. A Moll microphotometer was employed for recording densities of bands on the plates.

RESULTS

Intensities of the Cameron bands in comparison with the fourth positive bands were studied in order to distinguish between the effects of pressure and electron velocity. To illustrate the results, the region 2150–2190A, containing bands of the Cameron, the fourth positive, and the first negative systems has been chosen for comparison with previous experiments.[4] Microphotometer traces of this region, photographed under a variety of conditions, are reproduced in Fig. 2 and Fig. 3 and exposure data are listed in Table I.

Figure 2 shows a set of traces in which the pressure was kept constant at 0.025 mm of mercury while the filament-to-grid voltage was varied from 20 volts in exposure 1 to 150 volts in exposure 6. In these experiments the intensity of the Cameron bands as compared to the fourth positive bands has two maxima. At the lower voltages the Cameron bands are as strong as the fourth positive bands but they decrease in relative intensity at slightly higher potentials. They again reach a second maximum at about 25 volts above the minimum, becoming stronger than the fourth positive bands.

Figure 3 shows results obtained with the pressure kept constant at 0.006 mm of mercury

TABLE I. *Exposure data for Figs. 1 and 2.*

Exposure	Time (hr.)	Pressure (mm)	Filament Current (amp.)	Accel. Potential (volts)	Grid Current (ma)	Galv. Reading (ma)
1	12	0.025	9.5	20	250	7
2	8	0.025	7.2	35	250	10
3	4	0.025	7.2	50	245	14
4	6	0.025	4.0	60	245	50
5	8	0.025	8.4*	100	235	160
6	8	0.025	8.0*	150	225	180
7	5	0.006	9.8	30	260	110
8	5	0.006	8.6	35	250	85
9	9	0.006	6.9	50	245	25
10	5	0.006	6.7	65	240	90
11	6	0.006	6.0	75	240	130
12	5	0.006	5.0	95	235	55

* A different filament was used for these two exposures.

while the voltage was varied from 30 volts in exposure 7 to 95 volts in exposure 12. These exposures show the same relative form of electron-impact excitation function curve but give the minimum at a slightly higher voltage. Another set of exposures taken at a lower pressure gave the dip in the relative intensities of the two bands at still a higher voltage.

Discussion

The occurrence of the Cameron bands with good intensity at a pressure of 0.025 mm of mercury in this source was quite unexpected, since 0.005 mm was the highest pressure at which the bands were intense in the electrodeless discharge. This casts serious doubt on the lifetime of the $^3\Pi$ state computed on the basis of the extinction of the bands by increased pressure.

Actually, the conditions in the two sources differ so much that comparisons of results cannot be made with confidence. The gas temperature is definitely higher in the present experiments, possibly 350°C, in contrast with approximately 85°C in the electrodeless discharge. The high frequency electromagnetic field of the latter is absent in the present experiments, hence it is apparent that the emission of the Cameron bands does not depend on a weakening of selection rules by such a field.

It has been found[1] that the electron-impact excitation function for the $^3\Pi-{}^3\Pi$ second positive, N_2 bands behaves like that for triplet-triplet atomic transitions,[5] namely the function reaches a sharp maximum just above the excitation potential. One would also expect the $^1\Pi-{}^1\Sigma$ fourth positive system of CO to behave in a manner analogous to the corresponding atomic system. From a comparison of the relative intensities of the Cameron and fourth positive bands it is seen that if the above assumption holds, the Cameron bands which involve a $^3\Pi-{}^1\Sigma$ transition would have an excitation function similar to that of a $^3P-{}^1S$ atomic

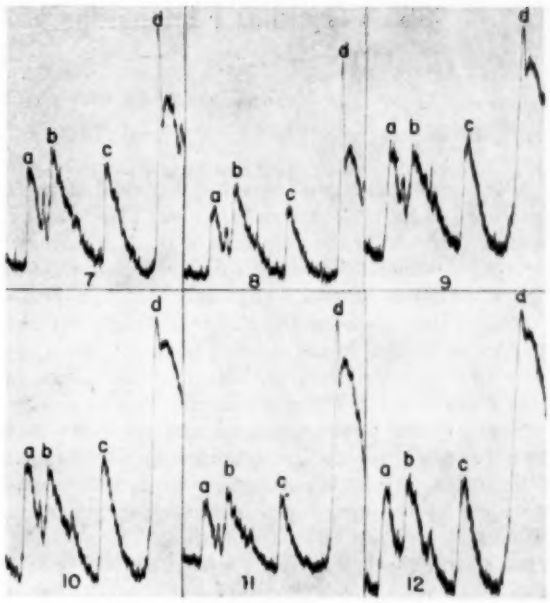

Fig. 3. Microphotometer traces of CO bands (see Table I for exposure data): *a*, (4, 12) fourth positive. *b*, (0, 1) Cameron. *c*, (5, 13) fourth positive. *d*, (0, 0) first negative (CO^+).

transition;[6] that is, a function with two maxima, one of which is reached shortly after the excitation potential while the other is reached at several times this value.

The precise effect of pressure changes on the excitation funcitons of the two band systems can only be inferred from the present experiments. However, the extreme sensitivity to pressure changes exhibited by the Cameron bands in previous experiments suggests that the excitation function of this system is more sensitive to pressure changes than that of the fourth positive system.

Acknowledgments

The author wishes to express his appreciation to Professor H. P. Knauss for suggestion of the problem, and valuable advice. He is also grateful to Mr. Paul Darby, who designed the filaments used in these experiments, and to Mr. Benjamin Clymer, who helped obtain the experimental results.

[5] W. Hanle, Zeits. f. Physik **56**, 94 (1929); J. H. Lees, Proc. Roy. Soc. **A137**, 173 (1932).

[6] W. Schaffernicht, Zeits. f. Physik **62**, 106 (1930); Ornstein, Lindeman and Oldeman, *ibid.* **83**, 171 (1933).

The Optimal Dimensions of a Clusius-Dickel Isotope Separator

WILLIAM KRASNY-ERGEN
Morley Chemical Laboratory, Western Reserve University, Cleveland, Ohio

(Received August 26, 1940)

A Clusius-Dickel isotope separator is treated on basis of the theory of Furry, Jones and Onsager. The dependence on the dimensions of the apparatus of H, A, K_d/K and P_e are derived without any assumption regarding the intermolecular forces in the isotope mixture. The problem treated is: How to choose the dimensions of the apparatus in order to obtain, at the smallest possible cost, a given quantity of isotope mixture, containing one isotope in a given concentration. The costs are assumed to consist of the costs of the power expended and the costs of the apparatus, the latter costs being proportional to the surface of the tubes. We need not include costs, which are independent of the dimensions of the apparatus, as, e.g., the cost of the natural isotope mixture. The question of how to choose the dimensions in order to obtain the output with the minimal power expenditure or with the minimal surface of the tubes is a special case of the general problem. The problem is solved for a single-stage apparatus, in which the concentration of the isotope in question always is small compared with unity. Formulae are given for the distance between the tubes, the mean circumference of the annular space between them and the length of the tubes, as well as for the minimum costs. Similarly, the problem is treated for an "ideal" multi-stage apparatus consisting of very many stages. In this case, the relative abundance of the isotope in question is not restricted to small values. It is shown that the costs are a minimum if the distance between the tubes has a constant value for all stages, this value being the same as for single-stage operation. The mean circumference however is different for different stages. Both in the single- and the multi-stage operation an increase in the pressure reduces the costs somewhat. The production of C^{13} is given as a numerical example.

NOTATION

c_1, relative abundance of the isotope in question.
c_1^0, natural relative abundance of this isotope.
κ_r, value of c_1 to be obtained by the separation process.
τ, quantity of isotope mixture, to be produced per unit time (in g/hour).
$1/\beta$, separation factor $=(\kappa_r/c_1^0)(1-c_1^0)/(1-\kappa_r)$. For κ_r, $c_1^0 \ll 1$: $1/\beta=\kappa_r/c_1^0$.
d, distance between the tubes, in cm.
L, length of the tubes, in cm, or sum of lengths of several stages.
B, mean circumference of the annular space between the tubes, in cm, or sum of circumferences of several tubes, working in parallel.
p, pressure, in atmospheres.
T, temperature, in °K.
T_1 (T_2), temperature of the colder (hotter) tube, in °K.
$G(T)$, H, A, K, K_d, defined in Furry, Jones and Onsager's paper.
D, coefficient of diffusion, in cm²/sec.
λ, thermal conductivity, in cal./cm-sec.-deg.
η, viscosity in poise.
α, thermal diffusion constant.
ρ, density, in g/cm³.
P, cost of running the apparatus one hour.
z, vertical coordinate in cm.

INTRODUCTION

LARGE scale isotope separation is of great interest, for instance, in the case of uranium where a comparatively great quantity of uranium containing U^{235} in an increased relative abundance is required in order to release nuclear energy by a radioactive chain reaction. Any large scale isotope separation is an expensive process. Consequently, the following problem is of special interest: Known is the natural relative abundance c_1^0 of the isotope in question. The relative abundance to be obtained is also given by the purpose for which the isotope shall be used and so is the output τ, i.e., the quantity of isotope mixture to be produced per hour. The question is, how to choose the variables of the apparatus in order to produce at the lowest cost the prescribed output of substance, containing the isotope in the desired relative abundance. This problem is, of course, also of interest in small scale separation. The costs will chiefly consist of: (1) the costs of the power expended;

(2) the price of the apparatus and the costs of replacement of worn out parts; (3) other costs which are independent of the dimensions of the apparatus and consequently can be omitted in our calculations, as for instance, the price of the natural isotope mixture and the wages of the operators.

We shall treat this problem for the *Clusius-Dickel* isotope separators based on the theory of Waldmann,[1] van der Grinten,[2] Furry, Jones and Onsager,[3] Debye,[4] and Bardeen.[5,6]

The energy expended during 1 hour at 1 cm² of the inner tube consists of two parts: The first, due to thermal conduction, and inversely proportional to the distance d between the tubes, can be written as p_c/d kw-hr.; the second part, p_r kw-hr., is due to radiation and independent of d. Thus the total power expenditure, in kw-hr., per hour and 1 cm² of the inner tube is $p'=p_c/d+p_r$. If we take the price of 1 kw-hr. as the unit of costs, p' gives us at the same time the cost of the power expended per hour and cm². We now assume that the costs of the apparatus, as defined under (2) are proportional to the outer surface of the inner tube. We denote by s these costs per cm², divided by the total number of hours during which the apparatus is used. Then

$$\bar{p}=p'+s=p_c/d+p_r+s=p_c/d+p_s \qquad (1)$$

is the total cost per hour and 1 cm².

If the costs of the apparatus are small compared with the costs of energy consumption, or if we are interested only in the problem of obtaining the given output with the minimum energy consumption, we have to put $p_s=p_r$. If the power costs are negligible compared with the costs of the apparatus, or if we are interested only in obtaining the output with the smallest surface of the apparatus, we put $p_c=0$. By integrating $\bar{p}$ over the whole surface of the inner tube, we obtain the total costs P which our apparatus causes every hour, producing τ gram/hour of the isotope mixture with the desired relative abundance κ_r. Our problem thus consists in making P a minimum. In solving this problem we shall use the same notation as Furry, Jones and Onsager, and refer to their formulae by giving the number of the formula and adding FJO. But we shall denote the length of the tubes by L instead of $2l$, and the distance between the tubes by d instead of $2w$.

First of all we need some knowledge about the dependence of the functions H, A and K_d on the dimensions of the apparatus, the pressure p and the temperatures T_1 and T_2 of the tubes. The formulae of Furry, Jones and Onsager for this dependence are based, however, on the specialization that the isotope mixture is a gas in which the molecules act as point centers of force, the force being proportional to r^{-5} (r, distance between the molecules). This assumption is not exactly justified, and the formulae are only meant as approximations. A comparison with the experiment by Nier[7] shows a difference of 60 percent between the approximate theory and the experiment. Because of the uncertainties in the approximations and the fact that the thermal diffusion constant α is not known in most cases, Furry, Jones and Onsager suggest preliminary experiments in order to measure H, A, and K_d. These measurements are especially necessary if the coefficient of diffusion D, the thermal conductivity λ, and the viscosity η are not known. How A and K_d/K can be determined for a gaseous isotope mixture is shown in Nier's paper.[7] H can subsequently be found by observation of the approach to the equilibrium and Bardeen's[5] formulae for this approach.

Of course, it would be very awkward to measure H, A, and K_d for different dimensions of the apparatus. Fortunately we see from Eqs. (6)

[1] L. Waldmann, Naturwiss. **27**, 230 (1939); Zeits. f. Physik **114**, 53 (1939).
[2] W. van der Grinten, Naturwiss. **27**, 317 (1939).
[3] W. H. Furry, R. Clark Jones, and L. Onsager, Phys. Rev. **55**, 1083 (1939).
[4] P. Debye, Ann. d. Physik **56**, 284 (1939).
[5] J. Bardeen, Phys. Rev. **57**, 35 (1940).
[6] A problem, similar to ours, has been treated by Waldmann (Zeits. f. Physik, reference 1, p. 80, 81). The difference in Waldmann's results and ours is chiefly due to the following facts: 1. Waldmann assumes that the velocity v of the gas current, constituting the small total transport of gas through the tube, should be constant (otherwise H/H^*, in Waldmann's notation, would vary). Constant v means, at a given output, that $B\cdot d=$const. This is a constraint to which Waldmann's minimum problem is subject, whereas, in our calculation, B and d can vary independently in order to find the optimum; 2. Waldmann takes a theoretical "maximum output," defined in his paper as a measure for the quantity yielded, whereas our calculations are based on the output actually obtained; 3. Waldmann neglects the energy lost by radiation and the costs of the apparatus.
[7] A. O. Nier, Phys. Rev. **57**, 30 (1940).

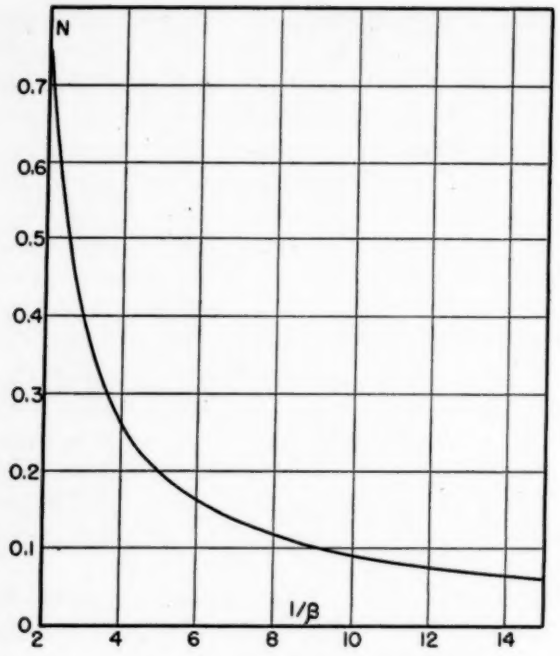

FIG. 1. N as a function of the separation factor.

FJO, (24) FJO, and (25) FJO, that

$$H=Bd^3h, \tag{2}$$

$$A=H/2K=a/d^4, \tag{3}$$

$$K_d/K=\gamma/d^6, \tag{4}$$

$$\left.\begin{aligned} h&=-\int_{T_1}^{T_2}(\rho D\alpha/\lambda T)G(T)dT\left\{\int_{T_1}^{T_2}\lambda dT\right\}^{-3}\\ a&=-\int_{T_1}^{T_2}(\rho D\alpha/\lambda T)G(T)dT\left\{\int_{T_1}^{T_2}\lambda dT\right\}^{4}\Big/\\ &\qquad 2\int_{T_1}^{T_2}(\rho D/\lambda)G(T)^2dT\\ \gamma&=\left\{\int_{T_1}^{T_2}\lambda dT\right\}^{6}\int_{T_1}^{T_2}\rho\lambda D dT\Big/\\ &\qquad \int_{T_1}^{T_2}(\rho D/\lambda)[G(T)]^2dT. \end{aligned}\right\} \tag{5}$$

h, a, and γ depend only on the pressure p and on T_1 and T_2, but not on d and B. If h, a, and γ are measured for one couple of values of d and B, H, A, and K_d are known for all other values of d and B, by Eqs. (2), (3) and (4). These equations are not based on any specializations regarding the intermolecular forces. They also can be applied to liquid isotope mixtures. But the results of our further calculations yield very awkward dimensions for the apparatus for most cases in which the isotope mixture is a liquid. Then our assumption that the costs of the apparatus should be proportional to the surface is no longer valid. For p_c and p_r (Eq. (1)) we obtain:

$$p_c=4.18\times10^{-3}\int_{T_1}^{T_2}\lambda dT, \tag{6}$$

$$p_r=5.7\times10^{-15}(1-R_1)(1-R_2)\times(1-R_1R_2)^{-1}(T_2^4-T_1^4), \tag{7}$$

where R_1 and R_2 are the average reflection coefficients of the tubes, which are supposed to be nontransparent. Of course, p_c and p_r cannot be calculated from these formulae but must be found by experiments, as described by Nier.[7]

SINGLE-STAGE APPARATUS

We specialize our calculations to the case in which c_1, the relative abundance of the molecule in question, is small ($c_1\ll1$). Then we get instead of (51) FJO:

$$[(1+n)c_1-n\kappa_r]^{-1}dc_1=2A_d dz, \tag{8}$$

$$(1+n)^{-1}\lg[(1+n)c_1-n\kappa_r]=2A_d(z-z_0), \tag{9}$$

$$-(1+n)^{-1}\lg[(1+n)\beta-n]=2A_dL, \tag{10}$$

where

$$1/\beta=\kappa_r/c_1^0 \tag{11}$$

is the separation factor required,

$$n=\tau/H=\tau/Bd^3h, \tag{12}$$

$$A_d=A/[1+(K_d/K)] \tag{13}$$

and lg means lg nat.

TABLE I. *Values of the roots N of Eq. (16) and of the functions X and X'.*

1/β	N	X	X'	1/β	N	X	X'
2	0.745	1.58	0.59	9	0.101	34.5	1.74
3	0.381	4.80	0.91	10	0.090	40.2	1.80
4	0.259	8.82	1.14	11	0.081	45.9	1.86
5	0.197	13.5	1.37	12	0.074	52.0	1.92
6	0.159	18.4	1.46	13	0.068	57.8	1.97
7	0.133	23.4	1.56	14	0.063	65.1	2.06
8	0.115	29.1	1.67	15	0.060	71.9	2.16

We now proceed to find out how to choose d and B in order to make P a minimum. Integration of (1) over the whole surface of the inner tube yields:

$$P=(p_c/d+p_s)LB. \tag{14}$$

Expressing L by (10), A_d by (13) and B by (12) we get:

$$P=\frac{\tau}{2ah}\cdot\frac{-\lg[(1+n)\beta-n]}{n(1+n)}\times(p_c+dp_s)\left(1+\frac{\gamma}{d^6}\right). \tag{15}$$

This equation gives us P as a function of d and n, or as n depends on B, of d and B. P is infinite for $n=0$ and $n=\beta/1-\beta$. The first case corresponds to $B=\infty$; in the second L is infinite, because the separation factor per unit length decreases to zero, if τ/B increases so much that n reaches $\beta/(1-\beta)$. Thus there must be at least one minimum for P regarded as a function of B. We find for this minimum

$$0=\partial P/\partial B=(\partial P/\partial n)(dn/dB)$$
$$(\beta-1)n(1+n)$$
$$=(1+2n)[(1+n)\beta-n]\lg[(1+n)\beta-n]. \tag{16}$$

This equation can be shown to have only one root N lying between the limits 0 and $\beta/(1-\beta)$. This root is, of course, a function of β. From Table I and Fig. 1 we can see the value of this function for separation factors $1/\beta$ lying between 2 and 15. For obtaining higher separation factors one probably always will use multi-stage operation (compare p. 1083, paragraph 3).

Substituting N into (15), we find

$$P=(\tau/2ah)(p_c+dp_s)(1+\gamma/d^6)X, \tag{17}$$

where

$$X=-[N(1+N)]^{-1}\lg[(1+N)\beta-N]$$
$$=(1-\beta)/\{(1+2N)[(1+N)\beta-N]\} \tag{18}$$

is a function of β, shown in Table I and Fig. 2.

P must also have a minimum if regarded as a function of d; too small d decreases the efficiency of the apparatus because of remixing due to ordinary diffusion along the tubes, and too great d causes a greater length L, thus increasing the surface and costs of the tubes and the energy losses by radiation. But a slight deviation of d from its optimal value does not increase P very much, as the remixing by diffusion, the costs of the apparatus and the energy lost by radiation are only small corrections. By $\partial P/\partial d=0$ we find from (17)

$$d^7-5\gamma d-6\gamma p_c/p_s=0. \tag{19}$$

This equation can in most cases be solved by finding a first approximation by

$$d_1=(6\gamma p_c/p_s)^{1/7} \tag{20}$$

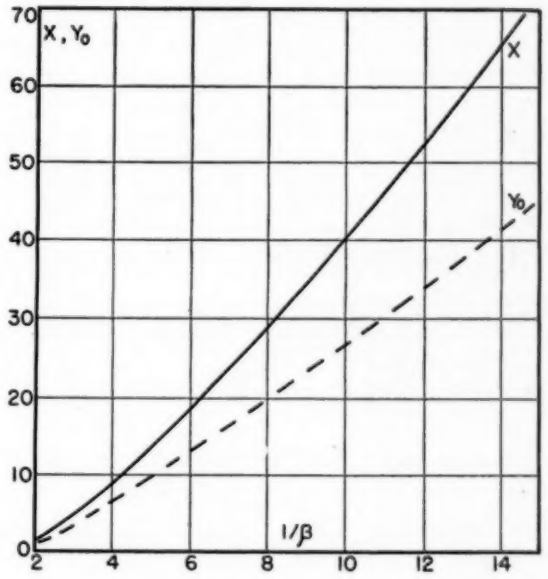

FIG. 2. Costs of a single-stage (——) and a multi-stage (– – – –) apparatus.

and subsequent approximations by

$$d_r=(6\gamma p_c/p_s+5\gamma d_{r-1})^{1/7}\quad r=2, 3, \cdots. \tag{21}$$

If, on the other hand, $p_s\gg p_c$, we have

$$d=(5\gamma)^{1/6}. \tag{22}$$

This equation gives us the optimum value of d, if we wish to obtain the given output with the smallest possible surface or if the cost of the energy lost by conduction is small compared with the other costs.

If we give d the value

$$d=0.89\gamma^{1/6} \tag{22a}$$[1]

we get a maximum of A_d (Eq. (13)) and consequently for a fixed n and β a minimum of L. The power consumption, however, will be considerably above its minimal value (in the numerical

example, given at the end of this paper, by more than 100 percent). In small scale operation, where the costs are not so important, it might happen that the advantage of a small L is greater than the disadvantage of the increase of P. But in large scale production it is essential to bring down the costs to a minimum even if that makes a greater length of the tubes necessary. Before relying upon Eq. (19)—(22a) we also must consider the fact that too large values of d cause a turbulent flow of the gas between the tubes and consequently an ineffective operation of the apparatus. This fact has been treated theoretically and experimentally by Onsager and Watson.[8] The theoretical calculations by these authors are based on the assumption that the molecules act as Maxwellian molecules in all respects except the thermal diffusion. The calculations can, however, be regarded as a good approximation even for non-Maxwellian molecules. Onsager and Watson find experimentally that turbulence occurs at a Reynolds number of about 150, whereas substitution of our Eq. (4) and (22) into Onsager and Watson's equations (1) and (3) yields a Reynolds number lying between 31 and 35. When using Eq. (22a) of this paper, we obtain still smaller Reynolds numbers. Thus application of Eq. (22) and (22a) does not involve any risk of turbulence.

Equation (19) of this paper, however, yields a Reynolds number over 150, if $p_c/(d\cdot p_s)$, the ratio between the costs of energy consumption by conduction and the other costs, turns out to be greater than 20. The Reynolds number lies at about 75, if $p_c/(d\cdot p_s)$ is 3.7. Onsager and Watson point out that it is necessary to know that the Reynolds number lies considerably below the critical value of about 150, in order to be sure, that no turbulence occurs. Therefore, if (19) yields a ratio $p_c/(d\cdot p_s)$ greater than 3.7, it is necessary to determine by experiment, at which d the turbulence sets on, and then the largest d, for which lamellar flow is certain, is to be used in the construction of the final apparatus. How the onset of turbulence can be determined, is shown in Onsager and Watson's paper.

Having found d by the above considerations and N by Table I or Eq. (16) we find B from (12), P from (17) and (18) or Table I. Then L is given by (14)

$$L=(d^4/a)(1+\gamma/d^6)X', \tag{23}$$

where

$$X'=XN/2=\{-\lg[(1+N)\beta-N]\}/2(1+N)$$
$$=(1-\beta)N/\{2(1+2N)[(1+N)\beta-N]\} \tag{24}$$

is a function of β, which can be seen in Table I and Fig. 2.

Multi-Stage Apparatus

We suppose, that the height dz of each stage is so great that the equation

$$\tau_1'=\tau\kappa_r=Hc_1(1-c_1)$$
$$-(K+K_d)(dc_1/dz)+\tau c_1 \tag{25}$$

for the transport τ_1' of the isotope through the apparatus and our Eqs. (2)–(4) for H, A, and K_d are valid at practically all points. Equation (25) is obtained from (48) FJO by taking into account the remixing by diffusion along the tubes. Here it is not necessary to assume $c_1\ll 1$. On the other hand, we use the approximation that summation over all stages can be replaced by integration with respect to z.

From (25) we obtain, by using (2), (3), (4), and (12):

$$dc_1/dz=2ad^{-4}(1+\gamma/d^6)^{-1}$$
$$\times[c_1(1-c_1)-n(\kappa_r-c_1)]. \tag{26}$$

The amount dP, which every stage contributes to P is

$$dP=dz\cdot B\cdot[(p_c/d)+p_s]. \tag{27}$$

Substitution of dz from (26) and B from (12) yields:

$$dP/dc_1=(\tau/2ah)(p_c+dp_s)(1+\gamma/d^6)n^{-1}$$
$$\times[c_1(1-c_1)-n(\kappa_r-c_1)]^{-1}. \tag{28}$$

The conditions necessary for

$$P=\int_{c_1}^{\kappa_r}(dP/dc_1)dc_1 \tag{29}$$

being a minimum, are:

$$\partial(dP/dc_1)/\partial n=0;\ \partial(dP/dc_1)/\partial d=0 \tag{30) (31}$$

(30) and (28) yield:

$$n=c_1(1-c_1)/2(\kappa_r-c_1) \tag{32}$$

[8] L. Onsager and W. W. Watson, Phys. Rev. **56**, 474 (1939).

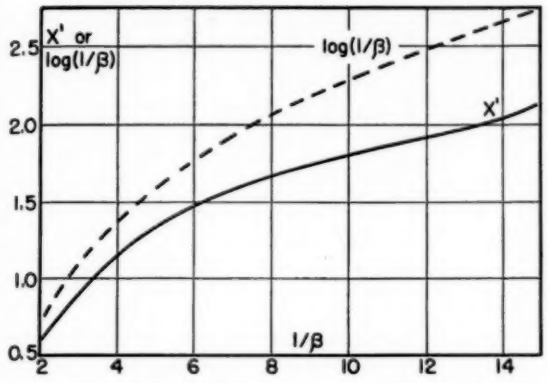

FIG. 3. Length of a single-stage (——) and a multi-stage (– – – –) apparatus.

and from (31) and (28) we find again Eq. (19), which can be solved in the same way as outlined above. As for the single-stage apparatus, we also can give d the value determined by (22a), thus making the total length a minimum, but increasing the costs or power expenditure P. The precautions against turbulence, described above for the single-stage apparatus, have also to be applied here. Having determined d, we obtain from (12) and (32)

$$B=(2\tau/hd^3)(\kappa_r-c_1)/c_1(1-c_1), \qquad (33)$$

where c_1 is according to (26) and (37) given by

$$c_1/(1-c_1)=[c_1^0/(1-c_1^0)](1/\beta)^{z/L} \qquad (33a)$$

and $z=0$ at the end, where the natural isotope mixture is supplied.

Thus we see, the minimum of P is obtained if d has a constant value throughout the whole apparatus, this value being the same as for single-stage operation. The mean circumference however varies along the tubes according to (33), having its greatest value

$$B_0=(2\tau/hd^3)(\kappa_r/c_1^0-1)/(1-c_1^0) \qquad (34)$$

at the end, where the natural isotope mixture is supplied, and being very small at the opposite end.

Substituting (32) into (29), and (28) we see that

$$P=(\tau/2ah)(p_e+dp_s)(1+\gamma/d^6)\,Y, \qquad (35)$$

$$Y=4(\kappa_r/c_1^0-1)[1-c_1^0/(1-c_1^0)] +4(1-2\kappa_r)\lg\beta. \qquad (36)$$

If c_1^0, $\kappa_r \ll 1$, we get instead of Y

$$Y_0=4(1/\beta-1+\lg\beta). \qquad (36a)$$

Figure 2 shows a comparison between X and Y_0, which is, for the case c_1^0, $\kappa_r \ll 1$ a comparison for the power expenditure (cost) in single- and multi-stage operation. For a separation factor of 15, for example, the value of P is 60 percent greater for single stage than for multi-stage operation.

The total length L can be found by the integral:

$$L=\int_{c_1^0}^{\kappa_r}(dz/dc_1)dc_1 =a^{-1}d^4(1+\gamma/d^6)\cdot\lg(1/\beta). \qquad (37)$$

A comparison between X' and $\lg(1/\beta)$, or, for $\kappa_r \ll 1$, between the length of a single-stage apparatus and a multi-stage apparatus is shown in Fig. 3.

We also have developed the formulae for a multi-stage apparatus, in which B is constant along the tubes, and d varies in such a way, that P is a minimum. These formulae, however, are too complicated to be used in practice.

VARIATION OF PRESSURE AND TEMPERATURE

So far we have treated the problem of how to choose the dimensions of the apparatus if the pressure and the temperatures of the tubes are constant. We now proceed to study the influence of the pressure and temperature on the power consumption and the costs.

For gases which are far enough from their condensation point, there is a good agreement between theory and experiment, as to the fact, that the coefficient of diffusion is inversely proportional to the pressure, p, whereas the viscosity and the thermal conductivity do not depend on the pressure.[9] The density is of course proportional to p. No experiments have been made to determine the dependence on p of the thermal diffusion constant α, and we assume, that α is independent of the pressure, as it should be according to the theory.

If the coefficient of diffusion, the viscosity, the thermal conductivity, the density, and α

[9] See, e.g., G. Jäger, in Geiger-Scheel, Handbuch d. Physik 9, p. 415.

are subject to these laws, we see, without any assumption regarding the intermolecular forces, that $G(T)$ must be proportional to p^2:

$$G(T) \propto p^2. \tag{38}$$

This follows from Eq. (20) FJO. Then, our Eqs. (5), (6), and (7) yield:

$$h \propto p^2, \quad (39) \qquad \gamma \propto p^{-4}, \quad (40) \qquad a \propto p^{-2}, \quad (41)$$
$$p_c \text{ and } p_r \text{ independent of } p. \tag{42}$$

We first consider the cases, that d has to be determined by Eqs. (22) or (22a) or that d has, at any pressure, the greatest value, which can be applied without causing turbulence. In all these cases, $\gamma/d^6 = K_d/K$ has a constant value. This value is 0.2 if (22) is used and 2, if (22a) is applied. That K_d/K must be constant in the third of the just named cases, follows from the assumption that turbulence always occurs at the same Reynolds number, and from the fact that the Reynolds number is proportional to $(K_d/K)^{-\frac{1}{2}}$, by a factor only involving T_1 and T_2, but not p. This fact has been pointed out by Onsager and Watson in the theoretical part of their paper.

In the three cases named above, we see from (40) that d can be written as:

$$d = d_0 p^{-\frac{1}{7}}. \tag{43}$$

Then we see from Eq. (17) for the single-stage apparatus and from Eq. (35) for the multi-stage apparatus, that

$$P = \text{const.}\ (p_c + p_s d_0 p^{-\frac{1}{7}}). \tag{44}$$

P consequently decreases, as p increases. For L we see from (23) and (37) for the single- and multi-stage apparatus, respectively, that L is proportional to $p^{-\frac{1}{7}}$. B is independent of p for the single-stage apparatus as can be seen from (12). The same result is obtained for the multi-stage apparatus from (33) and (33a) if B is measured for all pressures at heights z, for which z/L is constant.

For the case, that d is determined by Eq. (19) we see from (20) that d_1 varies as $\gamma^{1/7}$. Then if Eq. (21) is written for $r=2$ the term $5\gamma d_1$ varies more than γ and consequently the variation of d_2 is somewhat greater than the variation of $\gamma^{1/7}$. Writing (21) for $r=3, 4, \cdots$ we can prove the same for $d_3, d_4, \cdots$ and consequently for d. If p_c/p_s is very great, the influence of the terms $5\gamma d_{r-1}$ will be small, and d will vary nearly as $\gamma^{1/7}$. If p_c/p_s is small, we have nearly the case of Eq. (22) in which d varies as $\gamma^{1/6}$. Consequently, d varies always more than $p^{-4/7}$ and less than $p^{-4/6}$. (Compare Eq. (40)). Increase of p causes decrease of d, and also of $\gamma/d^6 = K_d/K$. The latter means that the Reynolds number and the risk of turbulence grow, if higher p is applied and d readjusted according to (19). Consequently, (19) only can be applied until a certain p is reached. With further increase of p, we have the case, treated above, in which γ/d^6 must be kept constant and d vary as $p^{-\frac{1}{7}}$, in order to avoid a further increase in the Reynolds number.

Furthermore, we see that the factors $(p_c + dp_s)$ and $(1+\gamma/d^6)$ which occur in expressions (17) and (35) for P, decrease if p increases. As the other factors in these expressions remain constant, it is, also in the case of Eq. (19), advantageous, to choose p as high as possible, in order to obtain the lowest possible P. From (41) it follows that the factor d^4/a, which occurs in Eq. (23) and (37) for L, varies more than $p^{-2/7}$ and less than $p^{-\frac{1}{7}}$. Anyway, this factor decreases, as p increases, and so does $(1+\gamma/d^6)$. As the rest of (23) and (37) is independent of p, we see that L gets smaller if p grows. From (12) and (39) it follows for the single-stage apparatus, that B also decreases, if p increases, the variation being at the utmost as $p^{-2/7}$. The same is, by (33) and (33a), true for the multi-stage apparatus, if B is measured for all pressures at constant values of z/L.

Thus we see, that an increase in p is advantageous, because it decreases P and L. A limit for the increase in p is given by the fact that it is difficult to make the apparatus resistant against very high p, and also by the fact that the small values of d, accompanying high p, make the operation more sensitive against the effect of unavoidable small asymmetries. This effect consists in an additional remixing and consequently in a lower separation factor.

In Eq. (5) we see that p cancels out in all terms except $G(T)$. In this term it only occurs in the combination $p^2 g$, as can be seen from (20) FJO. Thus, a variation of the effective value of

the gravity g by a factor f has the same effect as a variation of the pressure p by a factor $f^{\frac{1}{2}}$.

The temperature T_1 of the colder tube should always be as low as possible. Generally, T_1 will be given by the temperature of the cooling water or the condensation point of the isotope mixture, or similar factors. The influence of the temperature T_2 of the hotter tube cannot be treated mathematically, because there is no formula for the real temperature dependence of λ, η, D, and α. There must exist an optimum value of T_2, as too low T_2 makes the apparatus ineffective and too high T_2 causes too great energy losses by radiation. In most cases, however, this optimum value lies very high and cannot be reached because of thermal decomposition of the gas or similar causes. Then these causes will determine T_2. If one has the possibility of using very high temperatures T_2, one has to determine experimentally h, a, γ, p_c and p_s for different values of T_2 and then it can be determined which T_2 gives the lowest P.

A. Numerical Example

Experimental values for H, A and K_d/K have been obtained by Nier[7] and Bardeen[5] for the separation of $C^{12}H_4$ and $C^{13}H_4$. Based on these values, we will calculate the optimum dimensions of a $C^{12}H_4-C^{13}H_4$ separator, which yields 10 mg per hour of a mixture, containing the C^{13} in a concentration, corresponding to the tenfold of the natural relative abundance ($\beta=0.1$).

Table II. *Dimensions of a single-stage and a multi-stage apparatus for minimal power expenditure, for minimal surface, and for minimal length.*

	Minimal Power	Minimal Surface	Minimal Length	Derived From Equations
d	0.764 cm	0.66 cm	0.45 cm	(19), (22) (22a) resp.
		Single-stage		
B	12.5 cm	19.3 cm	61 cm	(12)
N	0.09	0.09	0.09	(16) or Table I
L	28 m	17.4 m	9.3 m	(23), (24) or Table I
$L\cdot B$	350 m²	336 m²	567 m²	
Power	10.15 kw	10.6 kw	22.8 kw	(17), (18) or Table I
		Multi-stage		
B_0	20.2 cm	31.2 cm	99 cm	(34)
L	35.8 m	22.2 m	11.9 m	(37a)
Power	6.77 kw	7.07 kw	15.2 kw	(35), (36a)

As Nier states that his apparatus might have had some imperfections, as, for instance, asymmetries, there is some uncertainty in the values of H, A, and K_d/K, and consequently in the following calculations. But the calculations will be a useful illustration of how the equations of this paper can be applied.

Experimental data given by Nier for his apparatus:

$L=730$ cm
$d=0.712$ cm
$B=12.5$ cm
$T_1=300°$K
$T_2=600°$K
energy consumption, due to radiation $=p_rLB=1.22$ kw
total energy consumption $=p'LB=2.75$ kw
$H=2.5\times10^{-5}$ g/sec. $=9\times10^{-2}$ g/hour.
(for $p=1$ atmosphere)
$A=9.18\times10^{-4}$ cm^{-1}, $K_d/K=0.126$ } For $p=1$ atmosphere, from Nier's Eq. (8)

From these values we obtain:

$p_r=1.34\times10^{-4}$ kw/cm³
$p'=3.01\times10^{-4}$ kw/cm³
$p_c=d(p'-p_r)=1.19\times10^{-4}$ kw/cm (from Eq. (1))
$h=2\times10^{-2}$ g/(hour·cm⁴) (from Eq. (2))
$a=2.37\times10^{-4}$ cm³ (from Eq. (3))
$\gamma=1.66\times10^{-2}$ cm⁶ (from Eq. (4))

Table II gives the dimensions of a single-stage and a multi-stage apparatus (a) for minimal power expenditure (b) for minimal surface (c) for minimal length. B_0 is the value of B at the top of the multi-stage apparatus. The value of B for the other stages can be seen from Eq. (33) and (33a), where the positive z axis is pointing downwards and $z=0$ at the upper end of the apparatus. The dimensions of an apparatus, for which the sum of the costs of energy and the costs of the apparatus has to be a minimum, lay somewhere between the values for "minimal power" and "minimal surface." The exact values depend on the ratio between the costs of power and the costs of the apparatus. We see from Table II that the power expenditure in an apparatus of minimal length lies 120 percent above the minimal power consumption necessary for the desired output.

Hyperfine Structure and Intensities of the Forbidden Lines of Pb I

S. MROZOWSKI*
Radiation Laboratory, Department of Physics, University of California, Berkeley, California
(Received October 25, 1940)

The hyperfine structure of the forbidden lines of lead is studied in order to establish the intensity rules in the hyperfine structure of such lines. Those here investigated arise from transitions between the levels of the $6p^2$ configuration, and show hyperfine structure because of the presence of a nuclear spin and magnetic moment in the isotope 207. They are excited very intensely by 3-meter standing waves in helium at about 5 mm pressure, containing saturated Pb vapor at 800°C. The type of discharge and its dependence on several factors are studied. Intensities are quantitatively determined from calibrated plates. For the quadrupole line λ5313, the intensity ratio (3 : 2), and the ratio of the distances from the center of gravity, are found to agree with the Rubinowicz formulas transcribed for hyperfine structure by Opechowski (selection rule $\Delta F=0, \pm1, \pm2$). For the magnetic dipole line λ4618, these ratios agree with the well-known rules for electric dipole transitions (2 : 1). In the case of λ7330, which is of mixed type, the intensities are approximately those for ordinary electric dipole transitions, showing that this line is mostly magnetic dipole radiation and that for such radiation the selection rule $\Delta F=0, \pm1$ holds. An upper limit of the admixture of electric quadrupole can be evaluated from these measurements. The measurements also show that the total transition probabilities for electric quadrupole and magnetic dipole are independent of the existence of a magnetic moment of the nucleus since they are the same for the various isotopes. Finally, the relative intensities of these three lines and of two others, λ4659 and a newly found line at λ9250($^3P_2-{}^1D_2$), have been measured for comparison with theory. The results are $I_{4618} : I_{5313} = 5.0\pm0.3$ and $I_{4659} : I_{7330} : I_{9250} = 0.023\pm0.006 : 1 : 0.84 \pm0.07$. These ratios are independent of the furnace temperature. The ratio $I_{5313} : I_{4659}$ varies somewhat with temperature, changing from about 15 to 12 in going from the lower to the higher temperatures.

THE selection rules and intensity formulas have been accurately checked in the hyperfine structure of ordinary electric dipole lines. Very little is known about the case of forbidden lines, probably because of the relatively greater experimental difficulties in investigating them. Of the four known types of forbidden lines three present certain features of interest for further investigation. (1) Quadrupole lines. For only one line of this type has the hyperfine structure been observed (λ2815 in Hg II[1]). Formulas for the relative intensities in the hyperfine structure of such lines have been obtained by Opechowski[1] from the Rubinowicz formulas for multiplet structure, using the same process as that used in getting the hyperfine structure formulas of Hill from the Hönl and Kronig multiplet formulas, namely by substitution of the quantum numbers F, J and I in place of J, L and S. The selection rule $\Delta F=0, \pm1, \pm2$ and the intensity formulas of Opechowski have been checked by the excellent agreement of the predicted and observed structures of the Hg II line mentioned above, but no exact photometric measurements were made. For this line, the proof would not have been completely satisfactory anyway, in view of the partial overlapping of components belonging to the two odd isotopes of Hg. It therefore seemed worth while to make an accurate test of the applicability of the formulas for this case. (2) Magnetic dipole lines. No hyperfine structure has been observed and no theoretical predictions made about the intensities in the hyperfine components of lines of this type. Furthermore, the problem of lines of mixed character (magnetic dipole+electric quadrupole) appeared to be of considerable interest.[1] (3) Forbidden lines caused by inner hyperfine structure perturbations. These have been the most extensively investigated. Not only has the case of perturbations by nearby levels been studied, as in Al[2] and Hg,[3] but also one[4] where an extremely small perturbation induces the emission of a line forbidden for all types of spontaneous radiation, namely λ2656 in Hg I, $^3P_0 \rightarrow {}^1S_0$. Although the intensities of the components in this line were found to agree roughly with theory,[5] the two components belong

* Now at Ryerson Physical Laboratory, University of Chicago.

[1] S. Mrozowski, Phys. Rev. **57**, 207 (1940).

[2] F. Paschen, Sitz. Preuss. Akad. Wiss. **32**, 502 (1932).

[3] S. Goudsmit and R. F. Bacher, Phys. Rev. **43**, 894 (1933).

[4] S. Mrozowski, Zeits. f. Physik **108**, 204 (1938).

[5] W. Opechowski, Zeits. f. Physik **109**, 485 (1938).

to different Hg isotopes. Hence it would be interesting to check the perturbation theory in a case where the intensities of different components emitted by the same isotope could be compared. For this purpose, the investigation of $\lambda 2270(^3P_2 \rightarrow {}^1S_0)$ of Hg I[6] offers an opportunity for comparison with the calculations of Einaudi.[7]
(4) The fourth type of forbidden transitions is caused by external fields, but these present no interest for hyperfine structure investigations because of the strong broadening of the lines.[1]

Some years ago Niewodniczanski[8] showed that the forbidden lines of Pb I are emitted very strongly in a discharge through a mixture of lead vapor and a rare gas excited by high frequency current. The intensity of these lines was great enough so that he not only found two new lines, λ5313 and λ4659, in addition to the two previously known ones, λ4618 and λ7330, but also was able to study the Zeeman effect in λ4618.[9] This was the first and, up to the present, the only proof of the existence of radiation of magnetic dipole character. A more detailed investigation of these forbidden transitions seemed to promise results of considerable interest. Having at my disposal an excellent oscillator built kindly by Messrs. W. W. Salisbury and L. W. Wouters for my investigations of the spectra of radioactive substances, I was able to get extremely high intensities of these forbidden lines of lead and to study their hyperfine structure. An investigation of their Zeeman effect, in collaboration with Professor F. A. Jenkins, has given successful results, and will be reported in the near future.

Experimental

In preparing the discharge tube, a small portion of chemically pure lead was inserted in a quartz tube 12 cm long and 2 cm in diameter, having a plane window fused on the end. During the experiments the tube was permanently connected to the vacuum system by a side tube of quartz with a constriction close to the discharge tube. The latter, and part of the connecting tube, were surrounded by an electric furnace. The tube could be used for a month or more of daily operation without refilling with fresh lead, because the distillation of lead was retarded by the constriction, and by the presence of helium at a pressure of several mm. One of the difficulties encountered was cracking of the tube at the places where the quartz came in contact with metallic lead. At high temperatures lead attacks the inner surface of the quartz, roughens it, and adheres to it very strongly. Cooling of the tube below the temperature of solidification of lead produces strains which cause the cracks. Therefore the furnace was always kept hot, the temperature being kept at about 400°C when the discharge was not running. The furnace was designed to give a slightly lower temperature at the end containing the lead near the constriction, thus preventing the distillation of lead onto the window at the other end, through which the discharge was observed end-on. This precaution is essential, because formation of a few drops of metallic lead on the surface of the window at high temperature (above 700°C) soon leads to roughness of a large part of the window, the drops acting as centers of the disturbance, which can spread a distance of some mm. A tube thus attacked can be renovated by a procedure devised more than ten years ago by Dr. W. Kessel in Warsaw, consisting of treatment with warm hydrofluoric acid and subsequent heating close to the melting point in an oxygen flame. Naturally the planeness of the window is destroyed in this process.

A liquid-air trap was used between the tube and the vacuum system to avoid the vapors of the diffusion pump oil and of stopcock grease. These vapors decompose in the discharge giving an absorbing layer of carbon, which can only be removed from the window by allowing the tube to cool and burning off the carbon in air. Cooling the trap merely during operation of the discharge does not avoid this difficulty completely. The carbon deposits chiefly in the neighborhood of the electrodes, that is on the ends of the tube. Another type of opaque deposit forms at the ends of the tube during operation, the presence of which is probably due to the presence of PbO molecules, since its formation seemed to be

[6] T. Takamine and M. Fukuda, Phys. Rev. **25**, 23 (1925).
[7] F. R. Einaudi, Rend. R. Accad. dei Lincei **17**, 552 (1933).
[8] H. Niewodniczanski, Acta Phys. Polonica **2**, 375 (1934).
[9] H. Niewodniczanski, Acta Phys. Polonica **3**, 285 (1934); see also his more general article on forbidden lines, *ibid.* **5**, 111 (1936).

correlated with the existence of PbO bands in the spectrum. This deposit evaporates rapidly if the discharge is discontinued, and hence the discharge was interrupted every 15 minutes for about 5 minutes. If the formation of a considerable thickness of this deposit is not prevented, the deposit grows more stable, and this again can only be removed by cooling the tube and heating the window in air to the softening point of quartz.

The electrical apparatus for exciting the discharge consisted of a self-excited half-wave resonant line oscillator using two 500-watt tubes, one at each end of the line. The plate voltage was furnished by a transformer with rectifiers, and the voltage in the primary could be changed in small steps. The electrodes of the discharge tube were two rings of platinum wire around the ends of the tube, and were connected to the oscillator by leads attached on both sides of, and close to the center of, the oscillating line. The best distance was 5–10 cm from the center. At greater distances, too much energy goes into the discharge and suppresses the forbidden lines (see below), at the same time spoiling the balance in the oscillator. At smaller distances the intensity of the discharge is insufficient. Protective condensers and a choke grounded at the middle were inserted in the lines leading to the tube. This was necessary to avoid burning the asbestos in the furnace around the platinum wires.

A careful study was made of the various factors influencing the type of discharge, and the intensity of the allowed and forbidden lines. The wave-length used was about 3 m and could only be varied within small limits (± 0.5 m). No effect of such small changes of frequency on the type and intensity of discharge was found. The most important factor was the temperature of the furnace, that is, the density of the lead vapor. With increase of temperature we first have a pure helium spectrum, but above 500°C the helium lines gradually become weaker and the spectra of both Pb II and Pb I appear, the lines first growing in intensity and then decreasing. The intensity maximum appears at higher temperatures for lines of lower excitation energy. The helium lines disappear completely a little earlier than the Pb II lines. A complete spectrum of Pb I (in the region 2500–11,000A) appears at relatively low temperatures, while the Pb II spectrum behaves quite differently. Of the ^2P levels in Pb II only those below 25,000 cm^{-1} are excited.[10] Lines were observed that originate from ^2D levels lying a little higher (17,000 cm^{-1}), from ^2F levels lying considerably higher (9300 cm^{-1}), and from ^2G levels very much higher (about 5400 cm^{-1}). This preferential excitation of the ^2G levels is probably connected with the mechanism of the discharge. The energy of an ionized He atom ($\sim$198,000 cm^{-1}) is just a little higher than the energy required to doubly ionize a Pb atom ($\sim$181,000 cm^{-1}). As long as there is a small concentration of Pb atoms there are many highly excited atoms and free ions of helium. The latter, because of their longer lifetime, have a chance to collide with Pb atoms and to transfer their energy, taking on an electron and expelling another in the process. The spectrum of Pb II at low temperatures looks like a typical recombination spectrum, in which the free electrons have a much greater probability of being bound into states with high L values, and thus high statistical weights, from which by successive jumps they reach levels with lower and lower L values. Probably a different mechanism of excitation must be assumed in the case of the levels 8^2S and 9^2S of Pb II. These are quite strongly excited, although no trace of the lines from 11^2S and 10^2P could be detected, and the levels 8^2P and 9^2P are excited rather weakly. Nothing can be said about the line from 10^2S as it is covered by strong Pb I line λ3262. The excitation in this case is probably produced by collisions with metastable He atoms ($\sim$160,000 cm^{-1}), whose energy is just about sufficient to excite the higher level 9^2S ($\sim$161,000 cm^{-1}). That in such collisions, accompanied by expulsion of an electron, a preferential excitation of ^2S levels occurs is perhaps connected with the operation of some selection rule. A somewhat similar intensity distribution in the spectrum of Pb II was observed by Earls and Sawyer.[10] No doubt this was also due to the admixture of helium.

An increase of the density of Pb vapor results in a decrease of the average energy of the free electrons, thus resulting in direct excitation of

[10] See the classification of L. T. Earls and R. A. Sawyer, Phys. Rev. **47**, 115 (1935).

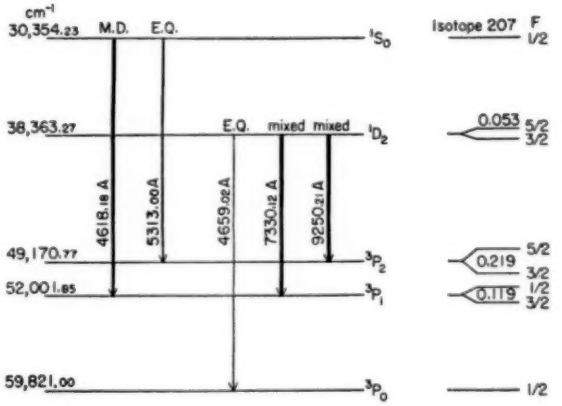

FIG. 1. The lowest levels of Pb I, all belonging to the $6s^26p^2$ configuration. Arrows show the transitions giving the forbidden lines investigated. On the right, the hyperfine splitting of levels of the isotope 207 is shown, but not to scale. M.D. = magnetic dipole, E.Q. = electric quadrupole.

lower and lower energy levels. At high temperatures, above 800°C, only a few lines, originating principally from low Pb I levels, are observed. Increase of the power of the oscillations produces an increase of the intensity of all lines, but the type of the spectrum is very little affected. The change apparently corresponds to a small lowering of the temperature of the furnace. Addition of helium enhances the whole spectrum, but the magnitude of the He pressure above 1 mm has little effect on the intensity. The intensity of most lines increases slowly in the range 1–10 mm of He.

The five lowest levels of Pb I arising from the normal $6p^2$ configuration are represented in Fig. 1. All transitions between these levels are forbidden for electric dipole radiation by Laporte's rule. The wave numbers of the levels were calculated using the very exact wavelengths of the Pb I lines contained in *M. I. T. Wavelength Tables*.[11] The separations of the levels were determined from different pairs of allowed transitions involving a common upper level. The disagreement between independent determinations did not exceed 0.3 cm^{-1}. Average values were used in finding the terms and the wavelengths of the forbidden lines studied. The five lines shown in Fig. 1 comprise all the forbidden lines found thus far. The remaining forbidden transitions which may occur for magnetic dipole or electric quadrupole radiation, namely $^1S_0 \rightarrow {}^1D_2$ and the transitions between the ^3P levels, lie far in infra-red region, and would be very difficult to identify or investigate. The two groups of observed lines are emitted from the two metastable states $^1S_0$ and $^1D_2$. Corresponding to the observations on the allowed lines described above is the fact that the maximum of intensity for the second group lies at higher temperatures (~850°C) than for the first (~800°C). But the forbidden lines differ markedly from the allowed ones in other respects. Their intensity first rises and then diminishes quite rapidly with increasing power and voltage of the oscillations. This is due to the destruction of metastable atoms by multiple excitation into higher levels. The influence of helium is very pronounced. The intensity of the forbidden lines is very small in a discharge through pure Pb vapor, but increases at first rapidly and then more slowly, tending to saturation as the He pressure is increased. All experiments were carried out with He at 5–6 mm. This is well above the range of the first rapid increase, and not far from saturation.

The forbidden lines are very sensitive to the slightest traces of impurities. Amounts which are small enough so that they do not affect the intensity of other lead lines at all, and which cannot be detected by visual observations of the spectrum, reduce the intensity of these lines very considerably. This does not refer to PbO molecules, which have comparatively small quenching effect. If the lead is slightly oxidized, PbO bands appear in the spectrum, but they are very weak in the temperature range used. Their intensity increases quite rapidly at the cost of the whole Pb spectrum above 850°C. The chief sources of impurities are the vapors of stopcock grease and the impurities coming out of the metallic lead. The latter source gives a constant supply of impurities, even though when starting with fresh lead it was always heated to well above 1000°C for at least ½ hour in order to outgas it. Therefore every few hours, at the start of a series of runs, the tube was pumped out and fresh helium introduced. In this way an exceptionally high intensity of the forbidden lines was achieved. Not only could the weak line λ4659 be easily seen in the spectrograph, but

[11] G. R. Harrison, *M.I.T. Wavelength Tables* (Wiley and Sons, New York, 1939).

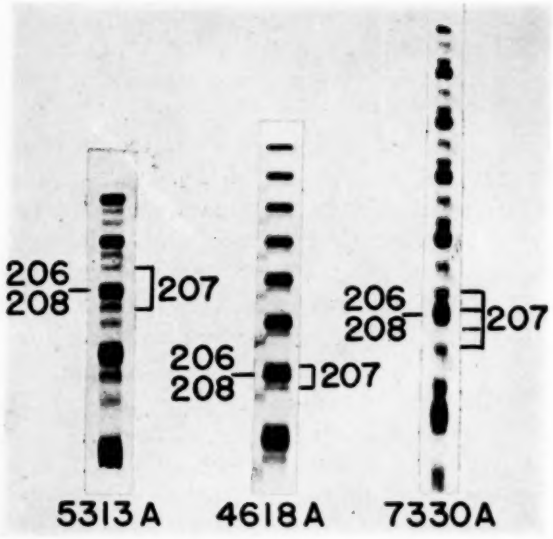

FIG. 2. Hyperfine structure of λ5313 (separator 17 mm); λ4618 (separator 15 mm); λ7330 (separator 19 mm).

also the line λ7330 appeared as a faint companion of the strong allowed line λ7229. After insertion of a Fabry-Perot etalon, the hyperfine structure of the lines 4618 and 5313 was visible. Since many attempts to increase further the intensity of these lines failed, it was concluded that in these experiments the concentration of metastable atoms had practically reached its saturation value, and was limited by the dimensions of the tube and the diffusion of metastable atoms to the walls.

The spectroscopic apparatus consisted of a one-prism glass spectrograph with lenses of 1-m focus, aperture 1 : 12, and a Fabry-Perot etalon, which was used between the prism and the collimator lens. The image of the source was projected on the slit by a short focus quartz lens. The Fabry-Perot plates were silvered, with the kind assistance of Mr. B. G. Saunders, the thickness of deposit being rather light, but still giving sufficient resolving power. (A very high resolving power was not necessary in view of the strong Doppler broadening of the lines.) Intensity marks were recorded on each plate above and below the interferometer pattern. This was done with a step-slit, removing the Fabry-Perot etalon and putting a sheet of white paper in front of the slit. The paper was illuminated from the side toward the slit by an ordinary frosted bulb, placed at such a distance as to make the time of exposure of the steps and of the Pb lines approximately the same. Photographic densities were measured with a Zeiss recording microphotometer and the intensity distribution was then evaluated by a method used by the author on the spectrum of boron and described in a previous paper.[12]

RESULTS

The hyperfine structure of the forbidden lines studied consisted of a strong main component belonging to the even isotopes of Pb (204, 206 and 208, comprising about 79 percent) and much weaker components belonging to the isotope 207 (20.2 percent), which has a nuclear spin of $\frac{1}{2}$. As all Pb levels involved belong to the same configuration, $6p^2$, practically no isotope shift in the lines is to be expected because whatever isotope shift occurs in the levels should be the same for all levels of one configuration. The hyperfine structure of the ordinary lead lines has been investigated by several different authors, and all find nearly equal shifts in all levels of the $6p^2$ configuration. The values given by them[13] of the hyperfine structure splitting of these levels for Pb^{207} are in excellent agreement with the values here measured, and shown in Fig. 1.

The quadrupole line λ5313[14]

In Fig. 2 is an enlargement of a 10-minute exposure of this line taken with a 17-mm Fabry-Perot separator. Eastman Super Panchro Press plates were used here. Two weaker components, on opposite sides of the main component, are observed. They obviously arise from the two transitions for the quantum number F $\frac{1}{2}\rightarrow\frac{5}{2}$ and $\frac{1}{2}\rightarrow\frac{3}{2}$, for the isotope 207. The distances from the main component are, in units of 10^{-3} cm^{-1}, 87.5 and 131.5, that is, exactly in the proportion 2 : 3. The possible error does not exceed a few percent. The relative intensities of these components were rather easy to evaluate, because, since the half-widths for all components are the same and much smaller than their separations, a direct measurement of peak intensities could

[12] S. Mrozowski, Zeits. f. Physik **112**, 223 (1939).
[13] See, for instance, H. Kopfermann, Zeits. f. Physik **75**, 363 (1932).
[14] The type of forbidden transitions in Pb I has been discussed by J. Blaton and H. Niewodniczanski, Phys. Rev. **45**, 64 (1934), and by J. Blaton, Zeits. f. Physik **89**, 155 (1934).

be used. A fairly large correction for the background had to be made because, besides the ordinary background due to the etalon,[12] a strong additional background is produced by the PbO bands in this region. The intensity of the first component was found to be 1.55 ± 0.06 times that of the weaker, so that they are within the limits of error in the proportion 3 : 2. This is clear *proof of the applicability of the Rubinowicz-Opechowski formulas to the intensities in the hyperfine structure of quadrupole lines*. The doublet here observed corresponds exactly to the forbidden (S, D) fine structure doublet first observed by Datta[15] in the spectrum of potassium.

The magnetic dipole line, λ4618

In Fig. 2 is shown an enlargement of a 40-second exposure of this line, taken with a 15-mm separator. Here Eastman 40 plates were satisfactory. This pattern shows one component well separated, and another on the opposite side, merging with the main line. They come from the two transitions of $F\ \frac{1}{2}\rightarrow\frac{1}{2}$ and $\frac{1}{2}\rightarrow\frac{3}{2}$, showing that the hyperfine structure in the level $^3P_1$ is inverted. This agrees with the results of other investigators.[13] The curve of the intensity distribution has been treated in the manner described before,[12] which consists essentially of reflection of the side of the main component not overlapped, and adjustment of its position so as to get from the remainder a component of the same Doppler width. The distances of the components and their relative intensities may then be found. A correction of 7.5 percent for the background was made.[12] The distances are 79.4 and 39.7, these being the mean values from the two best plates. Their ratio is 2.00 ± 0.06. The relative intensities are $1 : 2.05\pm0.08$. This shows that *for a magnetic dipole line the same intensity rules apply in the hyperfine structure as for electric dipole lines*. This result finds further confirmation in the structure of λ7330. Although not unexpected, it is also not quite evident, since in fine structure there is no such similarity of the two cases. This point needs some clarification on the theoretical side.

The mixed line, λ7330

The greatest experimental difficulties were encountered in the study of this line. In Fig. 2 is an enlargement of a 15-min. exposure taken with a 19-mm separator. Eastman I–U plates were used. In the lower part of Fig. 3 the predicted components for the isotope 207, and their intensities, are given for the two extreme cases of pure magnetic dipole and pure electric quadrupole radiation. A careful search for the extra component ($\Delta F=-2$; $\frac{5}{2}\rightarrow\frac{1}{2}$), which arises only from quadrupole radiation, was made. For this purpose excessive background had to be carefully avoided. Therefore the plates were not hypersensitized, although this would have considerably reduced the time of exposure. The presence of a very strong line at λ7229 gave a great deal of trouble, because it lies very close to the line investigated. An adjustable razor-blade edge was mounted in the plateholder to prevent this line from blackening the plate. Special care was taken to avoid scattered light in the spectrograph. A strong continuous background is also produced by the temperature radiation of the furnace; its influence was reduced by narrowing the spectrograph slit. Corrections of 8–15 percent for the furnace radiation alone had to be made on different plates (in addition to the normal correction), the variations depending on the furnace temperature and on the slit width. No trace of the extra component could be found. The distances from

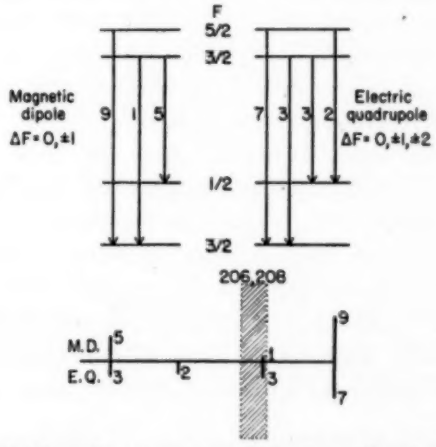

FIG. 3. Hyperfine structure level scheme for the isotope 207 and relative intensities of the components of λ7330 for the two extreme cases, pure magnetic dipole and pure electric quadrupole radiation. Below, the expected hyperfine structure of this line for both cases, in juxtaposition.

[15] S. Datta, Proc. Roy. Soc. **A101**, 539 (1922); see also W. Prokofjew, Zeits. f. Physik **57**, 387 (1929) for this and other alkalis.

the main line of the two components visible in Fig. 2 were measured, and found to be 112 and 60, from which the splitting of the $^1D_2$ level given in Fig. 1 was calculated. The ratio of intensities of the two components is 1.87 ± 0.08, or about 9 : 5.[16] This shows *that the line λ7330 is chiefly of a magnetic dipole character, and that for magnetic dipole radiation the selection rule* $\Delta F=0, \pm 1$ *holds.*

An upper limit to the percentage of quadrupole radiation can be roughly evaluated in the following way. We make the assumption, which as Dr. L. I. Schiff pointed out is not perfectly obvious and requires proof, that the intensities of the components are proportional to the sums of intensities of the two kinds of radiation. If we denote the percentage of quadrupole radiation by x, then the relative intensities of the two observed components will be $[9(100-x)+7x]/[5(100-x)+3x]$. This cannot be set equal to the observed value 1.87, as this ratio was obtained with the assumption of a certain correction for the background. If there is an extra component in the gap between the main line and the weaker component, the background correction must be taken as smaller, and the value for the relative intensity will also be a little smaller. We must adjust the background correction so as to have a consistent value of x from the three components (the last one being fictitious) in the ratio $[9(100-x)+7x] : [5(100-x)+3x] : 2x$. After thus adjusting the background, we find $x\sim 9$ percent, instead of 20 percent which we would obtain directly from the value 1.87. Naturally this estimate is very rough and only gives the order of magnitude. The method is only really sensitive around $x\sim 50$ percent.

In all three forbidden lines the ratio of the total intensity of the components belonging to the isotope 207 to that for the even isotopes is found to be in very good agreement with the known concentration of the isotopes. The ratio is 21 : 79 in λ5313, 21 : 79 in λ4618, and 21.5 : 78.5 in λ7330. This means that, in contradistinction to forbidden transitions caused by inner perturbations, *for spontaneous quadrupole and magnetic dipole radiation the transition probabilities are the same for all kinds of isotopes*, as is to be expected. The small deviation in the direction of too high an intensity for the isotope 207 probably arises from the underestimation of the peak value of the plate blackening resulting from the finite slit width of the microphotometer. This underestimation is especially important in the case of a high peak value, that is, for the main component. In the case of λ7330, where the slit width of the spectrograph was small, the slit had to be taken especially wide in order to get reasonable deflections on the microphotometer. Also connected with this microphotometer slit width are some inconsistencies in the results on the half-widths of the lines. The most reliable of these widths was the value 0.042 cm^{-1}, obtained for λ4618 from the lowest orders, with a separator of 28 mm. It probably differs very little from the true value. The Doppler half-width for a temperature of 830°C is computed to be 0.035 cm^{-1}. The temperature in the discharge is no doubt a little higher than that in the surrounding oven. At lower temperatures a gradual change of the spectrum was observed during the first few minutes of running, the change being of the sort to be expected from a heating up of the tube by the discharge. The difference of the measured and calculated half-widths may indicate the presence of a small isotope shift, much smaller however than the shift expected on the basis of Kopfermann's[13] data. For λ5313, the measured half-width was 0.040 cm^{-1}, and for λ7330, it was 0.038 cm^{-1}. These are to be compared with 0.030 and 0.022 cm^{-1}, calculated for 830°C. That this result is really a consequence of the finite slit width of the microphotometer is shown by the fact that the half-widths slowly increased with the order of interference, and were slightly greater for the main component than for the others. But it is possible that for λ5313 the isotope shift also plays a considerable role. According to Kopfermann[13] it should be greatest for this line, about 0.018 cm^{-1}, but this figure is certainly too high. For λ7330 which, according to Kopfermann,[13] should have practically no isotope shift, the whole discrepancy can be accounted for by the very wide microphotometer slit.

The hyperfine structure of the two remaining

[16] The weak line visible on Fig. 2 (7330A) close to the weakest component (below to right) is probably λ7346.0 of Cd. This line is much weaker at higher temperatures and therefore did not disturb the photometric measurements. The small hump in the curve may easily be seen, and was eliminated in the calculations.

lines, λ4659 and λ9250, was not investigated. A one-hour exposure of λ4659 showed that a pattern with sufficient blackening could be obtained in 3–4 hours for this line, but in view of the smallness of the $^1D_2$ level splitting, the attempt was not made. In any case, the component would not be clearly resolved from the main line. Furthermore, this line does not present anything new, as it is completely analogous to λ5313. The new line λ9250 occurs in an inconvenient spectral region and is similar in some respects to λ7330.

To complete the investigation of these forbidden transitions within the p^2 configuration, the relative intensities of all five lines were determined. After removal of the Fabry-Perot etalon, photographs of the spectrum of the discharge at different temperatures were taken. Two sets of intensity marks were photographed on each plate, using the step-slit and a Kipp and Zonen calibrated band-filament lamp in quartz. The lamp was placed as close to the discharge tube as possible to prevent errors due to lack of achromatism in the optical system. The blackening of the plates was measured on the microphotometer and the relative intensities determined by the usual method, including corrections for the background. The relative intensity of λ4618 and λ5313 was determined using the Super Panchro Press plates. The mean result, $I_{4618} : I_{5313} = 5.0 \pm 0.3$, was found to be independent of the temperature. The relative intensity of 5313 and 4659 was determined using the same kind of plates but longer exposures, to keep the blackenings in a suitable range. A large background correction had to be made for λ4659, due to the exact superposition of this line on the head of one of the PbO bands. The result was found to depend on the temperature $I_{5313} : I_{4659}$ being 15 for lower temperatures, and decreasing to 12 for the higher ones. The relative intensities of the three lines λ4659, λ7330 and λ9250 were measured, using hypersensitized Eastman I–M plates. Large background corrections were made for the first and last lines, amounting to about 35 percent. In the last case the background was produced by the very strong continuous furnace radiation. The average result was $I_{4659} : I_{7330} : I_{9250} = 0.023 \pm 0.006 : 1 : 0.84 \pm 0.07$, and was independent of temperature.

A comparison of these relative intensities with the theoretical formulas of Stevenson[17] cannot be made, because his formulas are derived for small deviations from Russell-Saunders coupling only, namely, when the intensities of the above triplet differ only slightly from 0 : 1 : 3. Since in this spectrum the coupling is very nearly j, j, the more general formulas of Condon[18] should be used. Unfortunately Condon does not give formulas for all the transitions here investigated. More complete, and independent, calculations have been carried out recently by Mr. E. Gerjuoy and will be published soon. The comparison of the experimental results with theory will be made in his paper, and at the same time other problems mentioned above will be discussed.

Finally, an attempt has been made to detect a possible forbidden line $^1S_0 \rightarrow {}^3P_0$, at λ3392.7, corresponding to the well-known Hg I line λ2655.8. This line would only be emitted by the isotope 207, as a result of the coupling of the electronic shell with the nuclear spin. A careful search, made with a small spectrograph, led to a negative result, and it was concluded that this line, if present, has an intensity smaller than 1/20 of the intensity of λ4659. This upper limit is high, because the presence of PbO bands in this region made it impossible to greatly increase the time of exposure. A very faint line was found quite close to the expected position, but it turned out to be λ3397.2 of Bi I. That the lead used contained not only Cd, but also traces of Bi was proved by the appearance of some of the other strong lines of the Bi I spectrum. It seems probable that the forbidden line λ3392.7 is not emitted at all, because of the operation of the Laporte's rule.

In conclusion, I wish to express my sincere thanks to Professor E. O. Lawrence for making possible my stay in Berkeley, and for extending to me the facilities of his laboratory. I also wish to thank Professor F. A. Jenkins for his many suggestions and his great kindness during the whole time of my stay. I am also much indebted to Dr. L. I. Schiff, to Mr. W. Opechowski (Leiden), and Mr. E. Gerjuoy for stimulating discussions.

[17] A. F. Stevenson, Proc. Roy. Soc. **137**, 298 (1932). See also J. Blaton, reference 14.
[18] E. U. Condon, Astrophys J. **79**, 217 (1934).

The Zeeman Effect of Krypton

J. B. GREEN, D. W. BOWMAN,* AND E. H. HURLBURT†
Mendenhall Laboratory of Physics, Ohio State University, Columbus, Ohio
(Received October 5, 1940)

Measurements on the Zeeman effect about 130 lines in the spectrum of neutral krypton have yielded a large number of additional g values to those already given by Pogany. In several cases, our results differ sharply from Pogany's, especially in the case of $4p^55s$. The g sum rule has been verified for $4p^55s$, $4p^55p$ and for $J=2$ of $4p^56p$, but for this last configuration, interaction with $4p^55f$ causes the breakdown of the rule for $J=1$. Other anomalies in the g values are also discussed.

THE classification of the first spectrum of krypton has been carefully carried out by Meggers, deBruin and Humphreys[1] and their classifications have been verified with few exceptions.

The earliest experimental work on the Zeeman effect of krypton was done by Bakker[2] in 1931 and extended by Pogany[3] in 1933 and 1935. Lörinczi[4] has made some calculations of the g factors for the $4p^55p$ and $4p^56p$ configurations. Green[5] has carried out the calculations of the g values of the $4p^55p$ configuration with results differing somewhat from Lörinczi's.

The present investigation covers about 150 lines in the first spectrum of krypton covering the region λλ3400–8950. The source and magnet were the same as that used by Green and Peoples[6] in previous work on the Zeeman effect of neon. In the present investigation the gas pressure was about 10 mm and the carbon trap was removed from the system in an attempt to eliminate some troublesome bands. A gas mixture of 95 percent helium and 5 percent krypton was used. Eastman special spectroscopic plates were used and developed in Edwal 12 developer. All the dyed plates were sensitized for one minute in a four-percent aqueous ammonia solution. Two sets of exposures were about 48 hours, the third 75 hours, and the fourth and the fifth taken in the perpendicular polarization with the aid of a calcite crystal lasted 98 and 111 hours, respectively.

Table I gives a summary of the patterns measured in the arc spectrum of krypton and of the g values calculated from these patterns. In certain cases where the pattern is not resolved the better known g value is assumed in order to calculate the other.

Table II is a summary of the average g values observed. In the cases of the $1s_2$, $1s_4$, $1s_5$, $2p_3$, $2p_4$, $2p_8$, $2p_9$, $2p_{10}$, $3p_4$, $3p_7$, and $3p_{10}$ levels only resolved patterns were averaged. For the remaining levels the values obtained from unresolved patterns were given only half the weight of the values obtained from the resolved patterns. The average values obtained from resolved patterns only are probably accurate to about 0.5 percent.

Tables III, IV, and V show the individual g values and the g sums for the $4p^55s$, $4p^55p$, and $4p^56p$ configurations with comparisons between the calculated values of Lörinczi, Green and the authors and the observed values of Pogany and the authors.

In the $4p^55s$ configuration the authors' observed g values for the s_4 and s_2 levels are in agreement with the calculated values but are opposite in relative magnitude to those observed by Pogany. (See Fig. 1.)

The authors' experimental results for the $4p^55p$ configuration are not in agreement with Pogany's results nor Lörinczi's theoretical results. However, the agreement with Green's calculated results and with the g sum rule is much better.

* Now at Hendrix College, Conway, Arkansas.
† Now at Fenn College, Cleveland, Ohio.
[1] W. F. Meggers, T. L. deBruin and C. J. Humphreys, Bur. Stand. J. Research 3, 129 (1929); C. J. Humphreys, *ibid.* 5, 1041 (1930); 7, 351 (1931); W. F. Meggers, T. L. deBruin, and C. J. Humphreys, *ibid.* 7, 643 (1931); W. F. Meggers, and C. J. Humphreys, *ibid.* 10, 427 (1933).
[2] C. J. Bakker, Diss. Amsterdam, (1931).
[3] B. Pogany, Zeits. f. Physik 86, 729 (1933); 93, 364 (1935).
[4] K. Lörinczi, Zeits. f. Physik 107, 177 (1937).
[5] J. B. Green, Phys. Rev. 52, 736 (1937).
[6] J. B. Green, and J. A. Peoples, Phys. Rev. 54, 602 (1938).

TABLE I. *Summary of Zeeman patterns.*

λ	Classification	J Values	Pattern	g_a	g_b
‡8928.693	$1s_5 - 2p_{10}$	2, 1	(0), (0.396), **1.105**, 1.494, 1.886	1.497	1.889
‡8776.790	$1s_4 - 2p_8$	1, 2	(0), (0.147), **0.950**, 1.094, 1.228	1.243	1.100
‡8508.874	$1s_2 - 2p_4$	1, 1	(−), 0.645, 1.256	1.256	0.645
‡8298.109	$1s_4 - 2p_1$	1, 1	(0.235), 1.006, 1.241	1.241	1.006
‡8281.06	$1s_2 - 2p_3$	1, 1	(0.191), 1.257, 1.448	1.257	1.448
‡*8263.241	$1s_2 - 2p_2$	1, 2	(0), 1.123	*1.258*	1.168
‡8190.057	$1s_4 - 2p_6$	1, 2	(0), (0.157), 1.225, 1.370, **1.530**	1.242	1.381
8112.902	$1s_5 - 2p_9$	2, 3	(0), (0.174), (0.363), **0.983**, 1.170, 1.338, 1.507, 1.676	1.507	1.338
8104.02	$1s_5 - 2p_8$	2, 2	(−), (−), −, **1.101**, **1.500**, 1.898	1.500	1.101
8059.505	$1s_3 - 2p_4$	0, 1	(0), 0.647	0/0	0.647
*7928.602	$2p_8 - 4d_4$	2, 3	(0), 0.999	*1.101*	1.050
7913.443	$2p_{10} - 4d_6$	1, 1	(−), 1.098, 1.901	1.901	1.098
7854.823	$1s_3 - 2p_2$	0, 1	(0), 1.452	0/0	1.452
7746.831	$2p_{10} - 4d_6$	1, 0	(0), 1.897	1.897	0/0
7741.37	$2p_9 - 4d_1'$	3, 3	(0.252), (−)	*1.336*	1.243
7694.540	$1s_5 - 2p_7$	2, 1	(0), (0.508), 1.006, 1.498, **1.993**	1.496	1.000
7685.247	$1s_2 - 2p_1$	1, 0	(0), 1.260	1.260	0/0
†7601.547	$1s_5 - 2p_6$	2, 2	(0.236), 1.451	1.516	1.386
7587.414	$1s_4 - 2p_5$	1, 0	(0), 1.244	1.244	0/0
7494.15	$2p_8 - 3s_5$	2, 2	P.B.	*1.100*	1.492
7493.58	$2p_8 - 4d_2$	2, 1	P.B.	*1.100*	0.935
7487.12	$2p_9 - 4d_2$ forbidden	3, 1	P.B.	*1.333*	0.935
7486.850	$2p_9 - 3s_5$	3, 2	P.B.	*1.333*	1.500
*7425.54	$2p_8 - 3s_4$	2, 1	(0), 1.102	*1.101*	1.098
7287.262	$2p_{10} - 2s_2$	1, 1	(−), 1.018, 1.895	1.895	1.018
7224.109	$2p_{10} - 4d_3$	1, 2	(−), (−), −, **0.697**, 1.297, 1.888	1.890	1.295
7143.45	$2p_{10} - 4d_1''$	1, 2	(0), [0.105], 1.011, −	1.896	1.006
7000.79	$2p_5 - 4s_4$	0, 1	(0), 1.160	0/0	1.160
6904.68	$2p_{10} - 3s_5$	1, 2	P.B.	1.898	1.496
6904.22	$2p_{10} - 4d_2$	1, 1	P.B.	1.898	0.940
*6869.63	$2p_8 - 5d_5$	2, 1	(0), 1.403	*1.387*	1.355
6846.40	$2p_{10} - 3s_4$	1, 1	(0.792), 1.093, 1.894	1.892	1.096
6829.09	$2p_7 - 5d_6$	1, 0	(0), 1.009	1.009	0/0
†6813.10	$2p_6 - 5d_5$	2, 2	(0.127), 1.352	1.387	1.317
6740.10	$2p_7 - 5d_3$	1, 2	(0), (0.317), −, −, **1.630**	1.000	1.315
*6652.24	$2p_7 - 5d_1''$	1, 2	(0), 0.964	*1.005*	0.978
†6576.42	$2p_6 - 4s_5$	2, 2	(0.212), 1.457	1.398	1.516
†6536.55	$2p_7 - 5d_2$	1, 1	(0.183), 0.914	1.005	0.823
6504.89	$2p_8 - 5d_5$	2, 1	(0), (0.252), **0.840**, 1.072, −	1.094	1.344
†6488.07	$2p_7 - 4s_4$	1, 1	(0.157), 1.101	1.022	1.179
*6456.293	$2p_9 - 5d_4'$	3, 4	(0), 1.052	*1.337*	1.231
*6448.78	$2p_9 - 5d_3$	3, 2	(0), **1.349**	*1.337*	1.325
*6421.028	$2p_8 - 5d_4$	2, 3	(0), 1.041	*1.102*	1.071
6415.65	$2p_9 - 5d_4$	3, 3	(0.262), (**0.550**), −, 0.808, **1.074**, **1.338**, 1.600, 1.868	1.337	1.074
6410.17	$2p_5 - 6d_2$	0, 1	(0), 0.797	0/0	0.797
†6373.58	$2p_8 - 5d_1''$	2, 2	(0.255), 1.023	1.094	0.952
*6351.90	$2p_8 - 5d_1'$	2, 3	(0), 1.441	*1.101*	1.271
†6346.66	$2p_9 - 5d_1'$	3, 3	(0.272), −	*1.336*	1.237
6241.39	$2p_8 - 4s_5$	2, 2	(0.398), (−), 0.716, **1.106**, **1.503**, 1.895	1.107	1.502
6236.34	$2p_9 - 4s_5$	3, 2	(0), (0.173), (0.341), **1.004**, 1.173, −, −, −.	1.334	1.502
*6222.71	$2p_8 - 4s_4$	2, 1	(0), 1.064	*1.101*	1.169
*ε6163.65	$2p_6 - 6d_5$	2, 1	(0), 1.392	*1.387*	1.377
†6151.38	$2p_6 - 6d_3$	2, 2	(0.122), 1.354	1.388	1.320
6091.81	$2p_7 - 6d_3$	1, 2	(0), (0.310), 1.031, 1.322, **1.627**	1.020	1.322
6082.85	$2p_{10} - 5d_6$	1, 0	(0), 1.898	1.898	0/0
‡6075.24	$2p_6 - 6d_1'$	2, 3	(0), (0.170), (0.356), **0.866**, 1.043, 1.245, 1.413, −.	1.397	1.218
‡6056.11	$2p_{10} - 5d_5$	1, 1	(0.551), 1.348, 1.895	1.896	1.346
*6035.82	$2p_7 - 6d_1''$	1, 2	(0), 0.930	*1.008*	0.956
6012.111	$2p_{10} - 5d_3$	1, 2	(0), (0.576), **0.740**, 1.318, 1.895	1.895	1.318
5993.850	$1s_4 - 2p_4$	1, 1	(−), 0.647, 1.244	1.243	[0.647
†5977.65	$2p_7 - 6d_2$	1, 1	(0.208), 0.892	0.996	0.798
‡5879.89	$1s_4 - 2p_3$	1, 1	(0.217), 1.247, 1.457	1.243	1.456
*5870.915	$1s_4 - 2p_2$	1, 2	(0), 1.150	*1.248*	1.181
‡5866.74	$1s_2 - 3p_{10}$	1, 1	(0.576), 1.266, 1.834	1.264	1.836
*5832.85	$2p_9 - 6d_4'$	3, 4	(0), 1.066	*1.337*	1.228
5827.07	$2p_{10} - 4s_5$	1, 2	(0), (0.411), 1.101, 1.515, 1.902	1.914	1.510
*5824.50	$2p_8 - 6d_4$	2, 3	(0), 1.072	*1.102*	1.086
5820.10	$2p_9 - 6d_4$	3, 3	(−), (0.490), (−), −, −, **1.098**, **1.344**, 1.600, 1.827	1.344	1.098
5810.80	$2p_{10} - 4s_4$	1, 1	(−), 1.178, 1.890	1.890	1.178
†5805.53	$2p_8 - 6d_1''$	2, 2	(0.260), 1.020	1.096	0.952
*5788.24	$2p_8 - 6d_1'$	2, 3	(−), 1.389	*1.101*	1.245
*5783.89	$2p_9 - 6d_1'$	3, 3	(−), 1.291	*1.337*	1.245
*5750.57	$2p_6 - 7d_1'$	2, 3	(0), 1.066	*1.385*	1.227
5723.56	$1s_2 - 3p_7$	1, 1	(0.221), 1.034, 1.267	1.263	1.036
*5721.88	$2p_8 - 5s_4$	2, 1	(0), 1.064	*1.102*	1.174
5707.51	$1s_2 - 3p_6$	1, 2	(0), (0.148), −, 1.405, **1.548**	1.257	1.403
*5702.19	$2p_7 - 7d_1''$	1, 2	(0), 1.003	*1.008*	1.005
5672.45	$1s_5 - 2p_4$	2, 1	(0), 0.647, (−), 1.503, **2.356**	1.502	0.648
†5662.67	$2p_7 - 6s_4$	1, 1	(0.176), 1.073	0.985	1.161
‡5649.563	$1s_2 - 3p_{10}$	0, 1	(0), 1.834	0/0	1.834
†5611.82	$2p_8 - 4s_1''$	2, 2	(0.382), −.	*1.101*	0.889
5580.39	$1s_2 - 3p_5$	1, 0	(0), 1.257	1.257	0/0
*5575.6	$2p_8 - 4s_1'''$	2, 3	(0), 1.179	*1.101*	1.140
*5570.289	$1s_5 - 2p_3$	2, 1	(0), 1.530	*1.502*	1.444
5562.225	$1s_5 - 2p_2$	2, 2	(0.315), (**0.635**), 0.863, **1.180**, **1.500**, 1.821	1.499	1.181
*5520.52	$2p_9 - 7d_4'$	3, 4	(0), 1.083	*1.336*	1.236
5516.66	$1s_3 - 3p_7$	0, 1	(0), 1.039	0/0	1.039
5504.34	$2p_{10} - 6d_6$	1, 0	(0), 1.897	1.897	0/0
*5504.04	$2p_8 - 7d_4$	2, 3	(0), 0.973	*1.101*	1.037
*5500.71	$2p_{10} - 6d_5$	1, 1	(0.547), 1.345, 1.887	1.888	1.344
5490.94	$2p_{10} - 6d_3$	1, 2	(0), (0.582), **0.722**, 1.303, 1.894	1.891	1.306
5379.64	$2p_{10} - 5s_5$	1, 2	(0), (0.411), **1.092**, 1.486, −.	1.898	1.495
*5339.13	$2p_9 - 8d_4'$	3, 4	(0), 1.086	*1.336*	1.182
5279.84	$2p_{10} - 4s_1''''$	1, 2	(0), **0.446**, (0.722), 1.169, −.	1.891	1.169
5274.61	$2p_{10} - 4s_1''$	1, 2	(0), (−), −, 0.904, −.	—	0.904
5228.18	$2p_{10} - 7d_5$	1, 1	(0.625), 1.301, 1.903	1.906	1.294
5215.81	$2p_{10} - 7d_6$	1, 0	(0), 1.899	1.899	0/0
5058.08	$2p_{10} - 8d_6$	1, 0	(0), 1.915	1.915	0/0
5040.34	$2p_{10} - 8d_5$	1, 1	(0.691), 1.205, 1.903	1.899	1.208
4812.607	$1s_3 - 4X$	0, 1	(0), 0.517	0/0	0.517
4724.89	$1s_2 - 4p_{10}$	1, 1	(0.544), 1.254, 1.792	1.253	1.792
4636.14	$1s_2 - 4p_5$	1, 0	(0), 1.265	1.265	0/0
4550.295	$1s_4 - 3p_{10}$	1, 1	(0.599), 1.250, 1.835	1.246	1.839
‡4463.6897	$1s_4 - 3p_7$	1, 1	(0.212), 1.030, 1.242	1.242	1.030
‡4454.9183	$1s_4 - 3p_6$	1, 2	(0), (0.184), 1.211, 1.375, **1.586**	1.214	1.401
‡4425.1909	$1s_2 - 3p_4$	1, 1	(−), 0.647, 1.253	1.253	0.647
4418.769	$1s_2 - 5Z$	1, 2	(0), 0.98	*1.26*	1.08
4416.88	$1s_2 - 5X$	1, 1	(−), 0.61, 1.25	1.25	0.61
†4410.369	$1s_2 - 3p_3$	1, 1	(0.145), 1.336	1.264	1.408
*4399.9675	$1s_2 - 3p_2$	1, 2	(0), 1.101	*1.258*	1.153
4376.1217	$1s_4 - 3p_5$	1, 0	(0), 1.246	1.246	0/0
‡4362.6429	$1s_5 - 3p_{10}$	2, 1	(0), (0.331), **1.168**, 1.498, 1.828	1.498	1.828
4351.3605	$1s_2 - 3p_1$	1, 0	(0), 1.259	1.259	0/0
4319.5798	$1s_5 - 3p_9$	2, 3	P.B.	*1.502*	1.333
4318.5523	$1s_5 - 3p_8$	2, 2	P.B.	*1.502*	1.107
‡4300.4877	$1s_2 - 3p_4$	0, 1	(0), 0.649	0/0	0.649
‡4286.4875	$1s_2 - 3p_2$	0, 1	(0), 1.402	0/0	1.402
‡4282.9686	$1s_4 - 3p_7$	2, 1	(0), (0.472), 1.032, 1.503, **1.975**	1.503	1.031
‡‡4273.9705	$1s_5 - 3p_8$	2, 2	(0.196), 1.455	1.509	1.401
4263.29	$1s_2 - 5p_5$	1, 0	(0), 1.256	1.256	0/0
4184.48	$1s_2 - 5p_{10}$	0, 1	(0), 1.794	0/0	1.794
3800.55	$1s_4 - 4p_7$	1, 1	(0.203), 1.025, 1.247	1.242	1.030
*3796.88	$1s_4 - 4p_6$	1, 2	(0), 1.508	*1.242*	1.417
3773.43	$1s_4 - 4p_5$	1, 0	(0), 1.236	1.236	0/0
3668.74	$1s_5 - 4p_7$	2, 1	(0), (0.461), −, 1.502, **1.963**	1.502	1.041
†3665.33	$1s_5 - 4p_6$	2, 2	(0.208), 1.448	1.506	1.390
*3628.17	$1s_4 - 5Z$	1, 2	(0), 1.031	*1.242*	1.101
*3615.48	$1s_4 - 3p_2$	1, 2	(0), 1.124	*1.242*	1.163
*3540.97	$1s_4 - 5p_7$	1, 1	(0), 1.128	*1.242*	1.014
*3539.55	$1s_4 - 5p_6$	1, 2	(0), 1.500	*1.242*	1.414
3522.68	$1s_4 - 5p_5$	1, 0	(0), 1.242	1.242	0/0
3502.56	$1s_5 - 3p_3$	2, 1	(0), 1.558	*1.502*	1.390
*3431.75	$1s_5 - 5p_9$	2, 3	(0), 1.032	*1.502*	1.267
†3424.97	$1s_5 - 5p_8$	2, 2	(0.179), 1.458	1.508	1.406

* Unresolved patterns.
Numbers in italics—Assumed value used to obtain other g value.
ε Slightly perturbed.
† Partially resolved patterns.
‡ Also measured by Pogany.
[ ] Mixed polarization.

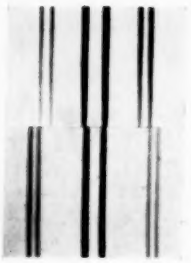

FIG. 1. Upper λ8298 $1s_4-2p_1$ (components $1\rightarrow 6=1s_4$). Lower λ8281 $1s_2-2p_3$ (components $2\rightarrow 5=1s_2$). Both photographs have exactly the same magnification, and even though the dispersion favors the longer wave-length line (proportional to λ^2), the separation of $1s_2$ is greater than $1s_4$. On the particular plate from which the enlargements were made, these separations were 2.251 mm and 2.260 mm, respectively. If Pogany's results were correct, the spread of the indicated components in the upper picture would be much larger than in the lower.

The $4p^5 6p$ configuration shows quite serious disagreement in all observed and calculated results and shows the breakdown of the g sum rule for $J=1$. Practically the entire discrepancy is to be attributed to the low g value of $2p_3$. The explanation for this discrepancy becomes obvious when we examine the energy level diagram. The lower states of $4p^5 5f$ intermingle with the upper states of $4p^5 6p$, so that the levels $3p_3$ and $5X$ are only 33.5 cm^{-1} apart. These two levels belong to configurations of the same parity (even) and both have $J=1$, so that they may perturb each other. In addition, the level $5X$ is the only level of $4p^5 5f$ with $J=1$ so that its g value should be $0.50(^3D_1)$. The only line involving this level available for measurement was λ4417, which was rather faint. This yielded a g value for $5X$ of 0.61 (with an accuracy of about 2 percent), which is 0.11 in excess of the theoretical value. The g sum for $J=1$ of $4p^5 6p$ is, according to our measurements, 0.083 less than the theoretical value, so that the total g sum is 5.527 instead of 5.500. These results are probably the same within experimental error. (It is interesting to note that if we use Pogany's g sum, the total g sum is 4.995.)*

The only other g sums available are for the $4p^5 5d$ configuration for $J=3$ and $J=2$. Here, the theoretical sums are 3.417 and 4.333, respectively, compared with 3.433 and 4.371 from

TABLE II. *Average observed g values.*

LEVEL	J	1	2	3	4	5	6	7	8
s_5	2	1.502	—	1.496	1.506	1.495			
s_4	1	1.242	—	1.097	1.171	1.174	1.161		
s_2	1	1.259	1.018						
Σg		2.501							
p_9	3		1.336	1.333					
p_3	2		1.099	1.107					
p_6	2		1.388	1.403	1.403	1.411			
p_2	2		1.181	1.158					
Σg			3.668	3.668					
p_{10}	1		1.898	1.834	1.795	1.795			
p_7	1		1.004	1.034	1.041	1.014			
p_4	1		0.647	0.648					
p_2	1		1.452	1.401					
Σg			5.001	4.917					
d_4'	4					1.231	1.228	1.236	
d_4	3				1.050	1.073	1.094	1.037	
d_1'	3				1.243	1.254	1.231	1.227	
s_1'''	3				1.140				
Σg					3.433				
d_3	2				1.295	1.318	1.315		
d_1''	2				1.006	0.965	0.954	1.005	
s_1''	2				0.899				
s_1''''	2				1.169				
Σg					4.371				
d_5	1				1.098	1.348	1.355	1.294	1.208
d_2	1				0.935	0.823	0.797		
s_1'	1				—	—	—		
Σg					—	—	—		

TABLE III. *$4p^5 5s$ g values.*

J	LEVEL	OBS. POGANY	OBS. AUTHORS	CALC.*
2	s_5	1.50	1.502	1.500
1	s_4	1.256	1.242	1.243
1	s_2	1.239	1.259	1.257
	Σg	2.495	2.501	2.500

* W. V. Houston, Phys. Rev. **33**, 297 (1929).

TABLE IV. *$4p^5 5p$ g values.*

J	LEVEL	CALC. LÖRINCZI	CALC. GREEN	OBS. POGANY	OBS. AUTHORS
1	p_3	1.392	1.461	1.425	1.452
1	p_4	0.708	0.653	0.631	0.647
1	p_7	1.041	1.002	1.028	1.004
1	p_{10}	1.907	1.884	1.891	1.898
	Σg	5.048	5.000	4.975	5.001
2	p_2	1.194	1.179	1.163	1.181
2	p_6	1.396	1.365	1.400	1.388
2	p_8	1.08	1.123	1.116	1.099
	Σg	3.670	3.667	3.679	3.668
3	p_9	1.333	1.333	1.33	1.336

* It should be pointed out that both $3p_3$ and $3p_4$ are perturbed by $5X$. $5X$ lies at 4434, $3p_3$ at 4400 and $3p_4$ at 4476. The tendency of the perturbation due to $5X$ is to push $3p_3$ and $3p_4$ farther apart than they would normally be, and to cause the g values of $3p_3$ and $3p_4$ to become smaller. But since the g value of $5X$ and $3p_4$ are nearly the same, the effect on its g value should be much smaller than on that of $3p_3$. The fact that $3p_4$ seems to be unperturbed must be regarded as fortuitous.

experiment. We are inclined to believe that these agree within experimental error.

Only one serious error occurs in the classification of the spectrum. This is the assignment of $4s_1'$. The level so classified has $J=2$ and hence is more probably $4s_1''''$ which has not been assigned. This level has a g value of 1.169 consistent with that classification, but it would be better to interchange the names $4s_1''$ and $4s_1''''$ to give uniformity to all of the rare gas spectrum classifications. With this change, we are left without any level assigned to $4s_1'$. This level should have a value of about 2200 cm^{-1}, and form a combination $2p_{10}-4s_1'$ at about 19,500 cm^{-1}. The only unclassified line in this neighborhood is λ5109.81 (ν19,564.76) which gives a value for $4s_1'$ of 2181.63. In the ultraviolet absorption spectrum, Beutler[7] finds a weak line

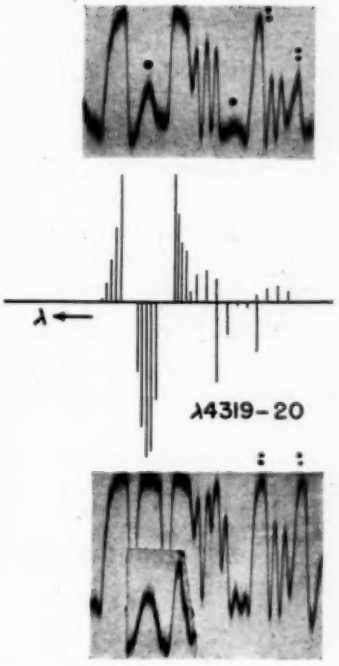

FIG. 2. λλ4319–20. Upper: perpendicular polarization. Lines marked with single dot represent parallel polarization "leaking" through. λ4320 was much over-exposed to bring out weak lines of λ4319. Lines with two dots are KrII. Middle: calculated pattern with perpendicular components above and parallel components below. Bottom: unpolarized pattern. The insert is the trace taken from a ghost to show the structure in the middle component of λ4320. Lines with two dots are KrII.

λ903.10 which yields a term value of 2184. This level he has temporarily assigned to $3s_2$. There are, unfortunately, no data on the Zeeman effect to support either classification.[8]

Attempts at a least-squares calculation of the configuration $4p^5 5d$ led nowhere; the levels are so badly perturbed that no agreement worth considering was obtained.

All of the rare gases show spectra which are very close to those due to jj-coupling; the upper state, in general, lead to very diffuse lines only very few of which have been found, so that it has not been possible to find total g sums. Partial g sums for the lower states yield the following results compared with theory. (See Table VI.)

In the case of the $4p^5ms$ levels, it was found that all of the s_5 levels were normal, with g values equal to 1.500 within experimental error. Both the $2s_2$ and the $3s_4$ levels showed serious perturbations. A comparison of the theoretical and observed patterns is given in Table VII.

The discrepancy in $3s_4$ may be accounted for by configuration interaction. It is only 122 cm^{-1} from $4d_2$ which itself shows a higher g value

TABLE V. *$4p^56p$ g values.*

J	LEVEL	CALC. LÖRINCZI	CALC.* AUTHORS	OBS. POGANY	OBS. AUTHORS
1	p_3	1.448	1.493	1.384	1.401
1	p_4	0.614	0.649	0.635	0.648
1	p_7	1.084	1.030	1.046	1.034
1	p_{10}	1.812	1.828	1.820	1.834
	Σg	4.958	5.000	4.885	4.917
2	p_2	1.168	1.169	—	1.158
2	p_6	1.343	1.379	1.406	1.403
2	p_8	1.156	1.119	1.110	1.107
	Σg	3.667	3.667	—	3.668
3	p_9		1.333	1.33	1.333

* These results were determined from a least-squares calculation yielding the following parameters: $F_0=-2034.09$, $F_2=45.09$, $G_0=204.07$, $G_2=12.71$, $\alpha=873.60$, $\beta=904.77$.

TABLE VI. *Partial g sums.*

CONFIG.	J	jj COUPLING	OBS.	CONFIG.	J	jj COUPLING	OBS.
$4p^56p$	1	2.833	2.836	$4p^56d$	2	2.277	2.283
$4p^58p$	1	2.833	2.809	$4p^57d$	2	2.277	2.269
$4p^55d$	1	2.167	2.023	$4p^56d$	3	2.306	2.327
$4p^56d$	1	2.167	2.171	$4p^57d$	3	2.306	2.325
$4p^57d$	1	2.167	2.152	$4p^58d$	3	2.306	2.264

TABLE VII. *g values for $4p^5ms$.*

LEVEL	THEORY[7]	OBSERVED	LEVEL	THEORY[7]	OBSERVED
$2s_2$	1.320	1.018	$4s_4$	1.170	1.171
$3s_5$	1.500	1.496	$5s_5$	1.500	1.495
$3s_4$	1.172	1.097	$5s_4$	1.169	1.174
$4s_5$	1.500	1.506	$6s_4$	1.168	1.161

[7] H. Beutler, Zeits. f. Physik 93, 177 (1934–5).

[8] Dr. J. C. Boyce, (private communication) finds a weak line at λ901.86 which yields a term value of 2032 cm^{-1} which fits the series of s_2 terms much better than 2182 cm^{-1}.

than any d_2 thus far found among the rare gases, and reacts with $3s_5$ (from which it is separated by only 1 cm^{-1}) to produce Paschen-Back effects.*

The very large discrepancy in $2s_2$ is not so easy to account for. It looks, almost, as if the level were improperly classified, although it appears to be in about the correct position. Perhaps $2s_2$ and $3s_1'$ should be interchanged.

The level $4d_5$ seems to have an abnormally low value when compared with the other rare gases, all of which have values about 1.4. Not too much importance can be placed on this point, however, for this configuration is badly distorted. Indeed, $4d_5$ seems to be far below its usual position, being lower than $4d_6$ which is usually the lowest level of the p^5d configuration.

The levels $3p_8$ and $3p_9$ are only 5.5 cm^{-1} apart and perturb each other sufficiently to distort the patterns of lines involving them. Their g values were determined by methods already described.[9] (See Fig. 2.)

* The calculations of the Paschen-Back interaction of $3s_8$ and $4d_2$ will be discussed in a separate communication.

[9] J. B. Green and J. F. Eichelberger, Phys. Rev. **56**, 51 (1939); J. B. Green and J. A. Peoples, *ibid.* **56**, 54 (1939).

DECEMBER 15, 1940 PHYSICAL REVIEW VOLUME 58

Field Dependence of the Intrinsic Domain Magnetization of a Ferromagnet

T. HOLSTEIN
New York University, New York, New York
AND
H. PRIMAKOFF*
Polytechnic Institute of Brooklyn, Brooklyn, New York

(Received July 31, 1940)

In this paper, the variation of the intrinsic domain magnetization of a ferromagnetic with the external magnetic field, is obtained. The basis of the treatment is the exchange interaction model amplified by explicit consideration of the dipole-dipole interaction between the atomic magnets. Approximations appropriate to low temperatures and equivalent to those used by Bloch in his derivation of the $T^{\frac{3}{2}}$ law, are introduced. The resultant expression for the intrinsic volume susceptibility decreases slowly with increasing field; at high fields the functional dependence is as the inverse square root of the field. The variation with temperature is linear; at room temperature and for fields of about 4000 gauss, the order of magnitude of the (volume) susceptibility is 10^{-4}. The results are compared with experiment and satisfactory agreement is found.

I. INTRODUCTION

CLOSELY allied to the problem of the temperature variation of the intrinsic magnetization, **M**, of a ferromagnetic body, is the problem of its variation with an external magnetic field, **H**. This intrinsic magnetization is characteristic of a single ferromagnetic domain and is identical with the experimentally observed magnetization when "technical saturation" has been achieved, i.e., when all of the domains in all of the individual crystal grains of the specimen have parallel magnetization vectors.[1]

When technical saturation has been reached, there are still, as a result of temperature agitation, some atomic magnetic moments which are not oriented in the direction of **H**. Further increase of magnetization is then to be ascribed to the progressive alignment of the temperature disoriented atomic magnets by an increasing field. The phenomenon is physically similar to that which obtains in the magnetization of a paramagnetic substance; however, the existence of the strong ferromagnetic coupling forces between the atomic magnets changes completely[2] both the magnitude of the effect, and its de-

* Present address: Queens College, Flushing, New York.

[1] "Technical saturation" is achieved at fields of 2000–4000 gauss, depending on the metallurgical treatment of the (polycrystalline) specimen.

[2] Cf. Eq. (30), (31) below.

pendence upon the external magnetic field and upon the temperature.

The problem of the variation of **M** with **H** has been treated by Akulov[3] on the basis of the phenomenological Weiss-Heisenberg internal field theory;[4] his result is in strong disagreement with subsequent experiments.[5]

The basis of the treatment of the variation of **M** with **H** given in the present paper is the exchange interaction model of a ferromagnetic,[6] wherein the electrons responsible for the ferromagnetism are anchored to the atomic cores and do not wander about the metallic interior. The essential approximation used in the treatment of this model is that the condition of "quasi-saturation" obtains; *viz.*, the percent deviation of the magnetization $\mathbf{M}(T, H)$ from its maximum possible value, $\mathbf{M}_0$, is small. This condition always prevails at temperatures sufficiently below the Curie temperature.[7]

It has also been found possible to take account of the magnetic interactions between the atomic magnets. These interactions are important, since, in most of the experiments thus far performed, the magnetic energy of an atom due to the magnetic moments of all of the other atoms, $\leqq 4\pi\beta M_0/3$ is usually larger than the magnetic energy due to an external magnetic field, $\leqq \beta H$.[8] It will be seen that the effect of the magnetic interactions cannot be expressed correctly by replacement of H by $H+\gamma M$[9] in the final expression for the magnetization (cf. (30), (31), (32), below).

II. The Hamiltonian

The exchange interaction model of a ferromagnetic, amplified by the inclusion of magnetic interactions, is described, in the space of the atomic spin variables by the following Hamiltonian,[9a]

$$\mathrm{H}=-\tfrac{1}{2}\sum_{l,m=1}^{N} 2J_{lm}(R_{lm})\mathbf{S}_l\cdot\mathbf{S}_m+\tfrac{1}{2}\sum_{l,m=1}^{N}(4\beta^2/R^5{}_{lm})(R^2{}_{lm}\mathbf{S}_l\cdot\mathbf{S}_m-3\mathbf{S}_l\cdot\mathbf{R}_{lm}\mathbf{S}_m\cdot\mathbf{R}_{lm})-\sum_{l=1}^{N}2\beta S_l{}^{(z)}H. \quad (1)$$

Here, N is the total number of atoms, while the sums over l and m each run from 1 to N, summands with $l=m$ being omitted. $R_{lm}=|\mathbf{R}_l-\mathbf{R}_m|$ is the distance between the centers of gravity of the lth and nth atoms; J_{lm} the exchange integral between these atoms; $\mathbf{S}_l$ the spin angular momentum operator of the atom at $\mathbf{R}_l$ in units of $\hbar$; the magnetic field H is directed along the z axis.

The first term in H is the Heisenberg exchange energy expressed in terms of the atomic spin operators (Dirac vector model).[10] The second term arises from the magnetic dipole-dipole interaction between electrons on different atoms. The effects of exchange and of higher magnetic poles on the magnetic interaction are both neglected;[11] hence, the centers of gravity of the atoms constitute the

[3] N. S. Akulov, Zeits. f. Physik **69**, 822 (1931). See, also, R. Becker and W. Döring, *Ferromagnetismus* (Julius Springer, Berlin, 1939), p. 35.

[4] See, for example, J. H. Van Vleck, *Theory of Electric and Magnetic Susceptibilities* (Oxford University Press, 1932), Ch. 12.

[5] A full discussion of the various experimental results and comparison with theory is given below in Section VI.

[6] W. Heisenberg, Zeits. f. Physik **49**, 619 (1928).

[7] The exchange interaction model, with the specimen in the condition of quasi-saturation, has been approximately treated by Bloch in his derivation of the temperature variation of the intrinsic magnetization. Cf. Zeits. f. Physik **61**, 206 (1930); **74**, 295 (1932). Using mathematical methods different from those in the present paper, Bloch derives the well-known $T^{\frac{3}{2}}$ law for atoms with spin $S=\frac{1}{2}$. Bloch's methods have been extended by Möller to the case $S>\frac{1}{2}$. Cf. Zeits. f. Physik **82**, 559 (1933).

[8] β is the Bohr magneton.

[9] γ is a numerical factor whose value lies between 0 and 4π.

[9a] It is to be noted that $(\mathbf{S}_l)^2$ commutes with the Hamiltonian of Eq. (1); therefore, the magnitude of the spin of each atom has a definite integral or half-integral value, S, and thus, each atomic magnetic moment should be an integral multiple of the Bohr magneton. However, experimental values of the intrinsic magnetization extrapolated to absolute zero, i.e. experimental values of M_0, give for the atomic magnetic moments, Fe: 2.2β; Ni: 0.6β; Co: 1.7β. The deviations of these magnetic moments from integral multiples of β is due, presumably, to the interchange of electrons between the atomic $3d$ shells, where the electrons contribute to the ferromagnetism, and the conduction states, where they do not. The problem of the extension of the exchange interaction model to include these interchanges has not yet been solved.

[10] See reference 4, Ch. 12.

[11] Magnetic quadrupole interactions have been invoked to explain ferromagnetic anisotropy, cf. R. Becker, *Theorie der Elektrizität*, Vol. II (Teubner, Leipzig, 1933) pp. 177–183; in order that these, alone, account for the observed ansiotropy their ratio to the dipole interactions need only be $\leqq 1/10$. In this connection it should further be mentioned that the use of magnetic quadrupole interactions to explain ferromagnetic anisotropy has been criticized by Van Vleck, Phys. Rev. **52**, 1178 (1937), p. 1188.

locations of magnetic dipoles, each with moment $2\beta S$. The last term is the interaction of the magnetic moment of each atom with the external magnetic field.

It is to be noted that spin orbit effects have been neglected in Eq. (1). How these effects are to be treated and what influence they have on the final result will be discussed in a later section.

III. Eigenvalues of the Hamiltonian

The first step in finding the magnetization is the determination of the eigenvalues, E of H. In conformance with the essential approximation of "quasi-saturation," $[M_0-M(T,H)]/M_0 \ll 1$ mentioned in the introduction, only those eigenvalues, E, are sought whose corresponding eigenfunctions, Ψ_E, specify states where the expectation value of the z component of the total spin of the specimen

$$\sum_{l=1}^{N} S^{(z)}{}_l$$

is close to its maximum possible value NS.[12]

To proceed, it is convenient to introduce the operators:

$$S^+{}_l = S^{(x)}{}_l + iS^{(y)}{}_l, \quad S^-{}_l = S^{(x)}{}_l - iS^{(y)}{}_l, \quad \mathfrak{n}_l = S - S^{(z)}{}_l. \tag{2}$$

n_l the eigenvalue of $\mathfrak{n}_l$, will be called the "spin deviation" of the lth atom; for the state

$$\Psi_{n_1, \cdots, n_l, \cdots n_N} \equiv \Psi_{n_l}$$

which is an eigenstate of $\mathfrak{n}_l$ and $S^{(z)}{}_l$, n_l obviously represents the difference between the z component of the spin of the lth atom and its maximum value. Also, by way of notation $\langle \mathfrak{n}_l \rangle_E$ is the expectation value of the spin-deviation operator, $\mathfrak{n}_l$, averaged over the eigenstate

$$\Psi_E = \sum_{n_1, \cdots, n_N} b_E(n_1, \cdots, n_l, \cdots n_N) \Psi_{n_1, \cdots, n_l, \cdots n_N},$$

i.e.,

$$\langle \mathfrak{n}_l \rangle_E = \sum_{n_1, \cdots, n_N} |b_E(n_1, \cdots, n_l, \cdots, n_N)|^2 n_l,$$

whereas,

$$\langle\langle \mathfrak{n}_l \rangle\rangle_{kT} \equiv \sum_E \langle \mathfrak{n}_l \rangle_E e^{-E/kT} / \sum_E e^{-E/kT}$$

is the expectation value of the spin-deviation operator when the temperature of the specimen is T, and involves, first an average over Ψ_E, and then an average over the Boltzmann distribution of the eigenstates of the specimen.

The operators of (2) have the following properties,

$$\begin{aligned} &S^+{}_l \Psi_{n_l} = (2S)^{\frac{1}{2}}(1-(n_l-1)/2S)^{\frac{1}{2}}(n_l)^{\frac{1}{2}}\Psi_{n_l-1}, \\ &S^-{}_l \Psi_{n_l} = (2S)^{\frac{1}{2}}(n_l+1)^{\frac{1}{2}}(1-n_l/2S)^{\frac{1}{2}}\Psi_{n_l+1}, \quad \mathfrak{n}_l \Psi_{n_l} = n_l \Psi_{n_l}. \end{aligned} \tag{3}$$

Introducing the well-known creation and destruction operators defined by[13]

$$a^*{}_l \Psi_{n_l} = (n_l+1)^{\frac{1}{2}} \Psi_{n_l+1}, \quad a_l \Psi_{n_l} = (n_l)^{\frac{1}{2}} \Psi_{n_l-1}, \tag{4}$$

one obtains, upon comparing (3) and (4)

$$S^+{}_l = (2S)^{\frac{1}{2}}(1-a^*{}_l a_l/2S)^{\frac{1}{2}} a_l, \quad S^-{}_l = (2S)^{\frac{1}{2}} a^*{}_l (1-a^*{}_l a_l/2S)^{\frac{1}{2}}, \quad \mathfrak{n}_l = a^*{}_l a_l. \tag{5}$$

---

[12] It is to be noted that $\sum_{l=1}^{N} S^{(z)}{}_l$ does not commute with the magnetic interaction portion of the Hamiltonian (1).

[13] In Eq. (4), n_l is allowed to run from 0 to ∞ rather than from 0 to $2S$ as in Eq. (3). The discrepancy is only apparent, since the transition from states with $n_l \leqq 2S$ to states with $n_l > 2S$ will never occur. e.g.

$$S^-{}_l \Psi_{2S} = (2S)^{\frac{1}{2}}(2S+1)^{\frac{1}{2}}(1-2S/2S)^{\frac{1}{2}}\Psi_{2S+1} = 0.$$

When substituted into the Hamiltonian of Eq. (1), (2) and (5) give:

$$\begin{aligned}H=&-\sum_{l,m}J_{lm}(2Sa^*_l(1-a^*_la_l/2S)^{\frac{1}{2}}(1-a^*_ma_m/2S)^{\frac{1}{2}}a_m+S^2-2Sa^*_la_l+a^*_la_la^*_ma_m)\\&+\tfrac{1}{2}\sum_{l,m}(4\beta^2/R^3_{lm})(2Sa^*_l(1-a^*_la_l/2S)^{\frac{1}{2}}(1-a^*_ma_m/2S)^{\frac{1}{2}}a_m+S^2-2Sa^*_la_l+a^*_la_la^*_ma_m)\\&+\tfrac{1}{2}\sum_{l,m}(4\beta^2/R^3_{lm})(-3)([z^2_{lm}(S^2-2Sa^*_la_l+a^*_la_la^*_ma_m)]\\&+[z_{lm}R^+_{lm}(S-a^*_la_l)(2S)^{\frac{1}{2}}a^*_m(1-a^*_ma_m/2S)^{\frac{1}{2}}+z_{lm}R^-_{lm}(S-a^*_la_l)(2S)^{\frac{1}{2}}(1-a^*_ma_m/2S)^{\frac{1}{2}}a_m]\\&+(2S/4)[(R^+_{lm})^2a^*_l(1-a^*_la_l/2S)^{\frac{1}{2}}a^*_m(1-a^*_ma_m/2S)^{\frac{1}{2}}+(R^-_{lm})^2(1-a^*_la_l/2S)^{\frac{1}{2}}\\&\times a_l(1-a^*_ma_m/2S)^{\frac{1}{2}}a_m+2R^-_{lm}R^+_{lm}a^*_l(1-a^*_la_l/2S)^{\frac{1}{2}}(1-a^*_ma_m/2S)^{\frac{1}{2}}a_m])\\&-\sum_{l=1}^{N}2\beta H(S-a^*_la_l),\end{aligned}\tag{6}$$

with $$R^+_{lm}=x_{lm}+iy_{lm};\quad R^-_{lm}=x_{lm}-iy_{lm}.$$

The condition of quasi-saturation

$$1\gg\tfrac{1}{2}[M_0-M(T,H)]/M_0=\langle\langle\mathfrak{n}_l\rangle\rangle_{\text{Av}}/2S=\langle\langle a^*_la_l\rangle\rangle_{\text{Av}}/2S$$

is now invoked to effect the following approximations in H.

I. Replacement of $(1-a_l^*a_l/2S)^{\frac{1}{2}}$ by 1. Such a replacement appears reasonable since the expectation value of $(1-a^*_la_l/2S)^{\frac{1}{2}}$ is $\leqq(1-\langle\langle\mathfrak{n}_l\rangle\rangle_{\text{Av}}/2S)^{\frac{1}{2}}\leqq 1$.

II. Neglect of terms proportional to $a^*_la_la^*_ma_m=\mathfrak{n}_l\mathfrak{n}_m$. Assuming that there is no correlation in the location of the different spin deviations, one obtains for the expectation value of these terms, $\langle\langle\mathfrak{n}_l\mathfrak{n}_m\rangle\rangle_{\text{Av}}\leqq\langle\langle\mathfrak{n}_l\rangle\rangle_{\text{Av}}\langle\langle\mathfrak{n}_m\rangle\rangle_{\text{Av}}$ which is smaller than the expectation value of $2Sa^*_la_l=2S\langle\langle\mathfrak{n}_l\rangle\rangle_{\text{Av}}$, by a factor $\langle\langle\mathfrak{n}_m\rangle\rangle_{\text{Av}}/2S\ll 1$.

III. Neglect of terms proportional to $(2S)^{\frac{1}{2}}a^*_la_la^*_m=(2S)^{\frac{1}{2}}\mathfrak{n}_la^*_m$. These are terms which cause the system to make transitions between states of different total spin. Unlike terms of the type $2Sa^*_la^*_m$ which also cause such transitions, they are different from zero only for transitions taking place near atoms on which spin deviations are already present; the ratio of the number of transitions arising from the two types of terms is thus $\leqq\langle\langle\mathfrak{n}_l\rangle\rangle_{\text{Av}}(2S)^{-\frac{1}{2}}\ll 1$.

A further discussion of the nature of the approximations I, II, III, is given in Appendix I. In anticipation of results to be obtained below (cf. Eq. (15′) and following text), it may be pointed out that, if the magnetic dipole-dipole interactions are omitted, these approximations lead to the same energy levels as obtained by Bloch in his derivation of the $T^{\frac{3}{2}}$ law,[7] and are thus equivalent to the approximations of his method.

An additional simplification of the Hamiltonian results from the fact that summations of the form:[14]

$$\textstyle\sum_{l,m}f(R_{lm})x_{lm}z_{lm}a^*_m=\sum_m a^*_m\sum_k f(R_k)x_kz_k$$

are zero. This fact is obvious if the direction of **H**, i.e., the z axis, coincides with one of the crystallographic cubical axes. In the more general case, a transformation of the sum over k to Cartesian coordinates which are referred to the cubical axes readily leads to the same result.

Applying approximations I, II, III, and the theorem just stated, one obtains for the Hamiltonian (6)

$$\begin{aligned}H=&\,C-\textstyle\sum_{l,m}2SJ_{lm}(a^*_la_m-a^*_la_l)+\tfrac{1}{2}\sum_{l,m}(4\beta^2/R^3_{lm})(2S)(a^*_la_m-a^*_la_l)\\&+\tfrac{1}{2}\textstyle\sum_{l,m}(4\beta^2/R^3_{lm})(-3)(2S)(\tfrac{1}{2}[x^2_{lm}+y^2_{lm}]a^*_la_m-z^2_{lm}a^*_la_l+\tfrac{1}{4}[(R^+_{lm})^2a^*_la^*_m+(R^-_{lm})^2a_la_m])\\&+\textstyle\sum_l 2\beta Ha^*_la_l,\end{aligned}\tag{7}$$

with $$C=-\textstyle\sum_{l,m}J_{lm}S^2-2\beta SNH-\tfrac{1}{2}\sum_l 2\beta S\{\sum_m(-2\beta S)/R^3_{lm}(1-3z^2_{lm}/R^2_{lm})\}.$$

[14] $f(\mathbf{R}_{lm})$ is any function of $\mathbf{R}_{lm}$ and $\mathbf{R}_k\equiv\mathbf{R}_l-\mathbf{R}_m$. The two sums are identical provided that contributions coming from atoms on the surface of the specimen are neglected; the justification of this neglect is given in the text before Eq. (11).

The numerical constant C is the value of the energy when all of the atomic magnets point in the direction of the field $\mathbf{H}$. The first sum in C is the exchange energy, the second the interaction between the atomic magnets and the external field, and the last the mutual dipole-dipole interaction of the atomic magnets. (In fact, the expression in the curly brackets is the sum of the Lorentz local-field, $4\pi M_0/3$, and the demagnetizing field, as will be shown in another connection below. Cf. text after Eqs. (44), (45) in Appendix II.

From the form of the Hamiltonian (7), it is apparent that the "spin deviations," specified by the integers n_l are not localized on any one atom, but are "propagated" through the crystal. That this propagation is essentially of a wave-like character is seen by the introduction of new variables defined by the following relations:

$$\begin{aligned} a_\lambda &= N^{-\frac{1}{2}} \textstyle\sum_l \exp(i\mathbf{K}_\lambda\cdot\mathbf{R}_l)a_l; \qquad a_l = N^{-\frac{1}{2}} \textstyle\sum_\lambda \exp(-i\mathbf{K}_\lambda\cdot\mathbf{R}_l)a_\lambda, \\ a^*_\lambda &= N^{-\frac{1}{2}} \textstyle\sum_l \exp(-i\mathbf{K}_\lambda\cdot\mathbf{R}_l)a_l; \qquad a^*_l = N^{-\frac{1}{2}} \textstyle\sum_\lambda \exp(i\mathbf{K}_\lambda\cdot\mathbf{R}_l)a^*_\lambda. \end{aligned} \tag{8}$$

The a_λ and a^*_μ satisfy the relation:

$$a_\lambda a^*_\mu - a^*_\mu a_\lambda = \delta_{\mu\lambda}, \tag{9}$$

since from Eq. (4),

$$a_l a^*_m - a^*_m a_l = \delta_{ml}. \tag{10}$$

In Eq. (8), $\mathbf{R}_l$ is the vector from an arbitrary origin to the lth atom, whose magnitude measures the corresponding distance in units of the lattice constant, in contrast to the formulae of the above text where $|\mathbf{R}_l|$ gives distance in centimeters. $\mathbf{K}_\lambda$ is a reduced wave-vector; the usual periodicity conditions require its components to take the values

$$\mathrm{K}^{(x)}_\lambda = 2\pi\lambda_x/G_x, \quad \mathrm{K}^{(y)}_\lambda = 2\pi\lambda_y/G_y, \quad \mathrm{K}^{(z)}_\lambda = 2\pi\lambda_z/G_z,$$

where λ_x, λ_y, λ_z assume any integral values between $-\frac{1}{2}G_x$ and $\frac{1}{2}G_x-1$, $-\frac{1}{2}G_y$ and $\frac{1}{2}G_y-1$, $-\frac{1}{2}G_z$ and $\frac{1}{2}G_z-1$, respectively.[15]

The replacement of the a_l by the a_λ constitutes the first step in the evaluation of the eigenvalues of the Hamiltonian. To carry out this replacement, one has to evaluate sums of the type,

$$\textstyle\sum_{l,m} f(\mathbf{R}_{lm}) a^*_l a_m.$$

Upon application of (10), this sum becomes

$$\sum_{l,m,\lambda,\lambda'} N^{-1} f(\mathbf{R}_{lm}) a^*_{\lambda'} a_\lambda \exp\{i(\mathbf{K}_{\lambda'}\cdot\mathbf{R}_l - \mathbf{K}_\lambda\cdot\mathbf{R}_m)\}.$$

Introducing the vector $\mathbf{R}_h = \mathbf{R}_l - \mathbf{R}_m = \mathbf{R}_{lm}$ one obtains

$$\sum_{l,h,\lambda,\lambda'} N^{-1} f(\mathbf{R}_h) a^*_{\lambda'} a_\lambda \exp\{i(\mathbf{K}_{\lambda'} - \mathbf{K}_\lambda)\cdot\mathbf{R}_l)\} \exp\{i\mathbf{K}_\lambda\cdot\mathbf{R}_h\}.$$

Now, the summations over l and h can be carried out independently if one neglects contributions arising from the surface of the specimen. Such contributions are obviously negligible for the exchange forces. In this case, the summation over h comprises only nearest neighbors of l, and hence surface terms arise only if the atom l is, itself, on the surface. However, the number of such terms is smaller than the total number of terms by a factor $\cong 1/G$. As far as the magnetic forces are concerned, although their short range character is not immediately obvious, one can show that, in the sum over h, again only small values of $|\mathbf{R}_h|$ are important; hence the argument given just above again applies. The summation over l then yields the factor $N\delta_{\lambda'\lambda}$ and the quadruple sum reduces to

$$\textstyle\sum_\lambda (\sum_h f(\mathbf{R}_h) \exp\{i\mathbf{K}_\lambda\cdot\mathbf{R}_h\}) a^*_\lambda a_\lambda.$$

[15] G_x, G_y, G_z are the lengths of the specimen in the x, y, z, directions, divided by the lattice spacing.

Treating all of the summations in H by this method, one obtains:

$$\mathrm{H}=C+\sum_\lambda A_\lambda a^*_\lambda a_\lambda+\sum_\lambda(\tfrac{1}{2}B_\lambda a_\lambda a_{-\lambda}+\tfrac{1}{2}B^*_\lambda a^*_\lambda a^*_{-\lambda}), \tag{11}$$

where

$$A_\lambda=3\beta\sum_h(-2\beta S/a^3R^3_h)(1-3z^2_h/R^2_h)+\beta\sum_h(2\beta S/a^3R^3_h)(1-3z^2_h/R^2_h)(1-\exp(i\mathbf{K}_\lambda\cdot\mathbf{R}_h))$$
$$+\sum_h 2SJ_h(R_h)(1-\exp(i\mathbf{K}_\lambda\cdot\mathbf{R}_h))+2\beta H. \tag{12}$$

$$B_\lambda=-3\beta\sum_h(2\beta S/a^3R^3_h)(x^2_h-y^2_h-2ix_hy_h)/R^2_h$$
$$+3\beta\sum_h(2\beta S/a^3R^3_h)((x^2_h-y^2_h-2ix_hy_h)/R^2_h)(1-\exp(i\mathbf{K}_\lambda\cdot\mathbf{R}_h)), \tag{13}$$

a being the lattice distance.

The sums over h in A_λ and B_λ are evaluated in Appendix II; the results for $|\mathbf{K}_\lambda|\ll 1$ are:

$$A_\lambda=A_{-\lambda}=2SJ\mathrm{K}_\lambda^2+2\beta H+4\pi\beta M_0\sin^2\theta_\lambda, \tag{14}$$

$$B_\lambda=B_{-\lambda}=4\pi\beta M_0\sin^2\theta_\lambda e^{-2i\phi_\lambda}. \tag{15}$$

Here, $J\equiv J_h(R_h)$ when R_h is the distance between nearest neighbors; θ_λ, ϕ_λ are polar angles of $\mathbf{K}_\lambda$ with polar axis parallel to the field, $\mathbf{H}$. As will be shown later in the text, the values of A_λ and B_λ which contribute importantly to the magnetization $\mathbf{M}$ are those with $|\mathbf{K}_\lambda|\ll 1$.

It might be instructive to point out that, if the magnetic interactions are omitted, H reduces to

$$-N\sum_h J_h S^2-2\beta SNH+\sum_\lambda(\sum_h J_h 2S(1-\exp(i\mathbf{K}_\lambda\cdot\mathbf{R}_h))+2\beta H)a^*_\lambda a_\lambda; \tag{15'}$$

since the eigenvalues, n_λ, of $\mathfrak{n}_\lambda\equiv a^*_\lambda a_\lambda$ are 0, 1, 2, 3, $\cdots$ [cf. Eq. (9)], it is seen that the eigenvalues of this Hamiltonian are just the energy values which have been found by Bloch and Möller.[7] In this connection, it is also apparent that n_λ can be interpreted as the number of "spin-wave quanta" associated with the wave vector $\mathbf{K}_\lambda$. Further, $\sum_\lambda\langle\langle\mathfrak{n}_\lambda\rangle\rangle_{Av}$ which is equal to $\sum_l\langle\langle\mathfrak{n}_l\rangle\rangle_{Av}$, gives directly the expectation value of the deviation from its maximum value of the z component of the total spin of the specimen.

However, the existence of the magnetic interactions, in particular the terms of (11) in $a_\lambda a_{-\lambda}$ and $a^*_\lambda a^*_{-\lambda}$ which do not commute with $\mathfrak{n}_\lambda$, necessitates further transformation before the Hamiltonian is brought to diagonal form. These transformations are, in order:

$$a_\lambda=2^{-\frac{1}{2}}e^{i\phi_\lambda}(b_\lambda+b_{-\lambda}); \quad a_{-\lambda}=2^{-\frac{1}{2}}e^{i\phi_{-\lambda}}(b_\lambda-b_{-\lambda}) \tag{16}$$

and similarly for a^*_λ, $a^*_{-\lambda}$. These transformations are defined only for the half-space of $\mathbf{K}_\lambda$, i.e., $-\pi<\mathrm{K}^{(x)}_\lambda<\pi$, $-\pi<\mathrm{K}^{(y)}_\lambda<\pi$, $0<\mathrm{K}^{(z)}_\lambda<\pi$.

$$b_\lambda=l_1c_\lambda+l_2c^*_\lambda; \quad b_{-\lambda}=l_1c_{-\lambda}-l_2c^*_{-\lambda}$$
$$b^*_\lambda=l_1c^*_\lambda+l_2c_\lambda; \quad b^*_{-\lambda}=l_1c^*_{-\lambda}-l_2c_{-\lambda} \tag{17}$$

with

$$l_1=\left(\frac{1}{2}\frac{A_\lambda+(A^2_\lambda-|B_\lambda|^2)^{\frac{1}{2}}}{(A^2_\lambda-|B_\lambda|^2)^{\frac{1}{2}}}\right)^{\frac{1}{2}}; \quad l_2=\left(\frac{1}{2}\frac{A_\lambda-(A^2_\lambda-|B_\lambda|^2)^{\frac{1}{2}}}{(A^2_\lambda-|B_\lambda|^2)^{\frac{1}{2}}}\right)^{\frac{1}{2}}. \tag{18}$$

In terms of c_λ, c^*_λ, the Hamiltonian (11), becomes:

$$\mathrm{H}=C+\sum_\lambda((A^2_\lambda-|B_\lambda|^2)^{\frac{1}{2}}C^*_\lambda C_\lambda+\tfrac{1}{2}(A^2_\lambda-|B_\lambda|^2)^{\frac{1}{2}}-\tfrac{1}{2}A_\lambda). \tag{19}$$

In (19) the sum over λ goes over the *whole* of $\mathbf{K}_\lambda$ space, as in (11).

The eigenvalues, E, of H are now immediately available since, by (9), (16), (17), the eigenvalues, N_λ of $C^*_\lambda C_\lambda$ are 0, 1, 2, 3, $\cdots$. Thus

$$\mathrm{E}\equiv\mathrm{E}_{\mathrm{N}_\lambda}=C+\sum_\lambda(\tfrac{1}{2}(A^2_\lambda-|B_\lambda|^2)^{\frac{1}{2}}-\tfrac{1}{2}A_\lambda)+\sum_\lambda(A^2_\lambda-|B_\lambda|^2)^{\frac{1}{2}}\mathrm{N}_\lambda. \tag{20}$$

IV. Calculation of the Magnetization, $M(T, H)$

The magnetization is obtained from the partition function, Z, by the relation,

$$M=\frac{kT}{V}\frac{\partial}{\partial H}\log Z \tag{21}$$

with

$$Z=\sum_E e^{-E/kT}=e^{-C/kT}\exp\left[-\sum_\lambda \tfrac{1}{2}((A^2_\lambda-|B_\lambda|^2)^{\frac{1}{2}}-A_\lambda)/kT\right]\sum_{N_\lambda}\exp\left[-\sum_\lambda(A^2_\lambda-|B_\lambda|^2)^{\frac{1}{2}}N_\lambda/kT\right]$$
$$=e^{-C/kT}\exp\left[-\sum_\lambda \tfrac{1}{2}((A^2_\lambda-|B_\lambda|^2)^{\frac{1}{2}}-A_\lambda)/kT\right]\prod_\lambda(1-\exp\left[(A^2_\lambda-|B_\lambda|^2)^{\frac{1}{2}}/kT\right])^{-1}. \tag{22}$$

Thus by (21), (22), and replacing $\sum_\lambda f(\mathbf{K}_\lambda)$ by $G_xG_yG_z(2\pi)^{-3}\int f(\mathbf{K})d\mathbf{K}$, one obtains

$$M(T,H)=\frac{2\beta SN}{V}-\frac{G_xG_yG_z2\beta}{(2\pi)^3V}\int\left[\left(\frac{A(\mathbf{K})}{((A(\mathbf{K}))^2-|B(\mathbf{K})|^2)^{\frac{1}{2}}}\right)\left(\frac{1}{\exp\left[((A(\mathbf{K}))^2-|B(\mathbf{K})|^2)^{\frac{1}{2}}/kT\right]-1}\right)\right]d\mathbf{K}$$
$$-\frac{G_xG_yG_z\beta}{(2\pi)^3V}\int\left[\frac{A(\mathbf{K})}{((A(\mathbf{K}))^2-|B(\mathbf{K})|^2)^{\frac{1}{2}}}-1\right]d\mathbf{K}\equiv M_0-M_T(T,H)-M_\beta(H). \tag{23}$$

M_0 is the value of the magnetization when all of the spins are parallel to each other—complete saturation. M_T is the deviation of M from M_0 due to temperature agitation; its magnitude, however, is also dependent on H and the magnetic dipole-dipole interaction. Finally, M_β is the deviation of M from M_0 due to the dipole-dipole interaction, itself; the magnitude of M_β is, in addition, a function of H. The presence of the term M_β indicates that, even at $T=0$, *complete* saturation can be attained only by the application of a field $H\gg 4\pi M_0$.

The $T^{\frac{3}{2}}$ law of Bloch is obtained from (23) by neglecting the magnetic interactions and by setting $\mathbf{H}=0$. Then, from (14) and (15), $A(\mathbf{K})=A(-\mathbf{K})=2SJ\mathrm{K}^2$; $B(\mathbf{K})=B(-\mathbf{K})=0$ and

$$M(T)^{\text{Bloch}}\equiv M_0-M_T{}^{\text{Bloch}}=M_0-G_xG_yG_z2\beta(2\pi)^{-3}V^{-1}\int(\exp\left[2SJ\mathrm{K}^2/kT\right]-1)^{-1}d\mathbf{K}$$
$$=M_0(1-[M^{-1}{}_0G_xG_yG_zV^{-1}2\beta(2\pi)^{-3}(k/2SJ)^{\frac{1}{2}}(2\pi)(2)(1.3)]T^{\frac{3}{2}})$$
$$=M_0(1-(\text{const.})T^{\frac{3}{2}}). \tag{24}$$

It is to be noted that in (24) the integration is extended over all $\mathbf{K}$-space rather than over a cube of side 2π, and the exchange energy $\sum_h 2SJ_h(R_h)(1-\exp\left[i\mathbf{K}\cdot\mathbf{R}_h\right])$ is approximated by $2SJ\mathrm{K}^2$. This procedure is permissible provided that $kT/2SJ\ll 1$, since in this case the main contributions to the integral come from regions of $\mathbf{K}$-space for which $|\mathbf{K}|\lessapprox(kT/2SJ)^{\frac{1}{2}}$.[16]

Turning now to the evaluation of the integral for M_T in (23), one proceeds most conveniently by finding the difference between M_T and the known integral for $M_T{}^{\text{Bloch}}$ in (24). Thus,

$$M_T-M_T{}^{\text{Bloch}}=\frac{G_xG_yG_z}{(2\pi)^3}\frac{2\beta}{V}\int\left[\left(\frac{A}{(A^2-|B|^2)^{\frac{1}{2}}}\right)\left(\frac{1}{\exp\left[(A^2-|B|^2)^{\frac{1}{2}}/kT\right]-1}\right)\right.$$
$$\left.-\frac{1}{\exp\left[2SJ\mathrm{K}^2/kT\right]-1}\right]d\mathbf{K} \tag{25}$$

with A and B satisfying relations (14) and (15), *viz.*:

$$A(\mathbf{K})=2SJ\mathrm{K}^2+4\pi\beta M_0\sin^2\theta_{\mathrm{K}}+2\beta H,\quad |B(\mathbf{K})|=4\pi\beta M_0\sin^2\theta_{\mathrm{K}}.$$

[16] The condition $kT/2SJ\ll 1$ is, in practice, not as well fulfilled as is theoretically desirable, e.g. for iron at room temperature $kT/2SJ\lessapprox 0.3$.

The important contributions to the integrand of (25) come from regions of **K**-space for which $|\mathbf{K}| \lesssim [(4\pi\beta M_0+2\beta H)/2SJ]^{\frac{1}{2}}$. Further, in all practical cases, $(4\pi\beta M_0+2\beta H)/kT \leqq 2\times 10^{-3}$. Thus, in the regions of **K**-space making important contributions to (25), both $(A^2-|B|^2)^{\frac{1}{2}}$ and $2SJK^2$ are small compared to kT. It is then permitted to expand the exponential in the integrand. Hence

$$M_T - M_T^{\text{Bloch}} = kT\frac{G_xG_yG_z}{V}\frac{2\beta}{(2\pi)^3}\int\left[\frac{A}{A^2-|B|^2}-\frac{1}{2SJK^2}\right]d\mathbf{K}. \tag{26}$$

From this point on, the integration is straightforward and yields:

$$M_T - M_T^{\text{Bloch}} = -\frac{G_xG_yG_z}{V}\frac{1}{S}\left(\frac{kT}{2SJ}\right)^{\frac{1}{2}}\frac{2\beta S}{(2\pi)^3}(2\pi)(2)(1.3)$$

$$\times\left\{\frac{3\pi}{8(1.3)}\left(\frac{2\beta H}{kT}\right)^{\frac{1}{2}}+\frac{\pi 2^{\frac{1}{2}}}{8(1.3)}\left(\frac{\beta}{kT}\right)^{\frac{1}{2}}\frac{H+4\pi M_0}{(4\pi M_0)^{\frac{1}{2}}}\sin^{-1}\left(\frac{4\pi M_0}{H+4\pi M_0}\right)^{\frac{1}{2}}\right\}. \tag{27}$$

As regards $M_\beta(H)$, it has not been found possible to evaluate the integral for it in a closed form for all values of H. However, in the two limits, $H \ll 4\pi M_0$ and $H \gg 4\pi M_0$, the integral has been evaluated. One obtains:

$$M_\beta(H) = \frac{G_xG_yG_z}{V}\beta\left(\frac{4\pi\beta M_0}{2SJ}\right)^2\left(\frac{2SJ}{2\beta H}\right)^{\frac{1}{2}}, \qquad \text{if } H \gg 4\pi M_0,$$

$$M_\beta(H) = \frac{G_xG_yG_z}{V}\beta\left(\frac{4\pi\beta M_0}{2SJ}\right)^2\left(\frac{2SJ}{4\pi\beta M_0}\right)^{\frac{1}{2}}, \quad \text{if } H \ll 4\pi M_0.$$

An estimate of the relative importance of the terms $M_\beta(H)$ and $M_T(T, H)$ is obtained by studying the change of these two quantities when H varies from zero to, say, $4\pi\beta M_0$. Then

$$\Delta M_T \equiv M_T(T, 4\pi\beta M_0) - M_T(T, 0) \lesssim \frac{G_xG_yG_z}{V}\beta\left(\frac{kT}{2SJ}\right)^{\frac{1}{2}}\left(\frac{4\pi\beta M_0}{kT}\right)^{\frac{1}{2}},$$

$$\Delta M_\beta \equiv M_\beta(4\pi\beta M_0) - M_\beta(0) \lesssim \frac{G_xG_yG_z}{V}\beta\left(\frac{2SJ}{4\pi\beta M_0}\right)^{\frac{1}{2}}\left(\frac{4\pi\beta M_0}{2SJ}\right)^2$$

and

$$\Delta M_\beta/\Delta M_T = 4\pi\beta M_0/kT. \tag{28}$$

This ratio is negligibly small (5×10^{-3} for iron, 1.5×10^{-3} for nickel); hence, M_β shall be omitted completely in what follows.

Thus, from (23), (24), and (27):

$$M(T, H) = M_0 - \frac{G_xG_yG_z}{V}(2\beta S)\frac{1}{S}\left(\frac{kT}{2SJ}\right)^{\frac{1}{2}}\frac{(2\pi)(2)(1.3)}{(2\pi)^3}\left(1-\frac{3\pi}{8(1.3)}\left(\frac{2\beta H}{kT}\right)^{\frac{1}{2}}\right.$$

$$\left.-\frac{\pi}{8(1.3)}\left(\frac{8\pi\beta M_0}{kT}\right)^{\frac{1}{2}}\frac{H+4\pi M_0}{4\pi M_0}\sin^{-1}\left(\frac{4\pi M_0}{H+4\pi M_0}\right)^{\frac{1}{2}}\right). \tag{29}$$

The quantity most often found in the experiments is the "intrinsic susceptibility," $\partial M/\partial H$. One obtains from (29),

$$\frac{\partial M}{\partial H}=\frac{G_xG_yG_z}{V}(2\beta S)\frac{1}{S}\left(\frac{kT}{2SJ}\right)^{\frac{1}{2}}\frac{(2\pi)(2)(1.3)}{(2\pi)^3}\frac{1}{M_0}$$

$$\times\frac{1}{16(1.3)2^{\frac{1}{2}}}\left(\frac{4\pi\beta M_0}{kT}\right)^{\frac{1}{2}}\left(\left(\frac{4\pi M_0}{H}\right)^{\frac{1}{2}}+\sin^{-1}\left(\frac{4\pi M_0}{H+4\pi M_0}\right)^{\frac{1}{2}}\right). \quad (30)$$

Up to the present time, it has not proved feasible to calculate J in terms of atomic constants; in practice its numerical value is obtained from an experimental measurement of $M_0-M(T,0)$. This latter quantity may be equated to M_T^{Bloch} since the other contribution to $M_0-M(T,0)$, namely $M_T(T,0)-M_T^{\text{Bloch}}$ and M_β, is relatively small. Thus from (30) and (24), one finally obtains:

$$\frac{\partial M}{\partial H}=\left(\frac{M_0-M(T,0)}{M_0}\right)\left(\frac{1}{(16)(2^{\frac{1}{2}})(1.3)}\right)\left(\frac{4\pi\beta M_0}{kT}\right)^{\frac{1}{2}}\left(\left(\frac{4\pi M_0}{H}\right)^{\frac{1}{2}}+\sin^{-1}\left(\frac{4\pi M_0}{H+4\pi M_0}\right)^{\frac{1}{2}}\right). \quad (31)$$

The application of this result to the experiments is considered in Section VI.

It is instructive to compare the above result for $\partial M/\partial H$ with what would be obtained if the magnetic interactions were *not* treated quantum-mechanically, but classically by means of the Lorentz local field. The result of such a procedure can be obtained directly from (30) by

(1) Passing to the limit $M_0\to 0$.

(2) Replacing H by $H+\gamma M$ where γ is a numerical factor $\cong 4\pi/3$.

The constant J can then be eliminated as above, and one obtains

$$\left(\frac{\partial M}{\partial H}\right)_{\text{Lorentz}}=\left(\frac{M_0-M(T,0)}{M_0}\right)\left(\frac{1}{(8)(1.3)(2^{\frac{1}{2}})}\right)\left(\frac{4\pi\beta M_0}{kT}\right)^{\frac{1}{2}}\left(\frac{4\pi M_0}{H+\gamma M_0}\right)^{\frac{1}{2}}. \quad (32)$$

The important differences between $(\partial M/\partial H)_{\text{Lorentz}}$ and $\partial M/\partial H$ of (31) occur for $H\ll 4\pi M_0$. In this case $(\partial M/\partial H)_{\text{Lorentz}}$ predicts a field-independent susceptibility, while (31) has an inverse square-root dependence on H. On the other hand for $H\gg 4\pi M_0$, the two expressions become identical; both then vary with H as $H^{-\frac{1}{2}}$. The inverse square-root dependence of the susceptibility on the magnetic field for $H\gg 4\pi M_0$ is thus seen to be a general feature of the exchange interaction model subject to approximations I, II, III, quite independent of the details of the treatment of the magnetic interaction.

It should finally be noted from (30) that the susceptibility is proportional to the absolute temperature.

V. Effects of Spin-Orbit Interactions

As was stated at the end of Section II, all spin-orbit effects have thus far been neglected in the formulation of the fundamental Hamiltonian (1). If one desires to treat these effects within the framework of the present development, i.e., supplementing the Hamiltonian (1) by additional terms, the first question which arises is whether spin-orbit effects can be described by an equivalent interaction energy in the space of the atomic spin variables. This question has been considered by Van Vleck in connection with the problem of ferromagnetic anisotropy.[11] In Van Vleck's work the spin-orbit effects are represented by equivalent "dipole-dipole" and "quadrupole-quadrupole" interactions

of the type:

$$\tfrac{1}{2}\sum_{l,m} C_{lm}(R_{lm})[\mathbf{S}_l\cdot\mathbf{S}_m - 3R_{lm}^{-2}\mathbf{S}_l\cdot\mathbf{R}_{lm}\mathbf{S}_m\cdot\mathbf{R}_{lm}], \tag{33}$$

$$\tfrac{1}{2}\sum_{l,m}\gamma_{lm}(R_{lm})R_{lm}^{-4}(\mathbf{S}_l\cdot R_{lm})^2(\mathbf{S}_m\cdot\mathbf{R}_{lm})^2. \tag{34}$$

These two terms are discussed in order.

(1) Conveniently, the equivalent "dipole-dipole" interaction (42) is just the same as the magnetic interaction provided that $4\beta^2/R^3_{lm}$ is replaced by $C_{lm}(R_{lm})$. The effect of this dipole-dipole interaction then merely consists of additions ΔA_λ, ΔB_λ to the coefficients A_λ which appear in the Hamiltonian (19), and therefore in the integral (23) for $M(T, H)$. One has: (cf. the first two sums in Eq. (12) for A_λ and Eq. (13) for B_λ)

$$\Delta A_\lambda = \sum_h\{(-3S/2)C(R_h)(1-3z^2{}_h/R^2{}_h)+(S/2)C(R_h)(1-3z^2{}_h/R^2{}_h)(1-\exp(i\mathbf{K}_\lambda\cdot\mathbf{R}_h))\}, \tag{35}$$

$$\Delta B_\lambda = \sum_h\{(-3S/2)C(R_h)((x^2{}_h-y^2{}_h-2ix_hy_h)/R^2{}_h)\exp(i\mathbf{K}_\lambda\cdot\mathbf{R}_h)\}. \tag{36}$$

It is also reasonable to suppose that $C(R_h)$ is of short range character;[17] in this case the sums in (35) and (36) have appreciable contributions only from the nearest neighbors of a given atom. Taking account of the crystalline cubical symmetry of the specimen, one obtains:

$$\Delta A_\lambda = \sum_h(S/2)C(1-3z^2{}_h/R^2{}_h)(1-\exp(i\mathbf{K}_\lambda\cdot\mathbf{R}_h)),$$

$$\Delta B_\lambda = \sum_h(3S/2)C((x_h{}^2-y_h{}^2-2ix_hy_h)/R^2{}_h)(\mathbf{K}_\lambda\cdot\mathbf{R}_h)^2+\text{terms in } K^4{}_\lambda, K^6{}_\lambda, \cdots$$

with $C\equiv C(R_h)$ for nearest neighbors,[17a] $\geqq 10$ wave-numbers $\geqq J/100$.

Equations (35), (36) and the above numerical estimate for C insure that the equivalent "dipole-dipole" interactions have no effect whatever on the magnetization. As far as the $A_\lambda+\Delta A_\lambda$ coefficient is concerned, the ΔA_λ term: $\sum_h(S/2)C(1-3Z^2{}_h/R^2{}_h)(1-\exp(i\mathbf{K}_\lambda\cdot\mathbf{R}_h))$ will be completely swamped by the exchange term in A_λ: $\sum_h 2SJ(1-\exp(i\mathbf{K}_\lambda\cdot\mathbf{R}_h))$. On the other hand, the $B_\lambda+\Delta B_\lambda$ coefficient is altogether important only when it is $\geqq A_\lambda+\Delta A_\lambda$, i.e., only when $4\pi\beta M_0\geqq\sum_h 2SJ(1-\exp(i\mathbf{K}_\lambda\cdot\mathbf{R}_h))$ $\geqq 2SJK^2{}_\lambda$. Under these circumstances, $\Delta B_\lambda\geqq SCK^2{}_\lambda\geqq SC4\pi\beta M_0/2SJ\ll 4\pi\beta M_0$, and thus, $\Delta B_\lambda\ll B_\lambda$, for the important B_λ.

(2) Concerning the quadrupole-quadrupole interaction, an examination of its diagonal matrix element in the representation where the Hamiltonian of Eq. (19) is diagonal indicates that its effect, to the first order in γ, is given by the addition to A_λ of a constant term $\geqq\gamma$. This term may be conveniently described by a fictitious "magnetic field": $H_a\equiv\gamma/2\beta\geqq$anistropy constant$/M_0\geqq 200$ gauss (Fe), 100 gauss (Ni).[17b] It can then be coupled together with the original $2\beta H$ term in A_λ in the form $2\beta(H+H_a)$ and carried through to the end of the evaluation of $M(T, H)$, without further ado. Thus, in the expressions for M and $\partial M/\partial H$ in Eqs. (30), (31), the term in γ has but little effect if H is, say, greater than 1000 guass.

(3) Finally, it is possible that some portion of the spin-orbit effects is incapable of description by interactions of the type (33), (34). Until explicit expressions are presented, one cannot, of course, estimate the resultant corrections. It is to be hoped, however, that these corrections will still be described by means of a fictitious field, H_a, whose order of magnitude will be the same as in the above numerical estimates.[17c]

---

[17] Van Vleck, reference 11, p. 1193.

[17a] This numerical estimate for C is due to Van Vleck, reference 11, p. 1184.

[17b] For experimental values of the anisotropy constant see Becker and Döring reference 3, p. 123, Table 12.

[17c] It may be remarked in passing that the methods of the present paper offer an approach to the problem of ferromagnetic anisotropy at low temperatures. For this purpose the eigenvalues $E_{N\lambda}$ of Eq. (20), with B_λ replaced by $B_\lambda+\Delta B_\lambda$ must be determined as functions of the direction of $\mathbf{M}_0$ with respect to the crystallographic axes. This calculation and its relation to other treatments of ferromagnetic anisotropy [Van Vleck, reference 11; Van Peype, Physica **5**, 465 (1938)] is now being considered.

VI. Comparison with Experiment

(1) Numerical estimates of theoretical values for the susceptibility

Equation (31) for the susceptibility $\partial M/\partial H$, when applied to iron and nickel at $T=287°\text{K}$ and $H=4000$ gauss, gives:

$$(\partial M/\partial H)_{\text{Fe}}=1.7\times10^{-4}, \tag{37}$$

$$(\partial M/\partial H)_{\text{Ni}}=1.2\times10^{-4}, \tag{38}$$

taking[18]

$$(M_0-M(T,0))/M_0]_{\text{Fe}}=0.018,$$

$$(4\pi M_0)_{\text{Fe}}=21{,}800;$$

$$(M_0-M(T,0))/M_0]_{\text{Ni}}=0.040,$$

$$(4\pi M_0)_{\text{Ni}}=6{,}400.$$

There exists no experimental data for cobalt for comparison with theory.

These numerical results for $\partial M/\partial H$, are to be compared with those of Akulov, which are based on the phenomenological Weiss-Heisenberg theory. In this theory,[19] for atoms with $S=\frac{1}{2}$,

$$M(T,H)=M_0\tanh[(\beta H+\beta qM)/kT],$$

$q=\frac{1}{2}zJ/\beta M_0$; whence, for low T, Akulov's results may be put in the form:

$$\left[\frac{\partial M}{\partial H}\right]_{\text{Akulov}}=\frac{[M_0-M(T,0)]}{M_0}\frac{1}{2\pi}\frac{4\pi\beta M_0}{kT}. \tag{39}$$

The numerical values for iron and nickel given by (39) are found from the experimentally observed values of $[M_0-M(T,0)]/M_0$. One has:

$$\partial M/\partial H]_{\text{Fe}}^{\text{Akulov}}=1.5\times10^{-5}, \tag{40}$$

$$\partial M/\partial H]_{\text{Ni}}^{\text{Akulov}}=1.2\times10^{-5}. \tag{41}$$

Thus Akulov's susceptibility is numerically smaller than the one derived in this paper by a factor of about ten;[20] this factor is due essentially to the appearance in Eq. (39) of the quantity $4\pi\beta M_0/kT$, which is $\ll1$, whereas in Eq. (31), there is instead the quantity $(4\pi\beta M_0/kT)^{\frac{1}{2}}$.

Further, Akulov's susceptibility is independent of H and is proportional to $e^{-zJ/kT}/T$, while the susceptibility of Eq. (31), as has already been noted at the end of Section IV, is proportional to $TH^{-\frac{1}{2}}$, for a large range of fields.

(2) Discussion of the various experiments

Information concerning the variation of the intrinsic magnetization with H, has been obtained from experiments[21] on polycrystalline samples of nickel and iron. In these experiments it has been customary to describe the variation of the observed magnetization with H by a formula of the type:

$$(\partial M/\partial H)_{\text{obs}}=A/H^2+B/H^3+C, \tag{42}$$

where A, B, C are supposed to be constants.

The constants A and B depend upon the metallurgical history of the polycrystalline specimen; A is conditioned by the plastic deformation of the material,[22] whereas B is determined by the crystalline properties and elastic state.[22] The physical significance of the constant A is at present a matter of speculation; the order of magnitude and dependence on temperature and elastic condition, of the constant B, as well as the field variation of the term B/H^3, shows that B originates from the ferromagnetic anisotropy of the component crystal grains of the specimen.[23] The latter observation is true whether the anisotropy is a consequence of the natural crystalline properties, or is induced by an external stress. Finally, the constant C has been

[18] The values of M_0 for Fe and Ni are obtained from Becker and Döring, p. 27, Table 5. At $T=287°\text{K}$, iron still obeys the $T^{\frac{1}{2}}$ law while nickel already shows some deviations. Under these circumstances one must take for $[(M_0-M(T,0))/M_0]_{\text{Ni}}$ in Eq. (31), not the experimentally observed value, 0.054, but the value obtained by extrapolation of the $T^{\frac{1}{2}}$ law, the constant $2SJ$ in it being determined from low temperatures. The resulting value for $[(M_0-M(T,0))/M_0]_{\text{Ni}}$ is 0.040. See the experimental work of Weiss and Forrer, and Fallot as quoted, e.g. in R. H. Fowler *Statistical Mechanics* (Cambridge University Press, 1936), p. 500.

[19] Cf. Reference 4. q is the internal field constant and z the number of nearest neighbors.

[20] Equation (39) and numerical values (40), (41), represent the maximum estimates which may be obtained for $\partial M/\partial H$ from the Weiss-Heisenberg phenomenological theory. Other estimates obtained by: (1) Use of theoretical value for $(M_0-M(T,0))/M_0$, i.e., $2e^{-zJ/kT}$. (2) Use of Langevin function appropriate to $S>\frac{1}{2}$, e.g. to $S=\infty$ —classical Weiss theory, give consistently smaller results.

[21] P. Weiss and R. Forrer, Ann. de physique **10**, 153 (1926); **12**, 279 (1929). E. Czerlinsky, Ann. d. Physik **13**, 89 (1932). A. R. Kaufmann, Phys. Rev. **55**, 1142, 1939 and private communication. H. Polley, Ann. d. Physik **36**, 625 (1939).

[22] A. R. Kaufmann, Phys. Rev. **51**, 1089 (1939).

[23] The theory of the term B/H^3 and of the constant B has been given by Akulov, reference 3; the experimental verification by Kaufmann, Czerlinsky, and Polley, reference 21. See also, Becker and Döring, reference 3, pp. 167–176.

observed to be independent of the metallurgical treatment.[22]

The independence of C from metallurgical treatment immediately suggests that it arises from the variation of the intrinsic domain magnetization with field. C is thus to be compared with expression (31) for $\partial M/\partial H$ derived in this paper, and with the expression (39) for $\partial M/\partial H$ derived by Akulov.

(*a*) *Field dependence of* $C=\partial M/\partial H]_{\text{intrinsic}}$.—Unfortunately, all the experiments[21] except those of Weiss and Forrer have been carried out in such a range of fields that, for most of the range, the A/H^2 and B/H^3 terms both predominate over C. A typical example is the work of Polley,[21] where the range of fields in which C is $\geqq A/H^2+B/H^3$ is from 3000–4000 gauss (cf. p. 641 of Polley's paper: Fig. 10). Under these conditions a weak dependence of C on H such as $H^{-\frac{1}{2}}$ could never be observed. All that can be obtained from these experiments, therefore, is the average numerical value of C over a field range of about 2000–5000 gauss.

The only experiments for which the determination of the field dependence of C is possible are those of Weiss and Forrer.[21] In these experiments the magnetization as a function of H was determined in a range of fields up to 20,000 gauss. From 5000 to 20,000 gauss C is the only term of importance; it was found to be independent of H. However, the slope of Weiss' M *vs.* H curves, i.e., C, is so small in absolute magnitude that it is difficult to decide whether this slope is actually a constant independent of H. In this connection, it should also be pointed out that Weiss' results have been criticized by other authors—particularly Czerlinsky;[21] *viz.*, Weiss measured directly M as a function of H, with the result that small errors in the measurement of M were capable of seriously affecting the determination of $\Delta M/\Delta H$; on the other hand, all the other experimenters measured $\Delta M/\Delta H$ directly. The relative inaccuracy of Weiss' procedure is indicated by the scattering of his observed values of C, i.e., from 0.72×10^{-4} to 1.2×10^{-4}.

(*b*) *Magnitude of* C.—The most consistent values of C for Ni have been obtained by Polley.[21] For $T=287°\text{K}$ and $H=4000$ gauss, Polley finds C to be 1.3×10^{-4}, which is in excellent agreement with Eq. (38) of this paper, but which is ten times larger than the value of C derived by Akulov [cf. Eq. (41)]. Other values of C have been obtained by Kaufmann;[21] these are $C=1.0\times10^{-4}$ and $C=0.7\times10^{-4}$.

For iron there are available the results of Kaufmann[21] and Czerlinsky;[21] Kaufmann obtained $C=3.8\times10^{-4}$ and 4.8×10^{-4}, while Czerlinsky found $C=4.4\times10^{-4}$. The average of these results[24] is about two and a half times the theoretical value found in this paper [cf. Eq. (37)] and more than twenty-five times Akulov's theoretical value [cf. Eq. (40)].

(*c*) *Temperature dependence of* C.—The expression (30) for $\partial M/\partial H$ predicts a linear variation of C with temperature. This is experimentally verified by Polley[21] in the temperature range 250°K–320°K.[25]

(3) Further possible experiments

A great complication in the experiments so far performed arises from the presence of the terms A/H^2 and B/H^3, which are due to the polycrystalline nature of the specimen. It would therefore be desirable to obtain experimental data with single crystals and with H in the direction of the various axes of symmetry in the crystal. These directions may be either the directions of "easy" or of "difficult" magnetization. In the first case, technical saturation is achieved for $H\geqq50$ gauss;[26] in the second case, technical saturation is achieved for $H\geqq3H_a\leqq600$ gauss (Fe), 300 gauss (Ni).[27] Any further observed variation of M with H, beyond its technical saturation value, is then to be ascribed to changes in the intrinsic magnetization. Thus, using single crystals, one may obtain, directly from the $\partial M/\partial H$ *vs.* H curves, the various features of theoretical interest.

(*a*) *Functional dependence of* $\partial M/\partial H$ on H, *with* $H\gg4\pi M_0$: Test of the $H^{-\frac{1}{2}}$ dependence.[28]

[24] Dr. Kaufmann, in a private communication, has stated that there exists a large experimental error (*ca.* 100 percent) in his determination of C.

[25] At higher temperatures, deviations from the linear variation of $\partial M/\partial H$ with T are to be expected, and have been found by Polley, reference 21. These deviations correspond to departures from the $T^{\frac{1}{2}}$ law in the same temperature range.

[26] See Becker and Döring, reference 3, p. 102, Fig. 61; p. 118, Fig. 71.

[27] Becker and Döring, reference 3, p. 102, Fig. 61; p. 118, Fig. 71; p. 124, Fig. 77.

[28] To determine experimentally the variation of $\partial M/\partial H$ with H, for $H\gg4\pi M_0$, one may also use polycrystalline specimens, since for such high fields the terms B/H^3 and A/H^2 are negligible.

(*b*) *Variation of* $\partial M/\partial H$ *with* H for $3H_a<H\leqq 4\pi M_0$: Test of effect of magnetic interaction in Eq. (31).

(*c*) *Effect of spin-orbit interactions:* With H parallel to the direction of "easy" magnetization, an investigation of the variation of $\partial M/\partial H$ with H, for $50<H<3H_a$, may be undertaken. There are then three possibilities:

(1) The spin-orbit effects are entirely described by the equivalent "dipole-dipole" interaction (33). In this case, the $\partial M/\partial H$ *vs.* H curves in this field range should be described by Eq. (31).

(2) An appreciable part of the spin-orbit effects is due to the equivalent "quadrupole-quadrupole" interaction (34). The $\partial M/\partial H$ *vs.* H curves in this field range should now be given by Eq. (31), with H replaced by $H+H_a$.

(3) An appreciable part of the spin-orbit effects cannot be described by equivalent interactions of the type (33), (34). The $\partial M/\partial H$ *vs.* H curves in this field range may then show a more radical departure from Eq. (31).

(4) Inadequacy of other possible mechanisms to account for the observed variation of the intrinsic magnetization with field

These mechanisms are:

(*a*) Ion-core diamagnetism of the atoms: resulting volume susceptibility, $\partial M/\partial H$ is $\leqq 10^{-6}$, and is negligible.

(*b*) Spin paramagnetism and orbital diamagnetism of the conduction electrons: resulting volume susceptibility $\partial M/\partial H$, is $\leqq 10^{-6}$, and is negligible.[29]

(*c*) Paramagnetism arising from the orbital motions of the electrons in the incomplete *d* shells. (The exchange coupling of the spins of these electrons gives rise to the ferromagnetism.) Precise estimates of the order of magnitude of this paramagnetism are difficult since little is known about the orbital states. Assuming that the orbital moment, **L**, of the incomplete *d* shell is what it would be in the vapor state, and that the various orbital magnetic moments do not at all influence each other, one obtains, with the usual Curie law:

$$\partial M/\partial H=(N/V)(\beta^2L(L+1)/3kT),$$

the following paramagnetic volume susceptibilities: 3×10^{-4} for iron; 7×10^{-4} for nickel. The gyromagnetic experiments, on the other hand, indicate that:

Either the orbital angular momentum of each incomplete *d* shell is destroyed or quenched by the crystalline electric field,[30a] in which case the corresponding susceptibility vanishes in first order;

Or, the orbital angular momentum vectors of the different atoms are "antiferromagnetically coupled."[30b] Then an estimate of the susceptibility may be obtained by replacing kT in the Curie law above by $kT+kT_c$, where kT_c, the interaction energy of the antiferromagnetic coupling, is $\leqq 1\frac{1}{4}$ ev.[31] The resulting paramagnetic volume susceptibility is thus cut down by a factor of fifty, and becomes negligibly small.

In conclusion, it should also be noted that the smallness of any paramagnetic susceptibility, described by the Curie-Weiss law, is directly shown by the experimentally observed temperature variation of the intrinsic magnetization; *viz.*, $C=\partial M/\partial H]_{\text{intrinsic}}=\text{const.}\ T$ (see Section VI).

The authors wish to thank Dr. A. R. Kaufmann of the Massachusetts Institute of Technology for helpful discussions of the experiments, and for communication of experimental data before publication.

Appendix I

The various approximations made at the beginning of the treatment are of the following type:

I. Neglect of $a^*_l(1-a^*_la_l/2S)^{\frac{1}{2}}-a^*_l$ in comparison with a^*_l.

II. Neglect of $a^*_la_la^*_ma_m/2S\equiv\mathfrak{n}_l\mathfrak{n}_m/2S$ in comparison with $a^*_la_l\equiv\mathfrak{n}_l$.

III. Neglect of $a^*_ma_ma^*_l\equiv\mathfrak{n}_ma^*_l$ in comparison with $a^*_la^*_m$.

[29] In making this estimate, it is assumed that the conduction electrons are perfectly free. This assumption is reasonable since the conduction electrons are valence electrons arising from the 4*s* atomic shells. The strong paramagnetism, with volume susceptibility $\leqq 5\times10^{-5}$, arising from electrons in the incomplete inner shells of some of the nonferromagnetic transition elements, e.g. Pd, plays no role in ferromagnetic elements, since the incomplete inner shells in this case, are responsible for the ferromagnetism itself.

[30a] Van Vleck, reference 4, Ch. 11.
[30b] Van Vleck, reference 11, p. 1182.
[31] Van Vleck, reference 11, p. 1184.

The neglected terms are important whenever two or more spin deviations are in close proximity, since all the neglected terms in I, II, III are multiplied by short range functions of R_{lm} i.e. $J_{lm}(R_{lm})$ or $R^{-3}{}_{lm}$. When spin deviations are to be found on atoms close to each other, the following situations may arise:

(A) The system makes transitions from states with $n_l \geqq 1$ to states with n_l+1. Cf. I, i.e.,

$$[a^*{}_l(1-a^*{}_l a_l/2S)^{\frac{1}{2}}-a^*{}_l]\Psi_{n_l} = (n_l+1)^{\frac{1}{2}}((1-n_l/2S)^{\frac{1}{2}}-1)\Psi_{n_l+1}=0,$$

unless $n_l \geqq 1$.

(B) The system occupies states with $n_l>0$, $n_m>0$. Cf. II, i.e.,

$$\frac{\mathfrak{n}_l\mathfrak{n}_m}{2S}\Psi_{n_l n_m}=\frac{n_l n_m}{2S}\Psi_{n_l n_m}.$$

(C) The system makes transitions from states with $n_m>0$, n_l to states with n_m, n_l+1. Cf. III, i.e.,

$$\mathfrak{n}_m a^*{}_l \Psi_{n_l n_m}=n_m(n_l+1)^{\frac{1}{2}}\Psi_{n_l+1,\,n_m}.$$

It is thus seen that I, II, III, imply that any atom having a spin deviation can always be regarded as surrounded by atoms with no spin deviations, i.e., the spin deviations are regarded as isolated independent units with no interactions.

Now, spin deviations may come into close proximity and give rise to (A), (B), and (C), as a result of two mechanisms, The first of these is temperature agitation, the second, the action of terms in the magnetic interaction of the form $R^{-3}{}_{lm}a^*{}_l a_m$ in creating two spin deviations close to each other.

In view of the lack of knowledge of the wave functions of the exact Hamiltonian (6) or (1), the approximate Hamiltonian (7) (which is the exact Hamiltonian (6) or (1), subject to approximation I, II, III) will be used to estimate the relative importance of the cases of close proximity of spin deviations.

(1) *Temperature agitation.*—The structure of the Hamiltonian (7), (without the part of the magnetic interaction proportional to $a^*{}_l a^*{}_m$ and $a_l a_m$) or better the Hamiltonian (11), (without the terms in B_λ and $B^*{}_\lambda$) obtained from (7) by the Fourier transformation (8), indicates that the position of each spin deviation is spatially uncorrellated with the position of any of the other spin deviations. Thus cases of close proximity of spin deviations due to temperature agitation are relatively infrequent in the condition of quasi-saturation.

To verify this lack of spatial correlation, one observes that

$$\langle\langle \mathfrak{n}_l\mathfrak{n}_m\rangle\rangle_{Av}\equiv\langle\langle a^*{}_l a_l a^*{}_m a_m\rangle\rangle_{Av}$$
$$=N^{-2}\sum_{\mu,\nu,\lambda,\rho}\exp\{i[(\mathbf{K}_\nu-\mathbf{K}_\mu)\cdot\mathbf{R}_l+(\mathbf{K}_\rho-\mathbf{K}_\lambda)\cdot\mathbf{R}_m]\}\langle\langle a^*{}_\mu a_\nu a^*{}_\lambda a_\rho\rangle\rangle_{Av}$$
$$=N^{-2}\textstyle\sum_{\mu,\lambda}\langle\langle \mathfrak{n}_\mu\mathfrak{n}_\lambda\rangle\rangle_{Av}+N^{-2}\sum_{\mu,\lambda}\exp\{i(\mathbf{K}_\mu-\mathbf{K}_\lambda)\cdot\mathbf{R}_\lambda\}\langle\langle \mathfrak{n}_\mu(\mathfrak{n}_\lambda+1)\rangle\rangle_{Av}(1-\delta_{\mu\lambda}).$$

The form of the partition function Z in Eq. (22) (with $B_\lambda=0$, and hence $N_\lambda=n_\lambda$), which is involved in averaging the $\mathfrak{n}_\lambda$ gives:

$$\langle\langle \mathfrak{n}_\mu\mathfrak{n}_\lambda\rangle\rangle_{Av}=\langle\langle \mathfrak{n}_\mu\rangle\rangle_{Av}\langle\langle \mathfrak{n}_\lambda\rangle\rangle_{Av}(1-\delta_{\mu\lambda})+(\langle\langle \mathfrak{n}_\mu\rangle\rangle_{Av}+2\langle\langle \mathfrak{n}_\mu\rangle\rangle_{Av}{}^2)\delta_{\mu\lambda}.$$

Hence,

$$\langle\langle \mathfrak{n}_l\mathfrak{n}_m\rangle\rangle_{Av}=N^{-2}\textstyle\sum_{\mu,\lambda}\langle\langle \mathfrak{n}_\mu\rangle\rangle_{Av}\langle\langle \mathfrak{n}_\lambda\rangle\rangle_{Av}+N^{-2}\sum_{\mu,\lambda}\exp\{i(\mathbf{K}_\mu-\mathbf{K}_\lambda)\cdot\mathbf{R}_\lambda\}\langle\langle \mathfrak{n}_\mu\rangle\rangle_{Av}\langle\langle \mathfrak{n}_\lambda\rangle\rangle_{Av}.$$

Also

$$S[M_0-M(T,0)]/M_0=\langle\langle n_l\rangle\rangle_{Av}=N^{-1}\textstyle\sum_m\langle\langle \mathfrak{n}_m\rangle\rangle_{Av}=N^{-1}\sum_\mu\langle\langle \mathfrak{n}_\mu\rangle\rangle_{Av}.$$

Thus $\langle\langle \mathfrak{n}_l\mathfrak{n}_m\rangle\rangle_{Av}$ and $\langle\langle \mathfrak{n}_l\rangle\rangle_{Av}\langle\langle \mathfrak{n}_m\rangle\rangle_{Av}$ are both of the same order of magnitude, and hence, there are no spatial correlations among the spin deviations. It follows that the probability for a spin deviation to be found on atom l when another spin deviation is known to be on atom m, is independent of the distance between atoms l and m, and is $\leqq\langle\langle \mathfrak{n}_l\mathfrak{n}_m\rangle\rangle_{Av}/\langle\langle \mathfrak{n}_m\rangle\rangle_{Av}\leqq\langle\langle \mathfrak{n}_l\rangle\rangle_{Av}\leqq S[M_0-M(T,0)]/M_0\ll 1$ in the condition of quasi-saturation.

(2) *Magnetic interactions proportional to* $a^*_l a^*_m$. —The effect of these magnetic interactions is contained in the terms, $\sum_\lambda \frac{1}{2}B^*_\lambda a^*_\lambda a^*_{-\lambda}$, of the Hamiltonian (11).

Now the B_λ which make the greatest contributions to $M(T,H)$ have $|\mathbf{K}_\lambda| \lesssim (4\pi\beta M_0/2SJ)^{\frac{1}{2}}$ [cf. text after Eq. (25)]. Also the main contributions to B_λ, (cf. (13)), come from summands for which $|\mathbf{R}_h|$, the relative separations of the spin deviations, is $\lesssim 1/K_\lambda$. Thus the effective spatial separation of the spin deviations created by the magnetic interaction is $\lesssim (2SJ/4\pi\beta M_0)^{\frac{1}{2}}$ lattice spacings $\lesssim 30$ lattice spacings. However the average spatial separation of the spin deviations created by the temperature agitation is $\lesssim (M_0/[M_0 - M(T,0)])^{\frac{1}{2}}$ lattice spacings $\lesssim 4$ lattice spacings. Thus from the point of view of causing cases of close proximity of spin deviations, the magnetic interaction is much less important than the temperature agitation.[32]

It should be emphasized that the above estimates as to the effective separation of the spin deviations created both by temperature agitation and by the magnetic interaction is given on the basis of the approximate Hamiltonian (7). The final justification of the validity of these estimates awaits a better knowledge of the wave functions of the exact Hamiltonian (6) or (1) than exists at present.

Appendix II

The sums for A_λ and B_λ in (12) and (13) will now be evaluated. The contribution to the first sum in A_λ, arising from near neighbors of a given atom vanishes because of the cubical symmetry of the specimen. A small sphere may now be drawn enclosing all these near neighbors, and the contributions to the sum for atoms lying outside of this sphere replaced by contributions to the corresponding integral, in accordance with the prescription:

$$a^{-3}\sum_h 2\beta S f(\mathbf{R}_h) \rightarrow M_0 \int f(\mathbf{R})\, d\mathbf{R}. \qquad (43)$$

Thus,

$$\sum_h (-2\beta S/a^3 R^3_h)(1-3z^2_h/R^2_h) \rightarrow (-M_0)\int [(1-3z^2/R^2)/R^3]\, d\mathbf{R}, \qquad (44)$$

where the integral is extended over all of the space outside the small sphere and inside the outer boundary of the specimen. Now by the divergence theorem,

$$(-M_0)\int [(1-3z^2/R^2)/R^3]\, d\mathbf{R} = (-\mathbf{M}_0)\cdot \int (\mathbf{n}z/R^3)\, d\Sigma + (-\mathbf{M}_0)\cdot \int (\mathbf{n}z/R^3)\, d\Sigma, \qquad (45)$$

where, on the right-hand side, the first integral is extended over the surface of the small sphere, and the second integral over the outer boundary of the specimen, $\mathbf{n}$ being the outer normal to the surfaces. The integral over the surface of the small sphere gives $4\pi M_0/3$ and is thus just the Lorentz local field. The second integral depends on the shape of the outer boundary of the specimen and is just the demagnetizing field. One takes the specimen to be an ellipsoid whose major axis is the z axis, and which is so elongated that the demagnetizing field may be neglected. Then,

$$3\beta \sum_h (-2\beta S/a^3 R^3_h)(1-3z^2_h/R^2_h) = 4\pi\beta M_0. \qquad (46)$$

The second sum in A_λ may be replaced by an integral at once, since this sum has no singularity at $\mathbf{R}_h = 0$. Thus:

[32] The portion of the equivalent dipole-dipole interaction of the form $C(R_{lm})a^*_l a^*_m$ (cf. Section V) creates spin deviations on atoms which are nearest neighbors, since C is short range. Nevertheless, the *effective* spatial separation of the spin deviations created by the *sum* of the magnetic and equivalent dipole-dipole interactions, *viz.* by terms of the type, $\sum_\lambda \frac{1}{2}(B^*_\lambda + \Delta B^*_\lambda)a^*_\lambda a^*_{-\lambda}$, is not appreciably different from 30 lattice spacings, since for $|\mathbf{K}| \lesssim (4\pi\beta M_0/2SJ)^{\frac{1}{2}}$, the values of $|\mathbf{K}_\lambda|$ where $B_\lambda + \Delta B_\lambda$ as well as B_λ makes its most important contribution to $M(T,H)$, one has $\Delta B_\lambda \lesssim SCK_\lambda^2 \lesssim (4\pi\beta M_0)(C/J) \ll 4\pi\beta M_0$. Thus, the contribution of ΔB_λ to the term $B_\lambda + \Delta B_\lambda$ is so small that the *effective* spatial separation of the spin deviations remains essentially unaltered.

$$\beta \sum_\lambda (2\beta S/a^3R^3_\lambda)(1-3z^2_\lambda/R^2_\lambda)(1-\exp(i\mathbf{K}_\lambda\cdot\mathbf{R}_\lambda))$$

$$\rightarrow \beta M_0 \int ((1-3z^2/R^2)/R^3)(1-\exp(i\mathbf{K}_\lambda\cdot\mathbf{R}))d\mathbf{R} = i\beta M_0 \mathrm{K}^{(z)}_\lambda \int (z/R^3)(\exp(i\mathbf{K}_\lambda\cdot\mathbf{R}))d\mathbf{R} \quad (47)$$

by an integration by parts.

The last integral is just equal to $4\pi i \mathrm{K}^{(z)}_\lambda/\mathrm{K}^2_\lambda$; (12), (46), (47) then yield:

$$A_\lambda = A_{-\lambda} = 4\pi\beta M_0 \sin^2\theta_\lambda + \sum_\lambda 2SJ_\lambda(R_\lambda)(1-\exp(i\mathbf{K}_\lambda\cdot\mathbf{R}_\lambda)) + 2\beta H. \quad (48)$$

To evaluate B_λ one proceeds similarly. Considering the first sum in B_λ, one draws a small sphere about $\mathbf{R}_\lambda = 0$, enclosing all the near neighbors. The contributions to the sum from atoms within the sphere is again zero because of cubical symmetry, while the contributions from atoms outside the small sphere are calculated by replacing the sum with the corresponding volume integral. Thus,

$$-3\beta \sum_\lambda (2\beta S/a^3R^3_\lambda)(x^2_\lambda - y^2_\lambda - 2ix_\lambda y_\lambda)/R^2_\lambda \rightarrow -3\beta M_0 \int [(x^2-y^2-2ixy)/R^5]d\mathbf{R}$$

$$= 3\beta M_0 \int [(\mathbf{a}_x - i\mathbf{a}_y)\cdot\mathbf{n}(x-iy)R^{-3}]d\Sigma + 3\beta M_0 \int [(\mathbf{a}_x - i\mathbf{a}_y)\cdot\mathbf{n}(x-iy)R^{-3}]d\Sigma, \quad (49)$$

where the first surface integral is extended over the boundary of the small sphere, the second over the outer boundary of the specimen, and $\mathbf{a}_x$, $\mathbf{a}_y$ are unit vectors in the x and y directions. Also the integral over the small sphere's surface vanishes by symmetry.

The second sum in B_λ, just like the second sum in A_λ may be replaced at once by an integral, which when integrated by parts gives:

$$-3\beta M_0 \int [(\mathbf{a}_x - i\mathbf{a}_y)\cdot\mathbf{n}(x-iy)R^{-3}]d\Sigma + 4\pi\beta M_0(\mathrm{K}^{(x)}_\lambda - i\mathrm{K}^{(y)}_\lambda)^2/\mathrm{K}^2_\lambda, \quad (50)$$

where the surface integral is extended over the outer boundary of the specimen. Thus from (13), (49), (50)

$$B_\lambda = B_{-\lambda} = 4\pi\beta M_0(\mathrm{K}^{(x)}_\lambda - i\mathrm{K}^{(y)}_\lambda)^2/\mathrm{K}^2_\lambda = 4\pi\beta M_0 \sin^2\theta_\lambda e^{-2i\phi_\lambda}. \quad (51)$$

It should finally be stated that the replacement of sums by integrals in A_λ, B_λ is an approximation with an error $\leqq(\mathrm{K}_\lambda)^2$. This introduces an error into $M(T,H) \leqq 4\pi\beta M_0/2SJ \ll 1$, since the greatest contributions to $M(T,H)$ from the magnetic interactions, both in A_λ and B_λ come from regions of $\mathbf{K}_\lambda$-space, where $|\mathbf{K}_\lambda| \leqq (4\pi\beta M_0/2SJ)^{\frac{1}{2}} \ll 1$. [Cf. text after Eq. (25).]

The difference between the sums and integrals becomes much more important for problems of other types: e.g., *can ferromagnetism arise from pure magnetic dipole-dipole interactions?*[33]

In this case $J=0$, and the use of (48), (51),

$$A_\lambda = 4\pi\beta M_0 \sin^2\theta_\lambda + 2\beta H;$$

$$B_\lambda = 4\pi M_0 \sin^2\theta_\lambda e^{-2i\phi_\lambda},$$

leads to a negative answer to the proposed question. It is to be expected, however, that the exact expressions for A_λ and B_λ determined by evaluation of the original sums (12), (13), will not be given by (48), (51), hence the existence of ferromagnetism arising from magnetic dipole-dipole interactions cannot be determined from the knowledge of A_λ and B_λ available at this time. The evaluation of the sums for A_λ and B_λ is being considered at present.

[33] This problem has been discussed by J. H. Van Vleck, J. Chem. Phys. 5, 320 (1937), Section 5; J. A. Sauer, Phys. Rev. 57, 142 (1940).

On the Satellite Lines in Atomic Spectra and the Excitation of Electrons from Closed Shells

TA-YOU WU
Department of Physics, National University of Peking, Kun-ming, China
(Received October 28, 1940)

RECENTLY Edlén and Tyrén have reported the observation of groups of weak lines on the long wave-length sides of the lines $1s^2\,{}^1S-1snp\,{}^1P$, $1s\,{}^2S-2p\,{}^2P$ in the spectra C V and C VI, respectively.[1] These "satellite" lines they ascribed to transitions in the preceding spectra with an additional external electron whose effect of screening on the energy of the transition giving rise to the main line is small. Thus the transition $1s^2\,{}^1S-1s2p\,{}^1P$ may have as satellites $1s^22s\,{}^2S-1s2s2p\,{}^2P$, ${}^2P$, $1s^22p\,{}^2P-1s2p^2\,{}^2P$, ${}^2D$, ${}^2S$, $1s^23s\,{}^2S-1s2p3s\,{}^2P$, ${}^2P$, etc. Dr. Edlén kindly sent to the writer a microphotometer tracing of the group of lines at 40.27A of C V $1s^2\,{}^1S-1s2p\,{}^1P$, together with their wave-lengths. The purpose of this note is to discuss these lines in greater detail.

With a view to examining the above explanation of the satellite lines, the writer has undertaken some calculations of the energy states involved in these transitions by the variational method of wave mechanics. The radial parts of the single electron wave functions employed for the $1s$, $2s$, $2p$ electrons are $\psi_{1s}=(4\alpha^3)^{\frac{1}{2}}e^{-\alpha r}$, $\psi_{2s}=(12\beta^5/\alpha^2-\alpha\beta+\beta^2)^{\frac{1}{2}}\cdot[1-\frac{1}{3}(\alpha+\beta)r]e^{-\beta r}$, $\psi_{2p}=(4\gamma^5/3)^{\frac{1}{2}}re^{-\gamma r}$, where α, β, γ are parameters to be determined by the variational process. The energy states calculated include the following: $2s2p\,{}^1P, {}^3P$; $2p^2\,{}^3P, {}^1D, {}^1S$; $1s2s^2\,{}^2S$; $1s2s2p\,{}^4P, {}^2P, {}^2P$; $1s2p^2\,{}^4P, {}^2P, {}^2D, {}^2S$; $2s^22p\,{}^2P$; $2s2p^2\,{}^4P, {}^2P, {}^2D, {}^2S$; $2p^3\,{}^4S, {}^2D, {}^2P$ in the 2 and 3 electron spectra of the atoms from Li to F. The accuracy of the calculated energies increases with the atomic number Z, and for carbon the error varies from $\frac{1}{2}$ to $\frac{1}{10}$ of a percent for the different configurations. The accuracy of the calculated positions of the various expected transitions is, however, somewhat better since the calculated energies always lie above the true values and in forming their differences the errors are partially compensated. Table I gives a comparison between the observed satellite lines and their tentative identifications based on the calculated energies. There are 5 very weak lines between 40.35 and 40.47A. They can be ascribed to such transitions as $1s^23s\,{}^2S-1s2p3s\,{}^2P$, $1s^23p\,{}^2P-1s2p3p\,{}^2P$, etc., which can be expected to lie closer to the main line since the interactions between a $3s$, $3p$, $3d$, etc., electron and the $1s$, $2p$ electrons are smaller.

Concerning the relative intensities of the main $1s^2\,{}^1S-1s2p\,{}^1P$ line and the transitions shown in Table I, one must consider the following factors: (1) the relative probabilities for the production of the initial states involved in these transitions, and (2) the relative values of the transition probabilities. In carbon, one needs for (1) to know the cross sections of the ionization and excitation processes $1s^22s^22p^2\rightarrow 1s2p$ and $1s^22s^22p^2\rightarrow 1s2s2p\,{}^2P$ by electron impact. Such calculations will be exceedingly lengthy on account of the large number of electrons ejected; and to obtain an estimate of their relative probabilities, the writer has made the calculations for Li, namely, for the process of simultaneous ionization and the excitation of an electron from a closed shell $1s^22s\,{}^2S\rightarrow 1s2p\,{}^1P$, and the process of excitation from a closed shell $1s^22s\,{}^2S\rightarrow 1s2s2p\,{}^2P$, ${}^2P$. The cross sections are obtained as functions of the energy of the colliding electron by using Born's approximation in which the ejected electron is represented by a plane wave. That this is justified is seen from the good agreement between the cross section for the ionization of helium calculated by this method and that calculated by a better approximation for the wave function of

TABLE I. *Suggested transitions and calculated wave-lengths for the satellite lines observed by Edlén on the long wave-length side* $1s^2\,{}^1S-1s2p\,{}^1P$.

OBS. λ (EDLÉN)		TRANSITION	CALC. λ
40.27A	very strong		
40.73	weak	$1s^22s\,{}^2S - 1s2s2p\,{}^2P$	40.7A
		$1s^22p\,{}^2P - 1s2p^2\,{}^2S$	40.7
41.33	weak	$1s^22p\,{}^2P - 1s2p^2\,{}^2D$	41.3
41.36	very weak	$1s^22p\,{}^2P - 1s2p^2\,{}^2P$	41.4
41.54	weak	$1s^22s\,{}^2S - 1s2s2p\,{}^2P$	41.5

[1] B. Edlén and F. Tyrén, Nature **143**, 940 (1939).

TABLE II. *Total cross sections for* Li *in* cm^2.

ELECTRON ENERGY (EV) →	5	10	30	50	70	100	200	400	800	
$1s^22s\ ^2S \rightarrow 1s^22p\ ^2P$	10.2	7.1	3.2	2.2	1.7	1.2	0.5	0.28	0.14	$\times 10^{-18}$
$1s^22s\ ^2S \rightarrow 1s^23p\ ^2P$	2.3	1.6	0.5	0.3						$\times 10^{-18}$
$1s^22s\ ^2S \rightarrow 1s^23d\ ^2D$	5.8	4.5	1.8	1.1						$\times 10^{-17}$
$1s^22s\ ^2S \rightarrow 1s2p\ ^1P$	—	—	—	—		3.1	3.8	3.1	2.5	$\times 10^{-17}$
$1s^22s\ ^2S \rightarrow 1s2s2p\ ^2P$	—	—	—	—	2.4	4.0	4.0	2.9	1.9	$\times 10^{-18}$
$1s^22s\ ^2S \rightarrow 1s2s2p\ ^2P$	—	—	—	—	1.9	3.1	3.1	2.3	1.5	$\times 10^{-18}$

the ejected electron.[2] Table II gives these cross sections together with those for the excitation of the valence electron for comparison.[3] An interesting result is that the cross section for the simultaneous ionization and excitation is roughly 10 times greater than that for excitation alone, for electron energy of about 400 volts. The ratio increases slowly with increasing energy of the electron.

The ratio of the transition probabilities of $1s^2\ ^1S-1s2p\ ^1P$ and $1s^22s\ ^2S-1s2s2p\ ^2P$ can be readily calculated with the variational wave functions for these states to be approximately 2.0. Thus in Li one would expect the ratio of the intensities of these two lines to be about 20 and 30 (for transitions from the $2\ ^2P$ states of $1s2s2p$) for excitation by electrons of a few hundred volts. These values would certainly be different for carbon; but their order of magnitude would perhaps be about the same.

[2] Compare W. W. Wetzel, Phys. Rev. **44**, 25 (1933) and N. E. Mott and H. S. W. Massey, *Theory of Atomic Collisions* (Oxford University Press, 1934), p. 180.

[3] The relative probabilities for the excitation of the valence electron and for the excitation of an electron in an inner closed shell are important in connection with the experiments of Lee and Whiddington, Proc. Roy. Soc. **A173**, 569 (1939) in which are observed energy losses of electrons during inelastic collisions with Zn, Cd and Hg atoms, which correspond to the excitation of a *d* electron in the closed shell, on comparison with the results of H. Beutler on their absorption spectra.

In his private communication, Dr. Edlén tentatively assigned the 40.73A line to the forbidden transition $1s^2\ ^1S_0-1s2p\ ^3P_1$. Now the intensity of this transition in C V can be readily calculated with the variational wave functions already obtained. The integral of the spin-orbit interaction

$$\xi=\frac{R\alpha^2}{4}\int \psi_{2p}^*\frac{1}{r}\frac{dV}{dr}\psi_{2p}d\tau,$$

where α is the fine structure constant, R the Rydberg constant, and

$$V=-\frac{2Z}{r}+\frac{2}{r}\int_0^r|\psi_{1s}|^2r^2dr+2\int_r^\infty|\psi_{1s}|^2rdr,$$

is found to be 120 cm^{-1}, and the ratio of the f values for the allowed $1s^2\ ^1S_0-1s2p\ ^1P_1$ and the forbidden $1s^2\ ^1S_0-1s2p\ ^3P_1$ transitions comes out to be of the order 10^5.[4] While it is not possible to determine the relative intensities of the 40.27A and 40.73A lines from his microphotometer tracing because the former was greatly overexposed, it is certain that the 40.73A line is more intense than the other satellite lines and is hence too intense to be the singlet-triplet transition, although its position agrees with the theoretically calculated value. For this reason, the suggested assignment in Table I is given.

Details concerning the variational wave functions and energies and the quantum-mechanical cross sections of these and other processes will be given in a forthcoming paper in the *Chinese Journal of Physics*.

[4] G. W. King and J. H. Van Vleck, Phys. Rev. **56**, 464 (1939). For C V, it is immaterial whether the same or different $2p$ wave functions are employed for $1s2p\ ^1P$ and $1s2p\ ^3P$, since the spin-orbit interaction is very small, of the order of 1/100, compared with the singlet-triplet separation.

LETTERS TO THE EDITOR

Prompt publication of brief reports of important discoveries in physics may be secured by addressing them to this department. Closing dates for this department are, for the first issue of the month, the eighteenth of the preceding month, for the second issue, the third of the month. Because of the late closing dates for the section no proof can be shown to authors. The Board of Editors does not hold itself responsible for the opinions expressed by the correspondents.

Communications should not in general exceed 600 words in length.

The Modified Reflections of Cu $K\alpha$ X-Rays from Rocksalt

We had obtained a few photographs of modified reflections of Cu $K\alpha$ x-rays from rocksalt in this laboratory when we received a reprint from Raman and Nilakantan[1] describing experiments on the modified reflections of Mo $K\alpha$ and Mo $K\beta$ rays from rocksalt. In their experiments, as in ours an, intense spectrum line radiation against a weak background of continuous radiation was used. Raman and Nilakantan sent a narrow beam of primary rays through a thin crystal plate as in the usual Laue arrangement while we allowed a narrow primary beam to fall on the front face of a thick crystal as in the usual Bragg arrangement. In both their and our experiments a crystal plane (the 100 cleavage face in our experiments) was set for a given photograph at a given value of the glancing angle of incidence i. Photographs were then taken for a series of values of i.

As i is varied we find it convenient to recognize two different types of spots on the photographs—the Bragg or B spots produced by the spectrum line radiation and the Laue or L spots produced by the continuous radiation. A B spot lights up (some of them can be seen with a fluorescent screen) only for a certain value of i, whereas when i is changed by Δ the L spots in the equatorial plane move by an amount 2Δ. Different values of i are obtained by turning the crystal about a principal axis which is vertical. An L_{hkl} spot or a B_{hkl} spot is produced by reflection from the hkl planes.

We have restricted ourselves to a study of the spots in the equatorial plane. Consequently we can treat rocksalt as a simple cubic crystal with $a=2.814$A. We find that as an $L_{h'k'0}$ spot is made to approach the position of a B_{hk0} spot a modified spot appears if h', $k'=h$, k. We therefore associate the modified spot with B_{hk0} and we designate it by mB_{hk0}.

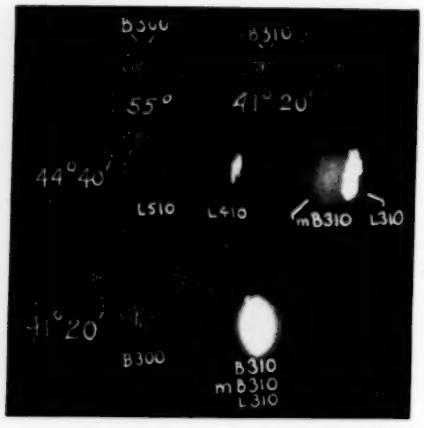

FIG. 1. Reflections of Cu $K\alpha$ x-rays at various angles from rocksalt.

Zachariasen[2] and independently Raman and Nath[3] have derived a theoretical formula

$$(\phi_{mB}-2\theta_B)=2(i-i_B)\sin^2\theta_B, \qquad (1)$$

where in our experiments ϕ_{mB} and $2\theta_B$ are the total scattering angles for mB_{hk0} and B_{hk0}, respectively, and where i_B is the glancing angle of incidence on the 100 crystal face which produces B_{hk0}. In (1) it is assumed that $(i-i_B)$ is small. Also Raman and Nath[3] have derived the theoretical formula

$$(\phi_{mB}-2\theta_B)=0 \qquad (2)$$

for all values of i.

Raman and Nilakantan[1] find that their experimental results for rocksalt conform to (2)—that mB_{hkl} continues in the position of B_{hkl} as L_{hkl} is moved away from this position. A sample of our experimental results is shown in Fig. 1. The top strip shows B_{300} and B_{310} produced by setting $i=55°$ and $i=41°20'$, respectively, and exposing the film for each setting of i for a few seconds. The B_{300} and B_{310} lines are double, showing separation of $K\alpha_1$ and $K\alpha_2$. The middle strip was obtained by setting $i=44°40'$ and exposing for 10 hours. The bottom strip was obtained for $i=41°20'$ and with an exposure of 10 hours. B_{300} was placed as a fiducial mark on the bottom strip by setting $i=55°$ and exposing for about 1 minute. We note the appearance of the blurred spot mB_{310} in the middle strip. The fiducial mark for this strip is outside the figure. The modified reflection mB_{310} does not occur at the position of B_{310} but between this position and L_{310}. Its position is not given by (2). In this result we differ from the conclusions of Raman and Nilakantan. We are not prepared to say whether or not the most intense part of mB_{310} is given by (1). We are continuing our investigation of this problem.

We wish to thank Sir C. V. Raman, Dr. Nilakantan, and Dr. Nath for the reprints they have sent us.

G. E. M. JAUNCEY
O. J. BALTZER

Wayman Crow Hall of Physics,
Washington University,
St. Louis, Missouri,
November 26, 1940.

[1] C. V. Raman and P. Nilakantan, Proc. Ind. Acad. Sci. 12A, 141 (1940).
[2] W. H. Zachariasen, Phys. Rev. 57, 597 (1940).
[3] C. V. Raman and N. S. G. Nath, Proc. Ind. Acad. Sci. 12A, 83 (1940).

The Possible Role of Neutrinos in Stellar Evolution

It can be considered at present as definitely established that the energy production in stars is caused by various types of thermonuclear reactions taking place in their interior. Since these reaction chains usually contain the processes of β-disintegration accompanied by the emission of high speed neutrinos, and since the neutrinos can pass almost without difficulty through the body of the star, we must assume that a certain part of the total energy produced escapes into interstellar space without being noticed as the actual thermal radiation of the star. Thus, for example, in the case of the carbon-nitrogen cycle in the sun, about 7 percent of the energy produced is lost in the form of neutrino radiation. However, since, in such reaction chains, the energy taken away by neutrinos represents a definite fraction of the total energy liberation, these losses are of but secondary importance for the problem of stellar equilibrium and evolution.

We want to indicate here that the situation becomes entirely different in cases where, as the result of the progressive contraction of the star, the density and temperature in its interior become sufficiently high to permit the penetration of free electrons into different nuclei resulting in the formation of unstable isobars with smaller atomic number.

The two processes which will take place under such conditions can be written schematically as:

$$(\text{Nucleus})^{s}+e\rightarrow(\text{Nucleus})^{s-1}+\text{neutrino},$$
$$(\text{Nucleus})^{s-1}\rightarrow(\text{Nucleus})^{s}+e+\text{neutrino}.$$

Since the neutrinos produced in both reactions cannot be held back by gaseous walls surrounding the central region of the star, no actual thermodynamic equilibrium is evidently possible, and the matter under these conditions will rapidly lose its extra heat content through the neutrino emission. Such a star can be considered as possessing in its interior a "negative energy source," the efficiency of which increases very rapidly with the temperature.

It is thus clear that when, in the process of progressive contraction, the star reaches the above-described state, the gas pressure in the interior will no longer be able to increase in order to support the weight of the outer layers, and the slow contraction will give place to a rapid collapse. Although the energy is actually lost in the central regions of such a collapsing star, a very large amount of heat will necessarily be produced in the rapidly contracting outer shells, and the thermal radiation from the surface of the star must increase enormously. This seems to give the possibility of applying the above-described process to the explanation of the vast stellar explosions of the supernova type.

More detailed calculations on this collapse process are now in progress.

G. Gamow

The George Washington University,
Washington, D. C.,

M. Schoenberg*

University of São Paulo,
São Paulo, Brazil,
November 23, 1940.

* Fellow of the Guggenheim Memorial Foundation. Now in Washington, D. C.

The Ground States of Be^{10} and C^{10}

Many properties of nuclei have been adequately interpreted through a model constructed of neutrons and protons interacting with each other with forces that are approximately the same between all pairs of particles. The only known forces which remove this symmetry, the Coulomb force and the interaction of magnetic moments, are believed to have a small effect in light nuclei. The question of the validity of this model is raised by the anomalous behavior of Be^{10}, which decays with a half-life $\sim 10^{6}$ years into stable B^{10} emitting 550-Kev β-particles.[1] In contrast to this activity C^{10}, which differs from Be^{10} only by the substitution of two protons for two neutrons, decays in 9 seconds also into B^{10} emitting 3.36-Mev positrons.[2] This difference in half-lives cannot be accounted for just by the difference in energy of the emitted particles so that the Be^{10} transition is classed as "forbidden," requiring a change of several units of angular momentum. Both transitions are presumably between ground states. Since the ground state of B^{10} is known, through measurement of its spin (1) and its magnetic moment (0.6 nuclear magneton),[3] to be a mixture of ^3S and $^3D_1$, it is to be expected from the observed lifetimes of Be^{10} and C^{10} and the Gamow-Teller selection rules that their ground states are ^1G and ^1S or ^1D, respectively. However, using the single particle model with a symmetric Hamiltonian,[4] one finds in both nuclei the same states having the same order and spacing with ^1S lowest separated from ^1G by 12 mc^2. From the theory of holes, the symmetry of Be^{10} and C^{10} about B^{10}, the center of the p shell, requires that the Coulomb energy does not in first order alter this level structure. We have estimated, by using closure, the contribution of the Coulomb energy in the second order where it, by interaction through excited configurations, disturbs this symmetry. The net result of the first- and second-order perturbations is to depress the ^1G state relative to ^1S state by 0.10 mc^2 in Be^{10} and by 0.07 mc^2 in C^{10}. This shift is in the right direction, but is very small compared to the calculated $^1S-{}^1G$ difference, 12 mc^2. Thus the Coulomb energy, which, on this model,[4] gives correctly the observed $Be^{10}-C^{10}$ ground state energy difference, would not lead us to expect *a priori* an inversion of levels in Be^{10}, and no inversion in C^{10}. In addition, it would seem that the interaction of magnetic moments (on account of the low velocities of nuclear particles and small nuclear moments) should introduce no significant shift. We are then led to the conclusion either that the level spacing given by the Hartree approximation is in error by more than an order of magnitude or that some asymmetry other than the known electromagnetic forces must appear in nuclear interactions.

The authors wish to thank Professor J. R. Oppenheimer for suggesting this work and for his guidance.

E. P. Cooper
E. C. Nelson

Department of Physics,
University of California,
Berkeley, California,
November 29, 1940.

[1] We are indebted to Dr. J. Halpern and Mr. R. C. Raymond for this information.
[2] L. A. Delsasso, M. G. White, W. Barkas and E. C. Creutz, Phys. Rev. **58**, 586 (1940).
[3] S. Millman, P. Kusch and I. I. Rabi, Phys. Rev. **56**, 165 (1939).
[4] E. Feenberg and M. Phillips, Phys. Rev. **51**, 597 (1937).

On the Theory of Mesons

In a recent paper by L. Rosenfeld and the present author[1] the theory of meson fields was formulated in a way which permits an unambiguous treatment of the problems of nuclear forces and stationary states of nuclei without having recourse to any "cutting off" prescriptions. The field variables in this theory are the field variables of the "vector" theory combined with those of the "pseudoscalar" theory. These two types of field variables are so far completely independent and satisfy equations which are separately covariant against Lorentz transformations. Each of these field equations contains a set of two universal constants g_1, g_2 and f_1, f_2 which determine the strength of the couplings between the nuclons[2] and the "vector" and "pseudoscalar" meson fields, respectively. In order to avoid the occurrence of strongly singular terms in the static interaction energy which, in general, would make an unambiguous treatment of the stationary states of nuclei impossible, the constants g_2 and f_2 must satisfy the condition $f_2^2=g_2^2$ but, otherwise, the four universal constants are completely independent.

Quite apart from the fundamental difficulties inherent in any quantum field theory, the occurrence of two independent types of field and of four universal constants is an unsatisfactory feature of the theory which leads to the view that this formalism is only part of a more comprehensive formalism in which the vector and pseudoscalar meson fields are more intimately connected and, consequently, the number of independent constants is reduced. A closer examination of the transformation properties of the source densities of the fields by rotations in a five-dimensional space shows, however, that the equations of the vector and pseudoscalar fields may be written compactly as tensor equations in five dimensions. These equations are covariant against all rotations in a five-dimensional space if the constants f_1 and f_2 are fixed by the relations $f_1=g_1$, $f_2=-g_2$ which are in accordance with the condition $f_2^2=g_2^2$ mentioned above. Since the Lorentz transformations only form a subgroup of the group of five-dimensional rotations the invariance properties of the field equations are in this way extended to a wider group of transformations in which the vector and pseudoscalar field variables are transformed into each other and the number of independent constants is reduced from four to two.

As regards the physical interpretation of the formalism it should be noticed that the group of five-dimensional rotations is homomorphous with the group of space-time rotations and translations in the de Sitter space, which may be pictured as the surface of a four-dimensional sphere embedded in a space of five dimensions.[3] A possible interpretation of the formalism is, therefore, obtained if the new field equations are regarded as the equations of meson theory in de Sitter space. In the approximation where the curvature of the de Sitter space is neglected, all consequences of the theory are then the same as in the previous formulation apart from the difference arising from the fixation of the constants f_1 and f_2, which of course makes the predictions of the new theory more precise. This is of importance, for instance, in the calculation of the quadrupole moment of the deuteron which in the earlier paper was explained by the occurrence of nonstatic directional terms in the Hamiltonian of first order in the velocities of the nuclons. The quadrupole moment arising from these terms, however, has a factor $f_1f_2+g_1g_2$ and vanishes if the constants f_1 and f_2 are fixed as above. Now, the Hamiltonian contains other directional terms of second order in the velocities of the nuclons which are proportional to the square of the constant g_2. The quadrupole moment arising from these terms will, therefore, have a definite sign independent of the choice of signs for the universal constants. Also the size of this quantity is uniquely determined and the result of a provisory evaluation agrees reasonably well with the empirical value of the quadrupole moment both as regards the order of magnitude and sign of this quantity.

A detailed account of the present theory has been given in a paper now in print in the *Proceedings of the Copenhagen Academy*.

C. MØLLER

Institute of Theoretical Physics,
Copenhagen,
October, 1940.

[1] C. Møller and L. Rosenfeld, Kgl. Danske Vidensk. Selsk. Mathem.-fys. Medd. **17**, 8 (1940).
[2] Following the proposal of Belinfante ("Theory of heavy quanta," Proefschrift, s'Gravenhage (1939)) we use the word nuclon as a common name for the nuclear constituents, the protons and neutrons.
[3] H. P. Robertson, Phil. Mag. **5**, 839 (1928).
[4] J. M. B. Kellogg, I. I. Rabi, N. F. Ramsey, Jr., and J. R. Zacharias, Phys. Rev. **55**, 318 (1939). See also A. Nordsieck, Phys. Rev. **57**, 556A (1940).

On the Vertical Shift of the Meson-Formation Layer

Quite recently, Loughridge and Gast have pointed out the "air-mass effect"[1] on cosmic-ray intensity, and Dr. Y. Nishina and the present author[2] have given additional confirmations. After Blackett[3] the "temperature effect" of the cosmic rays is caused by the vertical shift of the layer in which the mesons are formed.

In their first paper, Loughridge and Gast have given expression for vertical shift of the meson-producing layer, assuming the mesons are formed at a layer of given density. From a meteorological point of view a more probable expression seems to be desirable.

The International Commission for Air Navigation has put forward a specification of a standard atmosphere to secure uniformity in estimating aircraft performances. Up to 11 km this standard atmosphere is specified by the surface pressure $P=760$ mm Hg, the surface temperature 288°K and the lapse rate equal to 6.5°C per kilometer of height. Above 11 km the temperature is assumed constant at 216.5°K. By simple algebra we find the height of the meson-producing layer in the standard atmosphere as nearly 15,800 meters, assuming the mesons are formed at a layer of given pressure 80 mm Hg.

In aerology, the harmonic-mean temperature T_m is usually used for barometric altimetry. This is defined by $T_m=Z/\int_0^Z dZ/T$. The equation for determination of the height Z at which a particular pressure p is observed is given by the well-known formula:[4]

$$p=P\exp\left[-gZ/RT_m\right],$$

where g stands for the acceleration of gravity and R the

gas constant for air. In the I.C.A.N. atmosphere, the mean temperature up to 15.8 km is given by

$$\frac{15.8}{T_m}=\int_0^{11}\frac{dZ}{(288-6.5Z)}+\int_{11}^{15.8}\frac{dZ}{216.5}$$

or

$$T_m=239°\text{K}.$$

The shifts of the meson-formation layer are manifested by changes in height of given pressure (80 mm Hg). If the subscripts 0 and 1 refer to the initial and final values of the variables, we get,

$$P_0\exp\left[-gZ_0/RT_{m0}\right]=P_1\exp\left[-gZ_1/RT_{m1}\right].$$

The change of height at the meson-formation layer is then given by

$$\ln\frac{P_1}{P_0}=\frac{g}{R}\left(\frac{Z_1}{T_{m1}}-\frac{Z_0}{T_{m0}}\right),$$

or

$$Z_1-Z_0=\frac{T_{m1}-T_{m0}}{T_{m0}}Z_0+\frac{RT_{m1}}{g}\ln\left(1+\frac{P_1-P_0}{P_0}\right).$$

Since $(P_1-P_0)/P_0$ is always very small, we can safely get

$$\Delta Z=\frac{Z_0}{T_{m0}}\Delta T_m+\frac{H}{P_0}\Delta P, \qquad (1)$$

where $\Delta T_m=T_{m1}-T_{m0}$, $\Delta P=P_1-P_0$ and $H=RT_{m1}/g$.

If it is assumed that the height of the meson-formation layer Z, the surface pressure P and the mean temperature T_m have the standard values 15.8 km, 760 mm Hg and 239°K, respectively, Eq. (1) becomes

$$\Delta Z=0.0661\Delta T_m+0.0092\Delta P,$$

where ΔZ is measured in kilometers, ΔT_m in Celsius and ΔP in mm Hg. Assuming the mesons are formed at a layer of pressure 80 mm Hg, we find that the vertical shift of the meson-formation layer caused by an influx of warm air aloft amounts to 66 meters per °C and that the vertical shift of the meson-formation layer caused by the rising of the atmospheric pressure only amounts to 9 meters per mm Hg.

H. Arakawa

Central Meteorological Observatory,
Tokyo, Japan,
November 7, 1940.

[1] D. F. Loughridge and Paul F. Gast, Phys. Rev. **56**, 1169 (1939); **58**, 583 (1940).
[2] Y. Nishina, Y. Sekido, H. Simamura, and H. Arakawa, Phys. Rev. **57**, 663 (1940); **57**, 1050 (1940); Nature **145**, 703 (1940); **146**, 95 (1940).
[3] P. M. S. Blackett, Phys. Rev. **54**, 973 (1938).
[4] See any text on meteorology.

Decrease in Ionization of the F_2 Region During Solar Eclipse

During the total solar eclipse of October 1, 1940, ionospheric observations at three points in South Africa by the following three institutions: Cruft Laboratory (Harvard), Commonwealth Solar Observatory (Canberra), and Bernard Price Institute for Geophysical Research (Johannesburg), have revealed a marked ultraviolet light effect in the F_2 region. The maximum electron density in that region showed a decrease of about 20 percent, reaching a minimum about 30 minutes after totality. There was no evidence for corpuscular effects. The behavior of the E and F_1 regions was similar to what has been observed at previous eclipses.

J. A. Pierce,

Cruft Laboratory,
Harvard University,
Cambridge, Massachusetts,

A. J. Higgs,

Commonwealth Solar Observatory,
Canberra, Australia,

E. C. Halliday

Bernard Price Institute,
Johannesburg, South Africa,
October 14, 1940.

Proceedings of the American Physical Society

The Ohio Section

Minutes of the Symposium on the Physics of Rubber held at the University of Akron, October 11, 12, 1940

THE third meeting of the Ohio Section of the American Physical Society was held at the University of Akron, Akron, Ohio on Friday and Saturday, October 11 and 12, 1940. On Friday afternoon tours were taken through the aeronautical experimental laboratories of the Guggenheim Airship Institute and through the plant of the B. F. Goodrich Tire and Rubber Company.

A banquet held Friday evening was attended by 126 members and guests. After the banquet over 300 persons attended the evening program which included motion pictures depicting "physicists at work" by W. E. Forsythe, General Electric Company, Nela Park, Cleveland and an address on "Physical methods for investigating the structure of molecules" by Professor P. Debye, Cornell University.

The following invited papers were read at the Saturday morning session:

Physics in the Manufacture and Use of Rubber.—James W. Schade, *B. F. Goodrich Company.*

Thermal Problems in Rubber Manufacture.—Stuart H. Hahn, *B. F. Goodrich Company.*

The Optical Properties of Rubber.—Dr. Lawrence A. Wood, *National Bureau of Standards.*

Dielectric Constant and Power Factor of Koroseal at Radiofrequencies.—O. R. Fouts, *University of Akron.*

X-Ray Study of the Proportion of Crystalline and Amorphous Components in Stretched Rubber.—Dr. J. E. Field, *Goodyear Tire and Rubber Company.*

Infra-Red Spectra of Rubber.—Dr. W. C. Sears, *B. F. Goodrich Company.*

Some Applications of the Kinetic Theory of Rubber Elasticity.—Dr. H. Mark, *Brooklyn Polytechnic Institute.*

Physical Characteristics of Synthetic Rubber.—Dr. J. N. Street and Dr. J. H. Dillon, *Firestone Tire and Rubber Company.*

The mid-year meeting of the Ohio Section will be held on Saturday, March 29, 1941, at Muskingum College, New Concord, for which contributed papers will be solicited.

Richard H. Howe, *Secretary-Treasurer.*

The New England Section

Minutes of the Exeter Meeting, October 19, 1940

THE sixteenth regular meeting of the New England Section of the American Physical Society was held at Phillips Exeter Academy, Exeter, New Hampshire, on October 19, 1940. A hundred persons attended the meeting. The invited papers were as follows:

Symposium on Problems in the Logic of Physics

The Observer as Part of an Experimental System—Rogers D. Rusk, *Mount Holyoke College.*

Does Philosophy Help Us Understand Physics?—Philipp Frank, *Harvard University.*

What Do We Mean by an Explanation in Physics?—R. B. Lindsay, *Brown University.*

Phrasing of the Principle of Indefiniteness—K. K. Darrow, *Bell Telephone Laboratories.*

The Secondary School and Physics in General Education—A. Longacre, *Phillips Exeter Academy.*

Photography in the Physics Curriculum—Carl W. Miller, *Brown University.*

Electrostatic X-Ray Generators for Medical Use—J. G. Trump, *Massachusetts Institute of Technology.*

Abstracts of the contributed papers are given below.

The members of the society were guests of the Phillips Exeter Academy at luncheon at the Exeter Inn.

At the business meeting the following officers were elected for 1941: Chairman, F. H. Crawford; Vice Chairman, P. M. Morse; Secretary-Treasurer, J. C. Boyce; Members of the Program Committee, H. E. Farnsworth and J. H. Van Vleck.

A vote of thanks was extended to Dr. Perry, principal of the Academy, and to the members of its Science Department, for their most generous hospitality.

Because of the national meeting of the American Physcial Society to be held in Cambridge on February 21 and 22, 1941, there will be no winter meeting of the Section. The next section meeting will be held in October, 1941, at Smith College, Northampton, Massachusetts. The exact date will be announced later.

J. C. Boyce, *Secretary-Treasurer*

Abstracts of Contributed Papers

1. Model Showing Variable Astigmatism. Eric Rogers, *Mount Holyoke College.*—(Abstract to be published in *American Journal of Physics.*)

2. A Resistivity Study of the Order-Disorder Transformation in Cd-Mg. Mary Anne Benson* and Gladys A. Anslow, *Smith College.*—Specimens of 45 percent and 55 percent Cd, heat-treated to various states of order, were heated at 2, 4, and 5 degrees per min. and their resistivity measured at 5-degree intervals. Points of inflection on the resulting conductivity curves as well as on those which indicate the portion of the resistance resulting from increased disorder indicate several transition temperatures substantially below the Curie temperature. These may correspond to decreases in order within the nuclei, a short range order effect. A more definite inflection appears just below the Curie point, indicating general disorder. The initial state of order determines these temperatures; when the specimen is quenched from the disordered state the first transition temperatures have values lower than those for specimens nearly in equilibrium. The reverse occurs when the alloys are superordered. The variations in the final transition temperatures are effected by hysteresis resulting from the rate of heating, as well as the initial state of order. Studies of the activation energies confirm these conclusions.

* Now at Mount Holyoke College.

3. The Spectra of the Thermal Reaction Between Hydrogen and Oxygen. O. Oldenberg, E. G. Schneider and H. S. Sommers, Jr., *Harvard University and Stevens Institute of Technology.*—A mixture of hydrogen and oxygen (pressure about one atmosphere, temperature around 550°C) combines to form water with a nonexplosive, easily measurable rate. The several contradictory theories of this important reaction all postulate the presence of free hydroxyl radicals as carriers for a chain reaction. We made a search for these radicals during the fastest part of the reaction by hunting for their absorption spectrum photographed on a 21-foot grating, but found no trace of them. Hence their concentration is less than one radical in 300,000 molecules. The emission spectrum of the explosive reaction consists almost exclusively of hydroxyl bands. It is indistinguishable from the hydrogen-oxygen flame.

4. Atmospheric Pressure Geiger-Müller Counters. Sanborn C. Brown, *Massachusetts Institute of Technology.*—The usefulness of the ordinary Geiger-Müller counter for measuring soft radiation is limited by the thickness of the window which will withstand the pressure difference between the counter pressure and the atmosphere. To overcome this difficulty, Geiger-Müller counters filled to atmospheric pressure have been used successfully. The counters are filled with commercial tank helium, and have threshold voltages between 1500 and 1800 volts for counters 2 cm in diameter, so that they do not require special amplifiers or power supplies. No special treatment of the cathode surface is necessary. These counters have plateaus several hundred volts wide, and show the same γ-ray sensitivity as standard air counters of the same dimensions. If a coarse screen is substituted for the usual window in a counter, the helium may be flowed through the counter, out through the screen, and over the sample, eliminating any window between the counter volume and a source of very soft radiation. Having the helium flow through the counter does not affect its operation. Alcohol counters, to operate with a series resistance of 5 megohms in the anode circuit, have been made by bubbling the helium through alcohol while the counter is in operation. The threshold was found to be about 200 volts higher for these alcohol counters than for those filled with helium alone.

5. The Radioactivity of Sedimentary Rocks and Associated Petroleum. Clark Goodman, K. G. Bell and W. L. Whitehead, *Massachusetts Institute of Technology.*—Determinations of the radioactivity of 21 sedimentary rocks and 7 associated crude oils have been made by the precision method developed by R. D. Evans.[1] Considerable variability in radioactivity was found in the sandstones (1.4 to 0.19×10^{-12} g Ra/g) and limestones (1.3 to 0.18×10^{-12} g Ra/g). The radium content of limestones decreases with increasing purity. The shales were quite uniform (1.2 to 1.0×10^{-12} g Ra/g). Apparently discrete mineral particles in sandstone and impurities in limestone account for their occasional high radioactivity. The radon content of the crude oils (0.47 to 0.05×10^{-12} curie/g of oil) was in one sample 38 times, and averaged 10 times, the amount in equilibrium with the radium present. The results corroborate the inferences of former investigators that radon tends to concentrate in crude oils. Maximum radon content and maximum ratio of radon to radium were found in petroleum produced from a permeable, Oligocene sandstone of high radioactivity. Cracking of hydrocarbons with generation of hydrogen has been proved by S. C. Lind[2] to result from bombardment with alpha-rays. The amounts of radioactivity found in these crude oils are quantitatively sufficient to cause appreciable cracking by alpha-radiation during geologic time. These reactions, together with subsequent hydrogenation, may account for important changes in petroleum. This hypothesis would also explain the presence of hydrogen in some natural gases.

[1] R. D. Evans, Rev. Sci. Inst. **6**, 99–112 (1935).
[2] S. C. Lind, *The Chemical Effects of Alpha Particles and Electrons* (Chemical Catalog Co., 1928).

The Metropolitan Section

Minutes of the Meeting of November 15, 1940

THROUGH the courtesy of the Columbia Broadcasting System the first meeting of the Section for the season 1940–41 was held in the studios of the System at 49 East 52nd Street, New York City, at 8 P.M. on Friday, November 15, 1940. The following papers were presented:

The Coronaviser—A. M. Skellett

Color Television—Peter C. Goldmark

Some basic considerations in color television and a discussion and demonstration of the CBS color television system presented with the collaboration of J. N. Dyer, E. R. Piore and J. M. Hollywood.

W. S. Gorton, *Secretary-Treasurer*

Author Index to Volume 58

References with (A) are to abstracts of papers presented at meetings of the American Physical Society. References with (L) are to Letters to the Editor and those with (T) designate title only.

Allison, Samuel K., Leonard C. Miller, Gilbert J. Perlow, Lester S. Skaggs and Nicholas M. Smith, Jr. Energy released in the reaction $Li^6(p,\alpha)He^3$ and the mass of He^3—178(L)

Altmann, George O., H. N. Walker and Victor F. Hess. Counter studies on cosmic rays at sea level—1011

Alvarez, Luis W. High energy carbon nuclei—192(A)

—— (see Wiens, Jacob)—1005(L)

—— **and R. Cornog.** Radioactive hydrogen—a correction—197(A)

—— **and Kenneth S. Pitzer.** Scattering of 20° neutrons in ortho- and parahydrogen—1003(L)

Amaki, Toshio and Asao Sugimoto. Some experiments on the relative cross sections of the (n,α) and (n,p) reactions produced by fast neutrons—659(L)

Anslow, Gladys A. (see Benson, Mary Anne)—1121(A)

Aoki, K. (see Okuda, T.)—578(L)

Arakawa, H. On the vertical shift of the meson-formation layer—1118(L)

Araki, G. (see Tomonaga, S.)—90(L)

Bacher, R. F. (see Tomboulian, D. H.)—52

Backus, John. Low energy β-rays from copper^{64}—192(A)

Baker, Richard F. Halation on kinescope screens—208(A)

Baltzer, O. J. (see Jauncey, G. E. M.)—1116(L)

Band, William (see Ma, C. Y.)—479(L)

Baños, Alfredo, Jr. (see Schremp, E. J.)—662

Bardeen, J. Concentration of isotopes by thermal diffusion: Rate of approach to equilibrium—94(L)

—— Image and Van der Waals forces at a metallic surface—727

Barkas, W. H. (see Creutz, E. C.)—481, 1008(L)

—— (see Delsasso, L. A.)—586

——, **Phillip R. Carlson, J. E. Henderson and William H. Moore.** Concentration of radioactive bromine produced by gamma-radiation—577(L)

——, **E. C. Creutz, L. A. Delsasso, R. B. Sutton and M. G. White.** Beta-radiation from Si^{27} and P^{30}—194(A), 383(L)

Barnes, Arthur H. and Clarence Zener. Internal friction at high temperatures—87(L)

Barnóthy, J. and M. Forró. Absorption of cosmic rays in lead at a depth of 1000 m water equivalent—844(L)

Baroody, E. M. Directional dependence of electrical conductivity—793

Barrett, Charles S. and Alfred H. Geisler. Atomic distribution in aluminum-silver alloys during aging—206(A)

Barschall, H. H. (see Wheeler, John A.)—682

—— **and M. H. Kanner.** On the angular distribution of fast neutrons scattered by hydrogen, deuterium and helium—590; erratum—1010(L)

Bartunek, P. F. (see Cork, J. M.)—580(L)

Bayley, D. S. (see Huntoon, R. D.)—97

Bearden, J. A. (see Munier, J. H.)—537

—— **and W. W. Beeman.** K-absorption edges and $K\beta_{2,5}$-emission lines of two Zn-Ni alloys—396

—— **and H. Friedman.** X-ray $K\beta_{2,5}$-emission lines and K-absorption limits of Cu-Zn alloys—387

Beeman, W. W. (see Bearden, J. A.)—396

—— (see Friedman, H.)—400

Beers, Yardley (see Ladenburg, Rudolf)—757(L)

Bell, K. G. (see Goodman, Clark)—1121(A)

Bell, Paul H. (see Davey, Wheeler P.)—207(A)

Bennett, Clarence E. Optical dispersion and molar refraction at zero frequency for compressed nitrogen, argon, and carbon dioxide measured as functions of density—263

Bennett, W. E. (see Bonner, T. W.)—185(L)

—— (see Rogers, M. M.)—186(L)

—— **and T. W. Bonner.** Gamma-ray resonances from the bombardment of carbon by deuterons—183(L)

——, **T. W. Bonner, Emmett Hudspeth and Bob E. Watt.** Protons from $C^{13}+H^2$—478(L)

Bennett, Willard H. Mobilities in hydrogen at high current densities—992

Benson, Mary Anne and Gladys A. Anslow. Resistivity study of the order-disorder transformation in Cd-Mg—1121(A)

Berkey, W. E. (see Slepian, Joseph)—204(A), 210(A)

Bernardini, G., B. N. Cacciapuoti, B. Ferretti, O. Piccioni and G. C. Wick. Genetic relation between the electronic and mesotronic component of cosmic rays near and above sea level—1017

Bessey, William H. Diffraction and reflection of molecular beams—207(A)

Beyer, H. G. (see Nix, F. C.)—1031

Bidwell, C. C. Thermal conductivity of metals—561

Birge, Raymond T. Values of e, e/m, h/e and α—658(L)

Bitter, F. (see Starr, C.)—977

Bleakney, Walker (see Cummings, Charles S., II)—787

Bloch, F. Theory of the resonance scattering of protons and neutrons on helium—829

Bøggild, J. K. (see Bohr, N.)—839

—— (see Brostrøm, K. J.)—651

Bohr, N. Scattering and stopping of fission fragments—654

—— Successive transformations in nuclear fission—864

——, **J. K. Bøggild, K. J. Brostrøm and T. Lauritsen.** Velocity-range relation for fission fragments—839

Bonner, T. W. (see Bennett, W. E.)—183(L), 478(L)

—— (see Rogers, M. M.)—186(L)

——, **Emmett Hudspeth, and W. E. Bennett.** Resonances in the emission of neutrons from the reaction $C^{13}+H^2$—185(L)

Booth, E. T., J. R. Dunning, A. V. Grosse and A. O. Nier. Neutron capture by uranium (238)—475(L)

Booth, H. S. Chemistry through the microscope—96(T)

Bostick, W. H. (see Herzog, G.)—278(L)

Bound, M. (see Rossi, B.)—761

Bowman, D. W. (see Green, J. B.)—381(L), 1094

Bozorth, R. M. (see Williams, H. J.)—203(A)

—— **and H. J. Williams.** Explanation of anomalous magnetic torque curves—210(A)
——, **H. J. Williams and R. J. Morris, Jr.** Magnetic properties of iron-aluminum alloys—203(A)
Brady, James J. and Bruce Elle. Electrical conductivity of tartaric acid crystals—195(A)
Brasefield, Charles J. Effect of an activator on the absorption spectrum of zinc sulphide powders—436
Breit, G. Interpretation of resonances in nuclear reactions—506
—— Scattering matrix of radioactive states—1068
Bridgman, P. W. Second law of thermodynamics and irreversible processes—845(L)
Bright, William C. (see Murphy, Edgar J.)—88(L)
Brooks, Harvey. Ferromagnetic anisotropy and the itinerant electron model—909
Brostrøm, K. J. (see Bohr, N.)—839
——, **J. K. Bøggild and T. Lauritsen.** Cloud-chamber studies of fission fragment tracks—651
Brown, Harrison. On the temperature assignments of experimental thermal diffusion coefficients—661(L)
Brown, Sanborn C. Atmospheric pressure Geiger-Müller counters—1121(A)
Brown, William Fuller, Jr. Interpretation of torsional frequencies of crystal specimens—998
—— Theory of the approach to magnetic saturation—202(A), 736
Cacciapuoti, B. N. (see Bernardini, G.)—1017
Calus, H. and R. Smoluchowski. On the heat emission associated with the processes in oversaturated solid solutions ("aging")—205(A)
Carlson, Phillip R. (see Barkas, Walter H.)—577(L)
—— **and J. E. Henderson.** Photonuclear disintegration of iron and manganese—193(A)
Chao, K. T. (see Oleson, N. L.)—201(A)
—— (see Randels, R. B.)—201(A)
Chase, C. T. and R. T. Cox. Scattering of 50-kilovolt electrons by aluminum—243
Ch'en Shang-Yi. Broadening, asymmetry and shift of rubidium resonance lines under different pressures of helium and argon up to 100 atmospheres—1051
—— Pressure effect of homogeneous rubidium vapor on its resonance lines—884
—— **and Pao Chia-Shan.** Pressure effects of hydrogen and nitrogen on the second doublet of Rb principal series—1058
Christensen, H. (see Williams, H. J.)—203(A)
Christy, R. F. and J. M. Keller. Precise determination of the fine structure constant—658(L)
—— **and S. Kusaka.** Interaction of mesotrons with γ-rays—191(A)
Clancy, Edward P. Induced radioactivity of krypton—88(L)
Clarke, E. T. (see Murphy, Edgar J.)—88(L)
—— **and S. A. Korff.** Latitude effect in cosmic rays at far southern latitudes—179(L), 201(A)
Cleveland, Forrest F. Raman spectra evidence for the disappearance of the cyanate ion from an aqueous solution of potassium cyanate—189(A)
Cohn, Willi M. Note on the polarization of light emitted by electrically exploded wires—50, 188(A)
Collins, George B. (see Feldmeier, J. R.)—200(A)
Colwell, R. C. Variation in intensity of radio signals—204(A)
—— (see Thomas, C. D.)—203(A)
Compton, Arthur H. Effect of an eclipse on cosmic rays—841(L)
Condon, E. U. Development of high voltage for the production of neutrons and artificial radioactivity—96(T)
—— Simple calculation of klystron efficiency—204(A)
Cook, Emery. Complete data and boundary conditions for a superconductor—361
—— Phenomenological theory of superconductors—357
Cooley, R. A. (see Kalbfell, D. C.)—91(L)
Coon, J. B. Vibration analysis of the chlorine dioxide absoprtion spectrum—926(L)
Cooper, Densil. Fine structure in the directional intensity of cosmic rays—288
Cooper, E. P. and E. C. Nelson. Ground states of Be^{10} and C^{10}—1117(L)
Copeland, Paul L. Secondary emission from films of platinum on aluminum—604
Corben, H. C. and Julian Schwinger. Electromagnetic properties of mesotrons—191(A), 953
Cork, J. M. (see Lawson, J. L.)—580(L)
—— **and P. F. Bartunek.** Photographic registration of heavy particles emitted during bombardment—580(L)
—— **and J. Halpern.** Radioactive isotopes of gold—201(A)
—— **and W. Middleton.** Simultaneous emission of three particles from an excited nucleus—474(L)
Cornog, R. (see Alvarez, Luis W.)—197(A)
Corson, D. R., K. R. MacKenzie and E. Segrè. Artificially radioactive element 85—672
Cox, C. R. (see Hoag, J. Barton)—203(A)
Cox, R. T. (see Chase, C. T.)—243
Coy, Nettie H. and H. Sponer. Emission spectrum of antimony nitride—709
Crane, H. R. (see Oleson, N. L.)—201(A)
—— (see Randels, R. B.)—201(A)
Creutz, E. C. (see Barkas, W. H.)—194(A), 383(L)
—— (see Delsasso, L. A.)—586
——, **W. H. Barkas and N. H. Furman.** Gamma-radiation from rhenium—1008(L)
——, **L. A. Delsasso, R. B. Sutton, M. G. White and W. H. Barkas.** Radioactivity produced by proton bombardment of bromine and iodine—481
Critchfield, C. L. and W. E. Lamb, Jr. Note on a field theory of nuclear forces—46
Cummings, Charles S., II and Walker Bleakney. Products of ionization by electron impact in methyl and ethyl alcohol—787
Dancoff, S. M. Spin-orbit coupling in He^5—190(A), 326
Darrin, Marc (see Sidhu, S. S.)—206(A)
Darrow, K. K. Phrasing of the principle of indefiniteness—1120(T)
Davenport, L. L. Attempt to measure Young's modulus and Poisson's ratio by x-ray methods—206(A)
Davey, Wheeler P. and Paul H. Bell. X-ray study of liquid benzene, cyclohexane, and their mixtures—207(A)

Davidson, W. L., Jr. (see Schultz, H. L., Jr.)—198(A), 1043
Delsasso, L. A. (see Barkas, W. H.)—194(A), 383(L)
—— (see Creutz, E. C.)—481
——, **M. G. White, W. Barkas and E. C. Creutz.** Carbon isotopes of mass ten and eleven—586
DeVault, Don and W. F. Libby. Decay of the 4.5-hour Br^{80} isomer—688
Dickson, G. R. and E. J. Konopinski. Note on a possible scheme for the assignment and prediction of radioactive periods—949
Distad, M. (see Hagen, John P.)—208(A)
Drynski, T. and R. Smoluchowski. X-ray absorption edges in gaseous, liquid and solid states—207(A)
DuBridge, L. A. (see LePage, Wilbur R.)—61
—— **and John Marshall.** Radioactive isotopes of Sr, Y and Zr—7
DuMond, Jesse W. M. Complete isometric consistency chart for the natural constants e, m and h—457
Dunning, J. R. (see Booth, E. T.)—475(L)
—— (see Nix, F. C.)—1031
Eckart, Carl. Thermodynamics of irreversible processes. I. Simple fluid—267; II. Fluid mixtures—269; Correction —924; III. Relativistic theory of the simple fluid—919
Eisenstein, A. and N. S. Gingrich. Diffraction of x-rays by liquid argon—307
Elle, Bruce (see Brady, James J.)—195(A)
Ellett, A. (see Huntoon, R. D.)—97
—— (see McLean, W. B.)—500
—— (see Young, Victor J.)—498
Elliott, D. R. (see King, L. D. P.)—846(L)
Ellwood, W. B. Magnetic ultra-micrometer for measurement of thin films or nonmagnetic material superimposed upon a base of magnetic material—204(A)
Elmore, W. C. Interpretation of ferromagnetic colloid patterns on ferromagnetic crystal surfaces—640
Engstrom, R. W. and W. S. Huxford. Time-lag analysis of the Townsend discharge in argon with activated caesium electrodes—67
Evinger, H. H. (see Muskat, M.)—205(A)
Fajans, Kasimir and William H. Sullivan. Induced radioactivity of rhenium and tungsten—276(L)
—— **and Adolf F. Voigt.** Radioactivity produced by bombarding thallium—177(L)
Fano, Ugo. Theory on cathode luminescence—544
Farnsworth, H. E. and Ralph P. Winch. Photoelectric work functions of (100) and (111) faces of silver single crystals and their contact potential difference—812
Feldmeier, J. R. and George B. Collins. Pair production by electrons—200(A)
Ferguson, A. J. and L. R. Walker. Scattering of alpha-particles by carbon and oxygen—666
Ferretti, B. (see Bernardini, G.)—1017
Field, J. E. X-ray study of the proportion of crystalline and amorphous components in stretched rubber—1120(T)
Fitzsimmons, K. S., L. B. Loeb and J. M. Meek. Positive corona discharge—187(A)
Fleming, G. M. and Joseph E. Henderson. Energy losses attending field current and thermionic emission of electrons from metals—887
—— **and D. M. Holtoner.** Observations on field currents from tantalum—189(A)
Flerov and Petrjak. Spontaneous fission of uranium—89(L)
Fletcher, Harvey. Sound patterns—96(T)
Foote, Frank and Eric R. Jette. Fundamental relation between lattice constants and density—81
Forró, M. (see Barnóthy, J.)—844(L)
Fouts, O. R. Dielectric constant and power factor of Koroseal at radiofrequencies—1120(T)
Fowler, W. A. (see Lauritsen, C. C.)—193(A)
—— (see Streib, J. F.)—191(A)
—— **and C. C. Lauritsen.** Gamma-radiation from $M^{15}+H^1$ —192(A)
Frank, Philipp. Does philosophy help us understand physics?—1120(T)
Friedman, H. (see Bearden, J. A.)—387
—— **and W. W. Beeman.** Copper and nickel x-ray $K\beta_2$- and $K\beta_3$-emission lines and K-absorption limits in Cu-Ni alloys—400
Frye, William E. (see Hoyt, Frank C.)—784
Furman, N. H. (see Creutz, E. C.)—1008(L)
Gamow, G. and M. Schoenberg. Possible role of neutrinos in stellar evolution—1117(L)
Garbuny, Max and L. H. Matthias. Initial reignition voltage measurements—182(L)
Gast, Paul F. (see Loughridge, D. H.)—194(A), 583
—— **and D. H. Loughridge.** Latitude effect of cosmic rays above 50 degrees N latitude—194(A)
Geisler, Alfred H. (see Barrett, Charles S.)—206(A)
Gemant, Andrew. Ionic mobilities in insulating liquids —904
George, Henry H. (see Letner, Harold R.)—206(A)
Gerjuoy, E. On the angular distribution in the reaction $F^{19}(p,\alpha)$—503
Gingrich, N. S. (see Eisenstein, A.)—307
Glasoe, G. N. and J. Steigman. Radioactive products from gases produced in uranium fission—1
Goldhaber, M. (see O'Neal, R. D.)—574
Goldmark, Peter C. Color television—1121(T)
Goldsmith, H. H. (see Hornbostel, J.)—18
Good, William E. and Gertrud Scharff-Goldhaber. Scattering cross section of protons for 900-Kev neutrons —89(L)
Goodman, Clark, K. G. Bell and W. L. Whitehead. Radioactivity of sedimentary rocks and associated petroleum —1121(A)
Goss, W. H. and J. E. Henderson. High yield canal-ray ion source for nuclear disintegration—192(A)
Goudsmit, S. and J. L. Saunderson. Multiple scattering of electrons. II—36
Green, C. B. and G. L. Pearson. Thermistor voltage regulator—204(A)
Green, J. B., D. W. Bowman and E. H. Hurlburt. Zeeman effect of krypton—1094
——, **D. W. Bowman and E. H. Hurlburt.** Zeeman effect in krypton and xenon—381(L)
Gregg, E. C., Jr. Ultrasonic absorption in liquids—208(A)
Grinberg, A. P. and L. I. Roussinow. Structure of the lower excited levels of the Br^{80} nucleus—181(L)

Groetzinger, Gerhart (see Schein, Marcel)—1027
Grosse, A. V. (see Booth, E. T.)—475(L)
Hagen, John P., M. Distad and F. C. Iseley. Transmission line method of measuring the dielectric constant of gases and water vapor at ultra-high frequencies—208(A)
Hahn, Stuart H. Thermal problems in rubber manufacture—1120(T)
Halliday, E. C. (see Pierce, J. A.)—1119(L)
Halpern, J. (see Cork, J. M.)—201(A)
Hamilton, Donald R. On directional correlation of successive quanta—122
Hansche, George E. Intensity changes in Cameron bands of CO excited by electron impact—1075
Harrison, G. R. (see Roberson, J. H.)—895
—— **and J. Rand McNally, Jr.** Zeeman effects in the arc spectrum of ruthenium—703
Hartman, C. D. (see Wooldridge, D. E.)—381(L)
Harvey, G. G. (see Jauncey, G. E. M.)—179(L)
Haseltine, William R. Sparking threshold in air—188(A)
Haxby, R. O. (see Wells, W. H.)—162
——, **W. E. Shoupp, W. E. Stephens and W. H. Wells.** Fast neutron threshold for uranium fission—199(A)
——, **W. E. Shoupp, W. E. Stephens and W. H. Wells.** Photo-fission of uranium and thorium—92(L)
——, **W. E. Shoupp, W. E. Stephens and W. H. Wells.** Thresholds for the proton-neutron reactions of lithium, beryllium, boron and carbon—1035
Hay, Robert H. Nuclear magnetic moment of C^{13}—180(L)
Hazen, Wayne E. Sensitive time of a Wilson cloud chamber—194(A)
Healea, Monica and Charlotte Houtermans. Relative secondary electron emission due to He, Ne and A ions bombarding a hot nickel target—608
Hebb, M. H. and Eldred Nelson. Internal conversion of gamma-radiation in the *L* shell—486
Hellund, E. J. Temperature dependence of the viscosity of helium—192(A)
—— Transport cross section of helium—278(L)
Hemmendinger, Arthur. Proton induced radioactivity of manganese—929
Henderson, J. E. (see Barkas, Walter H.)—577(L)
—— (see Carlson, P. R.)—193(A)
—— (see Fleming, G. M.)—887
—— (see Goss, W. H.)—192(A)
—— (see Rubens, Sidney M.)—446
—— (see Wyckoff, H. O.)—187(A)
Henderson, Malcolm C. Heat of fission of uranium—200(A), 774
Herb, R. G., C. M. Turner, C. M. Hudson and R. E. Warren. Electrostatic generator with concentric electrodes—579(L)
Herring, Conyers, and A. G. Hill. Theoretical constitution of metallic beryllium—132
Herzfeld, K. F. (see Lyddane, R. H.)—1008(L)
Herzog, G. and W. H. Bostick. Pair production of mesotrons at 29,000 feet—278(L)
Hess, Victor F. (see Altmann, George O.)—1011
Hicks, Bruce L. Pressure-temperature dependence of the compressibility factor and density of hydrocarbons—209(A)
Higgs, A. J. (see Pierce, J. A.)—1119(L)
Hill, A. G. (see Herring, Conyers)—132
Hillier, James. Fresnel diffraction of electrons as a contour phenomenon in electron supermicroscope images—842(L)
Hirsh, F. R., Jr. Note on thin quartz crystals as used in the Cauchois focusing x-ray spectrograph—78
Hoag, J. Barton and C. R. Cox. High frequency resistance and permeability of iron in a magnetic field—203(A)
Holland, D. O. (see Stewart, G. W.)—174
Holloway, M. G. and B. L. Moore. Disintegration of N^{14} and N^{15} by deuterons—847
Holstein, T. and H. Primakoff. Field dependence of the intrinsic domain magnetization of a ferromagnet—1098
Holtoner, D. M. (see Fleming, G. M.)—189(A)
Hornbostel, J., H. H. Goldsmith and J. H. Manley. On the resonance levels of rhodium and indium—18
Houtermans, Charlotte (see Healea, Monica)—608
Hoyt, Frank C. and William E. Frye. On the calculation of force fields from scattering—784
Hsü Chang Pen. Propagation of electromagnetic waves inside a cylindrical metal tube and along other types of guides—193(A)
Hudson, C. M. (see Herb, R. G.)—579(L)
Hudson, G. G. (see Loeb, L. B.)—195(A)
Hudspeth, Emmett (see Bennett, W. E.)—478(L)
—— (see Bonner, T. W.)—185(L)
—— (see Richards, Hugh T.)—382(L)
—— (see Rogers, M. M.)—186(L)
Huntington, H. B. Self-consistent solution to the vacancy problem in metals—209(A)
Huntoon, R. D., A. Ellett, D. S. Bayley and J. A. Van Allen. Distribution in angle of protons from the deuteron-deuteron reaction—97
Hurlburt, E. H. (see Green, J. B.)—381(L), 1094
Hurwitz, H., Jr. Note on interaction energies in radiation theory—467
Hustrulid, Andrew (see Mann, Marvin M.)—340
Huxford, W. S. (see Engstrom, R. W.)—67
Ikawa, M. (see Nishina, Y.)—660(L)
Inglis, D. R. Nuclear spin of C^{13}—577(L)
Iseley, F. C. (see Hagen, John P.)—208(A)
Iverson, V. E. (see Kelly, Harry C.)—189(A)
Jacobs, James A. (see McLean, W. B.)—500
Jacobsen, I. C. and N. O. Lassen. Deuteron induced fission in uranium and thorium—867
Jaffé, George. On the theory of recombination—968
Jaffe, Hans von R. On the color of solutions of alkali metals in ammonia—207(A)
Jánossy, L. (see Rossi, B.)—761
Jauncey, G. E. M. and O. J. Baltzer. Modified reflections of Cu $K\alpha$ x-rays from rocksalt—1116(L)
—— **and G. G. Harvey.** Theory of the diffuse scattering of x-rays from crystals—179(L)
Jesse, William P. Study of time-variations in cosmic-ray intensity at high altitudes—281
Jette, Eric R. (see Foote, Frank)—81
Jones, R. Clark. On the theory of the thermal diffusion coefficient for isotopes—111
Jordan, E. B. $C^{13}H_2-N^{14}$ mass difference—1009(L)

Kalbfell, D. C. and R. A. Cooley. Radio-isotopes of Ba and Cs—91(L)
Kamen, Martin D. and Samuel Ruben. Production and properties of carbon (14)—194(A)
Kamogawa, Hirosi. Secondary emission and electron diffraction on the glass surface—660(L)
Kanne, W. R., R. F. Taschek and G. L. Ragan. Search for resonance scattered protons from B^{11} and F^{19}—693
Kanner, M. H. (see Barschall, H. H.)—590; erratum—1010(L)
Kaplan, Joseph (see Rubens, Sidney)—188(A)
—— **and Sidney M. Rubens.** Temporal effects in nitrogen afterglows—188(A)
Kaufmann, A. R. (see Starr, C.)—657(L), 977
Keller, J. M. (see Christy, R. F.)—658(L)
Kelly, Harry C. and V. E. Iverson. Fluorescence method of identifying potato tubers free from bacterial ring rot and other types of decay—189(A)
Kelsall, G. A. (see Nesbitt, E. A.)—203(A)
Kerst, D. W. Acceleration of electrons by magnetic induction—841(L)
Kettering, Charles F. Industry and science—96(T)
Keyes, Kenneth E. Electron band treatment of susceptibilities of nickel and nickel alloys—202(A)
Kimura, K. (see Nishina, Y.)—660(L)
King, L. D. P. and D. R. Elliott. Short-lived radioactivities of $_{14}Si^{27}$, $_{16}S^{31}$, and $_{18}A^{35}$—846(L)
King, Robert B. (see Russell, Henry Norris)—407
—— **and D. C. Stockbarger.** Absolute *f* values of Cd I and Cu I lines—187(A)
Kip, A. F. (see Loeb, L. B.)—195(A)
Koenig, Henry Paul. Solid angle subtended by the main and shadow cones of cosmic radiation—385
Konopinski, E. J. (see Dickson, G. R.)—949
Korff, S. A. (see Clarke, E. T.)—179(L), 201(A)
—— (see Murphy, Edgar J.)—88(L)
Krasny-Ergen, William. Optimal dimensions of a Clusius-Dickel isotope separator—1078
Kuper, J. B. Horner and Edward Teller. Scattering of fast electrons in helium—602
Kusaka, S. (see Christy, R. F.)—191(A)
Kusch, P. (see Millman, S.)—438
—— (see Shrader, E. F.)—925(L)
Ladenburg, Rudolf and Yardley Beers. Direct determination of the charge of the beta-particle—757(L)
Lamb, Willis E., Jr. Passage of uranium fission fragments through matter—696
—— (see Critchfield, C. L.)—46
Lampe, Isadore. Comparative study of neutron- and x-radiation upon biological tissues in the cancer problem—96(T)
Landé, Alfred. Ratio of *e*, *c*, and *h*—843(L)
Landau, L. On the "radius" of the elementary particles—1006(L)
—— **and I. Tamm.** On the nature of the nuclear forces—1006(L)
Langer, Alois and W. E. Stephens. Radioactive barium and strontium from photofission of uranium—759(L)
Lapointe, Christian and Franco Rasetti. Capture cross sections for thermal energy neutrons—554
Laporte, Otto and J. E. Mack. On the structure of the arc spectrum of tungsten—188(A)
Lark-Horovitz, K. (see Miller, E. P.)—207(A)
Lassen, N. O. (see Jacobsen, I. C.)—867
Lauritsen, C. C. (see Fowler, W. A.)—192(A)
—— (see Streib, W. A.)—191(A)
—— **and W. A. Fowler.** Gamma-radiation from $C^{13}+H^1$—193(A)
Lauritsen, T. (see Bohr, N.)—839
—— (see Brostrøm, K. J.)—651
Lawson, J. L. and J. M. Cork. Internally converted gamma-rays from radioactive gold—580(L)
Leatherberry, Daniel (see Thaxton, Hubert M.)—200(A)
LePage, Wilbur R. and L. A. DuBridge. Electron emission into dielectric liquids—61
Letner, Harold R., Henry H. George and S. S. Sidhu. X-ray diffraction studies of silver-rich, silver-magnesium alloys—206(A)
Libby, W. F. (see DeVault, Don)—688
Liebermann, Leonard N. Rotational analysis of some CS_2 bands in the near ultraviolet system—183(L)
Lindsay, R. B. What do we mean by an explanation in physics?—1120(T)
Little, E. M. Relativity misconceptions such as relative velocity—191(A)
Livingston, R. S. and B. T. Wright. $(d,2n)$ reaction in copper—656(L)
Loeb, L. B. (see Fitzsimmons, K. S.)—187(A)
——, **G. G. Hudson and A. F. Kip.** Occurrence of Trichell pulses in negative point-to-plane corona in air—195(A)
Longacre, A. Secondary school and physics in general education—1120(T)
Loughridge, D. H. (see Gast, Paul F.)—194(A)
—— **and Paul F. Gast.** Further investigations of air mass effect on cosmic-ray intensity—194(A), 583
Lu, Hoff and Ralph H. Schuman. Longitudinal extraction of ions from low pressure constricted arc discharge in H_2 and in BF_3—199(A)
Ludloff, H. F. Elasticity of solids at different temperatures, especially near phase transitions—209(A)
Lyddane, R. H., K. F. Herzfeld and R. G. Sachs. Electric fields in vibrating polar crystals—1008(L)
Ma, C. Y. and William Band. Law of magnus in single-crystal aluminum wires—479(L)
Mack, Edward. Protein molecule structure—96(T)
Mack, J. E. (see Laporte, Otto)—188(A)
—— (see Roberson, J. H.)—895
MacKenzie, K. R. (see Corson, D. R.)—672
Manley, J. H. (see Hornbostel, J.)—18
Mann, Marvin M., Andrew Hustrulid and John T. Tate. Ionization and dissociation of water vapor and ammonia by electron impact—340
Margenau, H. and E. Wigner. Magnetic moments of odd nuclei—103
Mark, H. Some applications of the kinetic theory of rubber elasticity—1120(T)
Marshall, Fitz-Hugh. Method for obtaining powders of uniform sodium chloride crystals in various size ranges, and the effect of size upon the intensity of x-ray reflection—642

Marshall, John (see DuBridge, L. A.)—7
Marshall, Lauriston C. (see Sloan, David H.)—193(A)
Marton, L. New electron microscope—57
Mason, R. C. Short time photographs of a low pressure copper arc—204(A)
Mason, W. P. Location of hysteresis phenomena in Rochelle salt crystals—744
Matthias, L. H. (see Garbuny, Max)—182(L)
McLean, W. B., A. Ellett and James A. Jacobs. Distribution in angle of the long range alpha-particles from fluorine bombarded with protons—500
McMillan, Edwin. Seven-day uranium activity—178(L)
McNally, J. Rand, Jr. (see Harrison, George R.)—703
Meek, J. M. Theoretical calculations of breakdown potential for sphere-gaps—195(A)
—— Variation of sparking potential with dense initial photoelectric currents—196(A)
—— (see Fitzsimmons, K. S.)—187(A)
Middleton, W. (see Cork, J. M.)—474(L)
Miller, Bernard L. Electron and x-ray diffraction study of the grain boundary substance in cadmium—206(A)
Miller, Bertrand J. Effect of hyperfine structure upon the magnetic rotation of the plane of maximum polarization of resonance radiation—258
Miller, Carl W. Photography in the physics curriculum—1120(T)
Miller, E. P. and K. Lark-Horovitz. Structure of liquid argon—207(A)
Miller, Leonard C. Electrostatic deflection studies of alpha-particles; the alphas from $Li^6(p, \alpha)He^3$—936
—— (see Allison, S. K.)—178(L)
Millman, S. (see Shrader, E. F.)—925(L)
—— **and P. Kusch.** On the radiofrequency spectra of sodium, rubidium and caesium—438
Møller, C. On the theory of mesons—1118(L)
Mooney, Robert Lee. Elastic scattering in helium at 15°C—871
Moore, B. L. (see Holloway, M. G.)—847
Moore, Charlotte E. (see Russell, Henry Norris)—407
Moore, William H. (see Barkas, Walter H.)—577(L)
Morgan, F., M. Muskat and D. W. Reed. Experiments on boundary lubrication—205(A)
Morris, R. J., Jr. (see R. M. Bozorth)—203(A)
Morrison, P. and L. I. Schiff. Radiative K capture—24, 190(A)
Morrison, R. A. and H. M. Parker. Some anomalies in the photographic recording of gamma-radiation—196(A)
Motz, Lloyd and Julian Schwinger. Scattering of thermal neutrons by deuterons—26
Mouromtseff, I. E. Influence of "cold ends" on performance of vacuum-tube air coolers—204(A)
Mouzon, J. C. (see Park, R. D.)—43
Mrozowski, S. Forbidden lines in the spectrum of Pb I—189(A)
—— Hyperfine structure and intensities of the forbidden lines of Pb I—1086
—— Nuclear isotope shift in the spectra of HgH^+ and HgD^+—332
—— Nuclear isotope shift in the spectrum of ZnH—597
Mueller, Hans. Properties of Rochelle salt. III—565, IV—805
Munier, J. H., J. A. Bearden and C. H. Shaw. Principal M-series emission lines of tungsten and the K absorption of magnesium and aluminum—537
Murphy, Edgar J., William C. Bright, Martin D. Whitaker, S. A. Korff and E. T. Clarke. Comparative efficiencies of radioactive neutron sources—88(L)
Muskat, M. (see Morgan, F.)—205(A)
—— **and H. H. Evinger.** Effect of pressure variation of viscosity on the lubrication of plane sliders—205(A)
Neher, H. Victor and William H. Pickering. Attempt to measure the latitude effect of extensive cosmic-ray showers—665
—— **and H. G. Stever.** Mean lifetime of the mesotron from electroscope data—191(A), 766
Neil, R. H. (see Warner, A. H.)—195(A)
Nelson, E. C. (see Cooper, E. P.)—1117(L)
Nelson, Eldred. Note on the Neher-Stever experiment—771
—— (see Hebb, M. H.)—486
Nesbitt, E. A. and G. A. Kelsall. Vicalloy, a new permanent magnet material—203(A)
Newman, M. S. Cancer-producing hydrocarbons—96(T)
Nielsen, H. H. (see Straley, J. W.)—1002(L)
Nielsen, R. A. Precipitation of dirt—205(A)
Nier, A. O. (see Booth, E. T.)—475(L)
Nishina, Y., T. Yasaki, K. Kimura and M. Ikawa. Fission products of uranium by fast neutrons—660(L)
Nix, F. C., H. G. Beyer and J. R. Dunning. Neutron studies of order in Fe-Ni alloys—1031
Nordsieck, A. On the value of the electric quadrupole moment of the deuteron—310
Norling, Folke. On the efficiency of γ-ray counters—277(L)
Northrup, D. L., C. M. Van Atta, R. J. Van de Graaff and L. C. Van Atta. Some experiments on the irradiation of deuterium, beryllium, and indium nuclei by x-rays—199(A)
Nottingham, W. B. Remarks on the temperature dependence of the work function of tungsten—927(L)
O'Connor, John (see Rudnick, Philip)—1003(L)
Ogata, K. (see Okuda, T.)—578(L)
Okuda, T., K. Ogata, K. Aoki and Y. Sugawara. On the isotopic weights of chlorine, argon and iron by the doublet method—578(L)
Oldenberg, O., E. G. Schneider and H. S. Sommers, Jr. Spectra of the thermal reaction between hydrogen and oxygen—1121(A)
Oleson, N. L., K. T. Chao and H. R. Crane. Effect of crystalline structure on the multiple scattering of electrons—201(A)
O'Neal, R. D. and M. Goldhaber. Decay constant of H^3—574
Ott, L. H. (see Schultz, H. L.)—198(A), 1043
Pao Chia-Shan (see Ch'en Shang-Yi)—1058
Park, R. D. and J. C. Mouzon. Evidence against the existence of an excited state of He^3—43
Parker, H. M. General purpose dosimeter—196(A)
—— (see R. A. Morrison)—196(A)

Parker, W. L. and L. W. Phillips. Spectra of highly ionized argon—93(L)
Pauli, W. Connection between spin and statistics—716
Pearson, G. L. (see Green, C. B.)—204(A)
Pecher, Charles. Long-lived isotope of yttrium—843(L)
Perlow, Gilbert J. Accurate measurement of the energy released in the disintegration of Li^6 by protons—218
—— (see Allison, S. K.)—178(L)
Petrjak, (see Flerov)—89(L)
Phillips, L. W. (see Parker, W. L.)—93(L)
Piccioni, O. (see Bernardini, G.)—1017
Pickering, William H. (see Neher, H. Victor)—665
Pierce, J. A., A. J. Higgs and E. C. Halliday. Decrease in ionization of the F_2 region during solar eclipse—1119(L)
Pincherle, Leo. Partially inverted multiplets in Mg I—251
Pitzer, Kenneth S. (see Alvarez, Luis W.)—1003(L)
Plain, G. J. (see Young, Victor J.)—498
Pollard, Ernest (see Shrader, E. F.)—199(A)
—— **and William W. Watson.** Transmutation of the separated isotopes of neon by deuterons—12
Potter, James G. Reply to remarks on the temperature dependence of the work function of tungsten—928(L)
—— Temperature dependence of the work function of tungsten from measurement of contact potentials by the Kelvin method—623
Powell, Wilson M. Photon production of mesotrons—474(L)
Primakoff, H. (see Holstein, T.)—1098
Privette, William (see Thaxton, Hubert M.)—200(A)
Ragan, G. L. (see Kanne, W. R.)—693
Ramsey, N. F., Jr. Diamagnetism and the quadrupole moment of hydrogen molecules—190(A)
—— Rotational magnetic moments of H_2, D_2, and HD molecules. Rotational radiofrequency spectra of H_2, D_2, and HD in magnetic fields—226
Ramsey, W. E. Period of photon emission in a counter discharge—476(L)
—— (see Swann, W. F. G.)—477(L)
Randall, R. H. and Clarence Zener. Internal friction of aluminum—472
Randels, R. B., K. T. Chao and H. R. Crane. Single scattering of electrons—201(A)
Rasetti, Franco. Capture cross sections for thermal energy neutrons. II—869
—— Scattering of thermal neutrons by crystals—321
—— (see Lapointe, Christian)—554
Read, Thomas A. Internal friction of single metal crystals—371
Reed, D. W. (see Morgan, F.)—205(A)
Regener, Victor H. (see Rossi, Bruno)—837
Reynolds, L. M. (see Stewart, G. W.)—174
Richards, Hugh T. and Emmett Hudspeth. Photographic plate spectrum of $d-d$ neutrons—382(L)
Rinehart, John S. Temperature dependence of Young's modulus of beta-brass single crystals—365
Ringo, Roy. Velocity spectrum of α-particles—942
Roberson, J. H., J. E. Mack and G. R. Harrison. Interactions in the tungsten atom, W I, in a magnetic field—895
Rochester, G. D. (see Rossi, B.)—761
Rogers, Eric. Model showing variable astigmatism—1121(T)
Rogers, M. M., W. E. Bennett, T. W. Bonner, and Emmett Hudspeth. Resonances in the emission of protons from the reaction $C^{12}+H^3$—186(L)
Rojansky, V. Cosmic rays and comets—1010(L)
Rose, M. E. Electron path lengths in multiple scattering—90(L)
Rossi, Bruno and Victor H. Regener. Production of mesotrons by penetrating non-ionizing rays—837
—— **L. Jánossy, G. D. Rochester and M. Bound.** On the production of secondary ionizing particles by non-ionizing agents in cosmic radiation—761
Roussinow, L. I. (see Grinberg, A. P.)—181(L)
Ruben, Samuel (see Kamen, Martin D.)—194(A)
Rubens, Sidney M. (see Kaplan, Joseph)—188(A)
—— **and J. E. Henderson.** Characteristics and function of anode spots in glow discharges—446
—— **and Joseph Kaplan.** Afterglow in nitrogen-helium mixtures—188(A)
Rubenstein, Pearl J. Relative intensities of $^1S-{}^3P$ and $^1S-{}^1P$ transitions in Mg—1007(L)
Rudnick, Philip, F. G. Slack and John O'Connor. Rotatory power of nickel sulphate at low temperatures—1003(L)
Rusk, Rogers D. Observer as part of an experimental system—1120(T)
Russell, Henry Norris, Robert B. King and Charlotte E. Moore. Arc spectrum of cobalt—407
Sachs, R. G. (see Lyddane, R. H.)—1008(L)
Sakata, Shoichi. Connection between the meson decay and the beta-decay—576(L)
Sampson, J. B. and Frederick Seitz. Theoretical magnetic susceptibilities of metallic lithium and sodium—633
Saunderson, J. L. (see Goudsmit, S.)—36
Sawyer, R. A. (see Schauls, Sister M. Roswitha)—781
Schade, James W. Physics in the manufacture and use of rubber—1120(T)
Scharff-Goldhaber, Gertrud (see Good, William E.)—89(L)
Schauls, Sister M. Roswitha and R. A. Sawyer. New lines and terms in the arc and first spark spectra of molybdenum: Mo I and Mo II—781
Schein, Marcel, E. O. Wollan and Gerhart Groetzinger. Study of the production and absorption of mesotrons in the substratosphere—1027
Schiff, L. I. (see Morrison, P.)—24, 190(A)
Schneider, E. G. (see Oldenberg, O.)—1121(A)
Schoenberg, M. (see Gamow, G.)—1117(L)
Schremp, E. J. and Alfredo Baños, Jr. On the fine structure pattern of cosmic rays at Mexico City—662(L)
Schuchard, E. A. On the ratio N of scattering to capture cross section for thermal neutrons in paraffin—189(A)
—— **and E. A. Uehling.** Further exact solutions of the Boltzmann equation applicable to the diffusion of neutrons—196(A)
—— **and E. A. Uehling.** Steady-state diffusion under conditions of generalized source and incident current distributions—611

Schultz, Howard L., W. L. Davidson, Jr. and L. H. Ott. Application of a cloud chamber to the detection of charged particle groups—198(A)
——, **W. L. Davidson, Jr. and L. H. Ott.** Protons from carbon and aluminum bombarded by deuterons—1043
—— **and William W. Watson.** Protons from the separated isotopes of carbon and neon under deuteron bombardment—1047
Schuman, Ralph H. (see Hoff, Lu)—199(A)
Schwinger, Julian. Neutron scattering in ortho- and para-hydrogen and the range of nuclear forces—1004(L)
—— (see Corben, H. C.)—191(A), 953
—— (see Motz, Lloyd)—26
Sears, W. C. Infra-red spectra of rubber—1120(T)
Seeger, R. J. and E. Teller. Electric breakdown of alkali halides—279(L)
Segrè, E. (see Corson, D. R.)—672
Seitz, Frederick (see Sampson, J. B.)—633
Seligmann, Paul. Theoretical maxima and minima in the anomalous scattering of alpha-particles—492
Shaw, C. H. (see Munier, J. H.)—537
—— **and T. M. Snyder.** Electron scattering in bromine gas—600
Sheppard, S. E. Photographic reversal—93(L)
Shoupp, W. E. (see Haxby, R. O.)—92(L), 199(A), 1035
—— (see Wells, W. H.)—162
Shrader, E. F. Nuclear spin of Cl^{37}—475(L)
—— **and E. Pollard.** Protons from deuteron bombardment of separated chlorine isotopes—199(A)
——, **S. Millman and P. Kusch.** On the nuclear gyromagnetic ratios of the chlorine isotopes—925(L)
Sibaiya, L. Hyperfine structure of ionized mercury lines—925(L)
Sidhu, S. S. (see Letner, Harold R.)—206(A)
—— **and Marc Darrin.** X-ray diffraction studies of anhydrous chromic oxides prepared by different methods—206(A)
Skaggs, Lester S. (see Allison, S. K.)—178(L)
Skellett, A. M. The coronaviser—1121(T)
Slack, C. M. Field emission x-ray tube—206(A)
Slack, F. G. (see Rudnick, Philip)—1003(L)
Slater, J. C. Note on the effect of pressure on the Curie point of iron-nickel alloys—54
Slepian, Joseph and W. E. Berkey. Arc cathodes of low current density at high amperage—204(A)
—— **and W. E. Berkey.** Spark gaps with short time lag—210(A)
Sloan, David H., and Lauriston C. Marshall. Ultra-high frequency power—193(A)
Smith, Fred H. (see Zartman, I. F.)—208(A)
Smith, Lincoln G. and V. Williams. Rotational structure of some fundamental infra-red bands of deuterated formic acid—208(A)
Smith, Nicholas M. (see Allison, S. K.)—178(L)
Smoluchowski, R. (see Calus, H.)—205(A)
—— (see Drynski, T.)—207(A)
Snyder, T. M. (see Shaw, C. H.)—600
Sommers, H. S., Jr. (see Oldenberg, O.)—1121(A)
Spedding, F. H. Absorption of praseodymium ion in solutions and in the solid state—255
Spees, A. H. and C. T. Zahn. Specific charge of the positron—861
Spitzer, Lyman, Jr. Impact broadening of spectral lines—348
Sponer, H. (see Coy, Nettie H.)—709
Squire, Charles F. Abnormal diamagnetism of Ge at low temperatures; specific heat of Zr—202(A)
Starr, C. Magnetic properties of the iron group anhydrous chlorides at low temperatures. II. Theoretical—984
—— **and A. R. Kaufmann.** Magnetic properties of metallic cerium—657(L)
——, **F. Bitter and A. R. Kaufmann.** Magnetic properties of the iron group anhydrous chlorides at low temperatures. I. Experimental—977
Staub, H. and H. Tatel. Anomalous scattering of neutrons by helium. (II)—820
Steigman, J. (see Glasoe, G. N.)—1
Stephens, W. E. (see Haxby, R. O.)—92(L), 199(A), 1035
—— (see Langer, Alois)—759(L)
—— (see Wells, W. H.)—162
Stephenson, S. T. Comparison of x-ray absorption fine structure for two elements in the same crystal—873
—— Note on possible Kronig fine structure in x-ray emission spectra—877
—— X-ray absorption fine structure comparison for two elements in the same crystal—195(A)
Stevenson, A. F. On the theory of the magnetic resonance method of determining nuclear moments—1061
Stever, H. G. (see Neher, H. V.)—191(A), 766
Stewart, G. W., D. O. Holland and L. M. Reynolds. Orientation of liquid crystals by heat conduction—174
Stockbarger, D. C. (see King, Robert B.)—187(A)
Straley, J. W., C. H. Tindal and H. H. Nielsen. Study of the frequencies ν_2 and ν_4 in the infra-red spectrum of SiH_4 and GeH_4—1002(L)
Streib, J. F., W. A. Fowler and C. C. Lauritsen. Disintegration of fluorine by protons—191(A)
Sugawara, Y. (see Okuda, T.)—578(L)
Sugimoto, Asao (see Amaki, Toshio)—659(L)
Sullivan, William H. (see Fajans, Kasimir)—276(L)
Sutton, R. B. (see Barkas, W. H.)—194(A), 383(L)
—— (see Creutz, E. C.)—481
Street, J. N. and J. H. Dillon. Physical characteristics of synthetic rubber—1120(T)
Swann, W. F. G. Theory of cosmic-ray phenomena based upon a single primary component—200(A)
—— **and W. E. Ramsey.** Secondary peak in the Rossi curve for tin—477(L)
Tamm, Ig. Mesons in a Coulomb field—952
—— (see Landau, L.)—1006(L)
Taschek, R. F. (see Kanne, W. R.)—693
Tate, John T. (see Mann, Marvin M.)—340
Tatel, H. (see Staub, H.)—820
Teller, Edward (see Kuper, J. B. Horner)—602
—— (see Seeger, R. J.)—279(L)
Thaxton, Hubert M., William Privette and Daniel Leatherberry. *P*-wave effects on proton-proton scattering in the meson theory—200(A)
Thomas, C. D. and R. C. Colwell. Wave reflections at oblique incidence—203(A)

Thomas, R. Internal pair production in radium C′—714
Tindal, C. H. (see Straley, J. W.)—1002(L)
Tomboulian, D. H. and R. F. Bacher. Evidence for a nuclear electric quadrupole moment for Sb^{123}—52
Tomonaga, S. and G. Araki. Effect of the nuclear Coulomb field on the capture of slow mesons—90(L)
Trump, J. G. Electrostatic x-ray generators for medical use—1120(T)
Turner, C. M. (see Herb, R. G.)—579(L)
Turner, Louis A. Radioactive isotopes of vanadium—679
—— Regularities among the heavy nuclei—181(L)
Uehling, E. A. Density distribution in steady-state diffusion—190(A)
—— (see Schuchard, E. A.)—196(A), 611
Umeda, Kwai. Accurate solution of the Thomas-Fermi-Dirac equation—92(L)
Valasek, Joseph. X-ray emission spectra and electronic energy bands of compounds—213
Van Allen, J. A. (see Huntoon, R. D.)—97
Van Atta, C. M. (see Northrup, D. L.)—199(A)
Van Atta, L. C. (see Northrup, D. L.)—199(A)
Van de Graaff, R. J. (see Northrup, D. L.)—199(A)
Vincent, Mabel S. (see Wick, Frances G.)—578(L)
Vinti, John P. Isotope shifts in boron—879
—— Theorem on nuclear motion in atomic spectra—882
Voigt, Adolf (see Fajans, K.)—177(L)
Walker, H. N. (see Altmann, George O.)—1011
Walker, L. R. (see Ferguson, A. J.)—666
Warner, A. H. and R. H. Neil. Four-gram radium pack of improved design—195(A)
Warren, R. E. (see Herb, R. G.)—579(L)
Watson, William W. (see Pollard, Ernest)—12
—— (see Schultz, Howard L.)—1047
Watt, Bob E. (see Bennett, W. E.)—478(L)
Wells, W. H. (see Haxby, R. O.)—92(L), 199(A), 1035
——, **R. O. Haxby, W. E. Stephens and W. E. Shoupp.** Design and preliminary performance tests of the Westinghouse electrostatic generator—162
Wet, J. S. de. On the spinor equations for particles with arbitrary spin and rest mass zero—236
Wheeler, John A. and H. H. Barschall. Scattering of 2.5-Mev neutrons in helium—682
Whitaker, Martin D. (see Murphy, Edgar J.)—88(L)
White, M. G. (see Barkas, W. H.)—194(A), 383(L)
—— (see Creutz, E. C.)—481
—— (see Delsasso, L. A.)—586
Whitehead, W. L. (see Goodman, Clark)—1121(A)
Wick, Frances G. and Mabel S. Vincent. Luminescence excited by exposure to neutrons—578(L)
Wick, G. C. (see Bernardini, G.)—1017
Wiens, Jacob and Luis W. Alvarez. Spectroscopically pure mercury (198)—1005(L)
Wigner, E. (see Margenau, H.)—103
Wilkins, T. R. and G. Wrenshall. Nuclear energy levels in magnesium—758(L)
Williams, A. O., Jr. Relativistic self-consistent field for Cu^+—723
Williams, E. J. Multiple scattering of fast electrons and alpha-particles, and "curvature" of cloud tracks due to scattering—292
Williams, H. J. (see Bozorth, R. M.)—203(A), 210(A)
——, **R. M. Bozorth and H. Christensen.** Change of length and Young's modulus with magnetization and heat treatment—203(A)
Williams, V. (see Smith, Lincoln G.)—208(A)
Wilson, G. Harold. Theory of gaseous isotope separation in a force field with application to the ultracentrifuge—209(A)
Winch, Ralph P. (see Farnsworth, H. E.)—812
Witmer, Enos E. Theoretical magnetic susceptibility of molecular deuterium as compared with that of molecular hydrogen—202(A)
Wollan, E. O. (see Schein, Marcel)—1027
Wood, Lawrence A. Optical properties of rubber—1120(T)
Wooldridge, D. E. Temperature effects in secondary emission—316
—— **and C. D. Hartman.** Effects of order and disorder on secondary electron emission—381(L)
Wrenshall, G. (see Wilkins, T. R.)—758(L)
Wright, B. T. (see Livingston, R. S.)—656(L)
Wu, C. S. Identification of two radioactive xenons from uranium fission—926(L)
Wu, Ta-You. On the satellite lines in atomic spectra and the excitation of electrons from closed shells—1114
Wyckoff, H. O. and J. E. Henderson. Spatial asymmetry of Cerenkov radiation as a function of electron energy—187(A)
Yasaki, T. (see Nishina, Y.)—660(L)
Yost, W. Jacque. Fock equations and diamagnetic susceptibility for magnesium III—202(A)
—— Self-consistent fields and diamagnetic susceptibility for magnesium III—557
Young, Victor J., A. Ellett and G. J. Plain. Distribution in angle of alpha-particles from lithium bombarded with protons—498
Yunker, E. A. Diurnal variation of the mobility spectrum of the atmospheric ions and the effect of age of ion—193(A)
Zahn, C. T. (see Spees, A. H.)—861
Zartman, I. F. and Fred H. Smith. Absorption of supersonic waves in gases—208(A)
Zener, Clarence (see Barnes, Arthur H.)—87(L)
—— (see Randall, R. H.)—472
Zwicky, F. Hydrodynamics and the morphology of nebulae—478(L); Erratum—758(L)

Analytic Subject Index to Volume 58

References with (A) are to abstracts of papers presented at meetings of the American Physical Society.
References with (L) are to Letters to the Editor.

Acoustics
Ultrasonic absorption in gases, I. F. Zartman, F. H. Smith—208(A)
Ultrasonic absorption in liquids, E. C. Gregg, Jr.—208(A)

Afterglow
In N_2–He, S. M. Rubens, J. Kaplan—188(A)
Temporal effects, J. Kaplan, S. M. Rubens—188(A)

Arcs (see **Discharge of electricity in gases**)

Astrophysics
Cosmic rays and comets, V. Rojansky—1010(L)
Morphology of nebulae, F. Zwicky—478(L); Erratum—758(L)
Neutrinos and stellar evolution, G. Gamow, M. Schoenberg—1117(L)

Atomic and molecular beams
Diffraction and reflection of molecular beams, W. H. Bessey—207(A)

Atomic structure (see also **Spectra, atomic**)
Relativistic self-consistent field for Cu^+, A. O. Williams, Jr.—723

Biophysics
Dosimeter, general purpose, H. M. Parker—196(A)
Electron microscope, Fresnel diffraction, J. Hillier—842(L)
Fluorescence method of identifying bacterial ring rot, H. C. Kelly, V. E. Iverson—189(A)
Photographic recording of gamma-radiation, R. A. Morrison, H. M. Parker—196(A)
Radium pack for treatment, A. H. Warner, R. H. Neil—195(A)

Constants, physical, standards
Charge of β-particle, R. Ladenburg, Y. Beers—757(L)
Fine structure constant, precise determination, R. F. Christy, J. M. Keller—658(L)
Isometric consistency chart for natural constants, J. W. M. DuMond—457
Ratio of e, c, and h, A. Landé—843(L)
Specific charge of positron, A. H. Spees, C. T. Zahn—861
Values of e, e/m, h/e and α, R. T. Birge—658(L)

Contact potentials
Of crystal faces, H. E. Farnsworth, R. P. Winch—812
Temperature dependence of work function, J. G. Potter—623, 928(L); W. B. Nottingham—927(L)

Cosmic radiation
Absorption in Pb at depth of 1000 m water, J. Barnóthy, M. Forró—844(L)
Air mass effect, D. H. Loughridge, P. F. Gast—194(A), 583; H. Arakawa—1118(L)
From comets, V. Rojansky—1010(L)
Decay of penetrating components, E. Nelson—771
Effect of an eclipse, A. H. Compton—841(L)
Electronic and mesotronic component, G. Bernardini, B. N. Cacciapuoti, B. Ferretti, O. Piccioni, G. C. Wick—1017
Fine structure in directional intensity, D. Cooper—288; E. J. Schremp, A. Baños, Jr.—662(L)
Ionizing particles from non-ionizing agents, B. Rossi, L. Jánossy, G. D. Rochester, M. Bound—761
Latitude effect above 50°N, P. F. Gast, D. H. Loughridge—194(A)
Latitude effect for showers, H. V. Neher, W. H. Pickering—665
Latitude effect at southern latitudes, E. T. Clarke, S. A. Korff—179(L), 201(A)
Lifetime of mesotron, H. V. Neher, H. G. Stever—191(A), 766
Main and shadow cones, H. P. Koenig—385
Production and absorption of mesotrons, M. Schein, E. O. Wollan, G. Groetzinger—1027
Production of mesotrons at 29,000 feet, G. Herzog, W. H. Bostick—278(L)
Rossi curve for tin, W. F. G. Swann, W. E. Ramsey—477(L)
At sea level, counter studies, G. O. Altmann, H. N. Walker, V. F. Hess—1011
Theory based upon single primary component, W. F. G. Swann—200(A)
Time-variation at high altitudes, W. P. Jesse—281

Crystalline state
Aging in oversaturated solid solutions, H. Calus, R. Smoluchowski—205(A)
Anhydrous chromic oxides, properties of, S. S. Sidhu, M. Darrin—206(A)
Constitution of metallic beryllium, C. Herring, A. G. Hill—132
Distribution in Al-Ag alloys during aging, C. S. Barrett, A. H. Geisler—206(A)
Electric breakdown of alkali halides, R. J. Seeger, E. Teller—279(L)
Electronic energy bands of compounds, J. Valasek—213
Ferromagnetic anisotropy and itinerant electron model, H. Brooks—909
Fields in crystals, R. H. Lyddane, K. F. Herzfeld, R. G. Sachs—1008(L)
Grain boundary substance in Cd, B. L. Miller—206(A)
Internal friction of Al, R. H. Randall, C. Zener—472
Internal friction at high temperatures, A. H. Barnes, C. Zener—87(L)
Internal friction single metal crystals, T. A. Read—371
Liquid crystals, orientation by heat conduction, G. W. Stewart, D. O. Holland, L. M. Reynolds—174
Order in Fe-Ni alloys; neutron transmission, F. C. Nix, H. G. Beyer, J. R. Dunning—1031
Resistance and order-disorder in Cd-Mg alloys, M. A. Benson, G. A. Anslow—1121(A)

Crystalline state (continued)
Rochelle salt, properties of, H. Mueller—565, 805
Self-consistent solution to vacancy problem in metals, H. B. Huntington—209(A)
Silver-rich, Ag-Mg alloys, H. R. Letner, H. H. George, S. S. Sidhu—206(A)
Single-crystal Al wires, law of Magnus, C. Y. Ma, W. Band—479(L)
Torsional frequencies of crystal specimens, W. F. Brown, Jr.—998
Van der Waals forces at metallic surfaces, J. Bardeen—727
Young's modulus of beta-brass single crystals, J. S. Rinehart—365

Dielectric constants (see **Dielectrics and dielectric properties**)
Dielectrics and dielectric properties
Electric fields in vibrating crystals, R. H. Lyddane, K. F. Herzfeld, R. G. Sachs—1008(L)
Of gases and water vapor at high frequencies, J. P. Hagen, M. Distad, F. C. Iseley—208(A)
Diffraction of electrons (see **Electron diffraction**)
Diffusion (see also **Thermal diffusion**)
Distribution in steady-state, E. A. Uehling—190(A)
Solutions of Boltzmann equation, E. A. Schuchard, E. A. Uehling—196(A)
Steady-state diffusion conditions, E. A. Schuchard, E. A. Uehling—611
Temperature in measurements of coefficients, H. Brown—661(L)
In ultracentrifuge, isotope separation, G. H. Wilson—209(A)
Discharge of electricity in gases
Anode spots in glow discharges, S. M. Rubens, J. E. Henderson—446
Arc cathodes of low current density, J. Slepian, W. E. Berkey—204(A)
Breakdown potential for sphere-gaps, J. M. Meek—195(A)
Photographs of copper arc, R. C. Mason—204(A)
Positive corona discharge, K. S. Fitzsimmons, L. B. Loeb, J. M. Meek—187(A)
Pulses in negative point-to-plane corona in air, L. B. Loeb, G. G. Hudson, A. F. Kip—195(A)
Reignition voltage measurements, M. Garbuny, L. H. Matthias—182(L)
Spark gaps with short time lag, J. Slepian, W. E. Berkey—210(A)
Sparking potential, initial photoelectric currents, J. M. Meek—196(A)
Sparking threshold in air, W. R. Haseltine—188(A)
Theory of recombination, G. Jaffé—968
Time-lag analysis of Townsend discharge, R. W. Engstrom, W. S. Huxford—67
Disintegration and excitation of nucleus (see also **Radioactivity**)
Anomalous scattering of α-particles, maxima and minima, P. Seligmann—492
Directional correlation of successive quanta, D. R. Hamilton—122
Distribution in angle, α-particles from F, W. B. McLean, A. Ellett, J. A. Jacobs—500
Distribution in angle, α-particles from Li, V. J. Young, A. Ellett, G. J. Plain—498
Distribution in angle in $F^{19}(p,\alpha)$, E. Gerjuoy—503
Distribution in angle of protons, R. D. Huntoon, A. Ellett, D. S. Bayley, J. A. Van Allen—97
Emission of three particles from excited nucleus, J. M. Cork, W. Middleton—474(L)
Energy of α-particles in $Li^6(p,\alpha)He^3$, G. J. Perlow—218; L. C. Miller—936
Energy released in $Li^6(p,\alpha)He^3$, S. K. Allison, L. C. Miller, G. J. Perlow, L. S. Skaggs, N. M. Smith, Jr.—178(L)
Of F by H^1, J. F. Streib, W. A. Fowler, C. C. Lauritsen—191(A)
γ-ray resonances from carbon, W. E. Bennett, T. W. Bonner—183(L)
γ-rays from $C^{13}+H^1$, C. C. Lauritsen, W. A. Fowler—193(A)
γ-rays from $N^{15}+H^1$, W. A. Fowler, C. C. Lauritsen—192(A)
Of H^2, Be and In by x-rays, D. L. Northrup, C. M. Van Atta, R. J. Van De Graaff, L. C. Van Atta—199(A)
Of isotopes of C and Ne, half-life of C^{14}, H. L. Schultz, W. W. Watson—1047
Neutrons from $C^{12}+H^2$, resonances, T. W. Bonner, E. Hudspeth, W. E. Bennett—185(L)
Of N^{14} and N^{15} by deuterons, M. G. Holloway, B. L. Moore—847
Photonuclear disintegration of Fe and Mn, P. R. Carlson, J. E. Henderson—193(A)
Protons from C and Al, H. L. Schultz, W. L. Davidson, Jr., L. H. Ott—1043
Protons from $C^{13}+H^2$, W. E. Bennett, T. W. Bonner, E. Hudspeth, B. E. Watt—478(L)
Protons from $C^{12}+H^2$, resonances, M. M. Rogers, W. E. Bennett, T. W. Bonner, E. Hudspeth—186(L)
Protons from Cl isotopes, E. F. Shrader, E. Pollard—199(A)
Reactions $B^{11}(p,n)C^{11}$ and $N^{14}(p,\alpha)C^{11}$, L. A. Delsasso, M. G. White, W. Barkas, E. C. Creutz—586
Resonances in nuclear reactions, G. Breit—506
Thresholds for (p,n) reactions of Li, Be, B, and C, R. O. Haxby, W. E. Shoupp, W. E. Stephens, W. H. Wells—1035
Dissociation
Of water vapor and ammonia by electron impact, M. M. Mann, A. Hustrulid, J. T. Tate—340

Elasticity
Compressibility of hydrocarbons, pressure-temperature dependence, B. L. Hicks—209(A)
Hysteresis phenomena in Rochelle salt, W. P. Mason—744
Internal friction of Al, R. H. Randall, C. Zener—472
Internal friction single metal crystals, T. A. Read—371
Near phase transitions, H. F. Ludloff—209(A)

Elasticity (continued)
Torsional frequencies, W. F. Brown, Jr.—998
Young's modulus of beta-brass single crystals, J. S. Rinehart—365
Young's modulus, heat treatment and magnetization, H. J. Williams, R. M. Bozorth, H. Christensen—203(A)
Young's modulus and Poisson's ratio by x-ray method, L. L. Davenport—206(A)
Electrical conductivity and resistance
Boundary conditions for superconductor, E. Cook—361
Directional dependence, E. M. Baroody—793
Electric breakdown of alkali halides, R. J. Seeger, E. Teller—279(L)
High frequency resistance of Fe, J. B. Hoag, C. R. Cox—203(A)
And order-disorder in Cd-Mg alloys, M. A. Benson, G. A. Anslow—1121(A)
Of tartaric acid crystals, J. J. Brady, B. Elle—195(A)
Theory of superconductors, E. Cook—357
Electromagnetic theory
Electromagnetic waves inside metal guide, Hsü Chang Pen—193(A)
Interaction energies in radiation theory, H. Hurwitz, Jr.—467
Wave reflections at oblique incidence, C. D. Thomas, R. C. Colwell—203(A)
Electron diffraction
On glass surface, Hirosi Kamogawa—660(L)
Electrons (see also **Positrons**)
Pair production, J. R. Feldmeier, G. B. Collins—200(A)
Electrons, secondary
Effects of order and disorder, D. E. Wooldridge, C. D. Hartman—381(L)
From Pt on Al, P. L. Copeland—604
Produced by He, Ne, and A ions on Ni, M. Healea, C. Houtermans—608
Temperature effects, D. E. Wooldridge—316
Errata
On the angular distribution of fast neutrons scattered by hydrogen, deuterium, and helium, H. H. Barschall, M. H. Kanner—1010(L)
Hydrodynamics and the morphology of nebulae, F. Zwicky—758(L)
Excitation of nuclei (see **Disintegration and excitation of nucleus**)

Field currents
Into dielectric liquids, W. R. LePage, L. A. DuBridge—61
Energy losses, G. M. Fleming, J. E. Henderson—887
From tantalum, G. M. Fleming, D. M. Holtoner—189(A)
In x-ray tube, C. M. Slack—206(A)
Fission of nucleus
Cloud-chamber studies of tracks, K. J. Brostrøm, J. K. Bøggild, T. Lauritsen—651
Deuteron induced in U and Th, I. C. Jacobsen, N. O. Lassen—867
Fast neutron threshold for U fission, R. O. Haxby, W. E. Shoupp, W. E. Stephens, W. H. Wells—199(A)
Heat of fission of U, M. C. Henderson—200(A), 774
Passage of U fission fragments through matter, W. E. Lamb, Jr.—696
Photo-fission, R. O. Haxby, W. E. Shoupp, W. E. Stephens, W. H. Wells—92(L)
Products from gases in U fission, G. N. Glasoe, J. Steigman—1
Radioactive Ba and Sr from photo-fission of U, A. Langer, W. E. Stephens—759(L)
Radioactive Xe isotopes, C. S. Wu—926(L)
Scattering and stopping of fragments, N. Bohr—654
Spontaneous fission of U, Flerov and Petrjak—89(L)
Successive transformations, N. Bohr—864
Of U by fast neutrons, Y. Nishina, T. Yasaki, K. Kimura, M. Ikawa—660(L)
Velocity-range relation for fragments, N. Bohr, J. K. Bøggild, K. J. Brostrøm, T. Lauritsen—839
Friction
Boundary lubrication, F. Morgan, M. Muskat, D. W. Reed—205(A)
Internal friction of Al, R. H. Randall, C. Zener—472
Internal friction, single metal crystals, T. A. Read—371

Geophysics
Magnetism of earth, J. C. Slater—54
Radioactivity of rocks and associated petroleum, C. Goodman, K. G. Bell, W. L. Whitehead—1121(A)
Gyromagnetization (see **Magnetic properties**)

High voltage tubes and machines
Electrostatic generator, concentric electrodes, R. G. Herb, C. M. Turner, C. M. Hudson, R. E. Warren—579(L)
Induction accelerator, D. W. Kerst—841(L)
Westinghouse electrostatic generator, W. H. Wells, R. O. Haxby, W. E. Stephens, W. E. Shoupp—162
Hyperfine structure (see also **Nuclear moments and spin**)
Of Sb^{121}, D. H. Tomboulian, R. F. Bacher—52
Of forbidden lines of Pb I, S. Mrozowski—1086
Upon magnetic rotation, B. J. Miller—258
Of Hg lines, L. Sibaiya—925(L)
Radiofrequency spectra of Na, Rb, and Cs, S. Millman, P. Kusch—438

Instruments (see **Methods and instruments**)
Ionization by collision (see **Ionization potentials**)
Ionization potentials
Of ions from methyl and ethyl alcohol, C. S. Cummings, II., W. Bleakney—787
Of H_2O and NH_3 vapor, M. M. Mann, A. Hustrulid, J. T. Tate—340
Ionosphere
Ionization during eclipse, J. A. Pierce, A. J. Higgs, E. C. Halliday—1119(L)
Ions, high speed
Of C^{++++++}, L. W. Alvarez—192(A)
Ions, mobility
Diurnal variation of atmospheric ions, E. A. Yunker—193(A)
In insulating liquids, A. Gemant—904
In pure H_2 high current densities, W. H. Bennett—992

Isotopes
Of carbon, L. A. Delsasso, M. G. White, W. Barkas, E. C. Creutz—586
$C^{13}H_2-N^{14}$ mass difference, E. B. Jordan—1009(L)
Clusius-Dickel isotope separator, W. Krasny-Ergen—1078
Isotopic weights of Cl, A, and Fe, T. Okuda, K. Ogata, K. Aoki, Y. Sugawara—578(L)
Mass of He^3, S. K. Allison, L. C. Miller, G. J. Perlow, L. S. Skaggs, N. M. Smith, Jr.—178(L)
Pure Hg^{198}, J. Wiens, L. W. Alvarez—1005(L)
Separation in centrifuge, G. H. Wilson—209(A)

Kinetic theory of gases
Transport cross section of He, E. J. Hellund—278(L)

Liquids
Diffraction of x-rays by liquid argon, A. Eisenstein, N. S. Gingrich—307
Structure of liquid argon, E. P. Miller, K. Lark-Horovitz—207(A)
Structure of liquid benzene, cyclohexane, and their mixtures, W. P. Davey, P. H. Bell—207(A)

Luminescence
Excited by neutrons, F. G. Wick, M. S. Vincent—578(L)
Spectrum of zinc sulphide powders, effect of activator, C. J. Brasefield—436
Theory of cathode luminescence, Ugo Fano—544

Magnetic moments (see also **Nuclear moments and spin**)
Of H_2, D_2, and HD, N. F. Ramsey, Jr.—226

Magnetic properties
Anisotropy and itinerant electron model, H. Brooks—909
Anomalous magnetic torque curves, R. M. Bozorth, H. J. Williams—210(A)
Change of length and Young's modulus, H. J. Williams, R. M. Bozorth, H. Christensen—203(A)
Colloid patterns on ferromagnetic crystal surfaces, W. C. Elmore—640
Curie point, effect of pressure, J. C. Slater—54
Diamagnetic susceptibility for Mg III, W. J. Yost—202(A), 557
Diamagnetism of H_2, N. F. Ramsey, Jr.—190(A)
Domain magnetization, T. Holstein, H. Primakoff—1098
Gyromagnetic ratios of Cl isotopes, E. F. Shrader, S. Millman, P. Kusch—925(L)
Of Fe-Al alloys, R. M. Bozorth, H. J. Williams, R. J. Morris, Jr.—203(A)
Of Ge, abnormal diamagnetism, C. F. Squire—202(A)
Of iron group chlorides, experimental, C. Starr, F. Bitter, A. R. Kaufmann—977
Of iron group chlorides, theoretical, C. Starr—984
Magnetic saturation, theory of, W. F. Brown, Jr.—202(A), 736
Of metallic Ce, C. Starr, A. R. Kaufmann—657(L)
Permeability of iron in a high frequency field, J. B. Hoag, C. R. Cox—203(A)
Susceptibilities of Ni and Ni alloys, K. E. Keyes—202(A)
Susceptibility of molecular deuterium, E. E. Witmer—202(A)
Theoretical susceptibilities of Li and Na, J. B. Sampson, F. Seitz—633
Vicalloy, a new permanent magnet material, E. A. Nesbitt, G. A. Kelsall—203(A)

Mass defects (see **Isotopes**)

Mechanics, quantum—atomic structure and spectra
Thomas-Fermi-Dirac equation, Kwai Umeda—92(L)

Mechanics, quantum—general
Force fields from scattering, F. C. Hoyt, W. E. Frye—784
"Radius" of elementary particles, L. Landau—1006(L)
Scattering matrix of radioactive states, G. Breit—1068
Spin and statistics, W. Pauli—716
Spinor equations for particles, J. S. de Wet—236

Mesotrons (see also **Cosmic radiation**)
Capture of slow mesons, S. Tomonaga, G. Araki—90(L)
In Coulomb field, Ig. Tamm—952
Electromagnetic properties, H. C. Corben, J. Schwinger—191(A), 953
Interaction with γ-rays, R. F. Christy, S. Kusaka—191(A)
Mean lifetime, H. V. Neher, H. G. Stever—191(A), 766; E. Nelson—771 (See footnote p. 1019)
Meson decay and beta-decay, Shoichi Sakata—576(L)
Produced by photon, W. M. Powell—474(L)
Production by non-ionizing rays, B. Rossi, V. H. Regener—837
Production at 29,000 feet, G. Herzog, W. H. Bostick—278(L)
In substratosphere, M. Schein, E. O. Wollan, G. Groetzinger—1027
Theory of, C. Møller—1118(L)

Methods and instruments
Atmospheric pressure G-M counters, S. C. Brown—1121(A)
Canal-ray ion source, W. H. Goss, J. E. Henderson—192(A)
Cauchois focusing x-ray spectrograph, F. R. Hirsh, Jr.—78
Charge of β-particle, direct determination, R. Ladenburg, Y. Beers—757(L)
"Curvature" of cloud tracks, E. J. Williams—292
Detection of charged particle groups with cloud chamber, H. L. Schultz, W. L. Davidson, Jr., L. H. Ott—198(A)
Dielectric constant at ultra-high frequencies, J. P. Hagen, M. Distad, F. C. Iseley—208(A)
Dosimeter, general purpose, H. M. Parker—196(A)
Efficiency of γ-ray counters, F. Norling—277(L)
Electron diffraction on glass surface, Hirosi Kamogawa—660(L)
Electron microscope, L. Marton—57
Electron microscope, Fresnel diffraction, J. Hillier—842(L)
Electrostatic deflection of α-particles, L. C. Miller—936
Electrostatic generator, concentric electrodes, R. G. Herb, C. M. Turner, C. M. Hudson, R. E. Warren—579(L)

Methods and instruments (continued)
Extraction of ions from low pressure arc, Hoff Lu, R. H. Schuman—199(A)
Fluorescence method of identifying bacterial ring rot, H. C. Kelly, V. E. Iverson—189(A)
Halation on kinescope screens, R. F. Baker—208(A)
High energy carbon ions, L. W. Alvarez—192(A)
Induction accelerator, D. W. Kerst—841(L)
Industrial radiography, C. Pecher—843(L)
Isotope separator; Clusius-Dickel, W. Krasny-Ergen—1078
Klystron efficiency, E. U. Condon—204(A)
Lattice constants and density, F. Foote, E. R. Jette—81
Magnetic resonance and nuclear moments; theory of, A. F. Stevenson—1061
Magnetic spectrograph for α-particles, R. Ringo—942
Magnetic ultra-micrometer, W. B. Ellwood—204(A)
Period of photon emission, counter discharge, W. E. Ramsey—476(L)
Photographic plate spectrum of $d-d$ neutrons, H. T. Richards, E. Hudspeth—382(L)
Photographic recording of gamma-radiation, R. A. Morrison, H. M. Parker—196(A)
Photographic registration of particles during bombardment, J. M. Cork, P. F. Bartunek—580(L)
Powders of uniform NaCl crystals in various sizes, F.-H. Marshall—642
Precipitation of dirt, R. A. Nielsen—205(A)
Radioactive neutron sources, E. J. Murphy, W. C. Bright, M. D. Whitaker, S. A. Korff, E. T. Clarke—88(L)
Radium pack for treatment, A. H. Warner, R. H. Neil—195(A)
Sensitive time of cloud chamber, W. E. Hazen—194(A)
Source of "forbidden" lines, S. Mrozowski—1086
Thermistor voltage regulator, C. B. Green, G. L. Pearson—204(A)
Ultra-high frequency power, D. H. Sloane, L. C. Marshall—193(A)
Vicalloy, a new permanent magnet material, E. A. Nesbitt, G. A. Kelsall—203(A)
Westinghouse electrostatic generator, W. H. Wells, R. O. Haxby, W. E. Stephens, W. E. Shoupp—162
Young's modulus and Poisson's ratio by x-ray methods, L. L. Davenport—206(A)

Mobility of ions (see **Ions, mobility**)

Molecular structure and constants (see also **Spectra, molecular** and **Raman spectra**)
Quadrupole moment of H_2, N. F. Ramsey, Jr.—190(A)

Neutrons
Capture cross sections, C. Lapointe, F. Rasetti—554; F. Rasetti—869
Capture by U^{238}, E. T. Booth, J. R. Dunning, A. V. Grosse, A. O. Nier—475(L)
From $C^{12}+H^2$, resonances, T. W. Bonner, E. Hudspeth, W. E. Bennett—185(L)
Cross sections for the (n, α) and (n, p) reactions, Toshio Amaki, Asao Sugimoto—659(L)
Photographic plate spectrum, H. T. Richards, E. Hudspeth—382(L)
Scattering capture cross section ratio, E. A. Schuchard—189(A)
Scattering in He, J. A. Wheeler, H. H. Barschall—682

Nuclear moments and spin (see also **Hyperfine structure**)
Of Cl^{37}, E. F. Shrader—475(L)
Gyromagnetic ratios of Cl isotopes, E. F. Shrader, S. Millman, P. Kusch—925(L)
Magnetic of C^{13}, R. H. Hay—180(L); D. R. Inglis—577(L)
Magnetic of odd nuclei, H. Margenau, E. Wigner—103
Quadrupole moment of Sb^{123}, D. H. Tomboulian, R. F. Bacher—52
Theory of magnetic resonance method, A. F. Stevenson—1061

Nuclear structure (see also **Disintegration of nucleus**)
Directional correlation of successive quanta, D. R. Hamilton—122
Energy levels in Mg, T. R. Wilkins, G. Wrenshall—758(L)
Excited state of He^3, R. D. Park, J. C. Mouzon—43
γ-ray resonances from carbon, W. E. Bennett, T. W. Bonner—183(L)
Ground states of Be^{10} and C^{10}, E. P. Cooper, E. C. Nelson—1117(L)
Lower levels of Br^{80}, A. P. Grinberg, L. I. Roussinow—181(L)
Nature of nuclear forces, L. Landau, I. Tamm—1006(L)
Nuclear forces, theory of, C. L. Critchfield, W. E. Lamb, Jr.—46
Quadrupole moment of Sb^{123}, D. H. Tomboulian, R. F Bacher—52
Quadrupole moment of deuteron, A. Nordsieck—310
Range of forces, J. Schwinger—1004(L)
Regularities among heavy nuclei, L. A. Turner—181(L)
Resonance levels of Rh and In, J. Hornbostel, H. H. Goldsmith, J. H. Manley—18
Resonances in nuclear reactions, G. Breit—506
Spin-orbit coupling in He^5, S. M. Dancoff—190(A), 326

Optical constants and properties
Of alkali metals in ammonia, H. von R. Jaffe—207(A)
Of N_2, A_1, CO_2, optical dispersion and molar refraction, C. E. Bennett—263
Rotatory power of nickel sulphate, P. Rudnick, F. G. Slack, J. O'Connor—1003(L)

Photoelectric effect and properties; cells
Work function of crystal faces, H. E. Farnsworth, R. P. Winch—812

Photography
Photographic reversal, S. E. Sheppard—93(L)

Photons
Period of photon emission, W. E. Ramsey—476(L)

Piezoelectric effect
Hysteresis phenomena in Rochelle salt, W. P. Mason—744
Rochelle salt, properties of, H. Mueller—565, 805

Polarization of radiation
Emitted by exploded wires, W. M. Cohn—50, 188(A)
Resonance radiation, B. J. Miller—258
Positrons
Pair production, J. R. Feldmeier, G. B. Collins—200(A)
Specific charge, A. H. Spees, C. T. Zahn—861
Proceedings of the American Physical Society
Metropolitan Section, Meeting, November 15, 1940—1121
New England Section, Meeting, October 19, 1940—1120
Ohio Section: Ohio State University Meeting, May 9–11, 1940—96; Akron Meeting, October 11–12, 1940—1120
Pittsburgh, Pennsylvania, Meeting, June 20–22, 1940—198
Seattle, Washington, Meeting, June 18–21, 1940—187

Radiation
Cerenkov radiation, spatial asymmetry, H. O. Wyckoff, J. E. Henderson—187(A)
Radio (see also **Ionosphere**)
Variation in intensity of signals, R. C. Colwell—204(A)
Wave reflections at oblique incidence, C. D. Thomas, R. C. Colwell—203(A)
Radioactivity (see also **Disintegration and excitation of nucleus**)
Of Ba and Cs, D. C. Kalbfell, R. A. Cooley—91(L)
β-radiation from Si^{27} and P^{30}, W. H. Barkas, E. C. Creutz, L. A. Delsasso, R. B. Sutton, M. G. White—194(A), 383(L)
β-rays from Cu^{64}, J. Backus—192(A)
Of Br and I bombarded by H^1, E. C. Creutz, L. A. Delsasso, R. B. Sutton, M. G. White, W. H. Barkas—481
Br^{80} isomer, decay of, D. DeVault, W. F. Libby—688
Of C^{14}, M. D. Kamen, S. Ruben—194(A); H. L. Schultz, W. W. Watson—1047
Decay constant of H^3, R. D. O'Neal, M. Goldhaber—574
$(d, 2n)$ reaction in Cu, R. S. Livingston, B. T. Wright—656(L)
Charge of β-particle, R. Ladenburg, Y. Beers—757(L)
Element 85, D. R. Corson, K. R. MacKenzie, E. Segrè—672
Of $_{14}Si^{27}$, $_{16}S^{31}$, and $_{18}A^{36}$, L. D. P. King, D. R. Elliott—846(L)
γ-ray resonances from carbon, W. E. Bennett, T. W. Bonner—183(L)
γ-rays from Re, E. C. Creutz, W. H. Barkas, N. H. Furman—1008(L)
Of Au, J. M. Cork, J. Halpern—201(A)
Internal conversion of γ-radiation, M. H. Hebb, E. Nelson—486
Internal conversion of γ-radiation from Au, J. L. Lawson, J. M. Cork—580(L)
Internal pair production, R. Thomas—714
Isotopes of V, L. A. Turner—679
K-electron capture, P. Morrison, L. I. Schiff—24, 190(A)
Of krypton, E. P. Clancy—88(L)
Long-lived isotopes of Y, C. Pecher—843(L)
Of Mn, proton induced, A. Hemmendinger—929
Multiple scattering of electrons and α-particles, E. J. Williams—292
Of Ne, separated isotopes, E. Pollard, W. W. Watson—12
Photographic recording of γ-radiation, R. A. Morrison, H. M. Parker—196(A)
Possible scheme of radioactive periods, G. R. Dickson, E. J. Konopinski—949
Products from gases in U fission, G. N. Glasoe, J. Steigman—1
Radioactive Br produced by γ-radiation, W. H. Barkas, P. R. Carlson, J. E. Henderson, W. H. Moore—577(L)
Radioactive hydrogen, L. W. Alvarez, R. Cornog—197(A)
Radioactive neutron sources, E. J. Murphy, W. C. Bright, M. D. Whitaker, S. A. Korff, E. T. Clarke—88(L)
Radium pack of improved design for treatment, A. H. Warner, R. H. Neil—195(A)
Resonance capture of neutrons by U^{238}, E. T. Booth, J. R. Dunning, A. V. Grosse, A. O. Nier—475(L)
Of Re and W, K. Fajans, W. H. Sullivan—276(L)
Of rocks and associated petroleum, C. Goodman, K. G. Bell, W. L. Whitehead—1121(A)
Scattering matrix of radioactive states, G. Breit—1068
Of Sr, Y and Zr, L. A. DuBridge, J. Marshall—7
Of Tl, K. Fajans, A. F. Voigt—177(L)
Of U, seven-day activity, E. McMillan—178(L)
Velocity spectrum of α-particles, R. Ringo—942
Of Xe from U fission, C. S. Wu—926(L)
Raman spectra
Cyanate ion, disappearance of, F. F. Cleveland—189(A)
Relativity
Relativity misconceptions, E. M. Little—191(A)
Resonance radiation (see also **Spectra, etc.**)
Magnetic rotation, B. J. Miller—258
Pressure effect, Ch'en Shang-Yi—884

Scattering of electrons, neutrons, and ions (see also **Electron diffraction**)
Of α-particles by C and O, A. J. Ferguson, L. R. Walker—666
Anomalous scattering of α-particles, P. Seligmann—492
Calculation of force fields, F. C. Hoyt, W. E. Frye—784
Capture cross sections for neutrons, C. Lapointe, F. Rasetti—554
Crystalline structure and scattering of electrons, N. L. Oleson, K. T. Chao, H. R. Crane—201(A)
Distribution in angle, α-particles from F, W. B. McLean, A. Ellett, J. A. Jacobs—500
Distribution in angle, α-particles from Li, V. J. Young, A. Ellett, G. J. Plain—498
Distribution in angle of protons from H^2+H^2, R. D. Huntoon, A. Ellett, D. S. Bayley, J. A. Van Allen—97
Electron path lengths, M. E. Rose—90(L)
Electron scattering in Br, C. H. Shaw, T. M. Snyder—600
Electron scattering in He, J. B. H. Kuper, E. Teller—602
Of electrons, S. Goudsmit, J. L. Saunderson—36

Scattering of electrons, neutrons, and ions (continued)
Of electrons by Al, C. T. Chase, R. T. Cox—243
Of fast neutrons scattered by H, D, and He, H. H. Barschall, M. H. Kanner—590, 1010(L)
Of He in He, R. L. Mooney—871
Of neutrons in He, J. A. Wheeler, H. H. Barschall—682; H. Staub, H. Tatel—820
Of neutrons in ortho- and parahydrogen, L. W. Alvarez, K. S. Pitzer—1003(L); J. Schwinger—1004(L)
Proton-proton scattering and meson theory, H. M. Thaxton, W. Privette, D. Leatherberry—200(A)
Of protons by neutrons, W. E. Good, G. Scharff-Goldhaber—89(L)
Resonance scattered protons from B^{11} and F^{19}, search for, W. R. Kanne, R. F. Taschek, G. L. Ragan—693
Resonance scattering of H^1 and n on He, theory of, F. Bloch—829
Scattering, capture cross section ratio for neutrons, E. A. Schuchard—189(A)
Single scattering of electrons, R. B. Randels, K. T. Chao, H. R. Crane—201(A)
Of thermal neutrons by crystals, F. Rasetti—321
Of thermal neutrons by deuterons, L. Motz, J. Schwinger—26
Secondary electrons (see **Electrons, secondary**)
Solid state (see **Crystalline state**)
Specific heat
Of Zr, C. F. Squire—202(A)
Spectra, absorption
CS_2 bands in ultraviolet, L. N. Liebermann—183(L)
Of ClO_2, J. B. Coon—926(L)
Of Pr ion in solutions and in solid state, F. H. Spedding—255
Of SiH_4 and GeH_4, J. W. Straley, C. H. Tindal, H. H. Nielsen—1002(L)
Solutions of alkali metals in ammonia, H. von R. Jaffe—207(A)
Of zinc sulphide powders, effect of activator, C. J. Brasefield—436
Spectra, atomic
Broadening of Rb lines in He and A, Ch'en Shang-Yi—1051
Of Co I, H. N. Russell, R. B. King, C. E. Moore—407
f values of Cd I and Cu I lines, R. B. King, D. C. Stockbarger—187(A)
Of highly ionized A, W. L. Parker, L. W. Phillips—93(L)
Inverted multiplets in Mg I, L. Pincherle—251
Isotope shift in B, J. P. Vinti—879
Of Pb I forbidden lines, S. Mrozowski—189(A)
Of Mo I and Mo II, M. R. Schauls, R. Sawyer—781
Ch'en Shang-Yi—884
Pressure effects, Rb lines, Ch'en Shang-Yi—884; Ch'en Shang-Yi, Pao Chia-Shan—1058
Radiofrequency spectra of Na, Rb, and Cs, S. Millman, P. Kusch—438
Satellite lines, excitation from closed shells, Ta-You Wu—1075
Theorem on nuclear motion, J. P. Vinti—882
Transitions in Mg, P. J. Rubenstein—1007(L)
Of W, O. Laporte, J. E. Mack—188(A)
Spectra, general
Hyperfine structure, magnetic rotation, resonance radiation, B. J. Miller—258
Impact broadening, L. Spitzer, Jr.—348
Interaction in W I in magnetic field, J. H. Roberson, J. E. Mack, G. R. Harrison—895
Pure Hg^{198} for spectroscopic use, J. Wiens, L. W. Alvarez—1005(L)
Spectra, molecular (see also **Molecular structure and constants**)
Of SbN, N. H. Coy, H. Sponer—709
Infra-red bands of deuterated formic acid, L. G. Smith, V. Williams—208(A)
Intensity of CO bands; electron impact, G. E. Hansche—1075
Isotope shift in HgH^+ and HgD^+, S. Mrozowski—332
Isotope shift in spectrum of ZnH, S. Mrozowski—597
Rotational radiofrequency spectra of H_2, D_2, and HD, N. F. Ramsey, Jr.—226
Thermal reaction between H_2 and O_2, O. Oldenberg, E. G. Schneider, H. S. Sommers, Jr.—1121(A)
Spectroscopy, technique
Source of "forbidden" lines, S. Mrozowski—1086
Superconductivity (see **Electrical conductivity and resistance**)

Thermal conductivity
Liquid crystals, orientation by heat conduction, G. W. Stewart, D. O. Holland, L. M. Reynolds—174
Of metals, C. C. Bidwell—561
Thermal diffusion
Approach to equilibrium, J. Bardeen—94(L)
Theory of, for isotopes, R. C. Jones—111
Thermionic emission of electrons; Emitting surfaces
Into dielectric liquids, W. R. LePage, L. A. DuBridge—61
Energy losses and thermionic emission, G. M. Fleming, J. E. Henderson—887
Temperature dependence of work function, J. G. Potter—623, 928(L); W. B. Nottingham—927(L)
Thermodynamics
Extension of second law, irreversible processes, P. W. Bridgman—845(L)
Irreversible processes, second law, simple fluid, C. Eckart—267; fluid mixtures—269, 924; relativistic theory of simple fluid—919
Thermoelectric effects
Single-crystal Al wires, law of Magnus, C. Y. Ma, W. Band—479(L)

Vacuum tubes
Halation on kinescope screens, R. F. Baker—208(A)
Influence of "cold ends," vacuum-tube air coolers, I. E. Mouromtseff—204(A)
Klystron efficiency, E. U. Condon—204(A)
Van der Waals forces
At metallic surfaces, J. Bardeen—727
Viscosity
Effect of pressure; lubricants, M. Muskat, H. H. Evinger—205(A)
Of He temperature dependence, E. J. Hellund—192(A)
Transport cross section of He, E. J. Hellund—278(L)

X-rays, absorption
Of Cu-Ni alloys, H. Friedman, W. W. Beeman—400
Of Cu-Zn alloys, J. A. Bearden, H. Friedman—387
Fine structure for two elements in same crystal, S. T. Stephenson—195(A), 873
In gaseous, liquid and solid states, T. Drynski, R. Smoluchowski—207(A)
Of Mg and Al, J. H. Munier, J. A. Bearden, C. H. Shaw—537
Of Zn-Ni alloys, J. A. Bearden, W. W. Beeman—396
X-rays, diffraction, scattering, reflection, refraction, and polarization
Diffuse scattering, theory of, G. E. M. Jauncey, G. G. Harvey—179(L)
Effect of crystal size on reflection, F.-H. Marshall—642
By liquid argon, A. Eisenstein, N. S. Gingrich—307
X-rays, emission (see also **X-rays, spectra and spectroscopy, etc.**)
Of Cu-Ni alloys, H. Friedman, W. W. Beeman—400
Of Cu-Zn alloys, J. A. Bearden, H. Friedman—387
Electronic energy bands of compounds, J. Valasek—213
Kronig fine structure, S. T. Stephenson—877
Modified reflections, G. E. M. Jauncey, O. J. Baltzer—1116(L)
M-series of W, J. H. Munier, J. A. Bearden, C. H. Shaw—537
Of Zn-Ni alloys, J. A. Bearden, W. W. Beeman—396
X-rays, spectra and spectroscopy, wave-length measurements (see also **X-rays, emission**)
Lattice constants and density, F. Foote, E. R. Jette—81
X-rays, tubes, apparatus
Cauchois focusing spectrograph, F. R. Hirsh, Jr.—78

Zeeman effect
In Kr, J. B. Green, D. W. Bowman, E. H. Hurlburt-1094
In Kr I and X I, J. B. Green, D. W. Bowman, E. H. Hurlburt—381(L)
In Ru I, G. R. Harrison, J. R. McNally, Jr.—703